

*Dissertation
zur Erlangung des Doktorgrades
Dr. rer. nat.
an der Mathematisch-Naturwissenschaftlichen Fakultät
der Christian-Albrechts-Universität zu Kiel*

Water mass dynamics around cold-water coral reefs in the North Atlantic



vorgelegt am:

GEOMAR
Helmholtz-Zentrum für Ozeanforschung Kiel
FB 1 Paläo-Ozeanographie

von

Dipl.-Geologin
Silke Glogowski

August 2017

1. Gutachter und Betreuer: Prof. Dr. W.-Christian Dullo

2. Gutachter: Prof. Dr. Martin Frank

Tag der Disputation: 29.09.2017

Zum Druck genehmigt: 29.09.2017

gez. Prof. Dr. Natascha Oppelt
(Die Dekanin)

Erklärung

Hiermit versichere ich an Eides statt, dass ich diese Dissertation selbstständig und nur mit Hilfe der angegebenen Quellen und Hilfsmittel erstellt habe. Ferner versichere ich, dass der Inhalt dieses Dokuments weder in dieser, noch in veränderter Form in einer weiteren Prüfungsbehörde vorliegt. Die Arbeit ist unter Einhaltung der Regeln guter wissenschaftlicher Praxis der deutschen Forschungsgemeinschaft entstanden.

Kiel, den 20.08.2017

Silke Glogowski

(Dipl.-Geologin)

Dedication

To Keke and Mika, without whom this would not have been possible.

I love you!

To Regina, Re-nate and Erika, for the inspiration long time ago.

I am deeply indebted to many people for their help throughout all aspects of this thesis.

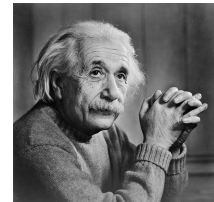
Citation

Albert Einstein (1879-1955):

“ The only real valuable thing is intuition.”

Albert Einstein (1879-1955):

“Das einzig wirklich wertvolle Ding ist Intuition.“



Contents

Abstract	XXI
Kurzfassung	XXV
Index of Symbols and Abbreviations	XXXI

Chapter 1.

Introduction

1.1 General Introduction	1
1.2 Motivation and main objective	2
1.3 The cold-water coral <i>Lophelia pertusa</i>	2
1.3.1 History	3
1.3.2 Distribution, occurrences and habitat characteristics of <i>L.pertusa</i>	5
References	10

Chapter 2.

The Eugen Seibold coral mounds offshore western Morocco: oceanographic and bathymetric boundary conditions of a newly discovered cold-water coral province

Abstract	23
2.1. Introduction	24
2.1.1 Physical Settings	26

2.2. Material and Methods	28
2.2.1 Hydrography	28
2.2.2 Hydroacoustic data	28
2.2.3 Box cores	29
2.2.4 Geochronology	29
2.3 Results	29
2.3.1 Hydrography	29
2.3.2 Hydroacoustic data	30
2.3.3 Box cores	32
2.3.4 Geochronology	33
2.4 Discussion	34
2.5 Conclusions	38
Acknowledgments	38
References	40
Supplementary Material	46

Chapter 3.

Geochemical, optical, microstructure and growth systematics of the scleractinian cold-water coral *Lophelia pertusa*

Abstract	52
3.1 Introduction	53
3.2 Material and Methods	55
3.2.1 Optical images	56
3.2.3 Preparation	57

3.2.4 Element distribution mapping with EPMA	57
3.2.5 Element distributions mapping with LA-ICP-MS	58
3.2.6 Analytical considerations	60
3.2.7 Calyx relative growth	61
3.3 Results	61
3.3.1 Optical visualisation	61
3.3.2 Mapping of Magnesium (Mg) distribution by EPMA	62
3.3.3 Mg/Ca ratios obtained by EPMA	62
3.3.4 Mg/Ca ratios obtained by LA-ICP-MS	63
3.3.5 Sr/Ca ratios obtained by EPMA	63
3.3.6 Sr/Ca ratios obtained by LA-ICP-MS	64
3.3.7 Na/Ca ratios obtained by LA-ICP-MS	65
3.3.8 Equations	65
3.3.9 Skeleton calyx length and cross-sectioned diameter	67
3.4 Discussion	67
3.4.1 Na/Ca ratios	68
3.5 Conclusions	75
Acknowledgments	76
References	77
Supplementary Material	84

Chapter 4.

Seawater mass density gradient of the Campeche cold-water coral province, southern Gulf of Mexico

Abstract	101
4.1 Introduction	102
4.1.1 Regional Settings	103
4.2 Material and Methods	104
4.2.1 Water column analyses	105
4.3 Results	106
4.3.1 Water column structures / dynamics	106
4.4 Discussion	108
4.4.1 Environmental control on the Campeche CWC ecosystem	110
4.5 Conclusions	112
Acknowledgments	113
References	114

Chapter 5.

Hydrographic properties of living cold-water coral reefs in the northern East Atlantic and the Gulf of Mexico

Abstract	118
5.1 Introduction	118
5.1.1 Water mass characteristics	120
5.1.2 Physical settings of investigated sites	122
5.1.3 Density gradient	127

5.2 Material and Methods	128
5.2.1 Hydrography	128
5.3 Results	129
5.3.1 Hydrography around living CWC reefs	129
5.4 Discussion	133
5.5 Conclusions	139
Acknowledgments	140
References	141
Supplementary Material	148
Summary	155
Index of Figures	157
Index of Tables	165
Acknowledgments	167
Apendix	171
CV based on the Europass Curriculum Vitae	172
List of Publications	174

Abstract

Cold-water coral reefs are distributed all over the world's oceans and form a high variety of ecosystems depending on their specific environmental factors. The surrounding parameter of cold-water coral reef growth is characterised by hydrophysical signals such as temperature and salinity, both yielded in potential density as a function of temperature, salinity and pressure. Within the past years a serious increase in knowledge on these cold-water coral occurrences and their hydrographic boundary conditions yielded worldwide, especially in the north-east Atlantic. This study investigates in the assessment of the environmental conditions of cold-water coral (CWC) growth in response to geochemical, hydrographic and oceanographic boundary processes. This study aims to unravel the environmental signals that influence CWC growth in different latitudes, which are of great importance for growth and occurrences. For this purpose, cold-water coral reefs in the north Atlantic margin, in the Gulf of Mexico, off Bahamas, in the Bay of Biscay, and off Morocco as well as Mauretania were selected. The comparison of data sets collected with identical tools yielded detailed information on the environmental conditions needed for healthy cold-water-reef growth.

The second chapter (Glogowski et al. 2015) reports on a new cold-water coral (CWC) province covering ~410 km² off western Morocco. Based on CTD measurements and associated with known oceanographic settings of CWC occurrences along the north-eastern Atlantic margin, hydroacoustic tools are additionally used to detect this CWC area. This comparable CWC reef is located in the upwelling regime within the North Atlantic Current Water (NACW), slightly above the Mediterranean Outflow Water (MOW). However, U-Th isotope systematics for macroscopically altered buried *Lophelia* material yielded absolute ages dating back to the late Holocene at least.

The third chapter (submitted) demonstrates geochemical investigations on *Lophelia pertusa*. Various geochemical proxies are investigated and used the determination of the coral skeleton into theca wall (TW) and center of calcification (CoC) without mentioning how and where exactly the boundary of both is settled. This study investigates into detailed measuring procedures in order to test the reliability of this differentiation process for distinct applications.

Combined measurements of trace element contents, such as Mg/Ca, Sr/Ca, Na/Ca ratios of CWC samples are applied to obtain a detailed record of the coral skeleton. These investigations into this difference show that by combined methods it is possible to differentiate geochemically between these microstructures. However, most CoC derived Me/Ca ratios exhibit better correlations to temperature and salinity than TW derived data. Additionally, Na/Ca data derived from CoC exhibit stronger correlations with salinity as well as temperature with respect to the TW, resulting in enriched crystal lattice defects (CLDs) within the CoC.

The fourth chapter (Hebbeln et al. 2014) focuses on the seawater mass density gradient in the Gulf of Mexico, at the Campeche Bank. This Campeche cold-water coral province was found during the cruise MSM20. The locality is particularly distinguished by an important oceanographic setting such as e.g. high current regime, high productivity right above the living CWC reefs system by vertical migration of nutrients. Thus an example, highlighting the density gradient as a trap for food source in order to supplemental serve the CWC reefs in the intermediate water depth. This observed hydrological setting fits the vividness of cold-water coral ecosystems.

The fifth chapter (to be submitted) also based on the density gradient, shows that it is derived by calculating the difference in water mass density between 10 m intervals resulting in the term of $\Delta\sigma_{\Theta_{10m}}$ and demonstrates the use of this hydrographic property in the northern East Atlantic and the Gulf of Mexico. Results show chances of finding living CWC reefs if the density gradient of maximum $\Delta\sigma_{\Theta_{10m}}$ values is $>0.02 \text{ kg/m}^3$. Moreover, results rather show that by using the maximum $\Delta\sigma_{\Theta_{10m}}$ values of the density gradient it forms layer within the water column. If these layers are thin, it might be an indication for well developed CWC reefs. In contrast, thick layers of maximum $\Delta\sigma_{\Theta_{10m}}$ values seem to present poor occurrences of living CWC reefs.

Kurzfassung

Kaltwasser-Korallenriffe sind weltweit in den Ozeanen verbreitet und bilden eine große Variabilität in ihrem Ökosystem und ihren damit einhergehenden, spezifischen ökologischen Faktoren. Die umgebenden hydrophysikalischen Parameter, die das Wachstum der Kaltwasser-Korallenriffe kennzeichnen, sind u.a. Temperatur und Salzgehalt, welche die potenzielle Dichte als eine Funktion aus Temperatur, Salzgehalt und Umgebungsdruck ergeben. Innerhalb der vergangenen Jahre haben sich die Erkenntnisse der weltweiten, hydrografischen Randbedingungen zu diesen existierenden Kaltwasser-Korallenriffen erheblich verstärkt, insbesondere im Nordost-Atlantik. Diese Studie untersucht und beurteilt die vorhandenen Wachstums- und Umweltbedingungen der Kaltwasser-Korallenriffe in Abhängigkeit zu den geochemisch, hydrographisch und ozeanographisch abgrenzenden Prozessen. Ein Ziel dieser Studie ist die Entwirrung der bestehenden Signale, welche das Wachstum der Kaltwasser-Korallenriffe in unterschiedlichen Breitengraden beeinflussen und von großer Bedeutung für deren Wachstum und Vorkommen sind. Zu diesem Zweck werden die Kaltwasser-Korallenriffe im Nord-Atlantik, im Golf von Mexiko, vor den Bahamas, im Golf von Biskaya, und vor Marokko und Mauretanien herangezogen. Für diesen Datenvergleich wurden identische Bedingungen, Instrumente und Methoden zur Datengewinnung verwendet, mit dem Ziel, detaillierte Informationen zu den umgebenden Bedingungen zu erzielen, die als Voraussetzung für ein gesundes Wachstum und zur Verbreitung der Kaltwasser-Korallenriffe benötigt werden. Kaltwasser-Korallenriffe sind weltweit in den Ozeanen verteilt und bilden eine große ökologische Bandbreite für das jeweilige Ökosystem, das von den dort vorherrschenden spezifischen Faktoren abhängig ist.

Das zweite Kapitel (Glogowski et al. 2015) berichtet über eine neu entdeckte Kaltwasser-Korallen-Provinz mit der Größe von $\sim 410 \text{ km}^2$, westlich vor Marokko. Basierend auf vorgenommenen CTD-Messungen aus dem Nordost-Atlantik, deren umgebende Ozeanographie bereits bekannt ist, wurde das neue Kaltwasser-Korallen-Vorkommen mit zusätzlichen hydroakustischen Daten assoziiert und entdeckt.

Lokalisiert wurde dieses vergleichbare Kaltwasser-Korallen-Vorkommen in einem Bereich mit starkem Tiefenwasserauftrieb in der Wassermasse des Nordatlantischen Strömungswassers (NACW), leicht oberhalb des ausströmenden Wassers aus dem Mittelmeer (MOW). Zusätzlich wurde per U-Th-Isotopie, anhand von makroskopisch verändertem *Lophelia* Material, ein Alter bis zum späten Holozän ermittelt.

Das dritte Kapitel (eingereicht) demonstriert die geochemischen Untersuchungen von *Lophelia pertusa*. Eine Vielzahl von geochemischen Proxies wurden bereits untersucht, und haben dazu die Unterscheidung innerhalb des Korallenskeletts in die äußere Seitenwand (TW) und inneres Zentrum der Kalzifikation (CoC) verwendet. Es wurde meist nicht genau benannt, wo exakt die Grenze zwischen diesen beiden Strukturen verläuft. Diese Studie untersucht im Detail, anhand von mehreren Messmethoden, wo genau diese Grenze verläuft und wie glaubwürdig verschiedene Anwendungsprozesse zur Differenzierung sind. Kombinierte Messungen der Verhältnisse der Spurenelemente, wie Mg/Ca, Sr/Ca, Na/Ca der jeweiligen Kaltwasser-Korallen-Proben wurden detailliert für jedes Korallenskelett aufgenommen. Diese Untersuchungen zur Differenzierung zeigen, dass eine Kombination der verschiedenen Methoden eine geochemische Möglichkeit zur Differenzierung der Mikrostruktur bietet. Allerdings zeigen die meisten Metall/Kalzium Verhältnisse in der CoC eine bessere Korrelation mit der Temperatur und dem Salzgehalt, im Vergleich mit den Daten der Verhältnisse in der TW. Zusätzlich zeigen die Spurenverhältnisse von Na/Ca aus dem CoC eine deutlichere Korrelation mit dem Salzgehalt und der Temperatur im Gegensatz zur TW, dieses resultiert aus der Anreicherung von Fehlstellen im Kristallgitter (CLDs) innerhalb der CoC.

Das vierte Kapitel (Hebbeln et al. 2014) konzentriert sich auf den Dichte-Gradienten des Ozeanwassers im Golf von Mexiko, an der Campeche Bank. Die an der Campeche Bank vorkommende Kaltwasser-Korallen-Provinz wurde während der Forschungsausfahrt MSM20 entdeckt. Diese Lokation ist besonders durch die umgebende Ozeanographie gekennzeichnet, wie zum Beispiel starkes Strömungsgebiet und hohe Produktivität direkt über den lebenden Kaltwasser-Korallen-Vorkommen durch die vertikale Migration der Nährstoffe.

Dies ist ein hervorragendes Beispiel dafür, dass die Dichte-Gradienten als eine Art Barriere dienen, an der Nährstoffpartikel, das Futter der Kaltwasser-Korallen-Vorkommen, akkumulieren und die Kaltwasser-Korallen-Vorkommen im Zwischenwasser damit bedienen. Diese hydrologische Entdeckung unterstützt die Vitalität der Kaltwasser-Korallen-Vorkommen und deren Ökosystem.

Das fünfte Kapitel (in Vorbereitung zum Einreichen) basiert ebenfalls auf den Dichte-Gradienten und zeigt, per Berechnung der jeweiligen Dichte-Gradienten in der Wassersäule im 10 m Intervall, ein hydrografisches Merkmal $\Delta\sigma_{\Theta_{10m}}$ und wird demonstriert für den Nordost-Atlantik und den Golf von Mexiko. Die erzielten Ergebnisse zeigen eine Möglichkeit zur Auffindung von lebenden Kaltwasser-Korallen-Vorkommen sobald das Maximum des Dichte-Gradienten $\Delta\sigma_{\Theta_{10m}}$ Werte von $>0.02 \text{ kg/m}^3$ zeigt. Weiterhin zeigen die Ergebnisse, anhand der Werte des maximalen Dichte-Gradienten $\Delta\sigma_{\Theta_{10m}}$, dass sich eine Gradienten-Schicht innerhalb der Wassersäule bildet. Ist diese Gradienten-Schicht dünn angelegt, so kann sie offensichtlich ein Indikator für lebende, gesunde und gut ausgeprägte Kaltwasser-Korallen-Vorkommen sein. Im Gegensatz dazu ist eine massiver ausgebildete Gradienten-Schicht der maximalen Werte des $\Delta\sigma_{\Theta_{10m}}$ ein Hinweis für weniger gut ausgeprägte lebende Kaltwasser-Korallen-Vorkommen.

Index of Symbols and Abbreviations

AAIW	Antarctic Intermediate Water
AC	Antilles Current
ACW	Antilles Current Water
AW	Atlantic Water
BB	Bay of Biscay
CB	Campeche Bank
CC	Canarian Current
CSW	Caribbean Surface Water
CTD	Conductivity-Temperature-Depth
CWC	Cold-Water Coral
DIC	Dissolved Inorganic Carbon
DOC	Dissolved Oxygen Concentration
DWBC	Deep Western Boundary Current
DWBCW	Deep Western Boundary Current Water
EGC	East Greenland Current
ENAW	Eastern North Atlantic Water
FC	Florida Current
FCSW	Florida Current Surface Water
FSSW	Florida Subsurface Water

GBB	Great Bahama Bank
GoM	Gulf of Mexico
GRS	Greenland Sea
GS	Gulf Stream
LAC	Labrador Current
LC	Loop Current
LSW	Labrador Sea Water
L. pertusa	<i>Lophelia pertusa</i> (Caryophylliidae)
MAC	Morocco Agadir Canyon
MOW	Mediterranean Outflow Water
NACW	North Atlantic Current Water
NADW	North Atlantic Deep Water
NAIW	North Atlantic Intermediate Water
NCW	North Coastal Current
NSDW	Norwegian Sea Deep Water
OFOS	Ocean Floor Observation System
ROV	Remote Operating Vehicle
SAIW	Subarctic Intermediate Water
STUW	Subtropical Intermediate Water
SUW	Subtropical Under Water
SoF	Strait of Florida
SoY	Strait of Yucatan
SW-FI	Southwest Florida

TSW	Tropical Surface Water
UNADW	Upper North Atlantic Deep Water
UTC	Universal Time Coordinated
VK	Viosca Knoll
WD	Water depth
W-FI	West Florida

Chapter 1

Introduction

1.1 General Introduction

Cold-water coral (CWC) reefs are under threat both by climate change and in turn by ocean acidification as well as by bottom trawling as a result of overfishing. To better protect these unique ecosystems, an improved understanding of the physical properties fit the surrounding seawater is required. Enhanced protection is needed to better protect the worldwide occurring CWC reefs (Bennecke et al. 2016), which even influence the global carbonate budget (Lindberg and Mienert 2005; Titschack et al. 2009). In this study, the habitats of the cold-water coral reefs were quantitatively described in relation to the surrounding oceanographic properties (e.g. depth, salinity, temperature, density, which is water masses) and geochemical signatures (e.g. Mg/Ca, Sr/Ca, Na/Ca ratios), which may portray ongoing climate changes. Although there are several CWC species, this study focussed on the primary frame builder *Lophelia pertusa* (Fig. 1.1).



Fig. 1.1 *Lophelia pertusa* caught during cruise MSM32 off Morocco and redrawn by Gabriel Engelen (Waldorfschule Kiel 2017)

1.2 Motivation and main objectives

Several studies show the mediation between the occurrence of living cold-water coral reefs and climate as well as environmental data which are locked in the skeletons of the cold-water corals, especially in *L. pertusa* (e.g. Cohen et al. 2006; Raddatz et al. 2013). The overall goal of this study is to focus on the oceanographic properties shaping the environment of living CWC reefs in the part north of the equator of the Atlantic Ocean. Therefore, the intention is to respond the several questions addressed: (1) What are the physical and geochemical boundary conditions / characteristics of living CWC reefs? What is the influence of bottom water (density) on CWC reefs? (3) What is the hydrographic (density) and hydrochemical signature of ambient bottom water masses bathing living cold-water corals in the northern Atlantic, where cold-water corals obviously live within a well defined hydrochemical window? (4) Which physical boundary conditions favour CWC growth and distribution? These questions are addressed and compared in three case studies from off Morocco (chapter 2), the geochemical analyses of different localities (chapter 3), and the study of density gradients within the water column above the living cold-water coral reef systems in chapter 4 and 5.

1.3 The cold-water coral *Lophelia pertusa*

The cold-water coral *Lophelia pertusa* (Fig. 1.1 and 1.2) is a cosmopolitan cold-water species. Taxonomically (Table 1.1) *L. pertusa* belongs to the order of Scleractinia. This cold-water coral occurs in different colour varieties, e.g. white, grey or red and builds cold-water coral reefs along the continental margins, which are among the most diverse deep-sea habitats. They are azooxanthellate and are able to live within the aphotic zone.



Table 1.1

Taxonomy *Lophelia pertusa* (Linnaeus 1758)

<u>Taxon</u>	<u>Name</u>
Phylum	Cnidaria
Class	Anthozoa
Subclass	Hexacorallia
Order	Scleractinia
Suborder	Caryophyllina
Family	Caryophyllioidea
Genus	<i>Lophelia</i>
Species	<i>Lophelia pertusa</i>

Fig. 1.2 Living *Lophelia pertusa* (Photo: R. Wynn; MSM32 off Morocco)

1.3.1 History

The existence of cold-water corals were mentioned and described first by Dr. Erich Pontoppidan (1752) and later included into the taxonomic description of Carl von Linné within the “Systema Naturae” (1758) as *Madrepora pertusa*. The occurrence of those cold-water corals were linked to “vegetables of the ocean“ and „carbonate knolls“ (Fig. 1.3) with only little interest, except the early studies of Gunnerus (1768) and Flemming (1846). The deep-sea CHALLENGER expedition (1872-1878) and fishermen dredging *Lophelia pertusa* during cruises to the Porcupine Seabight favoured the research on this species, e.g. Charles Wyville Thomson’s “The depths of the sea” (1873). Further research during mid 20th century was done by Le Danois (1948) with speculations that cold-water corals build reef-like structures in the same way as their tropical counterparts did. During the LOGATCHEV cruises in the 80ths of the last century, mound like CWC structures were discovered (Henriett et al. 1998).

Since technical improvements made it more easy to hydroacoustically map large seafloor areas, research efforts on the topic of CWC reefs increased (Roberts et al. 2006). The improvements allowed the detailed mapping and observation of the cold-water coral environment (e.g. Huvenne et al. 2003; Huvenne et al. 2005) and drastically expanded the knowledge of CWC provinces. By recognising their distribution, also the understanding of cold-water coral ecosystem functioning increased continuously, and CWC reefs were soon recognised as important biodiversity hotspot (Reed et al. 1982; Jensen and Fredericksen 1992; Buhl-Mortensen and Mortensen 2005; Mortensen and Fosså 2006; Roberts et al. 2006).

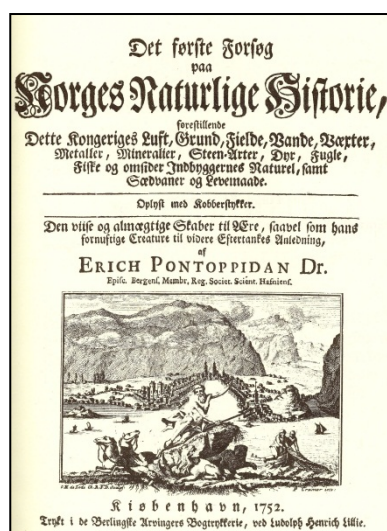


Fig. 1.3 Dr. Erich Pontoppidan, Bishop of Norway (1698 – 1764), “Meeresgemüse – vegetables of the ocean” (1755)

1.3.2 Distribution, occurrences and habitat characteristics of *Lophelia pertusa*

L. pertusa is widely distributed with dominant occurrences from 30°N to 70°N (Fig. 1.4) and seems to be most abundant in the Northeast Atlantic Ocean (Zibrowius 1980; Rogers 1999; Fosså et al. 2002). However, this distribution is certainly biased by the predominance of European initiated research projects, based both on national and European funding (Roberts et al. 2006).

The frame building cold-water coral *L. pertusa* forms habitats with highest abundances of associated species (e.g. McCloskey 1970; Connell 1978; Reaka-Kudla 1997) and supporting a hot spot biodiversity of continental margin marine life (Dons 1944; Burdon-Jones & Tambs-Lyche 1960; Jensen & Frederiksen 1992; Fosså & Mortensen 1998; Rogers 1999; Mortensen and Fosså 2006).

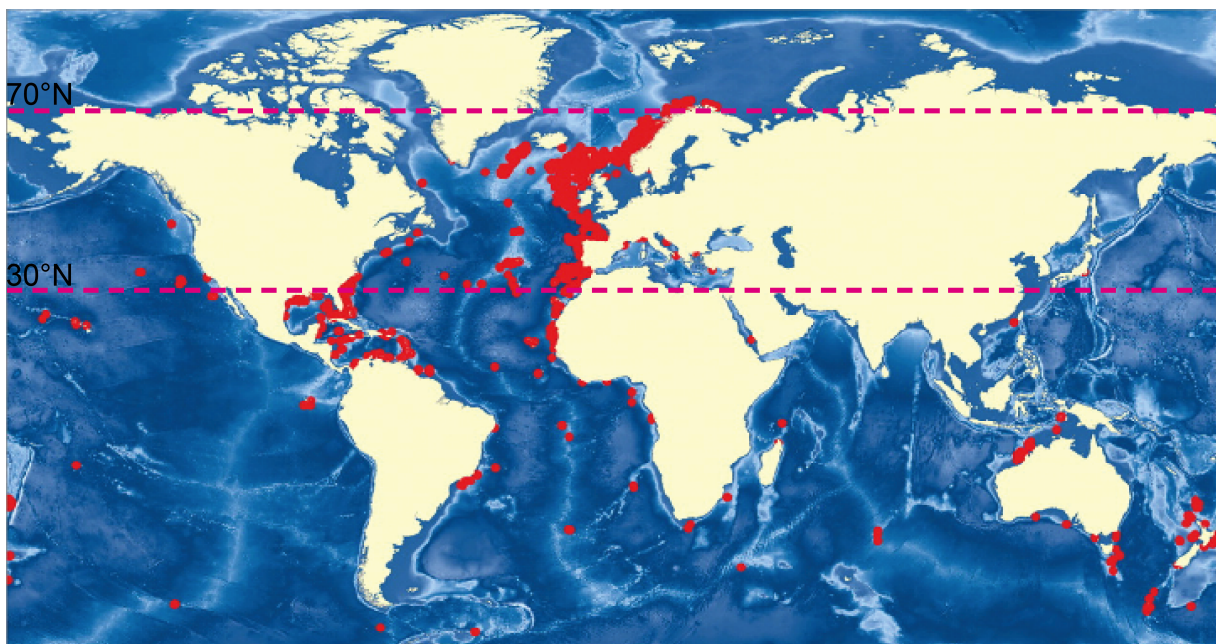


Fig. 1.4 Distribution of cold-water reefs after Roberts et al. (2006)

The present day known places of occurrences match the intensity of research along the continental margins and the number of identified reefs worldwide. Especially in the eastern Atlantic they range from the Norwegian margin at ~70°N (Roberts et al. 2006) down to tropical sites off Angola at ~7°S (Le Guilloux et al. 2009). To cite a few sites *L. pertusa* reefs were reported off the NE Atlantic on the Norwegian margin (Fosså et al. 2002; Freiwald 2002; Freiwald et al. 2004; Hovland et al. 2012) and on the Irish margin (Rüggeberg et al. 2005; Dorschel et al. 2005; White et al. 2007; Mazzini et al. 2012) along the eastern continental margin down to Bay of Biscaya (Huvenne et al. 2011; Dullo et al. 2017), the Mediterranean Sea (Taviani et al. 2005; Savini et al. 2014), off Morocco (Glogowski et al. 2015), off Mauretania (e.g. Eisele et al. 2014). Similar CWC reefs occur in the Gulf of Mexico (Hübscher et al. 2010), at the West Florida slope, the Florida Strait (Cairns 1984; Cairns et al. 2009), the Campeche Bank (Hebbeln et al. 2014) and around the Great Bahama Bank (e.g. Neumann et al. 1977; Mullins et al. 1981; Grasmueck et al. 2006; Reed et al. 2006; Correa et al. 2012).

L. pertusa tolerates a wide range of environmental settings in North Atlantic Ocean. This cold-water coral occurs in water depth from 39 m (Trondheimsfjord, Norway; Rapp and Sneli 1999) down to 3.383 m (New England Seamount Chain; Zibrowius 1980; Freiwald et al. 2004), with largest abundances from 200 m – 1.000 m water depth where this species forms reefs (Freiwald and Wilson 1998; Freiwald et al. 2004).

Lophelia-reefs are complex habitats constituted by coral colonies and fragments of dead skeleton with variable size and age (Wilson 1979; Mortensen et al. 1995; Hovland et al. 1998). According to Flögel et al. (2014) cold-water coral reefs were segmented in three major subhabitats with category I: real CWC framework of several 100 m elevation, category II: patchy CWC growth of some horizontal extension but very limited vertical elevation forming a thin veneer and category III: small, isolated colonies.

Cold-water corals are sessile filter feeders needing solid hard substratum to settle on. Preferring bathymetrical highs favouring increased water currents associated with high productivity (Jensen and Fredericksen 1992), they frequently form CWC reefs and as a result feedback intensifying CWC reef growth.

Moreover, *L. pertusa* is dependent on hydrographic regimes in order to advect nutrients and to remove suspended inorganic matter from the water column above the living *L. pertusa* (Freiwald 2002; Freiwald et al. 2004). The tolerated temperature ranges between 4° – 12 °C (Roberts et al. 2006; Freiwald et al. 2004) and dissolved oxygen levels are preferentially between 2.60 – 6.65 ml l⁻¹ (Schroeder 2002; Dodds et al. 2007; Davies et al. 2008). *L. pertusa* lives most commonly in salinities between 35 – 37 (Roberts et al. 2003; Freiwald et al. 2004; Davies et al. 2008), although they can tolerate ranges of <33 in Norwegian fjords up to >37 in the Mediterranean Sea (Taviani et al. 2005). As a result of temperature, the preferred density envelope proposed by Dullo et al. (2008) is $\sigma_{\Theta} 27.5 \pm 0.15$, this number is typical for all Atlantic sites. Although, cold-water corals in the Mediterranean Sea seem to occur in seawater densities around 29.1 kg m⁻³ (Freiwald et al. 2009). This density envelope may favour the accumulation and advection of nutrients (Duineveld et al. 2004; Waller and Tyler 2005) and to speculate the lateral transport of coral larvae. The CWCs feed on particulate organic matter and “other” nutrients derived from high productive sea surface waters (White et al. 2007). The process of nutrient transport to the CWCs is still not well understood (Davies et al. 2009). Strong bottom currents at tidal frequencies (Pingree and Le Cann 1989) seem to be important (Frederiksen et al. 1992; White 2007) as well as internal waves (Frederiksen et al. 1992; Messing et al. 1990; White 2007), local downwelling and associated mixing processes (Davies et al. 2009). Furthermore, hydrographic properties, such as e.g. density gradients (Dullo et al. 2008; Hebbeln et al. 2014) control the CWC settlement.

Several studies identified that CWC reefs often occur at a pycnocline that coincides with the interface of two different intermediate water masses (Dullo et al. 2008; Eisele et al. 2008; Hovland 2008; Rüggeberg et al. 2008; Roberts et al. 2008; Wheeler et al. 2008; Wienberg et al. 2008; Davies et al. 2009; De Haas et al. 2009; Dorschel et al. 2009; Foubert & Henriët 2009; Frank et al. 2009; Guinan et al. 2009; Huvenne et al. 2009; Lavaley et al. 2009; Mienis et al. 2009; Titschak et al. 2009; Wehrmann et al. 2009; Davies et al. 2010; McCulloch et al. 2010; Purser et al. 2010; Thierens et al. 2010; Van Rooij et al. 2010; Wienberg et al. 2010; Davies et al. 2011; De Mol et al. 2011; Eisele et al. 2011; Flögel & Dullo 2011; Frank et al. 2011; Foubert et al. 2011; Henriët et al. 2011; Hernández-Molina 2011; Howell 2011; Huvenne et al. 2011; Larmagnat et al. 2011; Maignien et al. 2011; Margreth et al. 2011; Pirlet et al. 2011; Raddatz et al. 2011;

Rüggeberg et al. 2011; Van Rooij et al. 2011; Wagner et al. 2011; Wheeler et al. 2011; Wheeler & Stadnitskaia 2011; Correa et al. 2012; Form et al. 2012; Mienis et al. 2012; Mienis et al. 2012b; Munoz et al. 2012; Tong et al. 2012; Allers et al. 2013; Amundsen et al. 2013; Brooke et al. 2013; Brooke & Järnegren 2013; Joseph et al. 2013; Fillinger & Richter et al. 2013; Findlay et al. 2013; Forster 2013; Gori et al. 2013; Naumann et al. 2013; Purser et al. 2013; Raddatz et al. 2013; Rogers et al. 2013; Spezzaferri et al. 2013; Thierens et al. 2013; Tong et al. 2013; Wienberg et al. 2013; Eisele et al. 2014; Findlay et al. 2014; Flögel et al. 2014; Gori et al. 2014; Gori et al. 2014b; Henriët et al. 2014; Iacono et al. 2014; Larsson et al. 2014; Mohn et al. 2014; Movilla et al. 2014; Naumann et al. 2014; Navas et al. 2014; Neves et al. 2014; Raddatz et al. 2014; Roberts & Cairns 2014; Sánchez et al. 2014; Smeulders et al. 2014; Somoza et al. 2014; Stalder et al. 2014; Stewart et al. 2014; Van der Land et al. 2014; Davies et al. 2015; Fink et al. 2015; Glogowski et al. 2015; Gori et al. 2015; Robert et al. 2015; Roik et al. 2015; Rüggeberg et al. 2015; Stalder et al. 2015; Stalder et al. 2015b; Titschack et al. 2015; Amaro et al. 2016; Anderson et al. 2016; Cordes et al. 2016; Fox et al. 2016; Georgian et al. 2016; Hebbeln et al. 2016; Raddatz et al. 2016; Rüggeberg et al. 2016; Soetaert et al. 2016; Tong et al. 2016; Victorero et al. 2016; Buhl-Mortensen et al. 2017; Fabri et al. 2017; Fernandez-Arcaya et al. 2017; Johanson et al. 2017; Kenchington et al. 2017; Lim et al. 2017; Reolid et al. 2017; Van Den Beld et al. 2017; Iacono et al. 2018). These water mass characteristics and the interaction of the associated hydrographic regimes are one of the major properties supporting the formation of living CWC reef systems (Davies et al. 2009; Flögel et al. 2014).

References

- Allers E, Abed RM, Wehrmann LM, Wang T, Larsson AI, Purser A, de Beer D (2013) Resistance of *Lophelia pertusa* to coverage by sediment and petroleum drill cuttings. *Mar poll bull* 74(1):132–40
- Amaro T, Huvenne VA, Allcock AL, Aslam T, Davies JS, Danovaro R, De Stigter HC, Duineveld GC, Gambi C, Gooday AJ, Gunton LM (2016) The Whittard Canyon—A case study of submarine canyon processes. *Prog Oceanog* 146:38–57
- Amundsen H, Anderson L, Andersson A, Azetsu-Scott K, Bellerby R, Beman M, Browman HI, Carlson C, Cheung WW, Chierici M, Clayton T (2013) AMAP Assessment 2013: Arctic Ocean Acidification. Arctic Monitoring and Assessment Programme (AMAP)
- Anderson OF, Guinotte JM, Rowden AA, Clark MR, Mormede S, Davies AJ, Bowden DA (2016) Field validation of habitat suitability models for vulnerable marine ecosystems in the South Pacific Ocean: Implications for the use of broad-scale models in fisheries management. *Ocean & Coastal Manag* 120:110–26
- Aristegui J, Barton ED, Álvarez-Salgado XA, Santos AMP, Figueiras FG, Kifani S, Hernández-León S, Mason E, Machú E, Demarcq H (2009) Sub-regional ecosystem variability in the Canary Current upwelling. *Prog Oceanog* 83:33–48
- Bennecke S, Kwasnitschka T, Metaxas A, Dullo W-C (2016) In situ growth rates of deep-water octocorals determined from 3D photogrammetric reconstructions. *Coral Reefs* 35(4):1227–1239. doi:10.1007/s00338-016-1471-7
- Brooke S, Ross SW, Bane JM, Seim HE, Young CM (2013) Temperature tolerance of the deep-sea coral *Lophelia pertusa* from the southeastern United States. *Deep-Sea Res II* 92:240–8
- Brooke S, Järnegren J (2013) Reproductive periodicity of the scleractinian coral *Lophelia pertusa* from the Trondheim Fjord, Norway. *Mar Biol* 160(1):139–53
- Burdon-Jones C and Tambs-Lyche H (1960) Observations on the fauna of the North Brattholmen stone-coral reef near Bergen. *Årbok for Universitetet i Bergen. Mat naturv Serie* (4):1–24
- Buhl-Mortensen L and Mortensen PB (2005) Distribution and diversity of species associated with deep-sea gorgonian corals off Atlantic Canada. In: Freiwald A, Roberts JM (eds) *Cold-water Corals and Ecosystems*. Springer-Verlag:849–879
- Buhl-Mortensen P, Gordon DC, Buhl-Mortensen L, Kulka DW (2017) First description of a *Lophelia pertusa* reef complex in Atlantic Canada. *Deep-Sea Res I* 126:21–30
- Cairns SD (1984) New records of ahermatotypic corals (Scleractinia) from the Hawaiian Islands and Line Islands. *Ocasional Papers of the Bishop Museum* 25:1–30
- Cairns SD, Jaap WC and Lang JC (2009) Scleractinia (Cnidaria) of the Gulf of Mexico, In: Felder DL and Camp DK (eds) *Gulf of Mexico – Origins, Waters and Biota*. Biodiversity:333–347. Texas A&M, University Press, College Station, Texas
- Cohen AL, Gaetani GA, Lundälv T, Corliss BH, George RY (2006) Compositional variability in a cold-water scleractinian, *Lophelia pertusa*: New insights into “vital effects”. *Geochem Geophys Geosyst* 7(12):Q12004. doi:10.1029/2006GC001354
- Connell JH (1978) Diversity in tropical rain forests and coral reefs. *Science* 199: 1302–1310

- Cordes E, Arnaud-Haond S, Bergstad O, da Costa Falcão AP, Freiwald A, Murray Roberts L, Bernal P (2016) Cold water corals. United Nations: In The first global integrated marine assessment. Division for ocean affairs and the law of the sea
- Correa ML, Montagna P, Joseph N, Rüggeberg A, Fietzke J, Flögel S, Dorschel B, Goldstein SL, Wheeler A, Freiwald A (2012) Preboreal onset of cold-water coral growth beyond the Arctic Circle revealed by coupled radiocarbon and U-series dating and neodymium isotopes. *Quat Sci Rev* 34:24–43
- Correa TBS, Grasmueck M, Eberli GP, Reed JK, Verwer K, Purkis S (2012b) Variability of cold-water coral mounds in a high sediment input and tidal current regime, Straits of Florida. *Sedimentology* 59(4):1278–1304
- Davies AJ, Wisshak M, Orr JC, Roberts JM (2008) Predicting suitable habitat for the cold-water coral *Lophelia pertusa* (Scleractinia). *Deep-Sea Res I* 55:1048–1062
- Davies AJ, Duineveld GCA, Lavaleye MSS, Bergmann MJN, van Haren H, Roberts JM (2009) Downwelling and deep-water bottom currents as food supply mechanisms to the cold-water coral *Lophelia pertusa* (Scleractinia) at the Mingulay Reef complex. *Limnol Oceanog* 54(2):620–629
- Davies AJ, Duineveld GC, van Weering TC, Mienis F, Quattrini AM, Seim HE, Bane JM, Ross SW (2010) Short-term environmental variability in cold-water coral habitat at Viosca Knoll, Gulf of Mexico. *Deep-Sea Res I* 57(2):199–212
- Davies AJ, Guinotte JM (2011) Global habitat suitability for framework-forming cold-water corals. *PLoS One* 6(4):e18483. doi:10.1371/journal.pone.0018483
- Davies JS, Stewart HA, Narayanaswamy BE, Jacobs C, Spicer J, Golding N, Howell KL (2015) Benthic assemblages of the Anton Dohrn seamount (NE Atlantic): defining deep-sea biotopes to support habitat mapping and management efforts with a focus on vulnerable marine ecosystems. *PloS One* 10(5):e0124815
- De Haas H, Mienis F, Frank N, Richter TO, Steinacher R, De Stigter H, Van der Land C, Van Weering TC (2009) Morphology and sedimentology of (clustered) cold-water coral mounds at the south Rockall Trough margins, NE Atlantic Ocean. *Facies* 55(1):1–26
- De Mol L, Van Rooij D, Pirlet H, Greinert J, Frank N, Quemmeraid F, Henriët JP (2011) Cold-water habitats in the Penmarch and Guilvinec Canyons (Bay of Biscay): Deep-water versus shallow-water settings. *Mar Geol* 282:40–52
- Dodds LA, Roberts JM, Taylor AC, Marubini F (2007) Metabolic tolerance of the cold-water coral *Lophelia pertusa* (Scleractinia) to temperature and dissolved oxygen change. *J Exp Mar Biol Ecol* 349:205–214
- Dorschel B, Wheeler AJ, Huvenne VA, De Haas H (2009) Cold-water coral mounds in an erosive environmental setting: TOBI side-scan sonar data and ROV video footage from the northwest Porcupine Bank, NE Atlantic. *Mar Geol* 264(3):218–29
- Duineveld GCA, Lavleye MSS, Berghuis EM (2004) Particle flux and food supply to a seamount cold-water coral community (Galicia Bank, NW Spain). *Mar Ecol Prog Ser* 277:13–23
- Dullo W-C, Flögel S, Rüggeberg A (2008) Cold-water coral growth in relation to the hydrography of the Celtic and Nordic European continental margin. *Mar Ecol Prog Ser* 371:165–176

- Dullo W-C, Flögel S, Rüggeberg A (2017) Water mass measurements around benthic communities: a comparative study between Yo-Yo Conductivity-Temperature-Depth (CTD) casts and high-resolution time series data acquisition of bottom waters from the Pagès Escarpment in the southern Bay of Biscay. In: Diversity in the Coastal Marine Sciences - A Festschrift Volume in Honor of Alexandru Bologa edited by Charles Finkel, Springer Verlag
- Dons C (1944) Norges korallrev. Det Kongelige Norske Videnskabers Selskabs Forhandlinger 16:37–82
- Dorschel B, Hebbeln D, Rüggeberg A, Dullo W-C, Freiwald A (2005) Growth and erosion of a cold-water coral covered carbonate mound in the Northeast Atlantic during Late Pleistocene and Holocene. *Earth Plan Sci Lett* 233:33–44
- Eisele M, Hebbeln D, Wienberg C (2008) Growth history of a cold-water coral covered carbonate mound—Galway Mound, Porcupine Seabight, NE-Atlantic. *Mar Geol* 253(3):160–9
- Eisele M, Frank N, Wienberg C, Hebbeln D, López Correa M, Douville E, Freiwald A (2011) Productivity controlled cold-water coral growth periods during the last glacial off Mauritania. *Mar Geol* 280:143–149
- Eisele M, Frank N, Wienberg C, Hebbeln D, López Correa M, Douville E, Freiwald A (2014) Productivity controlled cold-water coral growth periods during the last glacial off Mauretania. *Mar Geol* 280:143–149
- Fabri MC, Bargain A, Paireaud I, Pedel L, Taupier-Letage I (2017) Cold-water coral ecosystems in Cassidaigne Canyon: An assessment of their environmental living conditions. *Deep-Sea Res II* 137:436–53
- Fernandez-Arcaya U, Ramirez-Llodra E, Aguzzi J, Allcock AL, Davies JS, Dissanayake A, Harris P, Howell K, Huvenne VA, Macmillan-Lawler M, Martín J (2017) Ecological role of submarine canyons and need for canyon conservation. *Front Mar Sci* 4:00005
- Fillinger L, Richter C (2013) Vertical and horizontal distribution of *Desmophyllum dianthus* in Comau Fjord, Chile: a cold-water coral thriving at low pH. *Peer J* 1:e194
- Findlay HS, Artioli Y, Moreno Navas J, Hennige SJ, Wicks LC, Huvenne VA, Woodward EM, Roberts JM (2013) Tidal downwelling and implications for the carbon biogeochemistry of cold-water corals in relation to future ocean acidification and warming. *Global change biol* 19(9):2708–19
- Findlay HS, Hennige SJ, Wicks LC, Navas JM, Woodward EM, Roberts JM (2014) Fine-scale nutrient and carbonate system dynamics around cold-water coral reefs in the northeast Atlantic. *Scientific rep*:4
- Fink HG, Wienberg C, De Pol-Holz R, Hebbeln D (2015) Spatio-temporal distribution patterns of Mediterranean cold-water corals (*Lophelia pertusa* and *Madrepora oculata*) during the past 14,000 years. *Deep-Sea Res I* 103:37–48
- Flemming J (1846) On the recent Scottish Madrepores, with remarks on the climatic character of the extinct races. *Proc Roy Soc, Edinburgh* (2):82–83
- Flögel S and Dullo WC (2011) High-resolution water mass measurements around cold-water corals: a comparative test study between repeated Conductivity-Temperature-Depth (CTD) casts and continuous data acquisition of bottom waters from the West Florida Slope, Gulf of Mexico. *Annalen des Naturhistorischen Museums in Wien. Serie A für Mineralogie und Petrographie, Geologie und Paläontologie, Anthropologie und Prähistorie*:209–224

- Flögel S, Dullo W-C, Pfannkuche O, Kiriakoulakis K, Rüggeberg A (2014) Geochemical and physical constraints for the occurrence of living cold-water corals. *Deep-Sea Res II* 99:19–26
- Form AU, Ribesell U (2012) Acclimation to ocean acidification during long-term CO² exposure in the cold-water coral *Lophelia pertusa*. *Global Change Biol* 18: 843–853. doi: 10.1111/j.1365-2486.2011.02583.x
- Forster N (2013) Benthic foraminifers as tools to reconstruct high-latitude Holocene climate variability and processes during cold-water coral mound growth and development: A case study from Stjærnsund, northern Norway. *BoD–Books on Demand*
- Fosså JH, Mortensen PB (1998) Artsmangfoldet på *Lophelia*-korallrev og metoder for overvåkning. *Fisken og havet* Nr 17:95
- Fosså JH, Mortensen PB, Furevik DM (2002) The deepwater coral *Lophelia pertusa* in Norwegian waters; distribution and fishery impacts. *Hydrobiologia* 417:1–12
- Foubert A, Henriët JP (2009) Nature and significance of the recent carbonate mound record: the mound challenger code. *Springer Science & Business Media*
- Foubert A, Huvenne VA, Wheeler A, Kozachenko M, Opderbecke J, Henriët JP (2011) The Moira Mounds, small cold-water coral mounds in the Porcupine Seabight, NE Atlantic: Part B—Evaluating the impact of sediment dynamics through high-resolution ROV-borne bathymetric mapping. *Mar Geol* 282(1):65–78
- Fox AD, Henry LA, Corne DW, Roberts JM (2016) Sensitivity of marine protected area network connectivity to atmospheric variability. *Royal Society open science* 3(11):160494
- Frank N, Ricard E, Lutringer-Paquet A, van der Land C, Colin C, Blamart D, Foubert A, Van Rooij D, Henriët JP, de Haas H, van Weering T (2009) The Holocene occurrence of cold water corals in the NE Atlantic: implications for coral carbonate mound evolution. *Mar Geol* 266(1):129–42
- Frank N, Freiwald A, Correa ML, Wienberg C, Eisele M, Hebbeln D, Van Rooij D, Henriët JP, Colin C, van Weering T, de Haas H (2011) Northeastern Atlantic cold-water coral reefs and climate. *Geology* 39(8):743–6
- Frederiksen R, Jensen A, Westerberg H (1992) The distribution of the scleractinian coral *Lophelia pertusa* around the Faroe islands and the relation to internal tidal mixing. *Sarsia* 77:157–171
- Freiwald A, Henrich R, Pätzold J (1997) Anatomy of a deep-water coral reef mound from Stjærnsund, West-Finnmark, northern Norway. In: James NP, Clarke JAD (eds) *Cool-water carbonates*. *SEPM, Special Publication* 56:141–161
- Freiwald A and Wilson JB (1998) Taphonomy of modern deep, cold-temperate water coral reefs. *Hist Biol* 13:37–52
- Freiwald A (2002) Reef-forming cold-water corals. In: Wefer G, Billett D, Hebbeln D, Jørgensen BB, Schlüter M, Van Weering T (eds) *Ocean margin systems*. *Springer Verlag*:365–385
- Freiwald A, Fosså JH, Grehan A, Koslow T and Roberts JM (2004) *Cold-water coral reefs*. *UNEP-WCMC, Cambridge, UK*:84 pp
- Georgian SE (2016) *Environmental and energetic constraints on cold-water corals*. *Temple University*

- Georgian SE, DeLeo D, Durkin A, Gomez CE, Kurman M, Lunden JJ, Cordes EE (2016) Oceanographic patterns and carbonate chemistry in the vicinity of cold-water coral reefs in the Gulf of Mexico: Implications for resilience in a changing ocean. *Limnol Oceanog* 61(2):648–65
- Glogowski S, Dullo W-C, Feldens P, Liebetrau V, von Reumont J, Hühnerbach V, Krastel S, Wynn RB, Flögel S (2015) The Eugen Seibold coral mounds offshore western Morocco: oceanographic and bathymetric boundary conditions of a newly discovered cold-water coral province. *Geo-Mar Lett* 35(4):257–269. doi:10.1007/s00367-015-0405-7
- Gori A, Orejas C, Madurell T, Bramanti L, Martins M, Quintanilla E, Marti-Puig P, Iacono CL, Puig P, Requena S, Greenacre M (2013) Bathymetrical distribution and size structure of cold-water coral populations in the Cap de Creus and Lacaze-Duthiers canyons (northwestern Mediterranean). *Biogeosciences* 10(3):2049
- Gori A, Grover R, Orejas C, Sikorski S, Ferrier-Pagès C (2014) Uptake of dissolved free amino acids by four cold-water coral species from the Mediterranean Sea. *Deep-Sea Res II* 99:42–50
- Gori A, Reynaud S, Orejas C, Gili JM, Ferrier-Pages C (2014) Physiological performance of the cold-water coral *Dendrophyllia cornigera* reveals its preference for temperate environments. *Coral Reefs* 33(3):665–74
- Gori A, Reynaud S, Orejas C, Ferrier-Pagès C (2015) The influence of flow velocity and temperature on zooplankton capture rates by the cold-water coral *Dendrophyllia cornigera*. *J Exper Mar Biol Ecol* 466:92–7
- Grasmueck M, Eberli GP, Viggiano DA, Correa T, Rathwell G, Luo J (2006) Autonomous underwater vehicle (AUV) mapping reveals coral mound distribution, morphology, and oceanography in deep water of the Straits of Florida. *Geophys Res Lett* 33:L23616. doi:10.1029/2006GL027734
- Guinan J, Grehan AJ, Dolan MF, Brown C (2009) Quantifying relationships between video observations of cold-water coral cover and seafloor features in Rockall Trough, west of Ireland. *Mar Ecol Prog Ser* 375:125–38
- Gunnerus JE (1768) Om nogle Norske Coraller. *Konglige Norske Videnskabers Selskabs Skrifter*:38–73
- Hebbeln D, Wienberg C, Wintersteller P, Freiwald A, Becker M, Beuck L, Dullo C, Eberli GP, Glogowski S, Matos L, Forster N, Reyes-Bonilla H, Taviani M (2014) Environmental forcing of the Campeche cold-water coral province, southern Gulf of Mexico. *Biogeosciences* 11:1799–1815
- Hebbeln D, Van Rooij D, Wienberg C (2016) Good neighbours shaped by vigorous currents: Cold-water coral mounds and contourites in the North Atlantic. *Mar Geol* 378:171–85
- Henriet J-P, De Mol B, Pillen S, Vanneste M, Van Rooij D, Versteeg W, Croker PF, Shannon PM, Unnithan V, Bouriak S, Chachkine P (1998) Gas hydrate crystals may help build reefs. *Nature* 391:648–649
- Henriet JP, Spezzaferri S, Samankassou E, Foubert A, Van Rooij D, Rüggeberg A (2011) Carbonate mounds in shallow and deep time. *Mar Geol* 282(1-2):1–4
- Henriet JP, Hamoumi N, Da Silva AC, Foubert A, Lauridsen BW, Rüggeberg A, Van Rooij D (2014) Carbonate mounds: from paradox to world heritage. *Mar Geol* 352:89–110

- Hernández-Molina FJ, Serra N, Stow DAV, Llave E, Ercilla G, Van Rooij D (2011) Along-slope oceanographic processes and sedimentary products around the Iberian margin. *Geo-Mar Lett* 31:315–341
- Hovland M, Croker PF, Martin M (1994) Fault-associated seabed mounds (carbonate knolls?) off western Ireland and north-west Australia. *Mar Petrol Geol* 11:232–246
- Hovland M (2008) Deep-water coral reefs: Unique biodiversity hot-spots. Springer Science & Business Media
- Hovland M, Jensen S, Indreiten T (2012) Unit pockmarks associated with *Lophelia* coral reefs off mid-Norway: more evidence of control by ‘fertilizing’ bottom currents. *Geo-Mar Lett* 32:545–554
- Howell KL (2011) "When the species is also a habitat: comparing the predictively modelled distributions of *Lophelia pertusa* and the reef habitat it forms." *Biol Conser* 144(11):2656–2665
- Hübscher C, Dullo C, Flögel S, Titschack J, Schönfeld J (2010) Contourite drift evolution and related coral growth in the eastern Gulf of Mexico and its gateways. *Int J Earth Sci* 99:191–206
- Huvenne VA, Van Rooij D, De Mol B, Thierens M, O'Donnell R, Foubert A (2009) Sediment dynamics and palaeo-environmental context at key stages in the Challenger cold-water coral mound formation: clues from sediment deposits at the mound base. *Deep-Sea Res I* 56(12):2263–80
- Huvenne VA, Tyler PA, Masson DG, Fisher EH, Hauton C, Huehnerbach V, Le Bas TP, Wolff GA (2011) A picture on the wall: innovative mapping reveals cold-water coral refuge in submarine canyon. *PLoS One* 6:e28755
- Iacono CL, Gràcia E, Ranero CR, Emelianov M, Huvenne VA, Bartolomé R, Booth-Rea G, Prades J (2014) The West Melilla cold water coral mounds, Eastern Alboran Sea: Morphological characterization and environmental context. *Deep-Sea Res II* 99:316–26
- Iacono CL, Savini A, Basso D (2018) Cold-water carbonate bioconstructions. In: *Submarine Geomorphology*:425-455, Springer, Cham
- Jensen A and Fredericksen R (1992) The fauna associated with the bank-forming deep water coral *Lophelia pertusa* (Scleractinaria) on the Faroe shelf. *J Sarsia* 77(1):53–69. doi.org/10.1080/00364827.1992.10413492
- Johanson AN, Flögel S, Dullo WC, Linke P, Hasselbring W (2017) Modeling polyp activity of *Paragorgia arborea* using supervised learning. *Ecological Informatics* 39:109–18
- Joseph N, López Correa M, Schönfeld J, Rüggeberg A, Freiwald A (2013) Sub-arctic Holocene climatic and oceanographic variability in Stjærnsund, northern Norway: evidence from benthic foraminifera and stable isotopes. *Boreas* 42(3):511–31
- Kenchington E, Yashayaev I, Tendal OS, Jørgensbye H (2017) Water mass characteristics and associated fauna of a recently discovered *Lophelia pertusa* (Scleractinia: Anthozoa) reef in Greenlandic waters. *Polar Biol* 40(2):321–37
- Larmagnat S, Neuweiler F (2011) Exploring a link between Atlantic coral mounds and Phanerozoic carbonate mudmounds: Insights from pore water fluorescent dissolved organic matter (FDOM), Pen Duick mounds, offshore Morocco. *Mar Geol* 282(1):149–59

- Larsson AI, Järnegren J, Strömberg SM, Dahl MP, Lundälv T, Brooke S (2014) Embryogenesis and larval biology of the cold-water coral *Lophelia pertusa*. PLoS One 9(7):e102222
- Lavaleye M, Duineveld G, Lundälv T, White M, Guihen D, Kiriakoulakis K, Wolff GA (2009) Cold-water corals on the Tisler Reef: preliminary observations on the dynamic reef environment. Oceanog 22(1):76–84
- Le Danois E (1948) Les profondeurs de la mer. Payot, Paris:303
- Lindberg B and Mienert J (2005) Sedimentological and geochemical environment of the Fugløy Reef off northern Norway. In: Cold-Water Corals and Ecosystems: Springer Verlag:633–650
- Linnaeus C (1758) Systema naturae. 10th edn(1) Stockholm: Salvii L
- Lim A, Wheeler AJ, Arnaubec A (2017) High-resolution facies zonation within a cold-water coral mound: The case of the Piddington Mound, Porcupine Seabight, NE Atlantic. Mar Geol 390:120–30
- Maignien L, Depreiter D, Foubert A, Reveillaud J, De Mol L, Boeckx P, Blamart D, Henriot JP, Boon N (2011) Anaerobic oxidation of methane in a cold-water coral carbonate mound from the Gulf of Cadiz. Int J Earth Sci 100(6):1413–22
- Margreth S, Gennari G, Rüggeberg A, Comas MC, Pinheiro LM, Spezzaferri S (2011) Growth and demise of cold-water coral ecosystems on mud volcanoes in the West Alboran Sea: The messages from the planktonic and benthic foraminifera. Mar Geol 282(1):26–39
- Mazzini A, Akhmetzhanov A, Monteys X, Ivanov M (2012) The Porcupine Bank Canyon coral mounds: oceanographic and topographic steering of deep-water carbonate mound development and associated phosphatic deposition. Geo-Mar Lett 32:205–225
- McCloskey LR (1970) The dynamics of the community associated with a marine Scleractinian coral. Int Revue Hydrobiol 55:13–81
- McCulloch M, Taviani M, Montagna P, Correa ML, Remia A, Mortimer G. (2010) Proliferation and demise of deep-sea corals in the Mediterranean during the Younger Dryas. Earth Plan Sci Lett 298(1):143–52
- Mienis F, De Stigter HC, De Haas H, Van Weering TC (2009) Near-bed particle deposition and resuspension in a cold-water coral mound area at the Southwest Rockall Trough margin, NE Atlantic. Deep-Sea Res I 56(6):1026–38
- Mienis F, Duineveld GCA, Davies AJ, Ross SW, Seim H, Bane J and Van Weering TCE (2012) The influence of nearbed hydrodynamic conditions on cold-water corals in the Viosca Knoll area, Gulf of Mexico, Deep-Sea Res I 60:32–45
- Mienis F, De Stigter HC, De Haas H, Van der Land C, Van Weering TC (2012b) Hydrodynamic conditions in a cold-water coral mound area on the Renard Ridge, southern Gulf of Cadiz. J Mar Syst 96:61–71
- Mohn C, Rengstorf A, White M, Duineveld G, Mienis F, Soetaert K, Grehan A (2014) Linking benthic hydrodynamics and cold-water coral occurrences: A high-resolution model study at three cold-water coral provinces in the NE Atlantic. Prog Oceanog 122:92–104
- Mortensen PB, Hovland M, Brattegard T, Farestveit R (1995) Deep water bioherms of the scleractinian coral *Lophelia pertusa* (L.) at 64°N on the Norwegian shelf: structure and associated megafauna. Sarsia 80:145–158

- Mortensen PB and Fosså JH (2006) Species diversity and spatial distribution of invertebrates on deep-water *Lophelia* reefs in Norway. *Proc Int Coral Reef Symp*:1849–1868
- Movilla J, Orejas C, Calvo E, Gori A, López-Sanz À, Grinyó J, Domínguez-Carrió C, Pelejero C (2014) Differential response of two Mediterranean cold-water coral species to ocean acidification. *Coral Reefs* 33(3):675–86
- Mullins HT, Newton CR, Heath K and Vanburen HM (1981) Modern deep-water coral mounds north of Little Bahama Bank: criteria for recognition of deep-water coral bioherms in the rock record. *J Sed Petrol* 51:999–1013
- Munoz A, Cristobo J, Rios P, Druet M, Polonio V, Uchupi E, Acosta J, Group A (2012) Sediment drifts and cold-water coral reefs in the Patagonian upper and middle continental slope. *Mar Petro Geol* 36(1):70–82
- Naumann MS, Orejas C, Ferrier-Pagès C (2014) Species-specific physiological response by the cold-water corals *Lophelia pertusa* and *Madrepora oculata* to variations within their natural temperature range. *Deep-Sea Res II* 99:36–41
- Naumann MS, Orejas C, Ferrier-Pagès C (2013) High thermal tolerance of two Mediterranean cold-water coral species maintained in aquaria. *Coral Reefs* 32(3):749–54
- Navas JM, Miller PL, Henry LA, Hennige SJ, Roberts JM (2014) Ecohydrodynamics of cold-water coral reefs: a case study of the Mingulay Reef Complex (Western Scotland). *PLoS One* 9(5):e98218
- Neumann AC, Kofoed JW, Keller GH (1977) Lithoherms in the Straits of Florida. *Geology* 5:4–10
- Neves BM, Du Preez C, Edinger E (2014) Mapping coral and sponge habitats on a shelf-depth environment using multibeam sonar and ROV video observations: Learmonth Bank, northern British Columbia, Canada. *Deep-Sea Res II* 99:169–83
- Pirlet H, Colin C, Thierens M, Latruwe K, Van Rooij D, Foubert A, Frank N, Blamart D, Huvenne VA, Swennen R, Vanhaecke F (2011) The importance of the terrigenous fraction within a cold-water coral mound: A case study. *Mar Geol* 282(1):13–25
- Pollard S, Griffiths CR, Cunningham SA, Read JF, Perez FF, Rios AF (1996) Vivaldi 1991 – a study of the formation, circulation, and ventilation of the eastern North Atlantic Central Water. *Prog Oceanog* 37:167–1925
- Pontoppidan E (1755) *The natural history of Norway: containing, a particular and accurate account of the temperature of the air, the different soils, waters, vegetables, metals, minerals, stones, beasts, birds, and fishes; together with the dispositions, customs, and manner of living of the inhabitants; interspersed with physiological notes from eminent writers, and translations of academies. In two parts. Translated from the Danish original.* Linde A, London:206
- Purser A, Larsson AI, Thomsen L, van Oevelen D (2010) The influence of flow velocity and food concentration on *Lophelia pertusa* (Scleractinia) zooplankton capture rates. *Mar Biol Ecol* 395(1):55–62
- Purser A, Orejas C, Gori A, Tong R, Unnithan V, Thomsen L (2013) Local variation in the distribution of benthic megafauna species associated with cold-water coral reefs on the Norwegian margin. *Cont Shelf Res* 54:37–51
- Raddatz J, Rüggeberg A, Margreth S, Dullo WC, Expedition IO (2011) Paleoenvironmental reconstruction of Challenger Mound initiation in the Porcupine Seabight, NE Atlantic. *Mar Geol* 282(1):79–90

- Raddatz J, Liebetrau V, Rüggeberg A, Hathorne E, Krabbenhöft A, Eisenhauer A, Böhm F, Vollstaedt H, Fietzke J, López Correa M, Freiwald A, Dullo W-C (2013) Stable Sr-isotope, Sr/Ca, Mg/Ca, Li/Ca and Mg/Li ratios in the scleractinian cold-water coral *Lophelia pertusa*. *Chem Geol* 352:143–152
- Raddatz J, Rüggeberg A, Liebetrau V, Foubert A, Hathorne EC, Fietzke J, Eisenhauer A, Dullo WC (2014) Environmental boundary conditions of cold-water coral mound growth over the last 3 million years in the Porcupine Seabight, Northeast Atlantic. *Deep-Sea Res II* 99:227–36
- Raddatz J, Liebetrau V, Trotter J, Rüggeberg A, Flögel S, Dullo WC, Eisenhauer A, Voigt S, McCulloch M (2016) Environmental constraints on Holocene cold-water coral reef growth off Norway: Insights from a multiproxy approach. *Paleoceanog* 31(10):1350–67
- Rapp HT & Snell JA (1999) *Lophelia pertusa* – myths and reality. Second Nordic Marine Sciences Meeting, Hirtshals, Denmark
- Rahmstorf S (2002) Ocean circulation and climate change during the past 120,000 years. *Nature* 419:207–214
- Reaka-Kudla ML (1997) The global biodiversity of coral reefs: a comparison with rain forests. Pp 83-108 In Reaka-Kudla ML, Wilson DE, Wilson EO (eds) *Biodiversity II: Understanding and Protecting our Biological Resources*. Washington, DC, Joseph Henry Press: 551 pp
- Reed JK, Gore RH, Scotto LE, Wilson KA (1982) Community Composition, Structure, Areal and Trophic Relationships of Decapods Associated with Shallow- and Deep-Water *Oculina Varicosa* Coral Reefs: Studies on Decapod Crustacea from the Indian River Region of Florida, XXIV. *Bull Mar Sci* 32(3):761–786
- Reed JK, Weaver D, Pomponi SA (2006) Habitat and fauna of deep-water *Lophelia pertusa* coral reefs off the Southeastern USA: Blake Plateau, Straits of Florida, and Gulf of Mexico. *Bull Mar Sci* 78:343–375
- Reolid J, Reolid M, Betzler C, Lindhorst S, Wiesner MG, Lahajnar N (2017) Upper Pleistocene cold-water corals from the Inner Sea of the Maldives: taphonomy and environment. *Facies* 63(2):8
- Roberts JM, Henry LA, Long D, Hartley JP (2008) Cold-water coral reef frameworks, megafaunal communities and evidence for coral carbonate mounds on the Hatton Bank, north east Atlantic. *Facies* 54(3):297–316
- Roberts JM, Cairns SD (2014) Cold-water corals in a changing ocean. *Current Opinion in Environmental Sustainability* 7:118–26
- Robert K, Jones DO, Tyler PA, Van Rooij D, Huvenne VA (2015) Finding the hotspots within a biodiversity hotspot: fine-scale biological predictions within a submarine canyon using high-resolution acoustic mapping techniques. *Mar Ecol* 36(4):1256–76
- Rogers AD (1999) The biology of *Lophelia pertusa* (Linnaeus 1758) and other deep-water reef-forming corals and impacts from human activities. *Int Revue Hydrobiol* 84:315–406
- Rogers AD, Kemp KM, Davies AJ, Lisa Taylor M (2013) The Diseases of Deep-Water Corals. *Diseases of Coral*:416–41
- Roik A, Röthig T, Roder C, Müller PJ, Voolstra CR (2015) Captive rearing of the deep-sea coral *Eguchipsammia fistula* from the Red Sea demonstrates remarkable physiological plasticity. *Peer J* 3:e734

- Rüggeberg A, Dorschel B, Dullo C, Hebbeln D (2005) Sedimentary patterns in the vicinity of a carbonate mound in the Hovland Mound Province, northern Porcupine Seabight. In: Freiwald A, Roberts JM (eds) Cold-water Corals and Ecosystems, Springer Verlag:87–112
- Rüggeberg A, Dullo C, Dorschel B, Hebbeln D (2007) Environmental changes and growth history of Propeller Mound, Porcupine Seabight: Evidence from benthic foraminiferal assemblages. *Int J Earth Sci* 96:57–72
- Rüggeberg A, Fietzke J, Liebetrau V, Eisenhauer A, Dullo WC, Freiwald A (2008) Stable strontium isotopes ($\delta^{88/86}\text{Sr}$) in cold-water corals—A new proxy for reconstruction of intermediate ocean water temperatures. *Earth Plan Sci Lett* 269(3):570–5
- Rüggeberg A, Flögel S, Dullo W-C, Hissmann K, Freiwald A (2011) Water mass characteristics and sill dynamics in a subpolar cold-water coral reef setting at Stjærnsund, northern Norway. *Mar Geol* 282:5–12. doi:10.1016/j.margeo.2010.05.009
- Rüggeberg A, Spezzaferri S, Stalder C, Margreth S (2015) Cold-water coral reefs along the european continental margin: the role of foraminifera. In: Atlas of benthic foraminifera from cold-water coral reefs-Special Publication/Cushman Found Foram Res 44:3–11
- Rüggeberg A, Flögel S, Dullo WC, Raddatz J, Liebetrau V (2016) Paleoseawater density reconstruction and its implication for cold-water coral carbonate mounds in the northeast Atlantic through time. *Paleoceanog* 31(3):365–79
- Sánchez F, González-Pola C, Druet M, García-Alegre A, Acosta J, Cristobo J, Parra S, Ríos P, Altuna Á, Gómez-Ballesteros M, Muñoz-Recio A (2014) Habitat characterization of deep-water coral reefs in La Gaviera canyon (Avilés Canyon System, Cantabrian Sea). *Deep-Sea Res II* 106:118–40
- Savini A, Vertino A, Marchese F, Beuck L and Freiwald A: Mapping Cold-Water Coral Habitats at Different Scales within the Northern Ionian Sea (Central Mediterranean): An Assessment of Coral Coverage and Associated Vulnerability. *PLoS One* 9:e87108. doi:10.1371/journal.pone.0087108
- Schönfeld J, Dullo WC, Pfannkuche O, Freiwald A, Rüggeberg A, Schmidt S, Weston J (2011) Recent benthic foraminiferal assemblages from cold-water coral mounds in the Porcupine Seabight. *Facies* 57(2):187–213
- Schroeder WW (2002) Observations of *Lophelia pertusa* and the surficial geology at a deep-water site in the northeastern Gulf of Mexico. *Hydrobiol* 471:29–33
- Smeulders GG, Koho KA, De Stigter HC, Mienis F, De Haas H, Van Weering TC (2014) Cold-water coral habitats of Rockall and Porcupine Bank, NE Atlantic Ocean: Sedimentary facies and benthic foraminiferal assemblages. *Deep-Sea Res II*: 99:270–85
- Soetaert K, Mohn C, Rengstorf A, Grehan A, Van Oevelen D (2016) Ecosystem engineering creates a direct nutritional link between 600-m deep cold-water coral mounds and surface productivity. *Scientific rep* 6:35057
- Somoza L, Ercilla G, Urgorri V, León R, Medialdea T, Paredes M, Gonzalez FJ, Nombela MA (2014) Detection and mapping of cold-water coral mounds and living *Lophelia* reefs in the Galicia Bank, Atlantic NW Iberia margin. *Mar Geol* 349:73–90
- Spezzaferri S, Rüggeberg A, Stalder C, Margreth S (2013) Benthic foraminifer assemblages from norwegian cold-water coral reefs. *J Foram Res* 43(1):21–39

- Stewart HA, Davies JS, Guinan J, Howell KL (2014) The Dangeard and Explorer canyons, South Western Approaches UK: Geology, sedimentology and newly discovered cold-water coral mini-mounds. *Deep-Sea Res II* 104:230–44
- Stalder C, Spezzaferri S, Rüggeberg A, Pirkenseer C, Gennari G (2014) Late Weichselian deglaciation and early Holocene development of a cold-water coral reef along the LoppHAVet shelf (Northern Norway) recorded by benthic foraminifera and ostracoda. *Deep-Sea Res II* 99:249–69
- Stalder C, Vertino A, Rosso A, Rüggeberg A, Pirkenseer C, Spangenberg JE, Spezzaferri S, Camozzi O, Rappo S, Hajdas I (2015) Microfossils, a key to unravel cold-water carbonate mound evolution through time: evidence from the Eastern Alboran Sea. *PLoS One* 10(10):e0140223
- Stalder C, Székely-Szabolcs F, El Kateb A, Van Rooij D, Spezzaferri S (2015) *Schackoinella spina*, a new benthic foraminiferal species from cold-water coral ecosystems of the Alboran Sea and the Gulf of Cádiz. *J Foram Res* 45(4):344–53
- Taviani M, Remia A, Corselli C, Freiwald A, Malinverno E, Mastrototaro F, Savini A, Tursi A (2005) First geomarine survey of living cold-water *Lophelia pertusa* reefs in the Ionian Sea (Mediterranean basin). *Facies* 50(3):409–417
- Taviani M, Angeletti L, Canese S, Cannas R, Cardone F, Cau A, Cau AB, Follesa MC, Marchese F, Montagna P, Tessarolo C (2015) The “Sardinian cold-water coral province” in the context of the Mediterranean coral ecosystems. *Deep-Sea Res II*. doi.org/10.1016/j.dsr2.2015.12.008
- Thierens M, Titschack J, Dorschel B, Huvenne VA, Wheeler AJ, StuuT JB, O'donnell R (2010) The 2.6 Ma depositional sequence from the Challenger cold-water coral carbonate mound (IODP Exp. 307): Sediment contributors and hydrodynamic palaeo-environments. *Mar Geol Jun* 271(3):260–77
- Thierens M, Browning E, Pirlet H, Loutre MF, Dorschel B, Huvenne VA, Titschack J, Colin C, Foubert A, Wheeler AJ (2013) Cold-water coral carbonate mounds as unique palaeo-archives: the Plio-Pleistocene Challenger Mound record (NE Atlantic). *Quat Sci Rev* 73:14–30
- Thomson CW, Carpenter WB, Jeffreys JG (1873) *The depths of the sea: an account of the general results of the dredging cruises of H.M.S.S. 'Porcupine' and 'Lightning' during the summers of 1868, 1869, and 1870*. London, Macmillan & Co:527
- Titschack J, Thierens M, Dorschel B, Schulbert C, Freiwald A, Kano A, Takashima C, Kawagoe N, Li X (2009) Carbonate budget of a cold-water coral mound (Challenger Mound, IODP Exp. 307). *Mar Geol* 259:36–46
- Titschack J, Baum D, Pol-Holz D, Lopez Correa M, Forster N, Flögel S, Hebbeln D, Freiwald A (2015) Aggradation and carbonate accumulation of Holocene Norwegian cold-water coral reefs. *Sedimentology* 62(7):1873–98
- Tong R, Purser A, Unnithan V, Guinan J (2012) Multivariate statistical analysis of distribution of deep-water gorgonian corals in relation to seabed topography on the Norwegian margin. *PLoS One* 7(8):e43534
- Tong R, Purser A, Guinan J, Unnithan V (2013) Modeling the habitat suitability for deep-water gorgonian corals based on terrain variables. *Ecological informatics* 13:123–32

- Tong R, Purser A, Guinan J, Unnithan V, Yu J, Zhang C (2016) Quantifying relationships between abundances of cold-water coral *Lophelia pertusa* and terrain features: A case study on the Norwegian margin. *Cont Shelf Res* 116:13–26
- Van Den Beld I, Bourillet JF, Arnaud-Haond S, De Chambure L, Davies JS, Guillaumont B, Olu K, Menot L (2017) Cold-water coral habitats in submarine canyons of the Bay of Biscay. *Front Mar Sci* 4(118):1–30
- Van der Land C, Eisele M, Mienis F, de Haas H, Hebbeln D, Reijmer JJ, van Weering TC (2014) Carbonate mound development in contrasting settings on the Irish margin. *Deep-Sea Res II* 99:297–306
- Van Rooij D, De Mol L, Le Guilloux E, Wisshak M, Huvenne VA, Moeremans R, Henriët JP (2010) Environmental setting of deep-water oysters in the Bay of Biscay. *Deep-Sea Res I* 57(12):1561–72
- Van Rooij D, Blamart D, De Mol L, Mienis F, Pirlet H, Wehrmann LM, Barbieri R, Maignien L, Templer SP, De Haas H, Hebbeln D (2011) Cold-water coral mounds on the Pen Duick Escarpment, Gulf of Cadiz: The MICROSYSTEMS project approach. *Mar Geol* 282(1):102–17
- Wagner H, Purser A, Thomsen L, Jesus CC, Lundälv T (2011) Particulate organic matter fluxes and hydrodynamics at the Tisler cold-water coral reef. *J Mar Sys* 85(1):19–29
- Victorero L, Blamart D, Pons-Branchu E, Mavrogordato MN, Huvenne VA (2016) Reconstruction of the formation history of the Darwin Mounds, N Rockall Trough: How the dynamics of a sandy contourite affected cold-water coral growth. *Mar Geol* 378:186–95
- Waller R and Tyler P (2005) The reproductive biology of two deep-water, reef-building scleractinians from the NE Atlantic Ocean. *Coral Reefs* 24:514–522
- Wheeler AJ, Kozachenko M, Masson DG, Huvenne VA (2008) Influence of benthic sediment transport on cold-water coral bank morphology and growth: the example of the Darwin Mounds, north-east Atlantic. *Sedimentology* 55(6):1875–87
- Wheeler AJ, Kozachenko M, Henry LA, Foubert A, De Haas H, Huvenne VA, Masson DG, Olu K (2011) The Moira Mounds, small cold-water coral banks in the Porcupine Seabight, NE Atlantic: Part A—an early stage growth phase for future coral carbonate mounds? *Mar Geol* 282(1):53–64
- Wheeler AJ & Stadnitskaia A (2011) Benthic deep-sea carbonates: reefs and seeps. *Deep-Sea Sed*:397–455
- Wehrmann LM, Knab NJ, Pirlet H, Unnithan V, Wild C, Ferdelman TG (2009) Carbon mineralization and carbonate preservation in modern cold-water coral reef sediments on the Norwegian shelf. *Biogeosciences* 6(4):663–80
- White M, Bowyer P (1997) The shelf edge current northwest of Ireland. *An Geophysicae* 15:1076–1083. doi:10.1007/s00585-997-1076-0
- White M, Roberts JM, van Weering T (2007) Do bottom-intensified diurnal tidal currents shape the alignment of carbonate mounds in the NE Atlantic? *Geo-Mar Lett* 27:391–397
- Wienberg C, Beuck L, Heidkamp S, Hebbeln D, Freiwald A, Pfannkuche O, Monteys X (2008) In: Franken Mound - facies and biocoenoses on a newly-discovered 'carbonate mound' on the western Rockall Bank, NE Atlantic. *Facies* 54:1–24

- Wienberg C, Frank N, Mertens KN, Stuetz JB, Marchant M, Fietzke J, Mienis F, Hebbeln D (2010) Glacial cold-water coral growth in the Gulf of Cádiz: Implications of increased palaeo-productivity. *Earth Plan Sci Lett* 298(3):405–16
- Wienberg C, Wintersteller P, Beuck L, Hebbeln D (2013) Coral Patch seamount (NE Atlantic) - a sedimentological and megafaunal reconnaissance based on video and hydroacoustic surveys. *Biogeosciences* 10(5):3421
- Wilson JB (1979) 'Patch' development of the deep-water coral *Lophelia pertusa* (L.) on Rockall bank. *J Mar Biol Ass UK* 59:165–177
- Zibrowius H (1980) Les Scléactiniaires de la Méditerranée et de l'Atlantique nord-oriental. *Memo de l'Inst oceanogr* 11:226

The Eugen Seibold coral mounds offshore western Morocco: oceanographic and bathymetric boundary conditions of a newly discovered cold-water coral province

by Silke Glogowski, Wolf-Christian Dullo, Peter Feldens, Volker Liebetrau, Jonas von Reumont, Veit Hühnerbach, Sebastian Krastel, Russell B. Wynn and Sascha Flögel

Geo-Mar Lett 35(4):257–269 (2015)

Abstract

This study reports a new cold-water coral (CWC) province covering ~410 km² off western Morocco (ca. 31°N) ~40 nautical miles north of the Agadir Canyon system between 678 and 863 m water depth, here named the Eugen Seibold coral mounds. Individual mounds are up to 12 m high with slope angles varying between 3° and 12°. Hydroacoustic data revealed mound axes lengths of 80 to 240 m. Slope angle, mound height, and density of mounds decrease with increasing water depth. The deepest mounds are composed of dead and fragmented *Lophelia pertusa* branches. Living CWCs, mainly *L. pertusa*, were sampled with box cores between 678 and 719 m water depth. Conductivity-temperature-depth (CTD) measurements revealed living CWC colonies to occur within the deeper part of the North Atlantic Central Water (NACW; conservative temperature Θ of 9.78°–9.94°C, absolute salinity SA of ca. 35.632 g/kg, and seawater density σ_{Θ} of 27.31–27.33 kg/m³). Comparable CWC reefs off Mauritania (17°N–18°N) and on the Renard Ridge (35°N) in the Gulf of Cadiz, the latter consisting only of a dead CWC fabric, are also located in the deeper layer of the NACW slightly above the Mediterranean Outflow Water. The new CWC province, with its thin cover of living corals and much larger accumulations of dead thickets and fragmented coral rubble, was successfully discovered by CTD reconnaissance applying seawater density as a potential indicator of CWC occurrences, followed by hydroacoustic mapping. U-Th isotope systematics for macroscopically altered buried *Lophelia* material (25 cm sediment depth) yielded absolute ages dating back to the late Holocene at least.

2.1 Introduction

Cold-water coral (CWC) reefs are widespread along the continental margins of global ocean basins (Roberts et al. 2006). Since the discovery of spectacular CWC mounds in the Porcupine Seabight (Henriet et al. 1998), many more reef sites have been identified worldwide, predominantly in the North Atlantic. Indeed, the presence of *Lophelia pertusa* as a main frame-builder of CWC reefs is today known from, for example, the Norwegian margin (e.g. Freiwald 2002; Fosså et al. 2002; Hovland et al. 2012), the Porcupine, Rockall and Hatton banks (e.g. White et al. 2007; Sayago-Gil et al. 2010; Mazzini et al. 2012), the Celtic margin (e.g. Wheeler et al. 2007), the Armorican margin (e.g. Reveillaud et al. 2008), the Cantabrian Sea (e.g. Sánchez et al. 2014), the Iberian margin (e.g. Hernández-Molina et al. 2011; Somoza et al. 2014), the Mediterranean Sea (e.g. Freiwald et al. 2009; Palomino et al. 2011; Taviani et al. 2011; Fink et al. 2012; Gori et al. 2013; Savini et al. 2014), the Gulf of Cadiz (GoC; e.g. Van Rensbergen et al. 2005; Van Rooij et al. 2011; León et al. 2012), off northern Morocco (southern GoC; e.g. Foubert et al. 2008), off Mauritania (e.g. Eisele et al. 2011, 2014), the Angola margin (e.g. Le Guilloux et al. 2009), the Gulf of Mexico (e.g. Brooke and Schroeder 2007; Hübscher et al. 2010; Hebbeln et al. 2014), and around the Bahamas (e.g. Reed et al. 2006; Correa et al. 2012a, b). Many of these studies explored the impact of various hydrographic factors and nutrient availability (e.g. Hovland et al. 2012) on CWC reef growth. In addition, Martorelli et al. (2011) demonstrated the positive influence of topography-enhanced bottom current velocity on coral occurrences. Temperature and salinity are other key factors constraining the distribution of live corals (e.g. Davies et al. 2009; Davies and Guinotte 2011; Vierod et al. 2014), and indirectly ambient seawater density (e.g. Dullo et al. 2008; Flögel et al. 2014).

A new CWC province was discovered off western Morocco during research cruise 32 of *R/V Maria S. Merian* in October 2013, which mainly targeted the morphology, sedimentary processes and geohazards of giant landslides of the Agadir Canyon system (Krstel et al. 2013). This study explores the recent oceanographic and bathymetric boundary conditions of these CWCs, based on a combination of seafloor bathymetric and acoustic data as well as conductivity-temperature-depth (CTD) data collected from the overlying water masses. One of the cruise aims was to test whether seawater density can be used as a predictive tool to detect living CWC occurrences. The new province is here named the Eugen Seibold coral mounds in honour of the pioneering marine geologist Eugen Seibold (1918–2013).

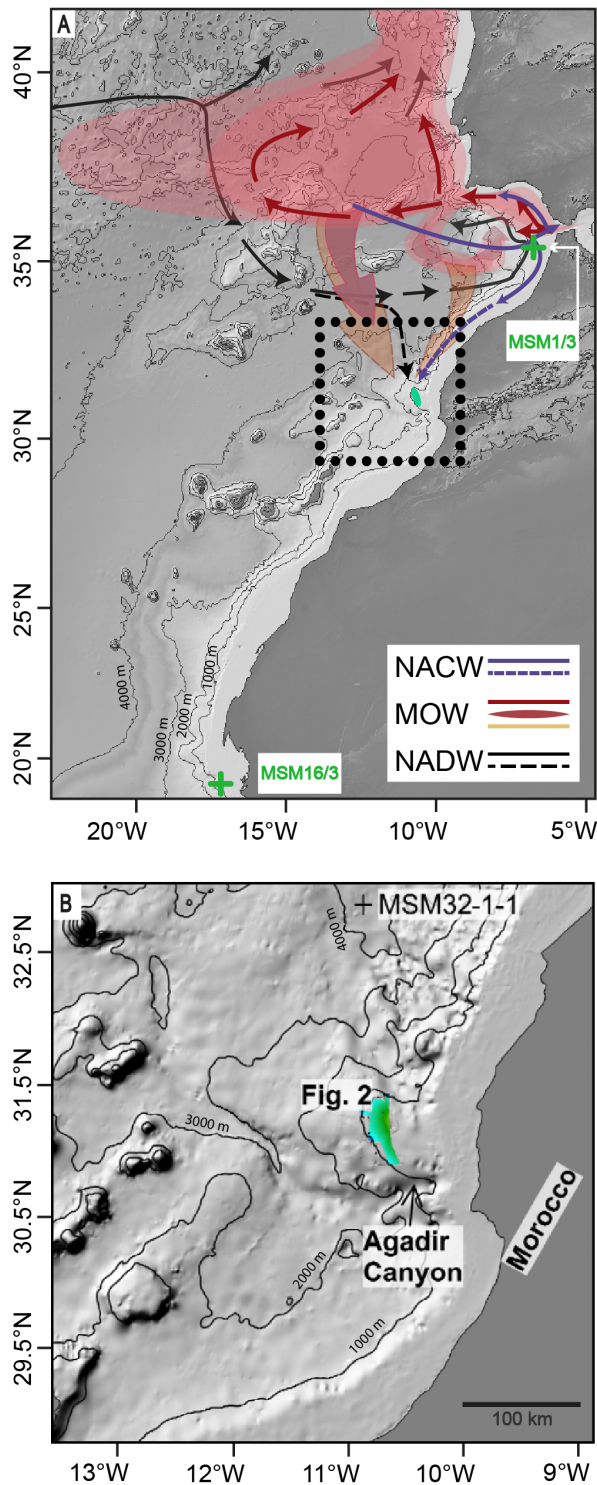


Fig. 2.1 *Top Map* showing the locations of the study area off western Morocco (*black box; green dot* mound field), and the CTD stations (*stars*) of earlier cruises off Mauritania (MSM16/3) and in the Gulf of Cadiz (MSM1/3; cf. Table 1), with depth contours and water masses. North Atlantic Central Water: *solid blue arrows* after Vandorpe et al. (2014); *dotted blue arrow* its continuation, present study. Mediterranean Outflow Water: *red area and arrows* after Hernández-Molina et al. (2011), including preferred meddy pathways; *orange arrows* its continuation, CTD data of present study. North Atlantic Deep Water: *solid dark grey arrows* after Hernández-Molina et al. (2011); *dark grey dotted arrow* its continuation, present study. *Bottom Green* Multibeam bathymetry coverage. Note the location of CTD station MSM32-1-1 (cf. Fig. 3, Table 1)

2.1.1 Physical Settings

This study focuses on the Atlantic Moroccan continental slope off northwest Africa at 32°54'–31°08'N and 10°34'–10°49'W (Fig. 2.1). Three investigated sites exhibit the following water masses from the surface to the seafloor. The Central Water (CW) masses comprise Subtropical Underwater (SUW), South Atlantic Central Water (SACW) and North Atlantic Central Water (NACW; Mittelstaedt 1991; Van Camp et al. 1991; Morigi et al. 2001; Vandorpe et al. 2014). According to Mittelstaedt (1991) and Arístegui et al. (2009), SACW and predominantly NACW upwell seasonally. The presence of Mediterranean Outflow Water (MOW) below the NACW is associated with a pronounced increase in salinity favouring the formation of a pycnocline—for example, in the GoC (Fusco et al. 2008). Alves et al. (2011) described the MOW off Morocco at 34°N, while Pelegrí et al. (2005) reported this water mass extending as far south as 30.5°N. In the present study area, the deepest part of the water column is formed by the North Atlantic Deep Water (NADW). Unpublished analogue TOPAS (TOpographic PArametric Sonar) sub-bottom profiles kindly supplied by G. Ercilla of the Institute of Marine Sciences (CSIC), Barcelona had revealed the presence of acoustically transparent mounds at more than 750 m water depth ~40 nautical miles north of the upper Agadir Canyon (Fig. 2.1), one of the largest submarine canyons worldwide (Wynn et al. 2002) and characterised by tectonic morphologies and giant landslides (Talling et al. 2007; Frenz et al. 2009). Examination of those preliminary data showed that the dimensions and acoustic character of the features were similar to those of known carbonate mounds in the northeast Atlantic (DeMol et al. 2002; Rüggeberg et al. 2011). Subsequent cruises gathered hydrographic data including seawater density, reported to be a predictive tool for coral occurrence in other regions (Foubert et al. 2008; Somoza et al. 2014). Prospective sites were mapped by swath bathymetry and side scan sonar in order to, amongst others, define targets for box coring. Indeed, these confirmed the suspected presence of mostly dead and some living corals in an extensive province of >400 km² (Fig. 2.2).

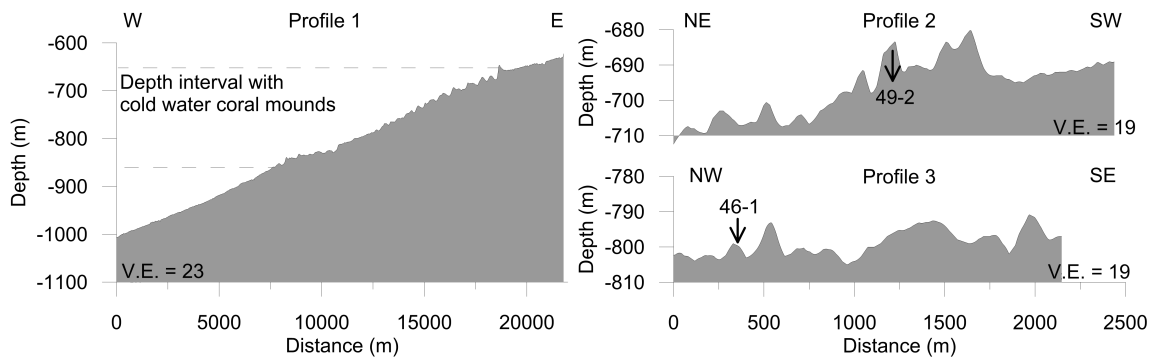
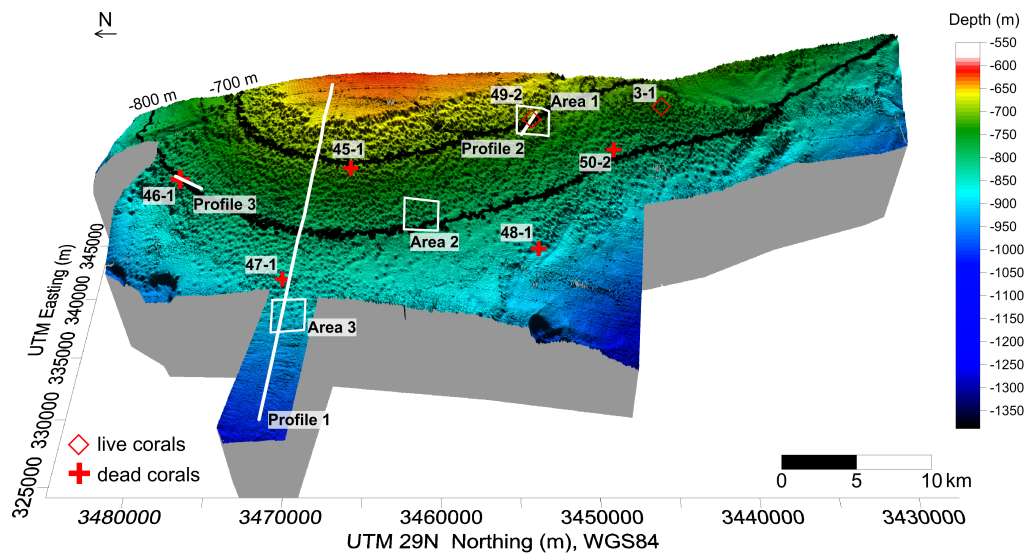


Fig. 2.2 *Top* 3D perspective view of multibeam bathymetry (lateral pixel resolution 30 m) across the Eugen Seibold coral mounds, and locations of the seven box corer stations (cf. Table 2) with live or dead corals, as well as three areas selected for estimation of coral mound density (cf. Fig. 4). With the exception of CTD station MSM32-1-1, situated further north beyond the currently known boundaries of the coral mound site (cf. Fig. 1), the locations of the other ten CTD stations were essentially identical or very close to those of the box corer stations (cf. Table 1). *Bottom* Bathymetric profile 1 crosses the site from its shallowest to its deepest part, profile 2 incorporates a coral mound with living CWCs, and profile 3 a coral mound with dead corals (box corer stations MSM32-49-2 and 46-1 respectively). *V.E.* Vertical exaggeration

2.2 Material and Methods

2.2.1 Hydrography

Water masses above the coral mounds were investigated by performing 11 CTD casts (Supplementary Material=SM Table 2.1) using a Seabird 'SBE 911 plus' underwater unit additionally equipped with two oxygen sensors and a turbidity sensor (including SBE data processing). CTD data were visualized using Ocean Data View (ODV) software, version 4.5.3 (Schlitzer 2013). Temperatures and salinities are reported as conservative temperature (Θ , °C) and absolute salinity (SA, g/kg; TEOS-10, McDougall and Barker 2011). T–S plots of temperature vs. salinity are commonly used to delineate water masses and their geographical distribution as well as dynamics (Tomczak 1999).

2.2.2 Hydroacoustic data

Water masses above the coral mounds were investigated by performing 11 CTD casts (SM Table 2.1) using a Seabird 'SBE 911 plus' underwater unit additionally equipped with two oxygen sensors and a turbidity sensor (including SBE data processing). CTD data were visualized using Ocean Data View (ODV) software, version 4.5.3 (Schlitzer 2013). Temperatures and salinities are reported as conservative temperature (Θ , °C) and absolute salinity (SA, g/kg; TEOS-10, McDougall and Barker 2011). T–S plots of temperature vs. salinity are commonly used to delineate water masses and their geographical distribution as well as dynamics (Tomczak 1999). Hydroacoustic data Multibeam bathymetric data were collected by means of the shipboard Kongsberg Simrad EM122 multibeam echo sound system (MBES) operating with a nominal frequency of 12 kHz. Data were processed by QPS Fledermaus and MBE-system software (Caress and Chayes 1995), including application of local sound velocity profiles, the creation of a CUBE surface (Calder and Mayer 2003) with a pixel resolution of 30 m, and manual removal of spikes. Coral mound heights and extensions were evaluated from these data for each of three sites within the mound field (Fig. 2.2). Mound heights were measured along N–S oriented depth profiles run parallel to the slope, in each case crossing the highest elevation down to the first break in slope. It should be noted that these values represent conservative approximations. A TOBI (Towed Ocean Bottom Instrument) system, comprising a 30 kHz side scan sonar (Flewellen et al. 1993) and 7 kHz sub-bottom profiler, served to collect a ~13 km long side scan sonar line across the south-eastern sector of the coral province.

Side scan sonar data were corrected for radiometric and geometric artefacts (Blondel 2009), and processed to a pixel size of ~3 m. The system was towed ~500 m above seafloor, producing a swath width of ~6 km (Murton et al. 1992).

3.2.3 Box cores

Based on hydroacoustic mapping, sites were selected for box coring (50x50 cm) to enable ground-truthing of seafloor sediments and potential CWC coverage. Seven box cores were taken (SM Table 2.2) distributed over the entire study area (Fig. 2.2).

3.2.4 Geochronology

Box core MSM32-3-1 was selected for a comparison of U-Th absolute ages of exposed surface branches of a living *Lophelia* reef structure with those of buried branch fragments from the underlying sediment.

Measurements were conducted on a multi-collector inductively coupled plasma mass spectrometer (MC-ICP-MS, VG-Axiom), following Fietzke et al. (2005). The required mineralogical pre-investigation was based on Xray diffractometry (XRD, Philips PW-1820). All analyses were performed using GEOMAR facilities.

Sample preparation, laboratory treatment and age determination followed Liebetrau et al. (2010). All uncertainties represent the 2 SE level, and the age data are rounded off to decades. Whole procedure blanks matched typical values of ca. 10 pg for U, 2 pg for ^{232}Th and 0.1 fg for ^{230}Th .

2.3 Results

2.3.1 Hydrography

In October 2013, assessments of regional oceanographic conditions characterising the deep-water MSM32-1-1 site to the north of the study area (4,224 m water depth; Figs. 2.1 and 2.3, SM Table 2.1) revealed an upper surface layer of ~30 m with a mean conservative temperature (Θ) of 23.06 °C, absolute salinity (SA) of 36.917 g/kg, and oxygen concentration of 4.53 ml/l. Below, the Central Water (CW) masses comprised Subtropical Under Water (SUW), South Atlantic Central Water (SACW) and North Atlantic Central Water (NACW). The SUW (31–64 m water depth) had Θ between 23.03°C and 17.73°C, SA of 36.914 to 36.526 g/kg, $\sigma\Theta$ of 25.23 to 26.38 kg/m³, and oxygen values of 4.51 to 5.09 ml/l.

The SACW (65–94 m) had Θ of 17.69°C to 16.52°C, SA of 36.535 to 36.483 g/kg, $\sigma\Theta$ of 26.38 to 26.66 kg/m³, and oxygen values of 4.67 to 5.10 ml/l. The top of the NACW (99–860 m) can be delimited by a strong decrease in Θ (from 16.71°C to 10.75°C) and in SA (from 36.512 to 36.072 g/kg). $\sigma\Theta$ varies between 26.60 and 27.52 kg/m³ and oxygen values between 4.56 and 3.65 ml/l. The deeper part of the NACW can be constrained by a minimum SA range of 35.769 to 35.530 g/kg between 774 and 904 m water depth. Below the NACW, the Mediterranean Outflow Water (MOW, 863–1,252 m) can be identified in terms of small Θ variations in the range 10.77–9.71 °C, and elevated SA of 36.088–36.200 g/kg. $\sigma\Theta$ ranges from 27.53 to 27.80 kg/m³, and oxygen values from 3.69 to 3.89 ml/l. Below the MOW at depths of 1,250–4,224 m, the North Atlantic Deep Water (NADW) had Θ =1.65°C, SA=35.065 g/kg, $\sigma\Theta$ =27.88 kg/m³ and [O₂]=4.60 ml/l (Fig. 2.3). In the vicinity of two living CWC sites discovered during the cruise—MSM32-3-2 and MSM32-51-2 at 704 and 678 m water depth respectively (see below)—local bottom water masses comprise the deeper part of the NACW. The deeper site at 704 m had Θ =9.78°C, SA=35.632 g/kg, oxygen=3.14 ml/l, whereas the shallow site at 678 m had Θ =9.94°C, SA=35.632 g/kg, oxygen=3.15 ml/l (SM Table 2.1). Conservative temperature and absolute salinity are lower than those of the deep MSM32-1-1 station in 700 m water depth, exhibiting Θ =10.79°C, SA=35.807 g/kg (Fig. 2.3).

2.3.2 Hydroacoustic data

Seafloor bathymetric data (Fig. 2.2) reveal that the mapped mound field extends up to 40 km alongslope (north to south) and up to 13 km downslope (east to west), covering an area of ~410 km². Cold-water coral mounds occur between 678 and 863 m water depth, immediately downslope of a relatively flat 'plateau' on the upper continental slope (Fig. 2.2). Individual mounds have circular to elliptical shapes in planform, and reach maximum heights of up to 12 m in the shallower part of the mound field. However, heights between 4 and 8 m are dominant (Fig. 2.2). Lengths of mound axes vary between 80 and 240 m, the longer axis being E–W aligned parallel to the direction of slope inclination. Maximum slope angle (12°) and maximum height (12 m) of individual mounds tend to decrease with increasing water depth (Fig. 2.4), as does the density of mounds.

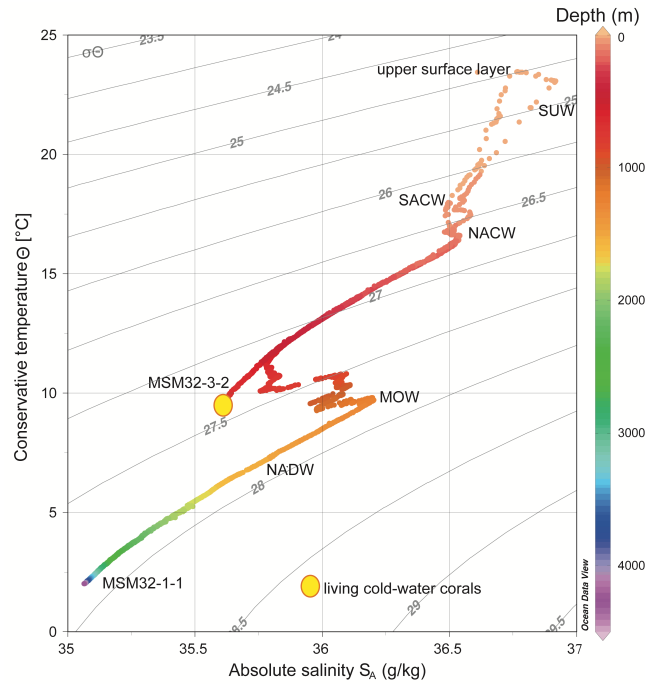


Fig. 2.3 T–S plot (Θ cons. temperature, S_A absolute salinity) for CTD stations MSM32-1-1 (see Fig. 1 for location) and MSM32-3-2 (location as for box corer station MSM32-3-1 in Fig. 2). Water masses comprise (from shallowest to deepest) an upper surface layer, Subtropical Under Water (SUW), South Atlantic Central Water (SACW), North Atlantic Central Water (NACW), Mediterranean Outflow Water (MOW), and North Atlantic Deep Water (NADW). Living CWCs, especially *Lophelia pertusa*, occur in the deeper part of the NACW roughly 150 m above the MOW characterised by still relatively elevated salinities and limited variation in temperature. Isopycnals are calculated with the reference pressure at 0 m (σ_Θ), i.e. sea level

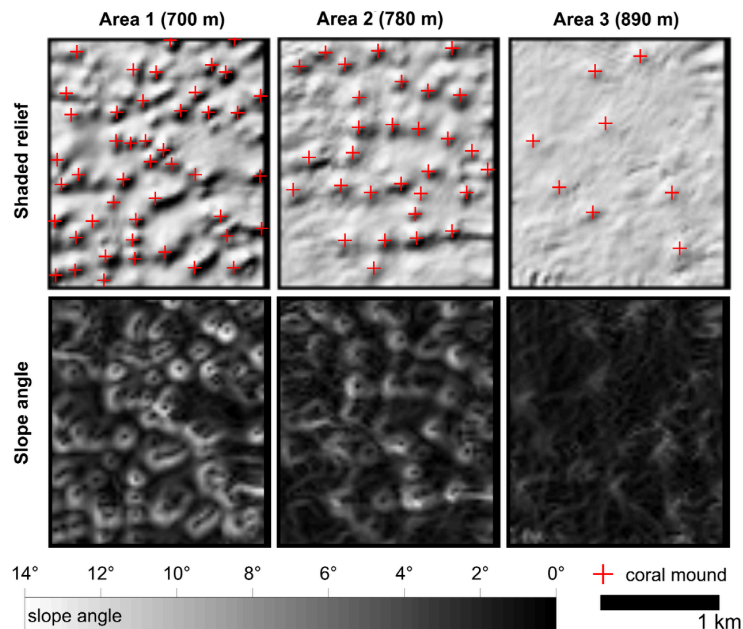


Fig. 2.4 Shaded relief (*top row*) and slope map (*bottom row*) across selected coral mound areas at three different water depths based on multibeam bathymetry data. Abundance, elevation and slope of coral mounds decrease as water depths increase from area 1 to area 3 (700, 780 and 890 m respectively). See Fig. 2 for locations of selected areas

Densities of mounds with slope inclinations larger than approx. 3° were assessed in three areas, each 4 km² in size (Fig. 2.2). Mound density varied from 12 mounds/km² (area 1) at ~700 m water depth, to 8 mounds/km² (area 2) at ~790 m water depth, and 2 mounds/km² (area 3) at ~880 m water depth (Figs. 2.4, Supplementary Material=SM Fig. 2.5). The individual mound-like structures appear as areas of higher backscatter (bright) in TOBI side scan sonar data compared to the lower backscatter of the surrounding seafloor (SM Fig. 2.6). Acoustic shadows (black) are commonly observed on the flanks of the steeper mounds. Shallower settings with more elevated mounds (~700 m water depth) display higher backscatter intensities compared to deeper settings (>750 m) with less elevated mounds (SM Fig. 2.6).

2.3.3 Box cores

All seven box cores (see Fig. 2.2 and SM Table 2.2) contained fragments of dead CWCs. The three box cores from the deeper sites (MSM32-46-1, 801 m; MSM32-47-1, 835 m; MSM32-48-1, 863 m) recovered 18–40 cm of a sandy to silty, light and pale brown mud containing dead *Lophelia pertusa* bioclasts of up to 2 cm. Most of the *Lophelia* branches are fragmented down to the size of one polyp. Two shallower box cores (MSM32-45-1, 701 m; MSM32-50-2, 788 m) sampled abundant dead *Lophelia* thickets up to 8 cm long. These are commonly accompanied by bivalve shells embedded in sandy to silty brown mud, with a maximum recovery of 15 cm. The abundance of bioclasts was more than twice as high in box core MSM32-50-2 and well exposed at the surface, in contrast to all other cores with dead CWC material. Box cores MSM32-49-2 (678 m) and MSM32-3-1 (719 m) contained large specimens of mainly dead but also a few living *Lophelia*. In box core MSM32-3-1, living branches of *Lophelia* exhibited up to 15 consecutive living polyps. Moreover, this box core had a single, live *Madrepora oculata* and *Desmophyllum* sp. specimen (Fig. 2.7). The coral framework stood well above the sediment between 10 and 20 cm. Further downcore, coral fragments and bioclasts associated with brown silty to sandy mud were recorded to at least 25 cm (maximum recovery). These shallower core sites are located within area 1 where highest elevations of coral mounds occur (see above). The box core sites deeper than 800 m are located within area 3 where the mounds are less elevated and less abundant (SM Table 2.2, Figs. 2.2, 2.4, SM Fig. 2.5).



Fig. 2.7 Photograph showing the contents of the box core recovered from station MSM32-3-1. The large colony of *Lophelia pertusa* (1) exhibits up to 15 consecutive living polyps in one branch. *Madrepora oculata* (2) settled on dead branches of *L. pertusa*, which evidently collapsed prior to settlement as indicated by the different orientation of the polyps of both corals. This is the only living *M. oculata* recovered during the cruise. *Desmophyllum* sp. (3) settled also on dead *L. pertusa* branches. In this box core, the numerous dead corals partly buried in the muddy, bioclast-rich sediment comprise only *L. pertusa*. Among the coral debris, a few bivalves occur. See Fig. 2 for location of box core station

These cores recovered only dead CWCs, except for box core MSM32-50-2 (788 m; see above) which also contained a single living polyp of *L. pertusa*, unlike box core MSM32-3-1 (719 m) earmarked by more profuse live corals. In all box cores *L. pertusa* is by far the dominant CWC species.

2.3.4 Geochronology

U-Th isotope systematics (SM Table 2.3) were determined for the youngest parts of growing (live) *Lophelia* branches recovered above the sediment surface, and for macroscopically altered material buried at 25 cm sediment depth (max. penetration depth of box core MSM32-3-1, 719 m water depth). All analysed samples had aragonite contents exceeding 98%.

Based on Liebetrau et al. (2010), and in addition to the common detrital Th correction, the data were normalised in terms of a potentially site-specific initial $^{230}\text{Th}/^{234}\text{U}$ activity ratio of 0.0005 ± 0.0002 , here deduced from three live juvenile branch tops. These integrate only the youngest 2 to 4 mm of sub-recent skeletal growth and are therefore assumed to provide zero age reference values. Their $\delta^{234}\text{U}$ signature of $149 \pm 2.5\text{‰}$ is in good agreement with the modern seawater reference of $146.8\pm 0.4\text{‰}$ (2 SE) proposed by Andersen et al. (2010). The growth systematics of this reef structure spanning approx. 40 cm (Fig. 2.7) enabled the identification of a root-like segment at its base with a maximum age of 60 ± 20 years before present (BP) and a modern seawater matching initial $\delta^{234}\text{U}$ value of $147.3\pm 2.1\text{‰}$. Uth data on two branch fragments from 25 cm sediment depth revealed ages of $1,810\pm 30$ years BP (initial $\delta^{234}\text{U}$ of $144.2\pm 2.2\text{‰}$) and $2,680\pm 30$ years BP (initial $\delta^{234}\text{U}$ of $141.9\pm 2.4\text{‰}$). Inherently, the different degree of morphologically visible alteration implies the former as more reliable than the latter. This is supported by the fact that only the former fragment displays a within error modern seawater matching initial $\delta^{234}\text{U}$ value.

2.4 Discussion

Hydrographic measurements above the Eugen Seibold CWC mounds (between 65 and 863 m water depth) revealed that the oceanic water column is controlled mainly by the interaction of SACW and NACW with underlying MOW, which enters the Atlantic Ocean via the Strait of Gibraltar (Figs. 2.1, 2.3). The subsurface SACW flows northwards and typically displays lower salinity, oxygen depletion and nutrient enrichment (Aristegui et al. 2009) relative to the deeper southwardflowing NACW (Mittelstaedt 1991; Pastor et al. 2008; Vandorpe et al. 2014).

The MOW is characterised by a very small temperature gradient, but shows a marked increase in salinity and density between 863 and 904 m water depth (Fig. 2.3). These water mass signatures are similar to those documented by Mittelstaedt (1991) and Pelegrí et al. (2005) off northwest Africa ($25\text{--}35^\circ\text{N}$, and Cape Ghir at $30\text{--}36^\circ\text{N}$). According to Dullo et al. (2008) and Flögel et al. (2014), most of the pristine and profuse live CWC coral reefs along the European continental margin occur at water mass densities of $\sigma_\theta=27.35\text{--}27.65\text{ kg/m}^3$. Living CWCs of the Eugen Seibold province at water depths between 678 and 719 m with density values of about $\sigma_\theta=27.33\text{ kg/m}^3$ correspond to the deeper part of the NACW.

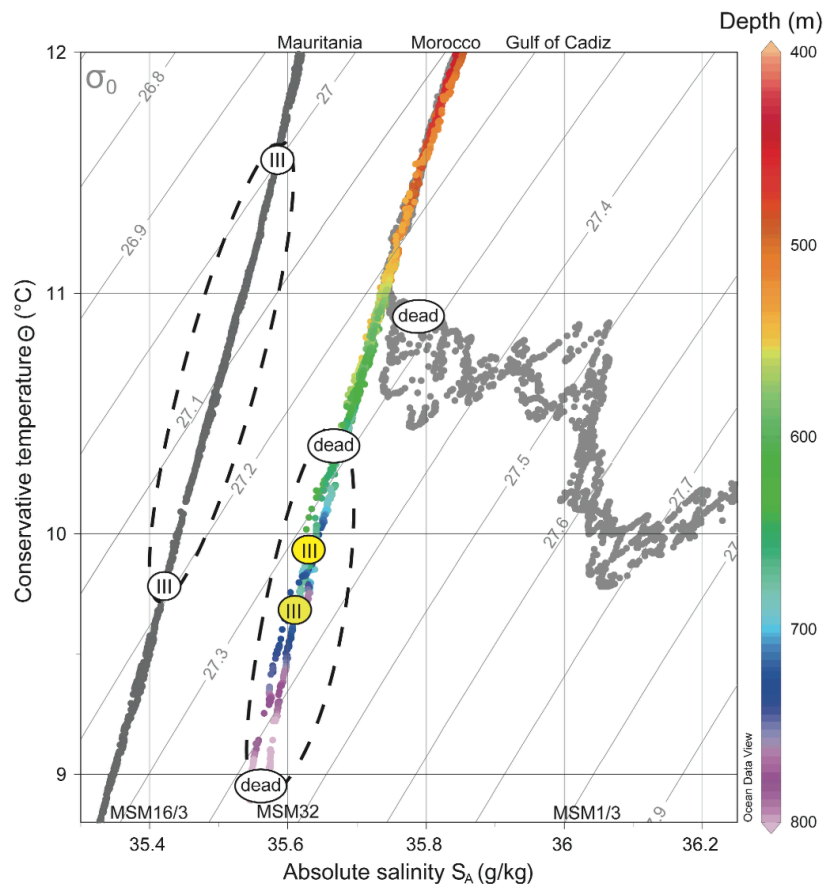


Fig. 2.8 Detailed T–S plot (cf. Fig. 3) of water masses bathing living and dead CWCs of the Eugen Seibold coral mounds north of Agadir Canyon (cruise MSM32 of the present study, *colour*), compared with dead CWC sites in the Gulf of Cadiz (cruise MSM1/3, *light grey*) and living CWC sites off Mauritania (cruise MSM16/3, *dark grey*). *Dashed ellipses* Temperature–salinity occurrence range of dead CWCs; *yellow, white circles* living CWCs, all category III of Flögel et al. (2014). Isopycnals are calculated with the reference pressure at 0 m (σ_Θ), i.e. sea level

Their occurrence is therefore just above the defined density window of Dullo et al. (2008), and ~150 m above the upper limits of the MOW (Figs. 2.3, 2.8) identified at ~863 m water depth.

Flögel et al. (2014) differentiated between three types of living CWC assemblages. Category I is characterised by dense horizontal and, most importantly, vertical reef growth, category II by patchy growth with colonies of some square meters, and category III by smaller and commonly more widely scattered isolated colonies. Living CWCs in the present study area are attributed to category III. This category is further supported by lower oxygen values of 3.14–3.15 ml/l at the study sites, contrasting with a global mean

of ~6 ml/l for ambient water masses around flourishing CWC reefs (Davies et al. 2008). The classification of three categories in combination with seawater density works well in the Atlantic, but can not be applied to the Mediterranean due to its higher density and higher alkalinity (cf. Flögel et al. 2014).

Although the information available to date from box cores represents only snapshots of the coral mounds, the general distinction between living mounds clustering around 700 m water depth and dead mounds in deeper waters (Figs. 2.2, 2.3, 2.8) is supported by the acoustic data (Fig. 2.4). Contrasting with presumably dead mounds, areas inhabited by living CWCs generally have more elevated (up to 12 m) and more steeply (up to 12°) inclined mounds (Figs. 2.4, SM Fig. 2.5) associated with higher backscatter intensities (SM Fig. 2.6). One might argue that high mounds may result from the higher baffling capacity of CWC fabrics. Less elevated mounds with lower slope inclinations may be a sign of partial burial of dead CWCs, which may explain the reduced occurrence of mounds in such areas. Another mechanism could be that the bathymetrically deeper mounds are already affected by erosion, but this awaits confirmation by additional optical ground-truthing and dating.

A similar situation has been described for CWC mounds off Mauritania—e.g. the Banda Mounds at 17–18°N, which were actively growing from 65 to 57 ka, 45 to 32 ka, and at about 14 ka (Eisele et al. 2011). The Banda Mounds are bathymetrically above the density envelope of Dullo et al. (2008; $\sigma_{\Theta}=27.5\pm 0.15 \text{ kg/m}^3$), and are also situated within the lower part of the NACW (*RV Maria S. Merian* cruise MSM16/3 in October 2010, Westphal et al. 2012; see Fig. 2.8). Today, these mounds show only a very thin cover of living *Lophelia* between 415 and 570 m water depth, corresponding to category III of Flögel et al. (2014).

The Renard Ridge (35°N) in the Gulf of Cadiz (GoC) is another prominent region of CWC mound occurrence; however, there are no living CWC colonies reported so far (e.g. Foubert et al. 2008; Wienberg et al. 2009, 2010). These dead CWCs are today found at relatively shallow water depths typified by densities not exceeding $\sigma_{\Theta}=27.5\pm 0.15 \text{ kg/m}^3$ (*RV Maria S. Merian* cruise MSM1/3 of January 2006, Pfannkuche and cruise participants 2006; see Fig. 2.8). There is evidence that, over the last 400 ka, these reefs also flourished during glacial times and up to the very early Holocene (Wienberg et al. 2010). Although Davies and Guinotte (2011) predict a high suitability for CWC growth, especially of *Lophelia pertusa*, between the GoC and Mauritania, to date living CWCs have been found only off Mauritania (17–18°N) and now off western Morocco (31°N) as small isolated colonies or forming a thin and patchy cover. Vigorous and extensive CWC reef

growth apparently occurred only during glacial times in this region, which would explain why the few modern living colonies reported to date do not match bathymetrically with the water mass density values known for CWC reefs belonging to category I of Flögel et al. (2014). The Eugen Seibold coral mounds exhibit a few living colonies (albeit based on limited sampling), and most sampled mound structures consist of a dead fabric.

Dating of a large living coral branch indicated a time span of 60 ± 20 years BP from the base to its living topmost part. The large uncertainty of ± 20 years mainly results from the correction for the initial $^{230}\text{Th}/^{234}\text{U}$ activity ratio. This implies a mean growth rate of 0.5 to 1 cm/year. An alternative age estimate is provided by counting the number of polyps in straight succession from the root segment to the juvenile top, which on average could correspond to the number of years according to Freiwald (2002). Resulting in 30 ± 5 polyps (varying with the sub-branch to follow), this approach suggests a slightly younger age. Based on CaCO_3 accumulation rates of $8.70 \pm 3.18 \times 10^{-3}\%$ per day (Form and Riebesell 2012), the maximum mass of 465 g of the dated branch implies a similar value of $9 \pm 2 \times 10^{-3}\%$ per day in terms of polyp counting age, and $5 \pm 2 \times 10^{-3}\%$ per day in terms of U-Th age. Deducing in first approximation a local sediment accumulation rate from the most reliable age of the dead fragments ($1,810 \pm 30$ years BP) and the observed burial depth results in 14 cm/1,000 years. This is consistent with the background flux of 12.15 ± 0.6 cm/1,000 years for the nearby Canary Basin reported by Hendericks et al. (2002).

In their overview of north-eastern Atlantic CWC reefs and climate change, Frank et al. (2011) argue that CWC reefs were growing south of 50°N predominantly during the last glacial periods and the deglacial on the Armorican margin (Reveillaud et al. 2008), the Iberian margin (Hernández-Molina et al. 2011), in the GoC (Wienberg et al. 2009, 2010) and the Banda Mounds (Eisele et al. 2011, 2014), including the Mediterranean (Savini et al. 2014), with the exception of sites in the Alboran Sea still growing until 5 ka (Fink et al. 2012). This would be in contrast with the CWC reef formation north of 50° being constrained to interglacials, including the late Holocene (e.g. Rüggeberg et al. 2007; Frank et al. 2009; Raddatz et al. 2013). The predominantly dead CWC assemblages of the newly discovered Eugen Seibold coral mounds off western Morocco may support the hypothesis of Frank et al. (2011). However, the initial dataset displays CWC growth since about 2 ka at least.

Therefore, interglacial growth periods cannot be excluded in general south of 50°N, as demonstrated also by the discovery of live juvenile corals in the present case. Providing a more comprehensive record of emplacement time intervals for the Eugen Seibold coral mounds requires more detailed archives, notably a drill core through at least one of the major mound structures well identified in this study.

2.5 Conclusions

The newly discovered Eugen Seibold coral mounds off western Morocco extend over more than 410 km², associated with known oceanographic settings of CWC occurrences along the north-eastern Atlantic margin. Mounds with living CWCs occur in a bathymetric range between 678 and 719 m characterised by *Lophelia pertusa*, at one site accompanied by a single *Madrepora oculata* excrescent and a single *Desmophyllum* sp. specimen. Most CWCs are represented by dead thickets which are more fragmented in the mounds at deeper water depths (>710 to 860 m). Shallower mounds are more elevated (12 m) and exhibit higher backscatter in contrast to mounds at deeper sites. Absolute ages of dead coral fragments indicate growth since the late Holocene at least, and imply a sediment accumulation rate of about 14 cm/1,000 years. These initial geochronological results and the patchy distribution of the cold-water corals suggest re-colonization of this area by *Lophelia*, rather than the continuous evolution of large flourishing reef build-ups. This interpretation for the Eugen Seibold coral mounds awaits confirmation based on additional evidence from optical ground-truthing and dating of longer downcore records.

Acknowledgments

We acknowledge the superb support by the captain and crew as well as the scientific shipboard party during cruise 32 aboard the *RV Maria S. Merian*, and the German Science Foundation (DFG) for funding ship time and providing financial support (Du 129/48-1). R.B.W. and the NOC TOBI team were supported by NERC grant NE/J012955/1.

We are grateful to Dr. Gemma Ercilla of CSIC, Barcelona for providing analogue TOPAS profiles which enabled us to target the coral mound province. In addition, thanks go to Dr. Steffen Hetzinger for providing data collected during cruise MSM16/3, Anke Bleyer and Bettina Domeyer for their helping hand in preparing the cruise, Jutta Heinze for XRD analyses, Ana Kolevica for clean-lab support (all from GEOMAR), Dr. Jan Fietzke for high

performance level of the Axiom MC-ICP-MS facility, Prof. A. Eisenhauer for unrestricted scientific and infrastructural support, and Prof. Peter Brandt for valuable discussions on water mass structures. Detailed comments provided by two anonymous reviewers, Prof. A. Foubert (Fribourg) and the editors proved useful in improving the paper.

References

- Alves JMR, Carton X, Ambar I (2011) Hydrological structure, circulation and water mass transport in the Gulf of Cadiz. *Int J Geosci* 2:432–456
- Andersen MB, Stirling CH, Zimmermann B, Halliday AN (2010) Precise determination of the open ocean $^{234}\text{U}/^{238}\text{U}$ composition. *Geochem Geophys Geosyst* 11(12):Q12003. doi:10.1029/2010GC003318
- Arístegui J, Barton ED, Álvarez-Salgado XA, Santos AMP, Figueiras FG, Kifani S, Hernández-León S, Mason E, Machú E, Demarcq H (2009) Sub-regional ecosystem variability in the Canary Current upwelling. *Prog Oceanog* 83:33–48
- Blondel PC (2009) *The Handbook of Sidescan Sonar. Computer-assisted interpretation*, Springer, Berlin:249–276
- Brooke S, Schroeder WW (2007) State of deep coral ecosystems in the Gulf of Mexico region. In: Lumsden E, Hourigan TF, Bruckner AW, Dorr G (eds) *The state of deep coral ecosystems of the U.S. NOAA Technical Memorandum CRCP-3*, Silver Spring, MD:233–270
- Calder BR, Mayer LA (2003) Automatic processing of high-rate, high-density multibeam echosounder data. *Geochem Geophys Geosyst* 4(6):1048. doi:10.1029/2002GC000486
- Caress DW, Chayes DN (1995) New software for processing sidescan data from sidescan-capable multibeam sonars. In: *Proc IEEE Oceans 95 Conf*:997–1000
- Correa TBS, Eberli GP, Grasmueck M, Reed JK, Correa AMS (2012a) Genesis and morphology of cold-water coral ridges in a unidirectional current regime. *Mar Geol* 326-328:14–27
- Correa TBS, Grasmueck M, Eberli GP, Reed JK, Verwer K, Purkis S (2012b) Variability of cold-water coral mounds in a high sediment input and tidal current regime, Straits of Florida. *Sedimentology* 59(4):1278–1304
- Davies AJ, Wisshak M, Orr JC, Roberts JM (2008) Predicting suitable habitat for the cold-water coral *Lophelia pertusa* (Scleractinia). *Deep-Sea Res I* 55:1048–1062
- Davies AJ, Duineveld GCA, Lavaleye MSS, Bergmann MJN, van Haren H, Roberts JM (2009) Downwelling and deep-water bottom currents as food supply mechanisms to the cold-water coral *Lophelia pertusa* (Scleractinia) at the Mingulay Reef complex. *Limnol Oceanog* 54(2):620–629
- Davies AJ, Guinotte JM (2011) Global habitat suitability for framework-forming cold-water corals. *PLoS One* 6(4):e18483. doi:10.1371/journal.pone.0018483
- De Mol B, Van Rensbergen P, Pillen S, Van Herreweghe K, Van Rooij D, McDonnell A, Huvenne V, Ivanov M, Swennen R, Henriët JP (2002) Large deep-water coral banks in the Porcupine Basin, southwest of Ireland. *Mar Geol* 188:193–231
- Dullo W-C, Flögel S, Rüggeberg A (2008) Cold-water coral growth in relation to the hydrography of the Celtic and Nordic European continental margin. *Mar Ecol Prog Ser* 371:165–176
- Eisele M, Frank N, Wienberg C, Hebbeln D, López Correa M, Douville E, Freiwald A (2011) Productivity controlled cold-water coral growth periods during the last glacial off Mauritania. *Mar Geol* 280:143–149
-

- Eisele M, Frank N, Wienberg C, Titschack J, Mienis F, Beuck L, Tisnerat-Laborde N, Hebbeln D (2014) Sedimentation patterns on a cold-water coral mound off Mauritania. *Deep-Sea Res II* 99:307–315
- Fietzke J, Liebetrau V, Eisenhauer A, Dullo Ch (2005) Determination of uranium isotope ratios by multi-static MIC-ICP-MS: method and implementation for precise U- and Th-series isotope measurements. *J Anal Atomic Spectrom* 20:395–401. doi:10.1039/b415958f
- Fink HG, Wienberg C, Hebbeln D, McGregor HV, Schmiedl G, Taviani M, Freiwald A (2012) Oxygen control on Holocene cold-water coral development in the eastern Mediterranean Sea. *Deep-Sea Res I* 62:89–96
- Flewellen C, Millard N, Rouse I (1993) TOBI, a vehicle for deep ocean survey. *Electronics Commun Eng J* 5:85–93
- Flögel S, Dullo W-C, Pfannkuche O, Kiriakoulakis K, Rüggeberg A (2014) Geochemical and physical constraints for the occurrence of living cold-water corals. *Deep-Sea Res II* 99:19–26
- Form AU, Riebesell U (2012) Acclimation to ocean acidification during long-term CO₂ exposure in the cold-water coral *Lophelia pertusa*. *Global Change Biol* 18:843–853
- Fosså JH, Mortensen PB, Furevik DM (2002) The deep-water coral *Lophelia pertusa* in Norwegian waters: distribution and fishery impacts. *Hydrobiologia* 471:1–12
- Foubert A, Depreiter D, Beck T, Maignien L, Pannemans B, Frank N, Blamart D, Henriët J-P (2008) Carbonate mounds in a mud volcano province off north-west Morocco: key to processes and controls. *Mar Geol* 248(1-2):74–96
- Frank N, Ricard E, Lutringer-Paque A, van der Land C, Colin C, Blamart D, Foubert A, Van Rooij D, Henriët J-P, de Haas H, van Weering TCE (2009) The Holocene occurrence of cold-water corals in the NE Atlantic: implications for coral carbonate mound evolution. *Mar Geol* 266:129–142
- Frank N, Freiwald A, López Correa M, Wienberg C, Eisele M, Hebbeln D, Van Rooij D, Henriët J-P, Colin C, van Weering T, de Haas H, Buhl-Mortensen P, Roberts JM, De Mol B, Douville E, Blamart D, Hatté C (2011) Northeastern Atlantic cold-water coral reefs and climate. *Geology* 39:743–746
- Freiwald A (2002) Reef-forming cold-water corals. In: Wefer G, Billett D, Hebbeln D, Jørgensen BB, Schlüter M, Van Weering T (eds) *Ocean margin systems*. Springer, Berlin:365–385
- Freiwald A, Beuck L, Rüggeberg A, Taviani M, Hebbeln D, R/V *Meteor* Cruise M70-1 Participants (2009) The white coral community in the central Mediterranean Sea revealed by ROV surveys. *Oceanography* 22:58–74
- Frenz M, Wynn RB, Georgiopoulou A, Bender VB, Hough G, Masson DG, Talling PJ, Cronin BT (2009) Provenance and pathways of late Quaternary turbidites in the deep-water Agadir Basin, northwest African margin. *Int J Earth Sci* 98:721–733
- Fusco G, Artale V, Cotroneo Y, Sannino G (2008) Thermohaline variability of Mediterranean Water in the Gulf of Cadiz, 1948–1999. *Deep-Sea Res II* 55:1624–1638
- Glogowski S, Dullo W-C, Feldens P, Liebetrau V, von Reumont J, Hühnerbach V, Krastel S, Wynn RB, Flögel S (2015) The Eugen Seibold coral mounds offshore western Morocco: oceanographic and bathymetric boundary conditions of a newly discovered cold-water coral province. *Geo-Mar Lett* 35(4):257–269. doi:10.1007/s00367-015-0405-7

- Gori A, Grover R, Orejas C, Sikorski S, Ferrier-Pagès C (2013) Uptake of dissolved free amino acids by four cold-water coral species from the Mediterranean Sea. *Deep-Sea Res II* 99:42–50
- Hebbeln D, Wienberg C, Wintersteller P, Freiwald A, Becker M, Beuck L, Dullo C, Eberli GP, Glogowski S, Matos L, Forster N, Reyes-Bonilla H, Taviani M (2014) Environmental forcing of the Campeche cold-water coral province, southern Gulf of Mexico. *Biogeosciences* 11:1799–1815
- Hendericks J, Freudenthal T, Meggers H, Nave S, Abrantes F, Bollmann J, Thierstein HR (2002) Glacial-interglacial variability of particle accumulation in the Canary Basin: a time-slice approach. *Deep-Sea Res II* 49:3675–3705
- Henriet JP, De Mol B, Pillen S, Vanneste M, Van Rooij D, Versteeg W, Croker PF, Shannon PM, Unnithan V, Bouriak S, Chachkine P (1998) Gas hydrate crystals may help build reefs. *Nature* 391:648–649
- Hernández-Molina FJ, Serra N, Stow DAV, Llave E, Ercilla G, Van Rooij D (2011) Along-slope oceanographic processes and sedimentary products around the Iberian margin. *Geo-Mar Lett* 31:315–341
- Hovland M, Jensen S, Indreiten T (2012) Unit pockmarks associated with *Lophelia* coral reefs off mid-Norway: more evidence of control by ‘fertilizing’ bottom currents. *Geo-Mar Lett* 32:545–554
- Hübscher C, Dullo C, Flügel S, Titschack J, Schönfeld J (2010) Contourite drift evolution and related coral growth in the eastern Gulf of Mexico and its gateways. *Int J Earth Sci* 99:191–206
- Krastel S, Böttner C, Cartigny M, Feldens P, Fu L, Glogowski S, Guggolz T, Hellmann S, Hühnerbach V, Jähmlich H, Kraus K, Kretschmer J, Matthew D, Meier D, Mücke I, von Reumont J, Schönke M, Schürer A, Stevenson C, Unverricht D, Voss D, Webb A, Wynn R (2013) Maria S. Merian Berichte. Morphology, processes and geohazards of giant landslides in and around Agadir Canyon, northwest Africa. Cruise No. MSM32. <http://eprints.uni-kiel.de/22613/1/msm32-short-cruise-report.pdf>
- Le Guilloux E, Olu K, Bourillet JF, Savoye B, Iglésias SP, Sibuet M (2009) First observation of deep-sea coral reefs along the Angola margin. *Deep-Sea Res II* 56:2394–2403
- León R, Somoza L, Medialdea T, Vázquez JT, González FJ, López-González N, Casas D, del Pilar Mata M, Fernández-Puga MC, Giménez-Moreno CJ, Díaz-del-Río V (2012) New discoveries of mud volcanoes on the Moroccan Atlantic continental margin (Gulf of Cádiz): morpho-structural characterization. *Geo-Mar Lett* 32:473–488
- Liebetrau V, Eisenhauer A, Linke P (2010) Cold seep carbonates and associated coldwater corals at the Hikurangi Margin, New Zealand: new insights into fluid pathways, growth structures and geochronology. *Mar Geol* 272:307–318
- Martorelli E, Petroni G, Chiocci FL and the Pantelleria Scientific Party (2011) Contourites offshore Pantelleria Island (Sicily Channel, Mediterranean Sea): depositional, erosional and biogenic elements. *Geo-Mar Lett* 31:481–493
- Mazzini A, Akhmetzhanov A, Monteys X, Ivanov M (2012) The Porcupine Bank Canyon coral mounds: oceanographic and topographic steering of deep-water carbonate mound development and associated phosphatic deposition. *Geo-Mar Lett* 32:205–225

- McDougall TJ, Barker PM (2011) Getting started with TEOS–10 and the Gibbs Seawater (GSW) Oceanog Toolbox, 28 pp, version 3.0. SCOR/IAPSO WG127, www.TEOS–10.org
- Mittelstaedt E (1991) The ocean boundary along the northwest African coast: circulation and oceanographic properties at the sea surface. *Prog Oceanog* 26:307–355
- Morigi C, Jorissen FJ, Gervais S, Borsetti AM (2001) Benthic foraminiferal faunas in surface sediments off NW Africa: relationship with organic flux to the ocean floor. *J Foram Res* 31(4):350–368
- Murton BJ, Rouse IP, Millard NW, Flewelling C (1992) Deep-towed instrument explores ocean floor. *Eos Trans Am Geophys Union* 73:225–228
- Palomino D, Vázquez J-T, Ercilla G, Alonso B, López-González N, Díaz-del-Río V (2011) Interaction between seabed morphology and water masses around the seamounts on the Motril Marginal Plateau (Alboran Sea, Western Mediterranean). *Geo-Mar Lett* 31:465–479
- Pastor MV, Pelegrí JL, Hernández-Guerra A, Font J, Salat J, Emelianov M (2008) Water and nutrient fluxes off Northwest Africa. *Cont Shelf Res* 28:915–936
- Pelegrí JL, Marrero-Díaz A, Ratsimandresy A, Antoranz A, Cisneros-Aguirre J, Gordo C, Grisolia D, Hernández-Guerra A, Láiz L, Martínez A, Parrilla G, Pérez-Rodríguez P, Rodríguez-Santana A, Sangrà P (2005) Hydrographic cruises off northwest Africa: the Canary Current and the Cape Ghir region. *J Mar Syst* 54:39–63
- Pfannkuche O and cruise participants (2006) Cruise Report Maria S. Merian 1/3. April - Mai 2006. http://www.senckenberg.de/files/content/forschung/abteilung/meeresforschung/meeresgeologie/expeditionen/msm1_3_final_report-olafsteil.pdf
- Raddatz J, Liebetrau V, Rüggeberg A, Hathorne E, Krabbenhöft A, Eisenhauer A, Böhm F, Vollstaedt H, Fietzke J, López Correa M, Freiwald A, Dullo W-C (2013) Stable Sr-isotope, Sr/Ca, Mg/Ca, Li/Ca and Mg/Li ratios in the scleractinian cold-water coral *Lophelia pertusa*. *Chem Geol* 352:143–152
- Reed JK, Weaver D, Pomponi SA (2006) Habitat and fauna of deep-water *Lophelia pertusa* coral reefs off the Southeastern USA: Blake Plateau, Straits of Florida, and Gulf of Mexico. *Bull Mar Sci* 78:343–375
- Reveillaud J, Freiwald A, Van Rooij D, Le Guilloux E, Altuna A, Foubert A, Vanreusel A, Olu-Le Roy K, Henriot J-P (2008) The distribution of scleractinian corals in the Bay of Biscay NE Atlantic. *Facies* 54:317–331. doi:10.1007/s10347-008-0138-4
- Roberts JM, Wheeler AJ, Freiwald A (2006) Reefs of the deep: the biology and geology of cold-water coral ecosystems. *Science* 312:543–547
- Rüggeberg A, Dullo C, Dorschel B, Hebbeln D (2007) Environmental changes and growth history of a cold-water carbonate mound (Propeller Mound, Porcupine Seabight). *Int J Earth Sci* 96:57–72
- Rüggeberg A, Flögel S, Dullo W-C, Hissmann K, Freiwald A (2011) Water mass characteristics and sill dynamics in a subpolar cold-water coral reef setting at Stjærnsund, northern Norway. *Mar Geol* 282:5–12
- Sánchez F, González-Pola C, Druet M, García-Alegre A, Acosta J, Cristobo J, Parra S, Ríos P, Altuna A, Gómez-Ballesteros M, Muñoz-Recio A, Rivera J, Díaz del Río G (2014) Habitat characterization of deep-water coral reefs in La Gaviera canyon (Avilés Canyon System, Cantabrian Sea). *Deep-Sea Res II* 106:118–140

- Savini A, Vertino A, Marchese F, Beuck L, Freiwald A (2014) Mapping cold-water coral habitats at different scales within the northern Ionian Sea (Central Mediterranean): an assessment of coral coverage and associated vulnerability. *PLoS One* 9(1):e87108. doi:10.1371/journal.pone.0087108
- Sayago-Gil M, Long D, Hitchen K, Díaz-del-Río V, Fernández-Salas LM, Durán-Muñoz P (2010) Evidence for current-controlled morphology along the western slope of Hatton Bank (Rockall Plateau, NE Atlantic Ocean). *Geo-Mar Lett* 30:99–111
- Schlitzer R (2013) Ocean Data View. <http://odv.awi.de>
- Somoza L, Ercilla G, Urgorri V, León R, Medialdea T, Paredes M, Gonzales FJ, Nombela MA (2014) Detection and mapping of cold-water coral mounds and living *Lophelia* reefs in the Galicia Bank, Atlantic NW Iberia margin. *Mar Geol* 349:73–90
- Talling PJ, Wynn RB, Masson DG, Frenz M, Cronin BT, Schiebel R, Akhmetzhanov AM, Dallmeier-Tiessen S, Benetti S, Weaver PPE, Georgiopoulou A, Zühlsdorff C, Amy LA (2007) Onset of submarine debris flow deposition far from original giant landslide. *Nature* 450:541–544
- Taviani M, Angeletti L, Antolini B, Ceregato A, Froglija C, López Correa M, Montagna P, Remia A, Trincardi F, Vertino A (2011) Geo - biology of Mediterranean deep-water coral ecosystems. *Mar Res at CNR*. <https://www.researchgate.net/publication/232628431>
- Tomczak (1999) Some historical, theoretical and applied aspects of quantitative water mass analysis. *J Mar Res* 57(2):275–303
- Van Camp L, Nykjær L, Mittelstaedt E, Schlittenhardt P (1991) Upwelling and boundary circulation off Northwest Africa as depicted by infrared and visible satellite observations. *Prog Oceanog* 26:357–402
- Vandorpe T, Van Rooij D, de Haas H (2014) Stratigraphy and paleoceanography of a topography-controlled contourite drift in the Pen Duick area, southern Gulf of Cádiz. *Mar Geol* 349:136–151
- Van Rensbergen P, Depreiter D, Pannemans B, Henriët J-P (2005) Seafloor expression of sediment extrusion and intrusion at the El Arraiche mud volcano field, Gulf of Cadiz. *J Geophys Res* 110:F02010. doi:10.1029/2004JF000165
- Van Rooij D, Blamart D, De Mol L, Mienis F, Pirllet H, Wehrmann LM, Barbieri R, Maignien L, Templer SP, de Haas H, Hebbeln D, Frank N, Larmagnat S, Stadnitskaia A, Stivaletta N, van Weering T, Zhang Y, Hamoumi N, Cnudde V, Duyck P, Henriët J-P (2011) Cold-water coral mounds on the Pen Duick Escarpment, Gulf of Cadiz: the MICROSYSTEMS project approach. *Mar Geol* 282:102–117
- Vierod ADT, Guinotte JM, Davies AJ (2014) Predicting the distribution of vulnerable marine ecosystems in the deep sea using presence-background models. *Deep-Sea Res II* 99:6–18
- Wedepohl KH (1995) The composition of the continental crust. *Geochim Cosmochim Acta* 59(7):1217–1232
- Westphal H, Beuck L, Braun S, Freiwald A, Hanebuth T, Hetzinger S, Klicpera A, Kudrass H, Lantzsch H, Lundälv T, Mateu-Vicens G, Preto N, v Reumont J, Schilling S, Taviani M, Wienberg C (2012) Phaeton – Report – Paleoceanographic and paleo-climatic record on the Mauritanian Shelf Cruise No. MSM16-3, Oct 13 – Nov 20, 2010, Bremerhaven (Germany) – Mindelo (Cap Verde). *Maria S. Merian – Berichte*:1–53

- Wheeler AJ, Beyer A, Freiwald A, de Haas H, Huvenne VAI, Kozachenko M, Olu-Le Roy K, Opperbecke J (2007) Morphology and environment of cold-water coral carbonate mounds on the NW European margin. *Int J Earth Sci* 9:37–56
- White M, Roberts JM, van Weering T (2007) Do bottom-intensified diurnal tidal currents shape the alignment of carbonate mounds in the NE Atlantic? *Geo-Mar Lett* 27:391–397
- Wienberg C, Hebbeln D, Fink HG, Mienis F, Dorschel B, Vertino A, López Correa M, Freiwald A (2009) Scleractinian cold-water corals in the Gulf of Cádiz - first clues about their spatial and temporal distribution. *Deep-Sea Res I* 56:1873–1893
- Wienberg C, Frank N, Mertens KN, Stuetz J-B, Marchant M, Fietzke J, Mienis F, Hebbeln D (2010) Glacial cold-water coral growth in the Gulf of Cádiz: implications of increased palaeo-productivity. *Earth Planet Sci Lett* 298:405–416
- Wynn RB, Weaver PPE, Masson DG, Stow DAV (2002) Turbidite depositional architecture across three interconnected deep-water basins on the north-west African margin. *Sedimentology* 49(4):669–695

Supplementary Material

Fig. 2.5 Number of mounds with respect to height for the three selected areas (each 4 km²) shown in Fig. 4. Mound height decreases from shallower depths of area 1, where living corals have been sampled, to deeper depths of area 3. Mean elevation and standard deviation for area 1 = 6.9±2.2 m, area 2 = 6.0±1.4 m, and area 3 = 3.6±1.0 m. Refer to Fig. 2 for area locations

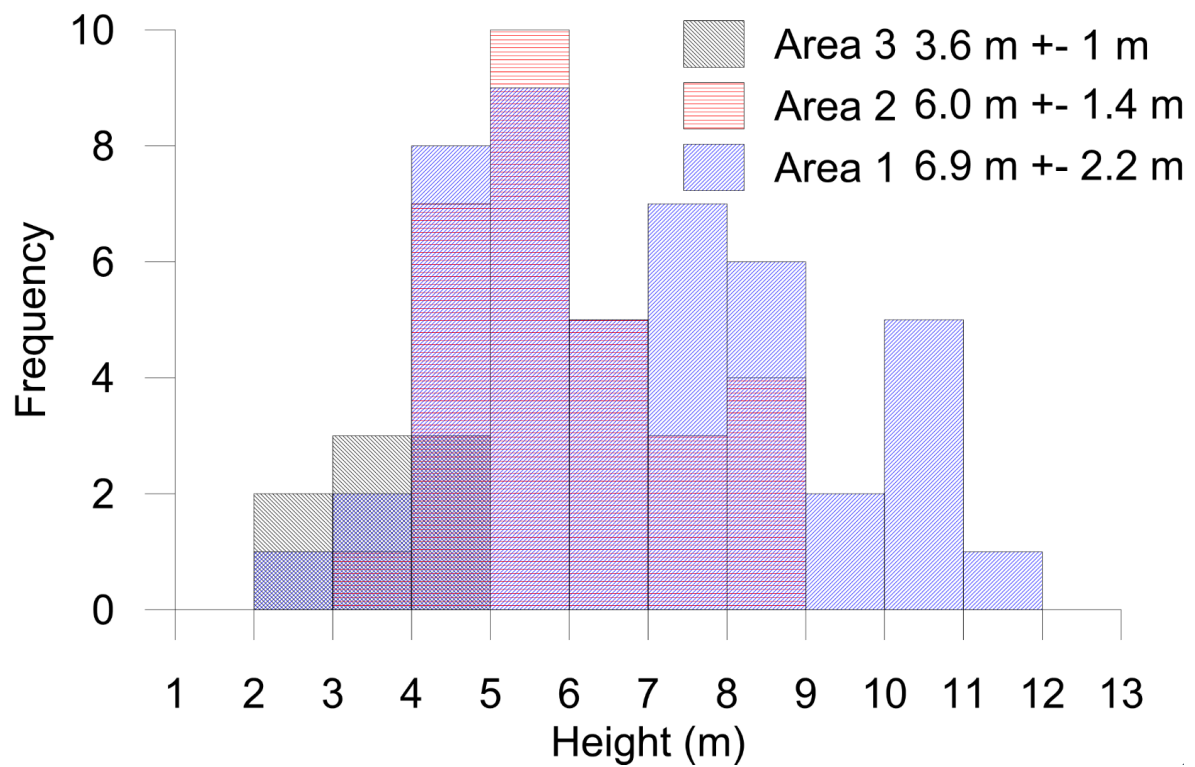
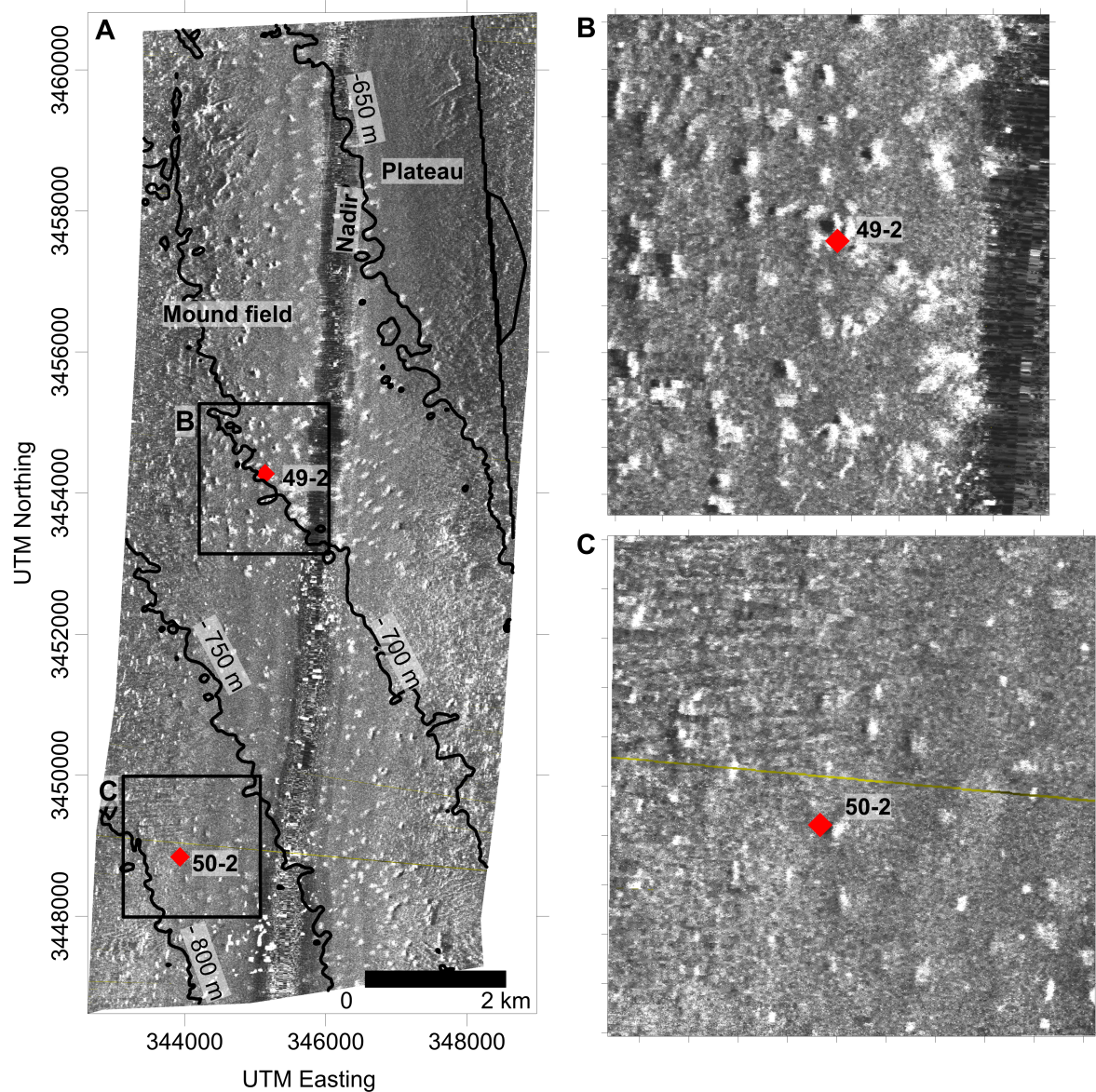


Fig. 2.6 *Left* TOBI side scan sonar (30 kHz) imagery across the carbonate mound province (swath width 6 km). Individual coral mounds are recognized by high acoustic backscatter on flanks inclined towards the side scan sonar track, and low backscatter shadows on the lee sides. *Right* Higher-resolution imagery in the vicinity of two box corer stations (red stars): *top right* MSM32-49-2, with living corals; *bottom right* MSM32-50-2, with dead corals. For corresponding locations in study area, see Fig. 2



Supplementary Material

Table 2.1 CTD stations off Morocco during cruise MSM32 (present study), and off Mauritania (cruise MSM16/3) and in the Gulf of Cadiz (cruise MSM1/3 (for data sources, see main text). T, S, density and oxygen values are given for the deepest sampling location

Station Number	Date	Time (UTC)	Bottom Depth* (m)	Lat. (°N)	Long. (°E)	<i>Lophelia pertusa</i>	Conservative Temperature (°C)	Absolute Salinity (S _A)	Density Sigma-theta (kg/m ³)
MSM32-41-1	24.10.13	16:09	90	30°18.170	09°47.440	unknown	15.56	36.403	26.78
MSM32-12-1	09.10.13	13:20	2667	30°42.240	10°59.710	unknown	2.71	35.156	27.88
MSM32-1-1	01.10.13	13:53	4224	32°54.400	10°49.060	unknown	1.65	35.065	27.88
MSM32-52-1	26.10.13	09:39	619	31°12.740	10°34.491	unknown	10.60	35.704	27.25
MSM32-51-2 ¹	25.10.13	18:37	678	31°12.740	10°37.530	living	9.94	35.632	27.31
MSM32-45-2	26.10.13	14:37	694	31°18.945	10°40.318	dead	10.31	35.678	27.28
MSM32-3-2	02.10.13	16:39	704	31°08.055	10°36.248	living	9.78	35.632	27.33
MSM32-50-3	25.10.13	11:02	763	31°09.784	10°38.236	dead	9.64	35.602	27.33
MSM32-46-2	26.10.13	16:17	794	31°25.094	10°40.067	dead	9.64	35.621	27.35
MSM32-47-2	26.10.13	17:55	830	31°21.020	10°44.794	dead	8.99	35.572	27.42
MSM32-48-2	26.10.13	12:38	857	31°12.470	10°42.850	dead	8.89	35.546	27.41

Table 2.1 CTD stations off Morocco during cruise MSM32 (present study), and off Mauritania (cruise MSM16/3) and in the Gulf of Cadiz (cruise MSM1/3 (for data sources, see main text). T, S, density and oxygen values are given for the deepest sampling location

CTD- stations with respect to Figure 5 off Mauretania taken during cruise MSM16/3 and Gulf of Cadiz taken during cruise MSM1/3

Station Number	Date	Time (UTC)	Bottom Depth* (m)	Lat. (°N)	Long. (°E)	<i>Lophelia pertusa</i> Conservative	Absolute Temperature (°C)	Salinity (S _A)	Density Sigma-theta (kg/m ³)
MSM16/327	10.10	20:40	504	19°41.990	17°11.479	cat. III 10.10	35.450	27.15	
(GeoB14778)									
MSM1/3-268	17.01.06	16:46	632	35°21.340	06°51.029	cat. III 10.68	35.758	27.26	

*CTD stopped ~5 m above the seafloor

¹repeated-CTD; first single data

Reference: MSM16/3, MSM1/3

Table 2.2 Box corer stations off Morocco taken during cruise MSM32

Station	Date	Time	Depth	Lat.	Long.	<i>Lophelia.</i>
Number		(UTC)	(m)	(°N)	(°E)	<i>pertusa</i>
MSM32-49-2	25.10.13	15:08	678	31°12.740	10°37.540	living
MSM32-45-1	25.10.13	07:55	701	31°18.945	10°40.318	dead
MSM32-3-1	02.10.13	15:06	719	31°08.055	10°36.248	living
MSM32-50-2	25.10.13	17:18	788	31°09.784	10°38.236	dead
MSM32-46-1	25.10.13	09:32	801	31°25.094	10°40.067	dead
MSM32-47-1	25.10.13	11:00	835	31°21.039	10°44.794	dead
MSM32-48-1	25.10.13	12:55	863	31°12.470	10°42.850	dead

Reference: MSM32, this study

Table 2.3 U-Th isotope systematics and age determination of *Lophelia pertusa* from box core MSM32-3-1-1 (719 m water depth), cruise MSM32 off Morocco (uncertainties at 2 SE level)

origin / lab-code *	ident No.	descript.	mean core depth of fragment (cm)	sample aliquot anal. (mg)	^{238}U conc. ($\mu\text{g/g}$)	^{232}Th conc. (ng/g)	$^{230}\text{Th}/^{232}\text{Th}$ act. ratio	$^{230}\text{Th}/^{234}\text{U}$ ⁽¹⁾ ratio	act.	$\delta^{234}\text{U}_{(o)}$ ⁽²⁾	$\delta^{234}\text{U}_{(t)}$ ⁽³⁾	Age ⁽⁴⁾ (y BP)
juvenile branch tops of sampling site												
969-14 *	# 3	<i>Loph. juv.</i>		38	4.08 ± 0.02	1.036 ± 0.011	9.3 ± 0.3	0.00062 ± 0.00003		147.6 ± 2.1		0
971-14 *	# 13	<i>Loph. juv.</i>	approx. 15 cm	83	3.97 ± 0.02	0.464 ± 0.003	9.8 ± 0.4	0.00030 ± 0.00001		151.5 ± 2.2		0
970-14 *	# 15	<i>Loph. juv.</i>	above sedim.	51	3.31 ± 0.01	0.509 ± 0.004	11.0 ± 0.5	0.00045 ± 0.00002		147.8 ± 2.3		0
average values:					3.79 ± 0.48	0.670 ± 0.637	10.0 ± 1.0	0.00046 ± 0.00019		149.0 ± 2.5		0
oldest growth segment of subrecent reef structure												
968-14	# 4	<i>Loph. root seg.</i>	0	109	3.50 ± 0.01	1.765 ± 0.010	7.6 ± 0.2	0.00053 ± 0.00019		147.3 ± 2.1	147.3 ± 2.1	60 ± 20
buried branch fragments of different macroscopical alteration status												
978-14	# 8	<i>Loph. str. alt.</i>	25	127	3.74 ± 0.02	0.616 ± 0.004	525.4 ± 4.7	0.02422 ± 0.00026		140.9 ± 2.4	141.9 ± 2.4	2680 ± 30
979-14	# 9	<i>Loph. sl. alt.</i>	25	141	3.42 ± 0.01	0.288 ± 0.002	707.5 ± 7.7	0.01647 ± 0.00024		143.5 ± 2.2	144.2 ± 2.2	1810 ± 30

All uncertainties are calculated on 2 SE level.

Whole procedure blanks of this sample set were around 10 pg for U, 2 pg for ^{232}Th and 0.1 fg for ^{230}Th , which is matching the typical range of applied method and used facilities.

Geochemical, optical, microstructure and growth systematics of the scleractinian cold-water coral *Lophelia pertusa*

by Silke Glogowski, Wolf-Christian Dullo, Sascha Flögel and Jacek Raddatz
(Submitted)

Abstract

Cold-water corals record environmental conditions during calcification by systematic variations in trace metal incorporation. This study presents geochemical ratios of Mg/Ca, Sr/Ca, and Na/Ca in *Lophelia pertusa* skeletons collected alive from the West- and East Atlantic Ocean and the Gulf of Mexico. In order to evaluate geochemical variability and empirical relationships between Me/Ca ratios and corresponding seawater parameters theca walls (TW) and centers of calcification (CoC) were analysed applying Laser Ablation-Inductively Coupled Plasma-Mass Spectrometry (LA-ICP-MS) and Electron Probe Microanalyser (EPMA) technique. Additionally, semi-quantitative element surface mapping and two different optical methods were applied. The results reveal that Mg/Ca ratios are increased within the CoCs and provide an excellent tool to differentiate between TW and CoC, whereas the Sr/Ca ratios variability is rather ubiquitous. Na/Ca ratios derived from LA-ICP-MS analysis correlate negative to both, salinity and temperature, hampering this potential proxy for seawater salinity reconstructions. However, there is a stronger correlation of Na/Ca data derived from CoC measurements with salinity ($R^2=0.73$) and temperature ($R^2=0.60$) compared to the TW (salinity: $R^2=0.51$; temperature: $R^2=0.34$). As Na may be enriched within crystal lattice defects (CLDs), this suggests a precipitation control on Na/Ca ratios in *L. pertusa*. Such defects preferentially occur in the fast precipitating and small crystals of the CoC in contrast to the fasciculate crystals of the TW. High precipitation rates result in an increase of CLDs and this is portrayed by ongoing calyx growth.

3.1 Introduction

Lophelia pertusa (Linnaeus 1758) is the dominant scleractinian cold-water coral (CWC) today, tolerating a wide range of physical and chemical environmental settings (e.g. Dullo et al. 2008; Flögel et al. 2014; Freiwald et al. 2004; Roberts et al. 2006). This species is found in various depth levels ranging from 39 m (Trondheimsfjord) to 3380 m (western Atlantic Ocean), whereas *L. pertusa* reefs are most abundant in water depths between 200 and 1000 m (Freiwald and Wilson 1998; Freiwald et al. 2004). Observed temperatures vary between 4°C – 14°C while measured salinities range between 34.85 g/kg and 38.75 g/kg (Davies et al. 2008; Dullo et al. 2008; Mienis et al. 2012; Flögel et al. 2014). The development of a density gradient (Dullo et al. 2008) appears to be important to favour lateral nutrient advection (Kiriakoulakis et al. 2004; Grasmueck et al. 2007; White et al. 2007) and/or larval dispersal. Dullo et al. (2008) indicated that living cold-water coral reefs occur at density surfaces supporting intermediate nepheloid layers (INLs), where food accumulation and availability for bottom biota increases.

During biomineralisation, CWCs, like their shallow water counterparts, incorporate distinct amounts of trace elements as well as specific isotope ratios, which are proxies for the physical and chemical conditions of the ambient seawater, such as e.g. temperature. In due consideration of the biological processes like “vital-effects” (e.g. Urey et al. 1951; Weber and Woodhead 1972; McConnaughey 1989; Adkins et al. 2003; Cohen et al. 2006) CWC-skeletons are a potential archive recording water mass variability (Smith et al. 2000; Lutringer et al. 2005). It has been demonstrated that *L. pertusa* is a reliable archive for temperature reconstructions (e.g. Case et al. 2010; Montero-Serrano et al. 2013; Raddatz et al. 2013; Raddatz et al. 2014a; Montagna et al. 2014; Raddatz et al. 2016).

Early studies (Wells 1956; Wainwright 1964) on *L. pertusa* skeletons have shown that they consist of a calcified outer part of the coral fibre, the theca wall (TW) and the inner part, the center of calcification (CoC). Rollion-Bard and Blamart (2015) refer to the aragonite fibres as Thickening Deposits (TDS) and the CoC is termed as Rapid Accretion Deposits (RAD), which was described as Early Mineralisation Zone (EMZ) by Cuif et al. (2003) and Centers of Rapid Accretion (CRA) by Stolarski (2003). In this paper the terms of TW and CoC are used.

Both, surrounding fibres (TW) and CoC have their own crystallographic characteristics and exhibit different compositions of trace element concentrations (Adkins et al. 2003; Gagnon et al. 2007; Robinson et al. 2006; Rollion-Bard et al. 2010; Raddatz et al. 2014b; Rollion-Bard and Blamart 2014). The TW consists of elongated aragonite crystals arranged with organic macromolecules forming the bulk of the total skeleton and providing mechanical robustness (Meibom et al. 2004). In contrast, the CoC is formed by submicron-sized granular aragonite crystals. These are encircled by short needle-like disorganised bundles of crystals (Gladfelter 1983; Cohen et al. 2001; Gagnon et al. 2007).

Previous investigations applying trace element and isotope ratios as proxies for past seawater mass reconstructions were performed in the skeletal parts either of the theca wall (TW; Cuif et al. 2003; Blamart et al. 2007) or in the center of calcification (CoC; Gladfelter 1982) or in a combination of both (e.g. Blamart et al. 2005; Lutringer et al. 2005; Rollion-Bard et al. 2009). Biomineralisation and calcification processes influence the skeletal architecture and the micro-fabric variability (Adkins et al. 2003; Rollion-Bard et al. 2003; Cohen and McConnaughey 2003; Meibom et al. 2004). Most authors agreed that CoC's represent the zone where skeletal growth and CaCO_3 precipitation is initiated (Cuif and Dauphin 1998). The higher precipitation rate of the CoC and the possible influence of an amorphous precursor phase also may lead to greater incorporation of organics and/or trace elements (Meibom et al. 2007; Sinclair et al. 2006; Gothmann et al. 2015), characterised also by different Me/Ca ratios, in particular highest ratios for Mg/Ca and Na/Ca are observed in the CoC (e.g. Cohen et al. 2006; Sinclair et al. 2006; Hoppe et al. 2013; Raddatz et al. 2013; Montagna et al. 2014; Rollion-Bard and Blamart 2015). Together with kinetic fractionation (Sinclair et al. 2006) they overprint the thermodynamic relationship, and obscure the primary environmental signal to derive e.g. precise temperature reconstructions (Montagna et al. 2005; Cohen et al. 2006; Gagnon et al. 2007; Meibom et al. 2008; Holcomb et al. 2009; Allison and Finch 2010).

Since geochemical proxy data in CWC skeletons vary between TW and CoC a distinct and careful differentiation between both is crucial. Based on two different optical methods and a semi-quantitative Mg-mapping this study presents Mg/Ca and Sr/Ca ratios measured by Electron Probe Microanalyser (EPMA) and Mg/Ca, Sr/Ca and Na/Ca ratios measured by Laser Ablation-Inductively Coupled Plasma-Mass Spectrometry (LA-ICP-MS) derived from TW and the CoC in *L. pertusa* specimen from eight different locations situated in the mid-latitude Atlantic.

Comparing the Me/Ca ratios of different microstructures with *in-situ* temperatures and salinities highlighted that most of the CoCs derived ratios exhibit stronger correlations than TW data.

3.2 Materials and Methods

Samples of living *L. pertusa* were collected at six different sites in the Gulf of Mexico (GoM) and on the western margin of the Bahama Bank during cruise MSM20-4 of R/V MARIA S. MERIAN in March/April 2012 (Hebbeln et al. 2014). Two additional samples derive from the Eugen Seibold coral garden ~40 nautical miles north of the Agadir Canyon off Morocco (Glogowski et al. 2015) sampled during cruise MSM32 with R/V MARIA S. MERIAN in October 2013 (SM Fig. 3.1).

Sample ID	Area	Station ID	Cruise / Samples	Lat. [°N]	Long. [°W]	Sampling Date	Depth [m]	Conservative Temperature [°C]	Absolute Salinity [psu]
GeoB 16312-1 [Yo-Yo CTD]	GoM, Campeche Bank	CB	MSM20-4, ROV 3, Sample 3	23°51.511	87°12.124	23.03.12	558	7.92	35.16
GeoB 16334-1 [Yo-Yo CTD]	GoM, West Florida Slope	W-FI	MSM20-4, ROV 6, Sample 1	26°20.201	84°45.597	27.03.12	513	7.67	35.14
GeoB 16347-1 [Single CTD]	GoM, Southwest Florida Slope	SW-FI1	MSM20-4, ROV 8, Sample 8	25°16.341	84°26.693	29.03.12	493	8.05	35.15
GeoB 16350-1 [Single CTD]	GoM, Southwest Florida Slope	SW-FI2	MSM20-4, ROV 9, Sample 4	24°58.164	84°17.973	30.03.12	483	8.29	35.17
GeoB 16362-1 [Single CTD]	Atlantic, Bimini Slope	BS	MSM20-4, ROV 11, Sample 6	25°56.230	79°18.611	02.04.12	487	12.95	35.81
GeoB 16373-1 [Yo-Yo CTD]	Atlantic, Great Bahama Bank Slope	GBB	MSM20-4, ROV 13, Sample 3	24°33.635	79°21.211	04.04.12	618	9.30	35.28
MSM32-3-2 [Single CTD]	Morocco, Agadir Canyon	MAC1	MSM32, Box Corer	31°08.055	10°36.248	02.10.13	704	9.87	35.63
MSM32-49-2 [Yo-Yo CTD]	Morocco, Agadir Canyon	MAC2	MSM32, Box Corer	31°12.740	10°37.540	25.10.13	674	10.12	35.65

Table 3.1 Sampling location and hydrographical *in-situ* data (according to Hebbeln et al. 2014; Glogowski et al. 2015). *Yo-yo-data represent mean values of 13 CTD casts covering a time window of 13 hours

The hydrography of the investigated sites such as Campeche Bank (CB; NE Yucatan Strait Peninsula), West-Florida Slope (W-FI), Southwest-Florida-Slope (SW-FI), Bimini Slope (BS) and Great Bahama Bank Slope (GBB) were reported in Hebbeln et al. (2014), while the respective data off Morocco (MAC; Agadir Canyon) are described in Glogowski et al. (2015). According to TEOS-10 (Thermodynamic Equation Of Seawater) all temperatures and salinities within this study are presented as conservative temperature (Θ ; °C) and absolute salinity (S_A ; g/kg), (McDougall and Barker 2011; Schlitzer 2013). During MSM20-4, samples were collected with the ROV „QUEST“ of MARUM (University of Bremen) while the samples off Morocco were collected with a standard box corer providing a sampling surface of 50x50 cm (Table 3.1).

The study of geochemical proxies requires detailed information of the microstructure of the coral skeleton (e.g. Blamart et al. 2005; Lutringer et al. 2005; Rollion-Bard and Blamart 2014).

The aim of this study was to define the location of the boundary between TW and CoC as accurate as possible. The microstructural differentiation is based on optical and electron optical as well as on high resolution geochemical analysis.

3.2.1 Optical images

In order to optically differentiate between the TW and CoC all polished sections of the corals were examined in reflected and insident light with two different cameras (SM Fig. 3.a). All samples were examined applying a standard Binocular-Microscope-Camera (binocular) equipped with a microscope camera (GEOMAR, Kiel). The other visualisation was applied by the Keyence-Digital-Highspeed-Camera (keyence) and digital microscope (University Kiel, Marine Micropaleontology Research Group). The samples have been visually observed before and after geochemical analyses. All images were analysed in detail with low-contrast and highly reflective targets and a magnification of 250 exhibiting the EPMA transect, the laser spots, and the difference of the coral skeleton structure.

3.2.3 Preparation

All samples were cleaned with Milli-Q water and dried overnight at 40°C. Every sample was photographed and optically scanned (SM Fig. 3.2 and SM Fig. 3.a). In order to measure the same individual coral calyx the samples were cut parallelly to the main axis of growth into two halves. Each half was prepared for measurements with EPMA and LA-ICP-MS, which require flat and highly polished sample surfaces. Therefore, the sample splits were vacuum embedded in epoxy resin and were afterwards polished to ensure a flat surface for signal stability during measuring EPMA and LA-ICP-MS (SM Fig. 3.2 and SM Fig. 3.a). Before the measurements each sample was cleaned in an ultrasonic bath, dried, optically scanned and photographed again. Sampling followed a line perpendicular to the longitudinal growth extension of the calices from the outer part of the TW crossing the CoC until the septum for both, EPMA and LA-ICP-MS analysis.

3.2.4 Element distribution mapping with EPMA

A section of each calyx from the CWC was used to study major and trace element distributions of Magnesium (Mg), Calcium (Ca), and Strontium (Sr) using the EPMA, a JEOL JXA-8200 super probe with five wavelength dispersive (WD) X-ray spectrometers, one energy dispersive (ED) X-ray detector, backscatter electron and secondary electron detectors and an optical microscope at the GEOMAR Helmholtz Centre for Ocean Research, Kiel. Sodium (Na) was not detectable with the EPMA due to the detection limit (<100 ppm) and measuring in ms. The revealed elemental precisions (relative standard deviation, 1σ) span for the ratios of Mg/Ca: $\pm 2.15\%$ and Sr/Ca: $\pm 5.06\%$ respectively. The uncertainties of the ratios obtained by EPMA span for the ratio of Mg/Ca from ± 0.39 – ± 0.62 mmol/mol, while the ratio of Sr/Ca range from ± 0.33 – ± 0.64 mmol/mol for the mean samples. Each scan was acquired at an acceleration voltage of 15.0 kV, a beam current of 100 nA, the width of the beam was 60 μm with a dwell time per pixel per accumulation of 100 ms per channel, the electron beam diameter was focused to a spot size of 3 μm and an amount of 4 accumulations for each image (400 ms dwell time per pixel). The defined pixel size was 3 x 3 μm . Calibration of Mg and Ca concentrations were based on an international major and minor element standard with known average concentrations Calcite-USNM 136321 (Jarosewich and MacIntyre 1983; Jarosewich 2002) and KAN-1 (Reay et al. 1993; Jarosewich 2002; SM Table 3.a), calibration of Sr

concentrations was based on Strontianite (R10065; Jarosewich 2002). The detailed position of each measurement is shown by a small red rectangle encircled within the bigger red rectangle in Fig. 2 for e.g. sample GeoB16312-1 (Campeche Bank, GoM). The calibration of the raw data was performed using an offline spreadsheet for data reduction and standardisation (Fietzke et al. 2015). The most recent recalibration of the EPMA at GEOMAR Kiel, applying a calcareous versus a siliceous standard revealed that the raw strontium concentrations (and calculated Sr/Ca ratios) presented in this study were underestimated and therefore corrected by a factor of 1.2 (Rüggeberg; personal comment) for aragonitic corals. This correction does not affect the other measured trace element signatures (Wisshak et al. 2009). Element composition of the calices was mapped and was arranged as a semi-quantitative contour plot for Magnesium (Mg). Mg compositions were displayed in colour and counts per pixel (cts/pxl; resolution 66 x 320 points, interval 3 μm ; SM Table 3.b), representing semi-quantitative Mg data. These cts/pxl show that the CoC has higher Mg values than the adjacent TW skeleton. This criterion is often used to determine growth bands within the coral skeleton (Shirai et al. 2008). Thus, element maps can be used to differentiate between microstructures of CWC skeletons.

3.2.5 Element distributions mapping with LA-ICP-MS

LA-ICP-MS, at GEOMAR, Kiel, is a double-focussing, high-resolution magnetic sector mass spectrometer (Nu Instruments, AttoM). The ICP-MS was combined with a 193 nm excimer laser ablation system (Coherent, GeoLasPro). Ablation was performed under He carrier gas, additionally Ar carrier gas was mixed prior to the plasma torch. Spot analyses were conducted by 30 s ablation with a laser repetition rate at 5 Hz, 3 J/cm², with 150 pulses/s (p/s). Spot diameters between 32 – 44 – 60 – 90 μm were tested for measurements (at sample GeoB16350-1 and GeoB16373-1), the best fit of 60 μm spot size were used for all samples. Additionally, 60 μm spot size was used 50 s of gas background data for pre-ablation prior to each ablation. NIST SRM 610 glass (30 s, 44 μm spot, 10 Hz, 5 J/cm², 32 μm spot, 300 p/s) was used as external reference material (Jochum et al. 2011). MPI-DING glass standards (ATHO-G and T1-G; 30 s, 44 μm spot, 10 Hz, 5 J/cm², 300 p/s) were used to check the accuracy of the measurements (<http://georem.mpch-inz.gwdg.de/sample>).

For example the reference material has been measured for sample GeoB16373-1 by the following way: NIST SRM 610 - 300 p/s, coral-spot 1 + 2 - 150 p/s, NIST SRM 610 - 300 p/s, coral-spot 3 + 4 - 150 p/s, NIST SRM 610 - 300 p/s, MPI-DING-ATHO-G - 300 p/s, MPI-DING-T1-G - 300 p/s, NIST SRM 610 - 300 p/s, coral-spot 5 + 6 - 150 p/s, NIST SRM 610 - 300 p/s, coral-spot 7 + 8 - 150 p/s, NIST SRM 610 - 300 p/s.

Backgrounds and standards were collected before and at the end of the measurements. The synthesised standard glass and the coral were pre-ablated to clean the surface of contaminants (10 shots / 60 μm) in order to remove the expected contamination at the upper few microns (Sinclair et al. 1998). The reproducibility (external errors) of the method is assessed by the repeated measurement of the standards with 300 measurements each. To correct for variations in ablation yield and instrumental drift, element signals were normalised to ^{43}Ca as the internal standard (Hathorne et al. 2013) obtained prior by EPMA analysis. The mean „minimum detection limits=m.d.l.“ for the relevant elements (ppm) are the following: Na(23)=0,31 (m.d.l.), Mg(25)=0,14 (m.d.l.), Ca(44)=2,2 (m.d.l.) and Sr(88)=0,02 (m.d.l.), this implicates that the element distribution of Sodium (Na) is detectable with LA-ICP-MS by using spot size with lower detection limits. The *in-situ* determination of the sampling transect was ablated parallelly along to the EPMA transect line with the same direction, across the TW of the *L. pertusa* specimens, from the external rim of the skeleton towards the CoC, for the isotopes ^{26}Mg , ^{25}Mg , ^{44}Ca , ^{43}Ca , ^{42}Ca , ^{86}Sr , ^{88}Sr , ^{23}Na simultaneously.

The whole measurement procedure for each sample contains 8 replicated single routine shot measurements. Spot sized analyses instead of lines or mapping were used in order to measure simply, quickly at low-cost, homogenous and free from cycle-variation. All element ratios were calculated using blank corrected rates for the isotopes selected ^{26}Mg , ^{44}Ca , ^{88}Sr , ^{23}Na and the corrected count rates of isotopes. The revealed elemental precisions (relative standard deviation, 1σ) span for the ratios of Mg/Ca: 2.06 – 2.75%, Sr/Ca: 1.50 – 1.91% and Na/Ca: 1.83 – 2.53% respectively. During the measurements of this study the „normalised argon index“ NAI values reclined between 36 and 39 with excellent „hot plasma“ conditions not influencing matrix effects as mentioned in Fietzke and Frische (2016).

3.2.6 Analytical considerations

EPMA provides good spatial resolution and accurate surface mapping of trace elements, which relies on the analysis of an individual track (line of EPMA spots). In contrast, LA-ICP-MS was used, characterised by a higher sensitivity for various elements and a higher precision, but with limitations of a larger diameter spot which in fact is a three-dimensional cylinder of 60 μm diameter, except for the tested measurements. Throughout this study, elemental ratios of Mg/Ca, Sr/Ca and Na/Ca are given in mmol/mol including the standard deviation (1σ). Each data represents the arithmetic mean of Me/Ca ratios at a specific point in a specific part, TW and CoC, of the coral skeleton. In addition, we calculated the arithmetic mean of the bulk sample to which we refer as the mean sample. For both analytical methods the analyses on the TW and CoC zone were focused. Measurements neither from the nucleation zones nor from the septum were included, since their Me/Ca ratios are frequently high due to the larger volumes of the „vital effects“. The calibration slopes, regression coefficients and associated errors were calculated using standard Microsoft Excel analyse function. The standard residuals were calculated by Analysis ToolPak. The coefficient of determination (R^2) was applied to test the significance of the relationships, being insignificant ($R^2 \leq 0.5$) or significant ($R^2 \geq 0.5$). Furthermore, related p -values for each element ratio are presented. Based on the calculated correlation coefficient (R) and corresponding p -value the probability of finding observed, or more extreme results when the null hypothesis (H_0) of a study question is true – statistically significant p -values are $p < 0.05$ and statistically highly significant p -values are $p < 0.001$. The correlation between linear regression residuals of the elemental ratios and seawater properties like conservative temperature and absolute salinity was tested, and no significant correlation was found. Therefore, with the present dataset it was not possible to disentangle dependency between the residuals and conservative temperature or absolute salinity (all $R^2 < 0.3$ for EPMA, all $R^2 < 0.6$ for LA-ICP-MS).

3.2.7 Calyx relative growth

Coral calices from the different locations were measured by using a sliding calliper (0.01 mm-scale). From each calyx its length was measured (SM Fig. 3.b), starting with the oldest part of the calyx (budding zone) with location to the youngest part of the calyx (apical zone), while the individual measurements of the diameter moving along the calyx beginning at the base of each calyx as shown in SM Fig. 3.b and SM Table 3.c, according to Buhl Mortensen (2001). The average values for each sample were calculated. Additionally, only the sectioned samples were measured which were used for the geochemical analysis with LA-ICP-MS (SM Table 3.d). The calyx length and calyx diameter was normalised by dividing length through diameter resulting in the calyx factor (CF). The CF was plotted against the arithmetic mean element ratios (measured by LA-ICP-MS and EPMA) of the mean sample, the TW and the CoC for each sample. Additionally, the CF was plotted against the single calyx measured by LA-ICP-MS.

3.3 Results

For all eight *L. pertusa* samples that were collected alive, temperature and salinity of the ambient seawater were measured with a conductivity, temperature and depth (CTD, Table 3.1) using a Seabird 'SBE 911 plus' underwater unit additionally equipped including SBE data processing.

Due to the different depth distribution of the samples (484 – 704 m), *in-situ* temperature (7.67°C – 12.95°C) varies considerably, while *in-situ* salinity (35.144 – 35.809 g/kg) exhibits little variations.

3.3.1 Optical visualisation

Differences between the TW and CoC are optically visible, since the CoC appears more opaque in contrast to the more translucent material of the TW. The TW is shown in dark grey (binocular) and in dark green (keyence; SM Fig. 3.a). The outer septal region is characterised by a slightly greyish colouration (keyence: darker greenish colouration respectively) and in some samples by a zone of almost colourless fibres. In contrast, the more opaque region in lighter grey (keyence: brighter green respectively) of the skeleton represents the CoC. In some samples, a metallic shimmer towards the inner rim to the septum can be observed.

Therefore, these regions were avoided for geochemical analyses. The optical differentiation between TW and CoC corresponds well to the geochemically derived data, which allows to assign the analytical sites to distinct CWC microstructures (SM Table 3.2). In all samples the profile of the EPMA analytical line is seen in lighter grey (binocular) or lighter green (keyence) respectively as well as the eight spots of LA-ICP-MS analysis represented as white circles (SM Fig. 3.a).

3.3.2 Mapping of Magnesium (Mg) distribution by EPMA

The distribution of Mg by semi-quantitative elemental EPMA mapping is visualised by the relationship between signal counts and elemental concentrations in different colours (SM Table 3.b). Red dots represent the highest concentration of number of counts (cts/pixel) from 217 – 313, whereas blue dots represent lowest Mg values ranging between 55 – 82 cts/pixel (SM Table 3.b). The transition zone is characterised by prismatic coloured dots and this mapping technique was applied to differentiate in-between TW and CoC. The Mg distribution pattern shows clear boundaries between the TW and the CoC, indicated by a sharp contrast of blue (and prismatic) and red dots (≥ 200 cts/pixel). This semi-quantitative mapping tool exhibits better results for Mg instead of Sr due to the higher range in cts/pixel for Mg, and therefore was combined with the different methods.

3.3.3 Mg/Ca ratios obtained by EPMA

The assignment of individual section lines to the microstructure of the skeleton is given in SM Table 3.2. Mg/Ca ratios are presented in detail in SM Table 3.3. Mg/Ca ratios exhibit no significant correlation to temperature (SM Fig. 3.3) neither in the arithmetic mean sample, the TW nor in the CoC. Mg/Ca ratios demonstrate no significant correlation to salinity (SM Fig. 3.c), neither in the arithmetic mean sample, the TW nor in the CoC. Considering the mean values of the TW and the CoC the Mg/Ca ratios are similar within uncertainties for five of the corals.

Irrespectively of their location Mg/Ca ratios are higher in the CoC with respect to the TW, this is evident in the arithmetic mean (SM Table 3.3), as well as by selecting the minimum (min.) value within the TW and the maximum (max.) value within the CoC. Both enrichment factors are presented in SM Table 3.3. The min./max. approach was previously used in other studies (e.g. Raddatz et al. 2013; Rollion-Bard and Blamart 2015), however, the arithmetic mean is the only appropriate approach because min./max. values overestimate the differences between the TW and the CoC.

In this study only the arithmetic mean values are further discussed, and the standard deviations were calculated for the different data sets in order to quantify the associated uncertainty. The arithmetic mean enrichment factor of Mg/Ca is up to 1.58 relative to TW (SM Table 3.3). For example, the minimum of sample GeoB16350-1 range from 0.404 mmol/mol at 116 μm , 0.653 at 147 μm , 0.658 at 105 μm to 0.681 at 182 μm . The data were corrected to 0.653 at 147 μm for the min. value, resulting in an enrichment factor of 4.26 for the EPMA measurement, which is representing the more reliable data. Therefore, the enrichment factor was corrected to 6.89 (SM Table 3.d).

3.3.4 Mg/Ca ratios obtained by LA-ICP-MS

Mg/Ca ratios obtained by the LA-ICP-MS exhibit no significant correlations to temperature (SM Fig. 3.3) and to salinity (SM Fig. 3.c), neither in the arithmetic mean sample, the TW nor in the CoC. The assignment of each spot to the microstructure is shown in SM Table 3.2 and distances at SM Table 3.e. Observed variabilities within TW and CoC for all samples and each spot are summarised in SM Table 3.3. Measuring was done from the outer wall to the inner wall of the CWC and parallel to the EPMA profile. The arithmetic mean enrichment factor ranges from 1.01 – 1.42.

In most of the CWCs, the Me/Ca ratios measured by LA-ICP-MS are slightly higher than those obtained by using EPMA, this is in accordance to the methodological comparison of both published by Weiss et al. (2008). Comparison between the line profil (EPMA) and the single spots (LA-ICP-MS) yields similar results within the analytical uncertainty e.g. for Mg/Ca ratios (mean sample: $R^2=0.97$; TW: $R^2=0.77$; CoC: $R^2=0.97$).

3.3.5 Sr/Ca ratios obtained by EPMA

In contrast to Mg/Ca ratios, Sr/Ca ratios exhibit small variabilities. The assignment of individual section lines to the microstructure of the skeleton is given in SM Table 3.2 and values for the Sr/Ca ratios are presented in SM Table 3.4. Sr/Ca ratios reveal significant correlations to temperature (Fig. 3.4) in the arithmetic mean sample (eq 1: $y = -0.1014x + 10.776$) and in the CoC (eq 2: $y = -0.198x + 11.735$), but demonstrate no significant correlation in the TW. Sr/Ca ratios exhibit significant correlations to salinity (SM Fig. 3.d) in the arithmetic mean sample (eq 3: $y = -0.7501x + 36.37$) and in the CoC (eq 4: $y = -1.3706x + 58.381$), but demonstrate no significant correlation in the TW. Sr/Ca ratios in the CoC are increased by the arithmetic mean enrichment factor of up to 1.06 with respect to the TW.

3.3.6 Sr/Ca ratios obtained by LA-ICP-MS

The assignment of each spot for the Sr/Ca ratios to the microstructure is given in SM Table 3.2, observed variabilities within TW and CoC are summarised in SM Table 3.4 and distances at SM Table 3.e, and values obtained differ within the same CWC and profile.

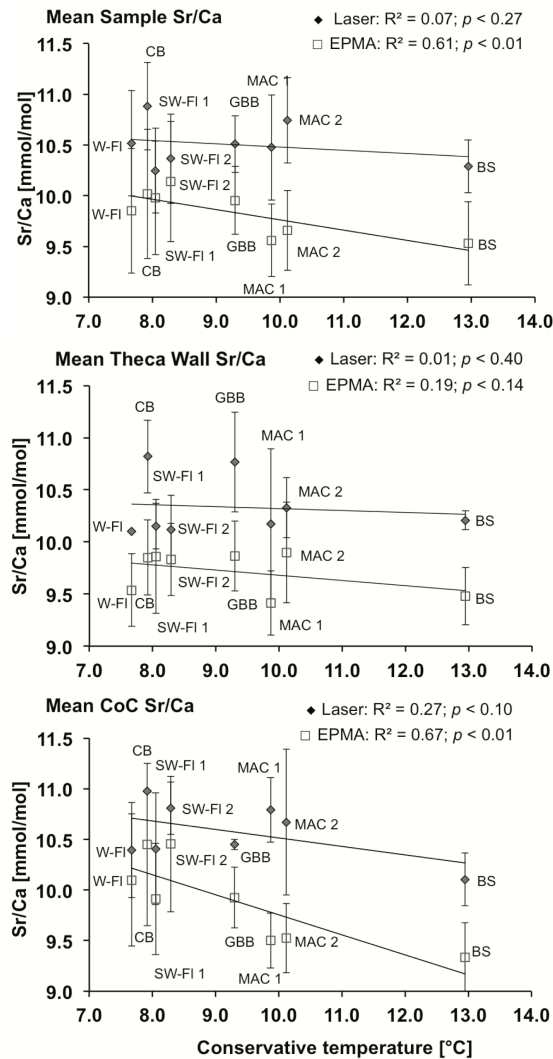


Fig. 3.4 Sr/Ca ratios (mmol/mol) versus *in-situ* temperature (°C) of EPMA and LA-ICP-MS in *L. pertusa*, differentiated in arithmetic mean sample (overview of the whole sample) *top*, the arithmetic mean TW plotted in the *middle* and the arithmetic mean CoC plotted at the *bottom*. Error bars = ± 1 SD (1σ). The linear regression, the corresponding R^2 and the p -values are given for both EPMA and LA-ICP-MS. Arithmetic mean enrichment factors are presented at SM Table 3.4

Sr/Ca ratios exhibit no significant correlation to temperature (Fig. 3.4), neither in the arithmetic mean sample nor in the TW, nor in the CoC (eq 5: $y = -0.0837x + 11.351$; $R^2=0.27$). Sr/Ca ratios exhibit no significant correlation to salinity (SM Fig. 3.d), neither in the arithmetic mean sample nor in the TW and nor in the CoC. Sr/Ca ratios of the arithmetic mean enrichment factor in the CoC are up to 1.07.

3.3.7 Na/Ca ratios obtained by LA-ICP-MS

All profiles show an increased Na/Ca ratio in the CoC with respect to the TW and the assignment of each spot for the Na/Ca ratios to the microstructure is given in SM Table 3.2. The observed distinct increase marks the transition from the TW into the CoC (SM Table 3.5 and distances at SM Table 3.e). Na/Ca ratios reveal a significant inverse correlation to temperature (Fig. 3.5) in the arithmetic mean sample (eq 6: $y = -1.0651x + 29.887$) and in the CoC (eq 7: $y = -1.2468x + 32.43$), but demonstrate no significant correlation in the TW (eq 8: $y = -0.6568x + 25.101$).

Na/Ca ratios exhibit significant correlations to salinity (Fig. 3.6) in the arithmetic mean sample (eq 9: $y = -7.0958x + 271.01$), and in the CoC (eq 10: $y = -8.6553x + 327.03$), but demonstrate a lower significant correlation in the TW (eq 11: $y = -5.0431x + 197.4$). The lowest value in the TW is increased by the arithmetic enrichment mean factor of 1.35 (GeoB16334-1) and 1.16 (GeoB16350-1).

3.3.8 Equations

Sr/Ca ratios display an inverse correlation with temperature measured by EPMA that was described by the eq 1 ($R^2=0.61$) in the arithmetic mean sample and eq 2 ($R^2=0.67$) in the CoC. The best fit to the Sr/Ca ratios was versus salinity measured by EPMA and can be described by eq 3 ($R^2=0.84$) in the arithmetic mean sample and in the CoC by eq 4 ($R^2=0.80$). The significant correlation between Na/Ca ratios and temperature measured by LA-ICP-MS are described by eq 6 ($R^2=0.58$) in the arithmetic mean sample and in the CoC by eq 7 ($R^2=0.60$), eq 8 ($R^2=0.34$) in the TW exhibit no significant correlation. The Na/Ca ratios versus salinity measured by LA-ICP-MS exhibits significant correlations described by eq 9 ($R^2=0.65$) in the arithmetic mean sample and demonstrated by the considerably higher value for the statistical R^2 in the CoC and described by eq 10 ($R^2=0.73$), and lower values in the TW by eq 11 ($R^2=0.51$).

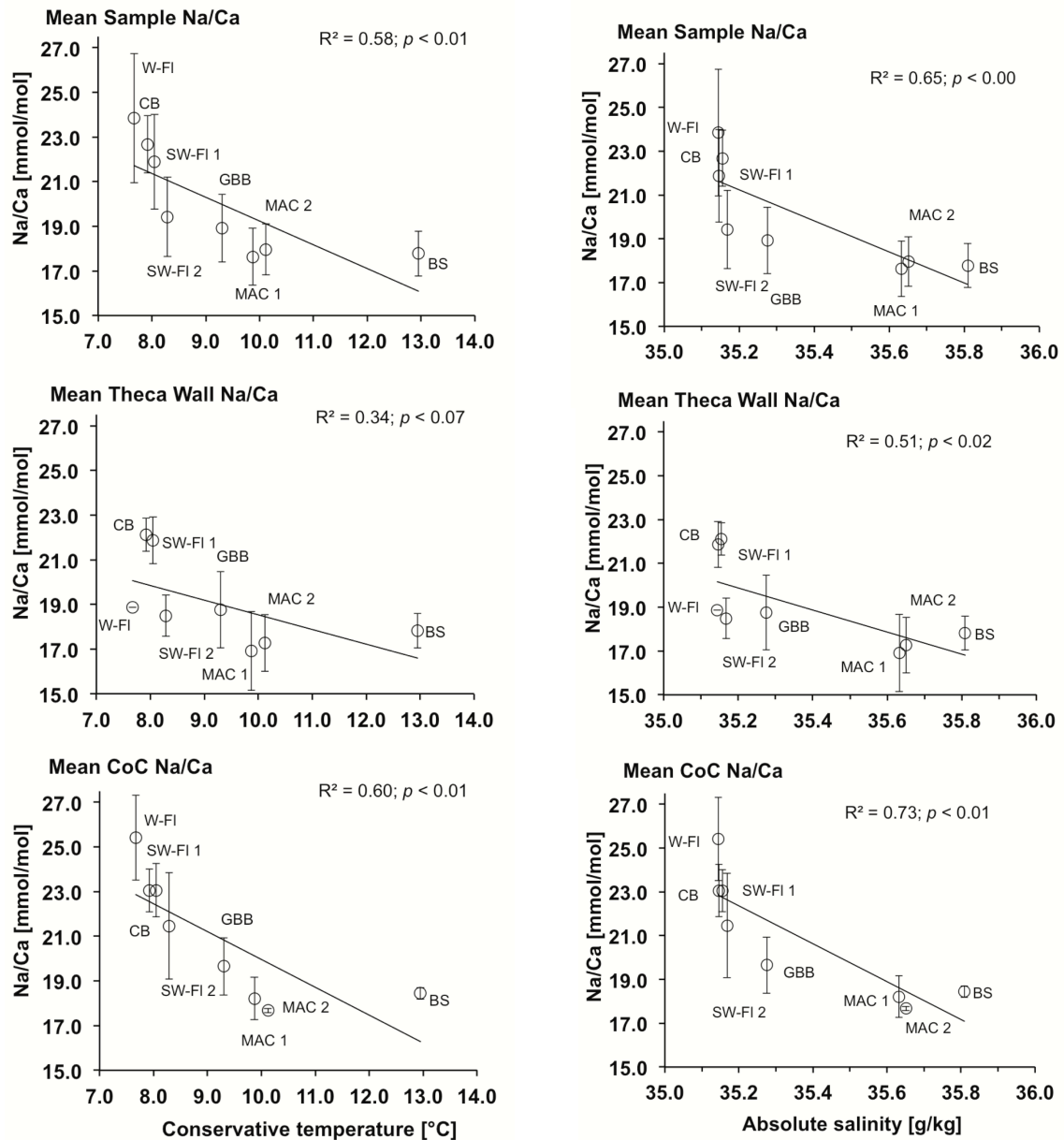


Fig. 3.5 (left) Na/Ca ratios (mmol/mol) versus *in-situ* temperature (°C) of LA-ICP-MS in *L. pertusa* and **Fig. 3.6** (right) Na/Ca ratios (mmol/mol) versus *in-situ* salinity (g/kg) of LA-ICP-MS in *L. pertusa*. Both figures are differentiated in arithmetic mean sample (overview of the whole sample) *top*, the arithmetic mean TW plotted in the *middle* and the arithmetic mean CoC plotted at the *bottom*. Error bars = ± 1 SD (1σ). The linear regression, the corresponding R^2 and the p -values are given for LA-ICP-MS. Arithmetic mean enrichment factors are presented at Table 3.5

3.3.9 Skeleton calyx length and cross-sectioned diameter / relative growth

Arithmetic mean in calyx length differs regionally at the eight different sample sites and range from 8.28 mm at BS and 10.32 mm at the GBB to 14.04 – 14.59 mm at Morocco and 15.14 – 21.03 mm in the GoM (SM Table 3.c, *bottom*). The arithmetic mean of the diameter ranges from 2.63 mm at BS and 4.84 mm at the GBB to 3.47 – 4.32 mm at Morocco and to 4.31 – 7.03 mm in the GoM (SM Table 3.c, *top*). The relationship between these averages of length and diameter show only a weak correlation ($R^2=0.25$; $p=0.10$; SM Fig. 3.e, *top*). Calyx length and the corresponding calyx diameter of the single, geochemically (LA-ICP-MS) analysed specimen (SM Table 3.d) do not exhibit a significant correlation ($R^2=0.15$; $p=0.18$; SM Fig. 3.e, *bottom*).

3.4 Discussion

Sr/Ca and Mg/Ca ratios

The results of this study do not exhibit a correlation between Mg/Ca ratios and temperature or salinity, neither in LA-ICP-MS nor in EMPA analyses, irrespectively from which microstructure the data derived (SM Fig. 3.3 and SM Fig. 3.c), eventhough such a relationship was initially proposed by Shirai et al. (2005) in *Caryophyllia*. The observed Sr/Ca to temperature sensivity are in line with more recent studies, albeit measured in other mineralogical parts of the skeleton (Allison and Finch 2004; Cohen et al. 2006; Gagnon et al. 2007; Montagna et al., 2014; Raddatz et al., 2013). The Sr/Ca ratios in this study exhibit a significant inverse relationship to temperature measured by EPMA (Fig. 3.4) in the arithmetic mean sample and in the CoC of *L. pertusa*, but no correlation was found in the TW neither for the EMPA nor for the LA-ICP-MS measurements. In contrast, the results of Raddatz et al. (2013) with 0.08 mmol/mol per °C the Sr/Ca ratios show a significant inverse correlation with temperature ($y=-0.083x+10.451$; $R^2=0.65$) in the TW. A similar observation was reported by Cohen et al. (2006) revealing a strong temperature sensitivity of 0.18 mmol/mol per °C in Sr/Ca ratios derived in the TW of *L. pertusa* ($Sr/Ca = -0.038(\pm 0.004)x + 10.43(\pm 0.19)$; $R^2=0.95$).

However, the corresponding measurements in this study obtained by laser ablation reveal no significant correlation to temperature (Fig. 3.4). This might be due to the limitation of eight LA-ICP-MS spots for some of the samples in the TW and CoC. The good correlation between Sr/Ca ratios and temperature within the TW reported by Cohen et al. (2006) with 4.8°C – 8.7°C for NE Skagerrak and Raddatz et al. (2013) with 6°C – 13.7°C (for European continental margin) may result from cooler temperatures of the sites they investigated in the NE Atlantic (4.8°C – 9.6°C), in contrast to the elevated temperatures in

this study (7.7°C – 13°C) with highest temperatures off the Bahama area. These previous studies reported only a significant correlation of Sr/Ca ratios with temperature but no correlation with salinity was observed. However, the corresponding Sr/Ca ratios (EPMA) of this study exhibit a significant inverse correlation with salinity in the data of the arithmetic mean sample and the CoC, but not with TW data.

DePaolo (2011) exhibits Sr incorporation as a function of calcite growth rates and the rate of solution-surface molecular exchange and therefore incorporation of Sr/Ca into calcite increases as calcification rate increases (Gabitov and Watson 2006; Dissard et al. 2010). If this is also true for aragonitic CWCs this may explain the observed Sr/Ca ratios in this study.

3.4.1 Na/Ca ratios

Rollion-Bard and Blamart (2015) presented Na/Ca ratios of *L. pertusa* with values in the TW from 23.19 – 27.37 mmol/mol and in the CoC from 19.55 – 28.88 mmol/mol. This range is in line with the results of this study, where Na/Ca ratios show an arithmetic enrichment mean factor of 1.35 (GeoB16334-1) and 1.16 (GeoB16350-1; SM Table 3.5). In contrast to published data with up to 1.5 for the min./max. method (Rollion-Bard and Blamart 2015) these are lower factors. Na/Ca ratios of this study decrease with increasing temperature especially derived from CoC crystals, while those derived from TW do not correlate significantly. Experimental precipitation studies of inorganic aragonite in relation to Na/Ca ratios were published already by Kinsmann (1970) for a temperature range between 15°C to 96°C and later by White (1977) for a temperature range between 25°C to 75°C.

They demonstrated a relation of decreasing Na/Ca ratios versus increasing temperature. Ragland et al. (1979) stated that Na⁺ is incorporated into biogenic carbonates in equilibrium to seawater. Swart (1981) showed a trend for the amounts of Na⁺ to be related to salinity, but this does not portray the Na/Ca ratios of the ambient seawater. Since no Na data were published from CWC in relation to salinity we have to refer to foraminifera and shallow water corals. Mitsugushi et al. (2010) studied Na concentrations in *Porites lobata* and suggested that the observed correlation with salinity is one but not the main controlling factor. Wit et al. (2013) observed no correlation between Na/Ca ratios and temperature in benthic foraminifera.

Na/Ca ratios demonstrate a significant positive correlation to salinity in the benthic foraminifera *Ammonia tepida* (Wit et al. 2013). Similar findings have been made in the planktonic foraminifera *Globigerinoides ruber* and *Globigerinoides sacculifer* (Allen et al. 2016; Mezger et al. 2016).

However, the Na/Ca ratios measured in the skeleton of CWCs in this study show a negative correlation to salinity (Fig. 6; TW: $R^2=0.51$; CoC: $R^2=0.73$). This inverse correlation rather excludes any influence of salinity on Na/Ca ratios in *L. pertusa* skeletons. The significant negative correlation of Na/Ca_(CoC) as well as Na/Ca_(TW) ratios to both temperature and salinity may indicate that possibly biomineralisation processes are influencing this ratio. In this study the relationship between *in-situ* salinity versus *in-situ* temperature correlates significantly ($R^2=0.85$), which points into the same direction and therefore temperature is not excluded as influencing factor.

Furthermore, Na/Ca ratios in the coral skeleton are significantly enriched in the CoC relative to the TW. Biological and/or mineralogical processes during calcification appear to be the main controlling mechanism with the effect of higher Na incorporation in the CoC. In particular, the crystallographic structure exhibits for both, TW and CoC, a nine-fold orthorhombic lattice (CaO₉ polyhedron) with potential different lattice defects (Gladfelter 1983; Busenberg and Plummer 1985; Mitsugushi et al. 2010; Brahmi et al. 2012; Rollion-Bard and Blamart 2015) and degrees of deformation (Mitsugushi et al. 2001). The number of these crystal lattice defects = CLDs in the crystallographic structure increases with higher precipitation rate (Mitsugushi et al. 2010; Rollion-Bard and Blamart 2015).

Since the CoC crystals are very small and result from very rapid precipitation, this may lead to irregular crystal growth (Gladfelter 1983) and CLDs (Okumura and Kitano 1986) are much more frequent in the CoC than in the TW (Mitsugushi et al. 2010). Moreover, the observed best fit between Na/Ca ratios and temperature as well as salinity within the CoC and to a lesser degree within the TW, implies a strong biological control on Na incorporation into the coral skeleton, as detected by Rollion-Bard and Blamart (2015). Amiel et al. (1973) hypothesised that the Na-ions fit into the aragonite lattice because of their similar ion radius of Na to Ca ($\text{Na}^+=0.95$ and $\text{Ca}^{2+}=0.97 \times 10^{-10}$ m).

Paquette and Reeder (1995, calcite), Reeder (1996, calcite) and Sinclair et al. (2005, aragonite, *Porites lobata*) argued that these cations may substitute their positions within the lattice and that this phenomenon is more common in crystals having higher CLDs.

This might explain the different Na/Ca ratios between TW and CoC and the enrichment within the CoC found in this study. In contrast, Yoshimura et al. (2017) described the altermultivalent substitution of Na into Ca sites in the lattice structures of calcite and aragonite. By using micro-X-ray fluorescence they showed for the fossil aragonitic coral *Desmophyllum* sp. that Na is homogeneously distributed throughout the skeletal microstructure, indicating that this process has only a minor influence on skeletal Na concentrations. The inhomogeneous distribution of Na/Ca ratios observed in this study seem to be controlled by the precipitation rate, the regional differences (Fig. 5 and 6) were linked to growth rates, without proving the variations in precipitation rates. Van de Locht et al. (2013) hypothesise that in *Porites lobata* the difference in growth between TW and CoC might be directly correlated to the coral growth, where the CoC is the result of rather rapid growth compared to the TW. If this is also true for CWCs, it could be explained by the calyx factor (CF) which is defined as calyx length / calyx diameter (SM Fig. 3.e) and is thus an expression of growth rate, assuming that one calyx is formed during one year (Freiwald et al. 1997; Buhl Mortensen 2001; Gass and Roberts 2010). Hence, a higher CF expresses more rapid growth and therefore an increased rate of precipitation. Maximum growth rates of *L. pertusa* were published by e.g. Gass and Roberts (2006 and 2010) with 26 ± 5 mm/year up to 33 ± 5 mm/year for the North Sea and by Brooke and Young (2009) with up to 16 mm/year in the GoM. Since the measurements of calyx length and calyx diameter vary considerably, the CF was applied for further analyses. The CF was calculated for the youngest calyx and the oldest calyx in each sample. The correlation between Na/Ca ratios and the CF exhibits a positive relationship for the arithmetic mean sample, and the CoC for the single calyx measured by LA-ICP-MS (Fig. 3.7). The non-existing correlation between Na/Ca TW data and CF factor results from a positive correlation between Na/Ca and CF of the youngest polyp and the negative correlation between the oldest polyp (SM Table 3.c). Therefore secondary thickening is crucial, however, it occurs obviously only in the TW. Since we argue that the variations in Na/Ca occur mainly in the CoC as a result of different rates of crystal precipitation this secondary thickening is only of minor or negligible importance. The incorporation of Na/Ca into the aragonitic TW and CoC seems to be linked to changes in the CLDs. The number of CLDs may depend on the precipitation rates: high rate corresponds to a higher number of CLDs.

Since high Na/Ca ratios positively correlate with high relative CFs it is assumed that also precipitation rates are high. Na/Ca ratios of the TW (SM Fig. 3.f) do not show a correlation with CF values but with CoC data applying all CF values of the respective coral branch. This is in accordance with the CF values derived from the analysed calyx for LA-ICP-MS measurements correlating in the CoC (Fig. 3.7). Therefore, Na/Ca ratios in *L. pertusa* are controlled by the rate of precipitation of aragonite in the CoC and to a lesser degree in the TW. This observation is further supported by the significant correlations of CF data and Mg/Ca_(CoC) ratios measured by LA-ICP-MS and EPMA (Fig. 3.8 and SM Fig. 3.g). However, Mg/Ca ratios in *L. pertusa* cannot be applied as a proxy for environmental controls like Na/Ca in contrast to Sr/Ca ratios (Fig. 3.9 and SM Fig. 3.h), which do not show any correlation to CF data in the coral skeleton. This is supported by Brahmi et al. (2012), who state also for scleractinian reef corals that there is no relationship between Sr/Ca und growth rate (CF).

Furthermore, the Sr/Ca ratios show ubiquitous variations within the coral architecture which indicates caution when applying Sr/Ca as a paleo-temperature proxy (Smith et al. 1979; Beck et al. 1992; Rüggeberg et al. 2008; Raddatz et al. 2013), though should future studies try to minimise the scatter.

Only Mg/Ca ratios inferred from EPMA show a clear distinction between TW and CoC and provide the proper tool for their differentiation as shown in Fig. 3.10. Both Mg/Ca ratios and Na/Ca ratios in combination with the two optical visualisations provide a method to select the proper site within CWC skeleton (Fig. 3.10), which is only the TW where suitable Me/Ca ratios may allow to reconstruct past environmental conditions (Cohen et al. 2006; Anagnostou et al. 2011; Raddatz et al. 2013).

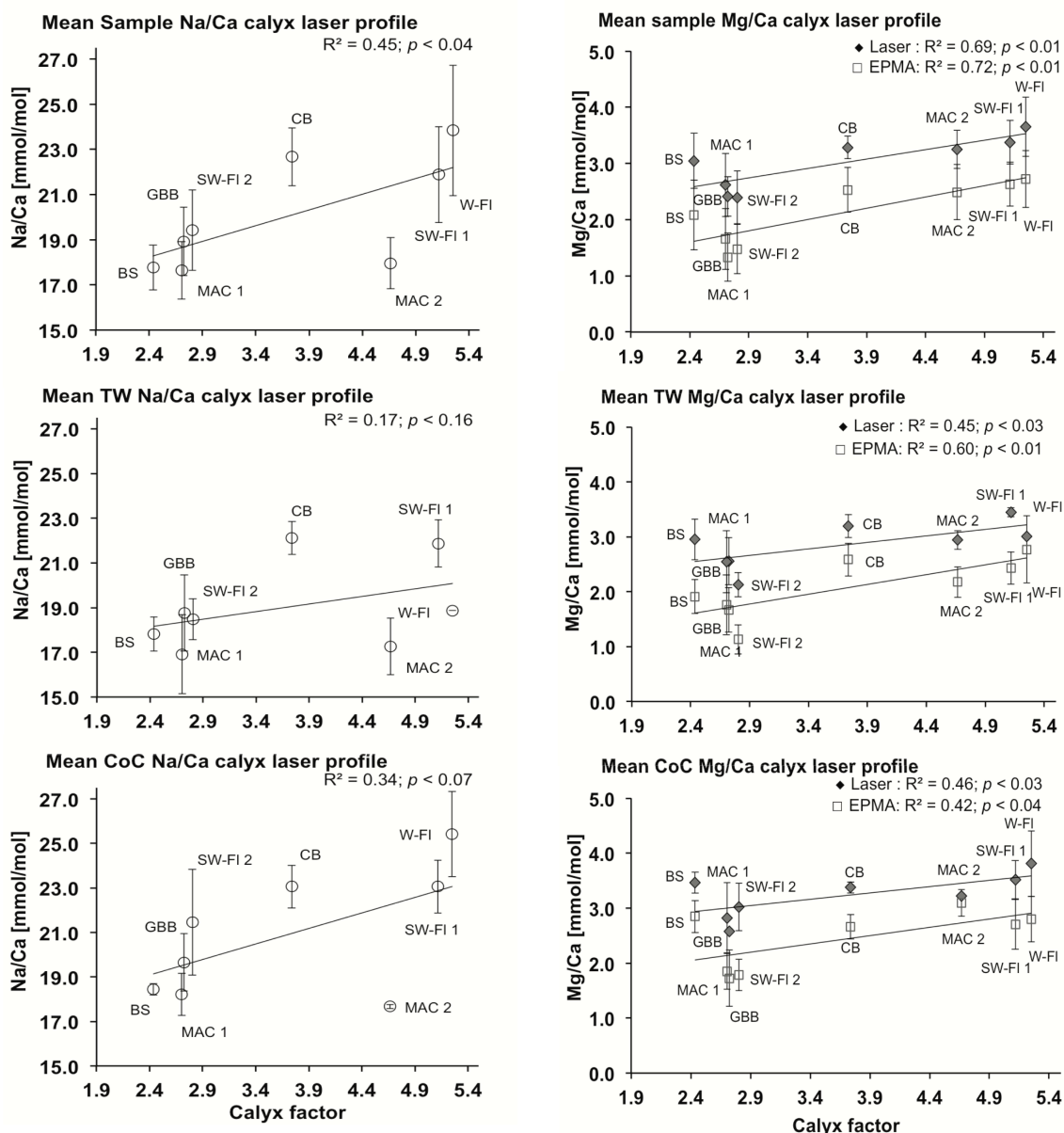
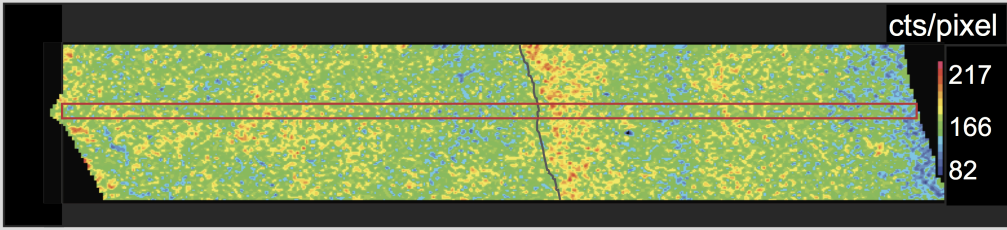
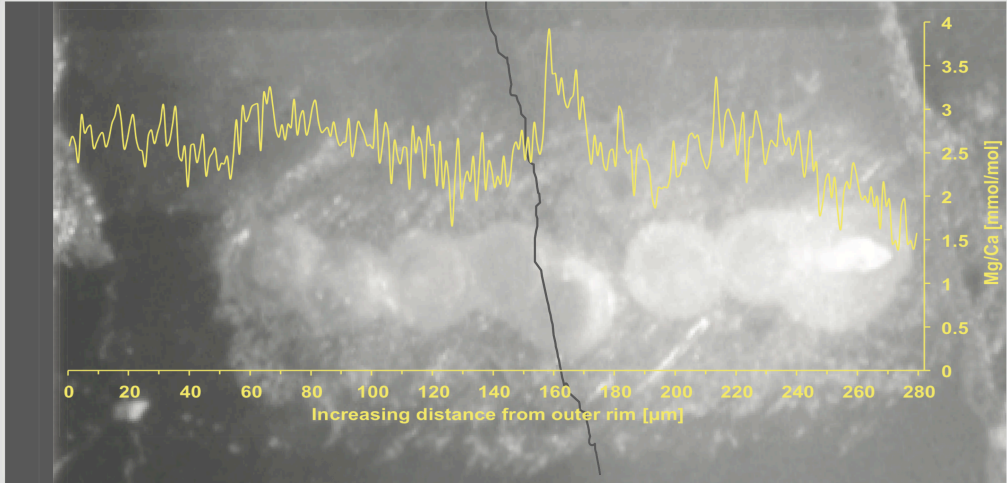


Fig. 3.7 (left) Na/Ca ratios versus Calyx factor (CF) derived from the analysed calices, differentiated in arithmetic mean sample (overview of the whole sample) *top*, the arithmetic mean TW plotted in the *middle* and the arithmetic mean CoC plotted at the *bottom*. Error bars = ± 1 SD (1σ). The linear regression, the corresponding R^2 and the p -values are given for LA-ICP-MS

Fig. 3.8 (right) Mg/Ca ratios versus Calyx factor (CF) derived from the analysed calices, differentiated in arithmetic mean sample (overview of the whole sample) *top*, the arithmetic mean TW plotted in the *middle* and the arithmetic mean CoC plotted at the *bottom*. Error bars = ± 1 SD (1σ). The linear regression, the corresponding R^2 and the p -values are given for both EPMA and LA-ICP-MS

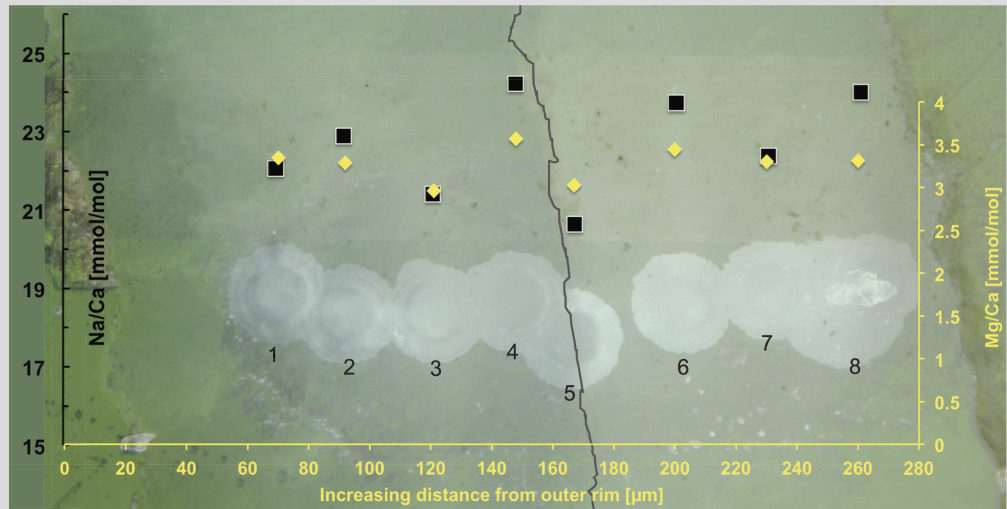


a)
EPMA
Mg



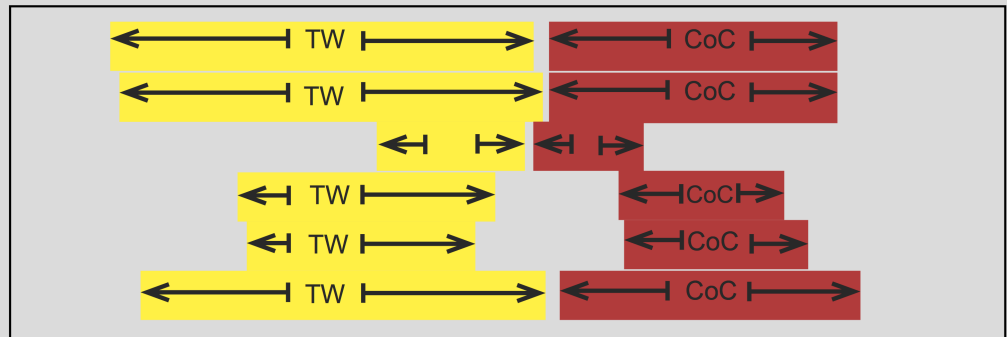
b)
EPMA
Mg/Ca

c)
Binocular
image



d)
LA-ICP-MS
Mg/Ca
Na/Ca

e)
Keyence
image



a)

b)

b)min/max

c)

d)

e)

Fig. 3.10 Mg concentrations and Me/Ca ratios derived by different methods from *L. pertusa* (GeoB16312-1; Campeche Bank) are shown to illustrate their distribution in relation to the different microstructures and are representative for all samples.

a) Semi-quantitative mapping of Mg distribution (EPMA) exhibiting low concentrations in blue (82 counts per pixel=cts/pixel) and high concentrations in red (>217 cts/pixel). The boundary between the theca wall (TW) and the center of calcification (CoC) would be assigned at ~150 μm distance from the outer rim (=DFOR). The elongated red rectangle indicates the measured profile in *b*

b) Mg/Ca ratio EPMA profile (spot size 3 μm) plotted as overlay on a black and white binocular image (*c*). The boundary between TW and CoC is almost identical to the mapping in *a*) and is located at 156 μm DFOR (Mg/Ca $1\sigma = \pm 0.4$; see Table 3). The spots refer to the LA-ICP-MS measurements in *d*)

c) The corresponding boundary between TW and CoC on the basis of the binocular image is indicated by the black line

d) The resolution of the LA-ICP-MS spot (light, large circles) is more than one order of magnitude larger than the EPMA spot. Note that the diameter of the shot spot is not similar to the diameter of the mapped spot. The boundary between TW and CoC based on minima for the TW and maxima for the CoC would assign it between spot 4 and 5. The large spot size of the laser may capture Mg/Ca ratios (mmol/mol) from the CoC crystals below the ablated surface and vice versa.

The lowest Mg/Ca ratios at spot 5 (Mg/Ca $1\sigma = \pm 0.2$; see Table 3), although visually located within the CoC, also according to the Keyence image (*e*) may result from such a “mixing” signal.

Na/Ca ratio (mmol/mol) measured by LA-ICP-MS (Na/Ca $1\sigma = \pm 1.28$; see Table 5) overlain on the Keyence image demonstrate the maximum within the TW at spot 4 and the minimum at the “mixing” signal of spot 5 within the CoC. The large spot size does not allow a clear differentiation between TW, CoC and the septum. The individual spot 8 might result from density differences within the material, or from a pore under the epoxy resin, or from an exploded crystal under the 150 shots of the laser ablation

e) Based on the Keyence© image the corresponding boundary between TW and CoC is indicated by the black line (bottom panel). Differentiation between TW and CoC on the basis of the different method *a*) – *e*) of TW (yellow) and CoC (red)

3.5 Conclusions

The aim of this research was to resolve the spatial variability of Mg/Ca, Sr/Ca and Na/Ca ratios with respect to the microstructure of the coral skeleton, e.g. TW versus CoC and the correlation / non-correlation of these Me/Ca ratios to *in-situ* seawater temperature and salinity. Normalised growth rates, calyx length / calyx diameter (CF) were used to evaluate the influence of crystal growth (kinetic effects) on these Me/Ca ratios:

- (1) A series of geochemical analyses applying EPMA and LA-ICP-MS measurements show that the spatial distributions of Mg/Ca and Na/Ca ratios in the CWC *L. pertusa* from eight environmentally different locations are strongly dependent on the skeletal architecture, i.e. differentiation between TW and CoC
- (2) The significant difference of Mg/Ca between TW and CoC, observed in previous studies, may as well strengthen the methodological approach to use Mg/Ca ratios to identify different skeletal features in CWCs
- (3) Most CoC derived Me/Ca ratios exhibit better correlations to temperature and salinity than TW derived data. Therefore, these differences can be used to differentiate geochemically between these microstructures
- (4) LA-ICP-MS spots a simple, quick, low-cost, homogenous, free from cycle-variation technique (instead of laser mapping) method is inappropriate to define the boundary between TW and CoC, since the large laser spot may „capture“ mixed signals between both. Furthermore, pre-ablation on the coral surface does not guarantee the full removal of altered material, which might be another source for mixed signals
- (5) Na/Ca data measured by LA-ICP-MS correlate negative both to salinity and temperature and correlate stronger for CoC data with respect to the TW data. This suggests a precipitation biomineralisation control (CLDs) of Na/Ca ratios in *L. pertusa* and therefore are crucial to use as a geochemical tracer
- (6) This twofold correlation in the present dataset does not allow to distinguish the primarily control of Na/Ca in the CWCs yet. Further investigations on this proxy are needed to develop it as a possible tool to reconstruct past oceanographic changes

Acknowledgments

We gratefully acknowledge the support of the MARUM (Bremen University) ROV team and Prof. Dr. Dierk Hebbeln, as well as Captain Friedhelm von Staa, his *R/V MARIA S. MERIAN* crew and the scientific shipboard party during cruise MSM20-4 in the GoM, funded by the Deutsche Forschungsgemeinschaft (DFG) and WACOM D1625–DU. A great “thank you!” also goes to Prof. Dr. Sebastian Krastel, Captain Ralf Schmidt, his crew, and the shipboard scientific party during cruise MSM32 off Morocco, funded by the DFG and the Bundesministerium für Bildung und Forschung (BMBF). We would like to thank Dr. Volker Liebetrau very much for his valuable discussions and critical comments (GEOMAR, Kiel). We express our appreciation to Dr. Nikolas Glock (GEOMAR, Kiel, binocular camera), Prof. Dr. Wolfgang Kuhnt (CAU University, Kiel, Keyence Digital High Speed Camera images), Dr. Matthias Frische and Dr. Jan Fietzke (GEOMAR, Kiel, LA-ICP-MS measurements), PD Dr. Thor Hansteen and Mario Thöner (GEOMAR, Kiel, EPMA), Dr. Steffanie Nordhausen (comments) and Dr. Marlene Wall (GEOMAR, Kiel, comments and data processing).

References

- Adkins JF, Boyle EA, Curry WB, Lutringer A (2003) Stable isotopes in deep-sea corals and a new mechanism for „vital effects“. *Geochim Cosmochim Acta* 67(6):1129–1143. doi:10.1016/S0016-7037(00)01203-6
- Allen KA, Hönisch B, Eggins SM, Haynes LL, Rosenthal Y, Yu J (2016) Trace element proxies for surface ocean conditions: A synthesis of culture calibrations with planktic foraminifera. *Geochim Cosmochim Acta* 193:197–221. doi: 10.1016/j.gca.2016.08.015
- Allison N and AA Finch (2004) High-resolution Sr/Ca records in modern *Porites lobata* corals: Effects of skeletal extension rate and architecture. *Geochem Geophys Geosyst* (5), Q05001. doi:10.1029/2004GC000696
- Allison N and Finch AA (2010) $\delta^{11}\text{B}$, Sr, Mg and B in a modern *Porites* coral: the relationship between calcification site pH and skeletal chemistry. *Geochim Cosmochim Acta* 74(6):1790–1800
- Amiel AJ, Friedmann GM, Miller DS (1973) Distribution and nature incorporation of trace elements in modern aragonitic corals. *Sedimentology* 20:47–64
- Anagnostou E, Sherell RM, Gagnon A, LaVigne M, Field MP, McDonough WF (2011) Seawater nutrient carbonate ion concentrations recorded as P/Ca, Ba/Ca, and U/Ca in the deep-sea coral *Desmophyllum dianthus*. *Geochem Geophys Geosyst* 75:2529–2543. doi:10.1016/j.gca.2011.02.019
- Beck JW, Edwards RL, Ito E, Taylor FW, Recy J, Rougerie F, Joannot P, Henin C (1992) Sea-surface temperature from coral skeletal strontium calcium ratios. *Science* 257(5070):644–647
- Blamart D, Rollion-Bard C, Cuif JP, Juillet-Leclerc A, Lutringer A, van Weering TCE, Henriot J-P (2005) C and O isotopes in a deep-sea coral (*Lophelia pertusa*) related to skeletal microstructure. In: Freiwald A, Roberts JM (eds), *Cold-Water Corals and Ecosystems*. Springer-Verlag, Berlin Heidelberg, ISBN:978-3-540-24136-2:1005–1020
- Blamart D, Rollion-Bard C, Meibom A, Cuif J-P, Juillet-Leclerc A, Dauphin Y (2007) Correlation of boron isotopic composition with ultrastructure in the deep-sea coral *Lophelia pertusa*: Implications for biomineralization and paleo-pH. *Geochem Geophys Geosyst* 8(12), Q12001. doi:10.1029/2007GC001686
- Brahmi C, Kopp C, Domart-Coulon L, Stolarski J, Meibom A (2012) Skeletal growth dynamics linked to trace-element composition in the scleractinian coral *Pocillopora damicornis*. *Geochim Cosmochim Acta* 99:146–158
- Brooke S and Young CM (2009) *In situ* measurement of survival and growth of *Lophelia pertusa* in the northern Gulf of Mexico. *Mar Ecol Prog Ser* 397:153–161. doi:10.3354/meps08344
- Buhl Mortensen P (2001) Aquarium observations on the deep-water coral *Lophelia pertusa* (L., 1758) (scleractinia) and selected associated invertebrates. *Ophelia* 54(2):83–104. doi:10.1080/00785236.2001.10409457
- Busenberg E Plummer LN (1985) Kinetic and thermodynamic factors controlling the distribution of SO_4^{2-} and Na^+ in calcites and selected aragonites. *Geochim Cosmochim Acta* 49:713–725
- Case DH, Robinson LF, Auro ME, Gagnon AC (2010) Environmental and biological controls on Mg and Li in deep-sea scleractinian corals. *Earth Plan Sci Lett* 300:215–225. doi:10.1016/j.epsl.2010.09.029
-

- Cohen AL, Layne GD and Hart SR (2001) Kinetic control of skeletal Sr/Ca in a symbiotic coral: Implications for the paleotemperature proxy. *Paleoceanography* 16. doi:10.1029/1999PA000478
- Cohen AL and McConnaughey TA (2003) Geochemical Perspectives on Coral Mineralization. In: *Biom mineralization*, edited by Dove PM, Weiner S and de Yoreo JJ. *Rev Mineral Geochem* 54:151–187. doi:10.2113/0540151
- Cohen AL, Gaetani GA, Lundälv T, Corliss BH, George RY (2006) Compositional variability in a cold-water scleractinian, *Lophelia pertusa*: New insights into “vital effects”. *Geochem Geophys Geosyst* 7(12):Q12004. doi:10.1029/2006GC001354
- Cuif J-P, Dauphin Y (1998) Microstructural and physico-chemical characterization of 'centers of calcification' in septa of some Recent scleractinian corals. *Pal Zeitschrift* 72(3/4):257–270
- Cuif J-P, Lecointre G, Perrin C, Tillier A & Tillier S (2003) Patterns of septal biomineralization in Scleractinia compared with their rRNA phylogeny: a dual approach for a new taxonomic framework. *Zoologica Scripta* 32(5):459–473. doi:10.1046/j.1463-6409.2003.00133.x
- Davies AJ, Wisshak M, Orr JC, Roberts JM (2008) Predicting suitable habitat for the cold-water coral *Lophelia pertusa* (Scleractinia). *Deep-Sea Res I* (55):1048–1062. doi:10.1016/j.dsr.2008.04.010
- DePaolo DJ (2011) Surface kinetic model for isotopic and trace element fractionation during precipitation of calcite from aqueous solutions. *Geochim Cosmochim Acta* 75:1039–1056. doi:10.1016/j.gca.2010.11.020
- Dissard D, Nehrke G, Reichart GJ, Bijma J (2010) Impact of seawater $p\text{CO}_2$ on calcification and Mg/Ca and Sr/Ca ratios in benthic foraminifera calcite: results from culturing experiments with *Ammonia tepida*. *Biogeoscience* 7:81–93
- Dullo W-C, Flögel S, Rüggeberg A (2008) Cold-water coral growth in relation to the hydrography of the Celtic and Nordic European continental margin. *Mar Ecol Prog Ser* 371:165–176. doi:10.3354/meps07623
- Fietzke J and Frische M (2016) Experimental evaluation of elemental behaviour during LA-ICP-MS: influences of plasma conditions and limits of plasma robustness. *J Anal Atom Spec* 31:234–244. doi:10.1039/c5ja00253b
- Fietzke J, Ragazzola F, Halfar J, Dietze H, Foster LC, Hansteen TH, Eisenhauer A and Steneck RS (2015) Century-scale trends and seasonality in pH and temperature for shallow zones of the Bering Sea. *PNAS* 112(10):2960–2965. doi:10.1073/pnas.1419216112
- Flögel S, Dullo W-Chr, Pfannkuche O, Kiriakoulakis K, Rüggeberg A (2014) Geochemical and physical constraints for the occurrence of living cold-water corals. *Deep-Sea Res II* 99:19–26. doi:10.1016/j.dsr2.2013.06.006
- Freiwald A, Henrich R, Pätzold J (1997) Anatomy of a deep-water coral reef mound from Stjernsund, West-Finnmark, northern Norway. In: James NP, Clarke JAD (eds) *Cool-water carbonates*. SEPM, Special Publication 56:141–161
- Freiwald A and Wilson JB (1998) Taphonomy of modern deep, cold-temperate water coral reefs. *Historical Biology* 13:37–52

- Freiwald A, Fosså JH, Grehan A, Koslow T and Roberts JM (2004) Cold-water coral reefs. UNEP-WCMC, Cambridge, UK, pp 84
- Gabitov RI and Watson EB (2006) Partitioning of strontium between calcite and fluid. *Geochem Geophys Geosyst* 7(11):Q11004. doi:10.1029/2005GC001216
- Gagnon AC, Adkins JF, Fernandez DP, Robinson LF (2007) Sr/Ca and Mg/Ca vital effects correlated with skeletal architecture in a scleractinian deep-sea coral and the role of Rayleigh fractionation. *Earth Plan Sci Lett* 261:280–295. doi:10.1016/j.epsl.2007.07.013
- Gass SE, Roberts JM (2006) The occurrence of the cold-water coral *Lophelia pertusa* (Scleractinia) on oil and gas platforms in the North Sea: Colony growth, recruitment and environmental controls on distribution. *Mar Poll Bull* 52:549–559. doi:10.1016/j.marpolbul.2005.10.002
- Gass SE, Roberts JM (2010) Growth and branching patterns of *Lophelia pertusa* (Scleractinia) from the North Sea. *J Mar Bio Ass* 91(4):831–835. doi:10.1017/S002531541000055X
- Gladfelter WB (1982) White-band disease in *Acropora palmata*: Implications for the structure and growth of shallow reefs. *Bull Mar Sci* 32(2):639–643
- Gladfelter EH (1983) Skeletal development in *Acropora cervicornis*, II. Diel patterns of calcium carbonate accretion. *Coral Reefs* 2(2):91–100. doi:10.1007/BF_02395279
- Glogowski S, Dullo W-C, Feldens P, Liebetau V, von Reumont J, Hühnerbach V, Krastel S, Wynn RB, Flögel S (2015) The Eugen Seibold coral mounds offshore western Morocco: oceanographic and bathymetric boundary conditions of a newly discovered cold-water coral province. *Geo-Mar Lett* 35(4):257–269. doi:10.1007/s00367-015-0405-7
- Gothmann AM, Stolarski J, Adkins JF, Schoene B, Dennis KJ, Schrag DP, Matzur M, Bender ML (2015) Fossil corals as an archive of secular variations in seawater chemistry since the Mesozoic. *Geochim Cosmochim Acta* 160:188–208. doi:10.1016/j.gca.2015.03.018
- Grasmueck M, Eberli GP, Correa TBS, Viggiano DA, Luo J, RSMAS University of Miami; Wyatt GJ, Qvester Tangent; Reed JK, Wright AE and Pomponi SA, Harbor Branch Oceanographic Institution (2007) AUV-Based Environmental Characterization of Deep-Water Coral Mounds in the Straits of Florida. Offshore Technology Conference, held in Houston, Texas, U.S.A., 30 April–3 May 2007, OTC 18510
- Hathorne EC, Gagnon A, Felis T, Adkins J, Asami R, Boer R, Caillon N, Case D, Cobb KM, Douville E, deMenocal P, Eisenhauer A, Garbe-Schönberg D, Geibert W, Goldstein S, Hughen K, Inoue M and Kawahata H, Kölling M, Cornec FL, Linsley BK, McGregor HV, Montagna P, Quinn TM, Raddatz J, Robinson L, Sadekov A, Sherrell R, and Sinclair D, Tudhope AW, Wei G, Wong H, Wu HC, You C-F (2013) Interlaboratory study for coral Sr/Ca and other element/Ca ratio measurements. *Geochem Geophys Geosyst* 14(9):3730–3750. doi:10.1002/ggge.20230
- Hebbeln D, Wienberg C, Wintersteller P, Freiwald A, Becker M, Beuck L, Dullo C, Eberli GP, Glogowski S, Matos L, Forster N, Reyes-Bonilla H, Taviani M and the MSM 20-4 shipboard scientific party (2014) Environmental forcing of the Campeche cold-water coral province, southern Gulf of Mexico. *Biogeosciences* 11:1799–1815. doi:10.5194/bg-11-1799-2014
- Holcomb M, Cohen AL, Gabitov RI, Hutter JL (2009) Compositional and morphological features of aragonite. *Geochim Cosmochim Acta* 73:4166–4179. doi:10.1016/j.gca.2009.04.015

- Hoppe P, Cohen S, Meibom A (2013) NanoSIMS: Technical Aspects and Applications in Cosmochemistry and Biological Geochemistry. *Geostand Geoanal Res*, I Ass Geoanal 37(2):111–154. doi:10.1111/j.1751-908X.2013.00239.x
- Jarosewich E and MacIntyre IG (1983) Carbonate reference samples for electron microprobe and scanning electron microscope analyses. *J Sedimentary Res* 53(2):677–678
- Jarosewich E (2002) Smithsonian Microbeam Standards. *J Res Natl Inst Stand Technol* 107:681–685
- Jochum KP, Weis U, Stoll B, Kuzmin D, Yang Q, Raczek I, Jacob DE, Stracke A, Birbaum K, Frick DA, Günther D,ENZWEILER J (2011) Determination of reference values for NIST SRM 610–617 glasses following ISO guidelines. *Geostand Geoanal Res* 35(4):397–429
- Kinsman DJJ (1970) Trace cations in aragonite. *Geol Soci Am* 2:596–597
- Kiriakoulakis K, Bett BJ, White M, Wolff GA (2004) Organic biogeochemistry of the Darwin Mounds, a deep-water coral ecosystem of the NE Atlantic. *Deep-Sea Res I* 51:1937–1954. doi:10.1016/j.dsr.2004.07.010
- Linné C (1758) *Systema naturae*. “The system of Nature”
- Lutringer A, Blamart D, Frank N, Labeyrie L (2005) Paleotemperatures from deep-sea corals: scale effects. In: Freiwald A, Roberts JM (eds), *Cold-Water Corals and Ecosystems*. Springer-Verlag, Berlin Heidelberg, ISBN:978-3-540-24136-2, pp 1081–1096
- McConnaughey T (1989) ¹³C and ¹⁸O isotopic disequilibrium in biological carbonates: I. Patterns. *Geochim Cosmochim Acta* 53:151–162
- McDougall TJ and Barker PM (2011) Getting started with TEOS–10 and the Gibbs Seawater (GSW) Oceanog Toolbox, 28 pp, version 3.0. SCOR/IAPSO WG127, www.TEOS-10.org
- Meibom A, Cuif J-P, Hillion F, Constantz BR, Juillet-Leclerc A, Dauphin Y, Watanabe T and Dunbar RB (2004) Distribution of magnesium in coral skeleton. *Geophys Res Lett* 31, L23306. doi:10.1029/2004GL021313
- Meibom A, Cuif JP, Hillion F, Constantz BR, Juillet-Leclerc A, Dauphin Y, Watanabe T and Dunbar RB 2007. Biological forcing controls the chemistry of reef-building coral skeleton. *Geophys Res Lett* 34, L02601. doi:10.1029/2006GL028657
- Meibom A, Cuif J-P, Houlbreque F, Mostefaoui S, Dauphin Y, Meibom KL, Dunbar R (2008) Compositional variations at ultra-structure length scales in coral skeleton. *Geochim Cosmochim Acta* 72:1555–1569. doi:10.1016/j.gca.2008.01.009
- Mezger EM, de Nooijer LJ, Boer W, Brummer GJA, and Reichert GJ (2016) Salinity controls on Na incorporation in Red Sea planktonic foraminifera. *Paleoceanography* 31(12):1562–1582. doi: 10.1002/2016PA003052
- Mienis F, Duineveld GCA, Davies AJ, Ross SW, Seim H, Bane J, vanWeering TCE (2012) The influence of near-bed hydrodynamic conditions on cold-water corals in the Viosca Knoll area, Gulf of Mexico. *Deep-Sea Res I* 60:32–45. doi:10.1016/j.dsr.2011.10.007
- Mitsugushi T, Uchida T, Matsumoto E, Isdale PJ and Kawana T (2001) Variations in Mg/Ca, Na/Ca, and Sr/Ca ratios of coral skeletons with chemical treatments: Implications for carbonate geochemistry. *Geochim Cosmochim Acta* 65(17):2865–2874
- Mitsugushi T, Uchida T, Matsumoto E (2010) Na/Ca variability in coral skeletons. *Geochem J* 44:261–273. doi:10.2343/geochemj.1.0067

- Montagna P, McCulloch M, Taviani M, Remia A, Rouse G (2005) High-resolution trace and minor element compositions in deep-water scleractinian corals (*Desmophyllum dianthus*) from the Mediterranean Sea and the Great Australian Bight. In: Freiwald A, Roberts JM (eds), Cold-Water Corals and Ecosystems. Springer-Verlag, Berlin Heidelberg, ISBN:978-3-540-24136-2:1109–1126
- Montagna P, McCulloch M, Douville E, López Correa M, Trotter J, Rodolfo-Metalpa R, Dissard D, Ferrier-Pagès C, Frank N, Freiwald A, Goldstein S, Mazzoli C, Reynaud S, Rüggeberg A, Russo S, Taviani M (2014) Li/Mg systematics in scleractinian corals: Calibration of the thermometer. *Geochim Cosmochim Acta* 132:288–310. doi:10.1016/j.gca.2014.02.005
- Montero-Serrano J-C, Frank N, Tisnérat-Laborde N, Colin C, Wu C-C, Lin K, Shen C-C, Copard K, Orejas C, Gori A, De Mol L, Van Rooij D, Reverdin G, Douville E (2013) Decadal changes in the mid-depth water mass dynamic of the Northeastern Atlantic margin (Bay of Biscay). *Earth Plan Sci Lett* 364:134–144. doi.org/10.1016/j.epsl.2013.01.012
- Okumura M and Kitano Y (1986) Coprecipitation of alkali metal ions with calcium carbonate. *Geochim Cosmochim Acta* 50:49–58
- Paquette J and Reeder RJ (1995) Relationship between surface structure, growth mechanism, and trace element incorporation in calcite. *Geochim Cosmochim Acta* 59:735–749
- Raddatz J, Liebetrau V, Rüggeberg A, Hathorne E, Krabbenhöft A, Eisenhauer A, Böhm F, Vollstaedt H, Fietzke J, López Correa M, Freiwald A, Dullo W-C (2013) Stable Sr-isotope, Sr/Ca, Mg/Ca, Li/Ca and Mg/Li ratios in the scleractinian cold-water coral *Lophelia pertusa*. *Chem Geol* 352:143–152. doi:10.1016/j.chemgeo.2013.06.013
- Raddatz J, Rüggeberg A, Liebetrau V, Foubert A, Hathorne EC, Fietzke J, Eisenhauer A, Dullo W-Chr (2014a) Environmental boundary conditions of cold-water coral mound growth over the last 3 million years in the Porcupine Seabight, Northeast Atlantic. *Deep-Sea Res II* 99:227–236. doi:10.1016/j.dsr.2.2013.06.009
- Raddatz J, Rüggeberg A, Flügel S, Hathorne EC, Liebetrau V, Eisenhauer A and Dullo W-Chr (2014b) The influence of seawater pH on U/Ca ratios in the scleractinian cold-water coral *Lophelia pertusa*. *Biogeosciences* 11:1863–1871. doi:10.5194/bg-11-1863-2014
- Raddatz J, Liebetrau V, Trotter J, Rüggeberg A, Flügel S, Dullo W-C, Eisenhauer A, Voigt S, McCulloch M (2016) Environmental constraints on Holocene cold-water reef growth off Norway: Insights from a multiproxy approach. *Paleoceanography* 31(10):1350–1367. doi:10.1002/2016PA002974
- Ragland PC, Pilkey OH, Blackwelder BW (1979) Diagenetic changes in the elemental composition of unrecrystallized mollusk shells. *Chem Geol* 25:123–134
- Reay A, Johnstone RD, Kawachi Y (1993) Anorthoclase, a second microprobe standard from Kakanui, New Zealand. *Geostand Newslett* 17:135–136
- Reeder RJ (1996) Interaction of divalent Co, Zn, Cd, and Ba with the calcite surface during layer growth. *Geochim Cosmochim Acta* 60:1543–1552
- Roberts JM, Wheeler AJ, Freiwald A (2006) Reefs of the deep: the biology and geology of cold-water coral ecosystems. *Science* 312:543–547. doi:10.1126/science.1119861
- Robinson LF, Adkins JF, Frank N, Gagnon AC, Prouty NG, Roark EB, Flierdt T (2006) The geochemistry of deep-sea coral skeletons: A review of vital effects and applications for palaeoceanography. *Deep-Sea Res II* 99:184–198. doi: 10.1016/j.dsr.2013.06.005

- Rollion-Bard C, Chaussidon M, France-Lanord C (2003) pH control on oxygen isotopic composition of symbiotic corals. *Earth Plan Sci Lett* 215:275–288. doi:10.1016/S0012-821X(03)00391-1
- Rollion-Bard C, Vigier N, Meibom A, Blamart D, Reynaud S, Rodolfo-Metalpa R, Martin S, Gattuso J-P (2009) Effect of environmental conditions and skeletal ultrastructure on the Li isotopic composition of scleractinian corals. *Earth Plan Sci Lett* 286:63–70. doi:10.1016/j.epsl.2009.06.015
- Rollion-Bard C, Blamart D, Cuif J-P, Dauphin Y (2010) *In situ* measurements of oxygen isotopic composition in deep-sea coral, *Lophelia pertusa*: Re-examination of the current geochemical models of biomineralization. *Geochim Cosmochim Acta* 74:1338–1349. doi:10.1016/j.gca.2009.11.011
- Rollion-Bard C, Blamart D (2014) SIMS method and examples of applications in coral biomineralization. In: Gower LB, DiMasi E (eds), *Biomineralization Handbook. Characterization of Biominerals and Biomimetic Materials*. Taylor & Francis, United Kingdom:249–260
- Rollion-Bard C, Blamart D (2015) Possible controls on Li, Na and Mg incorporation into aragonite coral skeletons. *Chem Geol* 396:98–111. doi:10.1016/j.chemgeo.2014.12.011
- Rüggeberg A, Fietzke J, Liebetrau V, Eisenhauer A, Dullo W-C, Freiwald A (2008) Stable strontium isotopes ($\delta^{88/86}\text{Sr}$) in cold-water corals — A new proxy for reconstruction of intermediate ocean water temperatures. *Earth Plan Sci Lett* 269:570–575. doi:10.1016/j.epsl.2008.03.002
- Schlitzer R (2013) Ocean Data View. <http://odv.awi.de>
- Shirai K, Kusakabe M, Nakai S, Ishii T, Watanabe T, Hiyagon H, Sano Y (2005) Deep-sea coral geochemistry: Implication for the vital effect. *Chem Geol* 224:212–222. doi:10.1016/j.chemgeo.2005.08.009
- Shirai K, Kawashima T, Sowa K, Watanabe T, Nakamori T, Takahata N, Amakawa H, Sano Y (2008) Minor and trace element incorporation into branching coral *Acropora nobilis* skeleton. *Geochim Cosmochim Acta* 72:5386–5400. doi: 10.1016/j.gca.2008.07.026
- Sinclair DJ, Kinsley LPJ, McCulloch MT (1998) High resolution analysis of trace elements in corals by laser ablation ICP-MS. *Geochim Cosmochim Acta* 62(11):1889–1901
- Sinclair DJ, Sherwood OA, Risk MJ, Hillaire-Marcel C, Tubrett M, Sylvester P, McCulloch M, Kinsley L (2005) Testing the reproducibility of Mg/Ca profiles in the deep-water coral *Primnoa resedaeformis*: putting the proxy through its paces. In: Freiwald A, Roberts JM (eds), *Cold-water Corals and Ecosystems*. Springer-Verlag, Berlin Heidelberg:1039–1060
- Sinclair DJ, Williams B and Risk M (2006) A biological origin for climate signals in corals – Trace element ‘vital effects’ are ubiquitous in Scleractinian coral skeletons. *Geophys Res Lett* 33, L17707. doi:10.1029/2006GL027183
- Smith SV, Buddemeier RW, Redalje RC, Houck JE (1979) Strontium–calcium thermometry in coral skeletons. *Science* 204(4391):404–407. doi: 10.1126/science.204.4391.404
- Smith JE, Schwarcz HP, Risk MJ, McConnaughey TA, Keller N (2000) Paleotemperatures From Deep-Sea Corals: Overcoming ‘Vital Effects’. *BioOne Palaios* 15(1):25–32. doi:10.1669/0883-1351

- Stolarski J (2003) Three-dimensional micro- and nanostructure characteristics of the scleractinian coral skeleton: a biocalcification proxy. *Acta Palaeo Polonica* 48:497–530
- Swart P (1981) The strontium, magnesium and sodium composition of recent scleractinian coral skeletons as standards for palaeoenvironmental analysis. *Palaeogeogr Palaeoclimatol Palaeoecol* 34:115–136
- Urey HC, Lowenstam HA, Epstein S, McKinney CR (1951) Measurement of paleotemperatures and temperatures of the upper cretaceous of England, Denmark, and the southeastern United States. *Bull Geol Soc America* 62(4):399–416
- van de Locht R, Verch A, Saunders M, Dissard D, Rixen T, Moya A, Kröger R (2013) Microstructural evolution and nanoscale crystallography in scleractinian coral spherulites. *J Struc Biol* 183:57–65. doi:10.1016/j.jsb.2013.05.005
- Wainwright SA (1964) Studies of the mineral phase of coral skeleton. *Exp Cell Res* 34:213–230
- Weber JN and Woodhead PMJ (1972) Temperature dependence of oxygen-18 concentration in reef coral carbonates. *J Geophys Res* 77:463–473. doi:10.1029/JC077i003p00463
- Weiss Y, Griffin WL, Elhlou S, Navon O (2008) Comparison between LA-ICP-MS and EPMA analysis of trace elements in diamonds. *Chem Geol* 252:158–168. doi:10.1016/j.chemgeo.2008.02.008
- Wells JW (1956) Treatise on Invertebrate Paleontology, Part F, Scleractinia. Geol Soc Am and University of Kansas Press, New York and Lawrence/Kansas, Scleractinia. In: Moore RC (eds), pp F328–F344
- White AF (1977) Sodium and potassium coprecipitation in aragonite. *Geochim Cosmochim Acta* 41:613–625
- White M, Roberts JM, van Weering T (2007) Do bottom-intensified diurnal tidal currents shape the alignment of carbonate mounds in the NE Atlantic? *Geo-Mar Lett* 27:391–397. doi:10.1007/s00367-007-0060-8
- Wit JC, de Nooijer LJ, Wolthers M, Reichardt GJ (2013) A novel salinity proxy based on Na incorporation into foraminiferal calcite. *Biogeosciences* 10:6375–6387. doi:10.5194/bg-10-6375-2013
- Yoshimura T, Tamenori Y, Suzuki A, Kawahata H, Iwasaki N, Hasegawa H, Nguyen LT, Kuroyanagi A, Yamazaki T, Kuroda J, Ohkouchi N (2017) Altrivalent substitution of sodium for calcium in biogenic calcite and aragonite. *Geochim Cosmochim Acta* 202:21–38. doi:10.1016/j.gca.2016.12.003

Supplementary Material

Fig. 3.1 Coral sample locations. Gulf of Mexico (GoM; MSM20-4), CB = Campeche Bank, W-FI = West-Florida Slope, SW-FI (1,2) = South-West-Florida Slope. Left: West-Atlantic (MSM20-4), BS = Bimini Slope, GBB = Great Bahama Bank. Right: East-Atlantic (MSM32), MAC (1,2) = Morocco

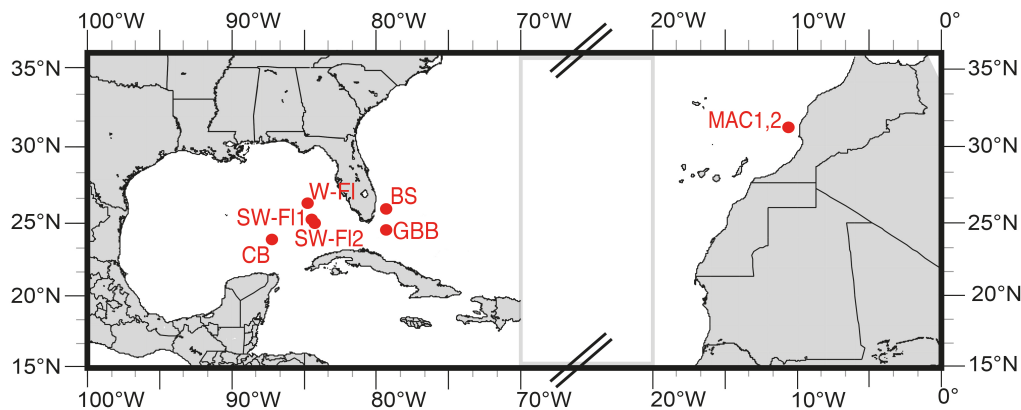


Fig. 3.2 a) ROV image showing the coral habitat at the Campeche Bank (image copyright MARUM, Bremen, ROV Cherokee team, MSM20-4). Note the squat lobster within. b) – c) Sample GeoB16312-1, b) the analysed calyx shown within the red rectangle and c) the resin embedded, polished *L. pertusa*. The red point within the red rectangle indicates the location used for geochemical analyses exactly (in order to avoid the organic interior lining in brownish colour)

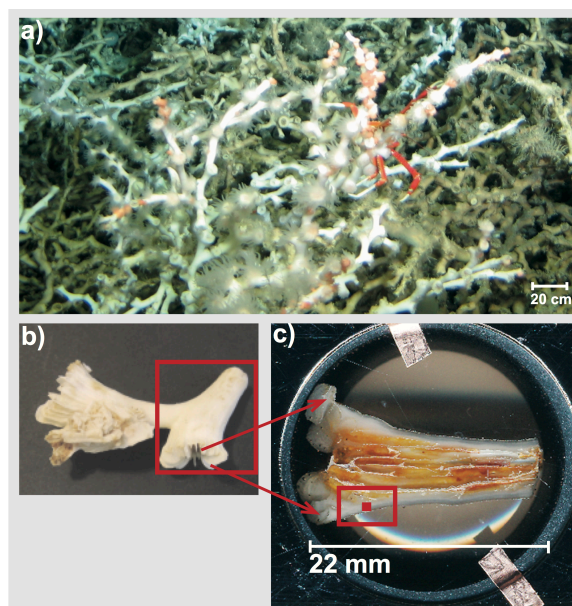


Fig. 3.3 Mg/Ca ratios (mmol/mol) versus *in-situ* temperature (°C) derived by EPMA and LA-ICP-MS in *L. pertusa*, differentiated in arithmetic mean sample (overview of the whole sample) *top*, the arithmetic mean TW plotted in the *middle* and the arithmetic mean CoC plotted at the *bottom*. Error bars = ±1 SD (1σ). The linear regression, the corresponding R^2 and the p -values are given for both EPMA and LA-ICP-MS. Arithmetic mean enrichment factors are presented at Table 3.3

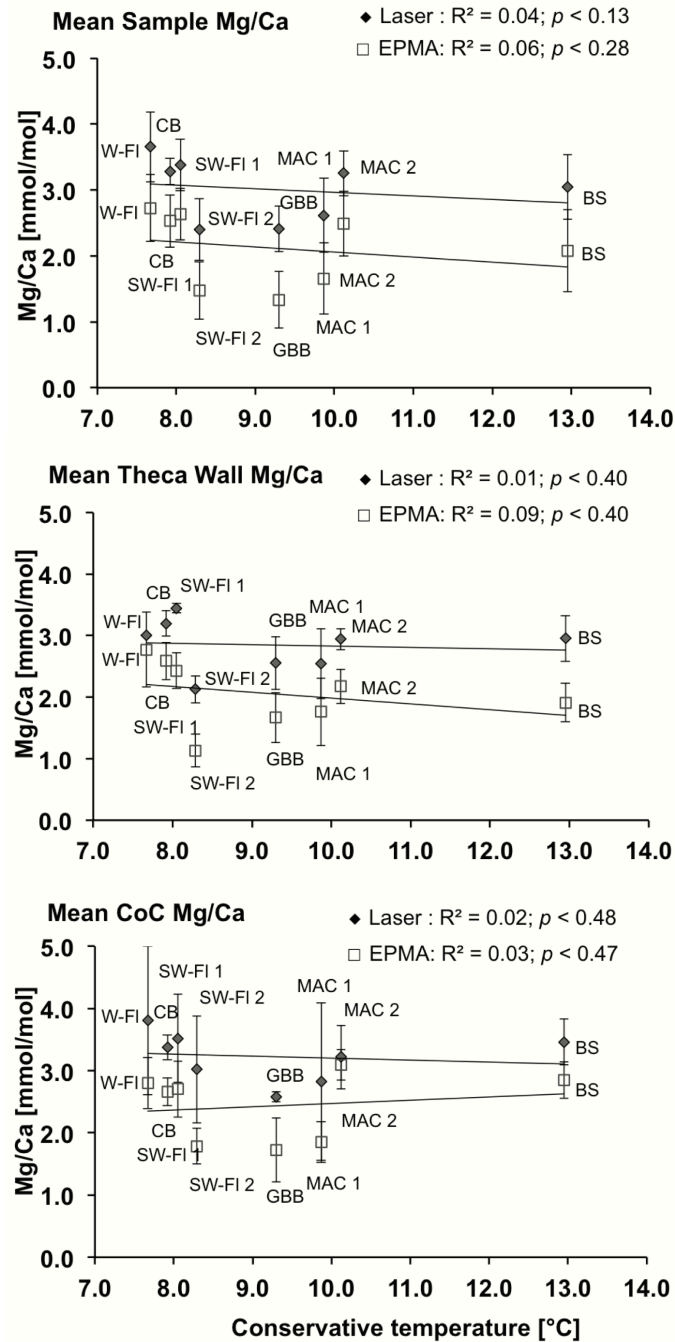
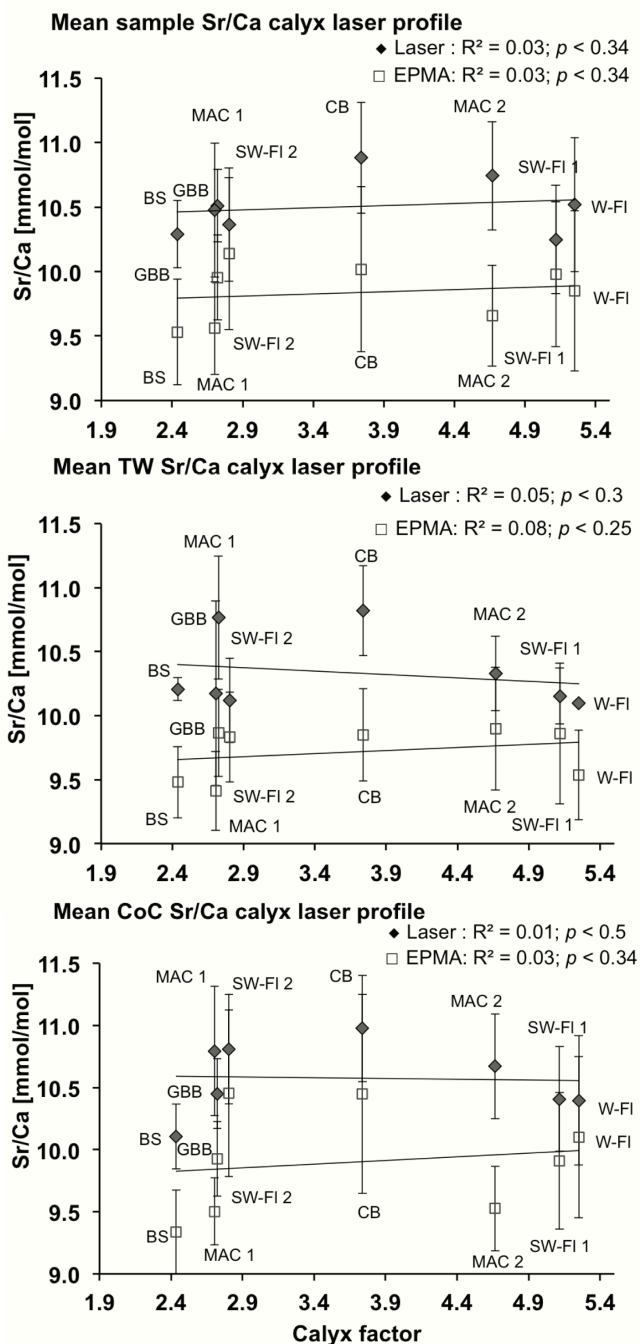


Fig. 3.9 Sr/Ca ratios versus Calyx factor (CF) derived from the analysed calices, differentiated in arithmetic mean sample (overview of the whole sample) *top*, the arithmetic mean TW plotted in the *middle* and the arithmetic mean CoC plotted at the *bottom*. Error bars = ± 1 SD (1σ). The linear regression, the corresponding R^2 and the p -values are given for both EPMA and LA-ICP-MS



Supplementary Material

Fig. 3.a Sample GeoB16312-1 under a) binocular-microscope-camera and b) Keyence-Digital-Highspeed-Camera. Images display sections from the TW to the CoC. The EPMA analyses track is indicated by the thin rectangle above the laser spots (white circles). The CoC exhibits lighter colours in contrast to the TW and is indicated by the black line

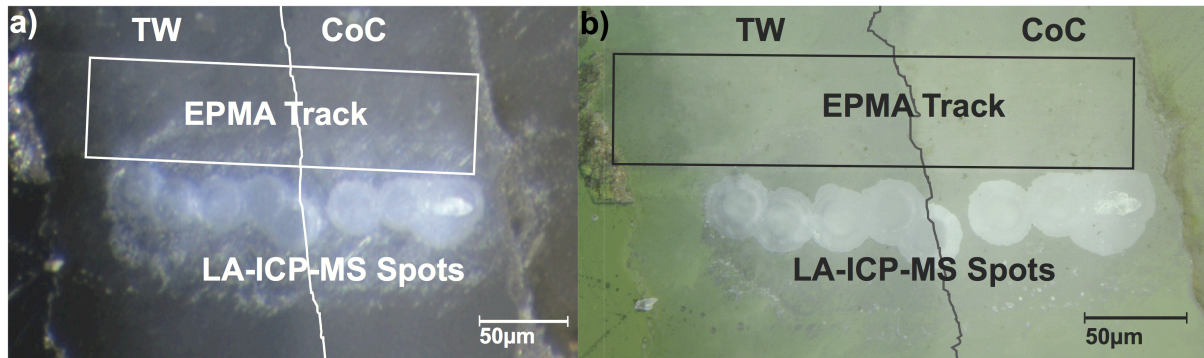


Fig. 3.b Position of measurements in *L. pertusa* sample GeoB16347-1 (SW-F11) of calyx length and calyx diameters a) used for mean sample (1 – 6), and b) used for geochemical analyses (7 – 8)

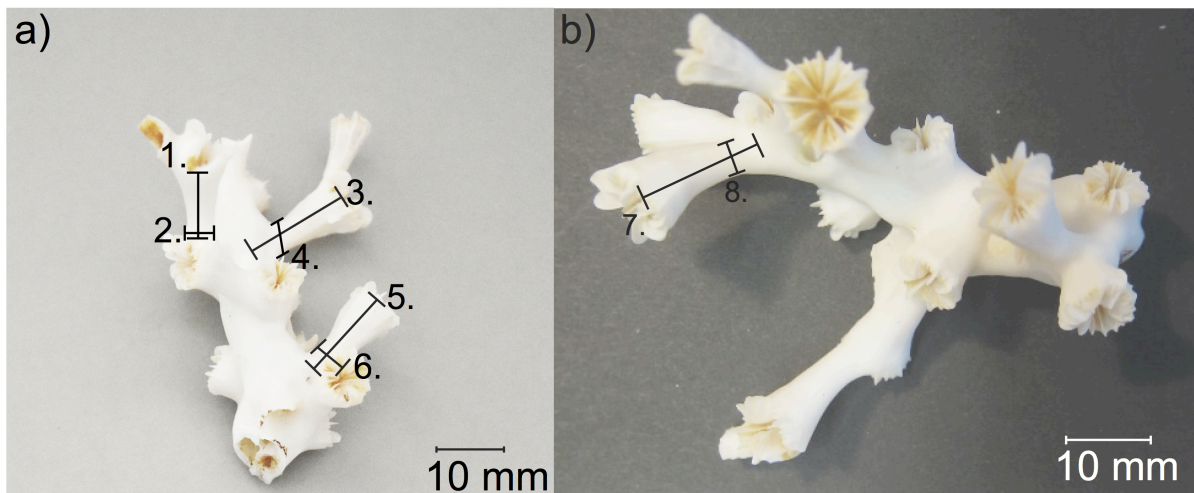


Fig. 3.c Mg/Ca ratios (mmol/mol) versus *in-situ* salinity (g/kg) of EPMA and LA-ICP-MS in *L. pertusa*, differentiated in arithmetic mean sample (overview of the whole sample) *top*, the arithmetic mean TW plotted in the *middle* and the arithmetic mean CoC plotted at the *bottom*. Error bars = ± 1 SD (1σ). The linear regression, the corresponding R^2 and the p -values are given for both EPMA and LA-ICP-MS. Arithmetic mean enrichment factors are presented at Table 3.3. n = the number of individual data points

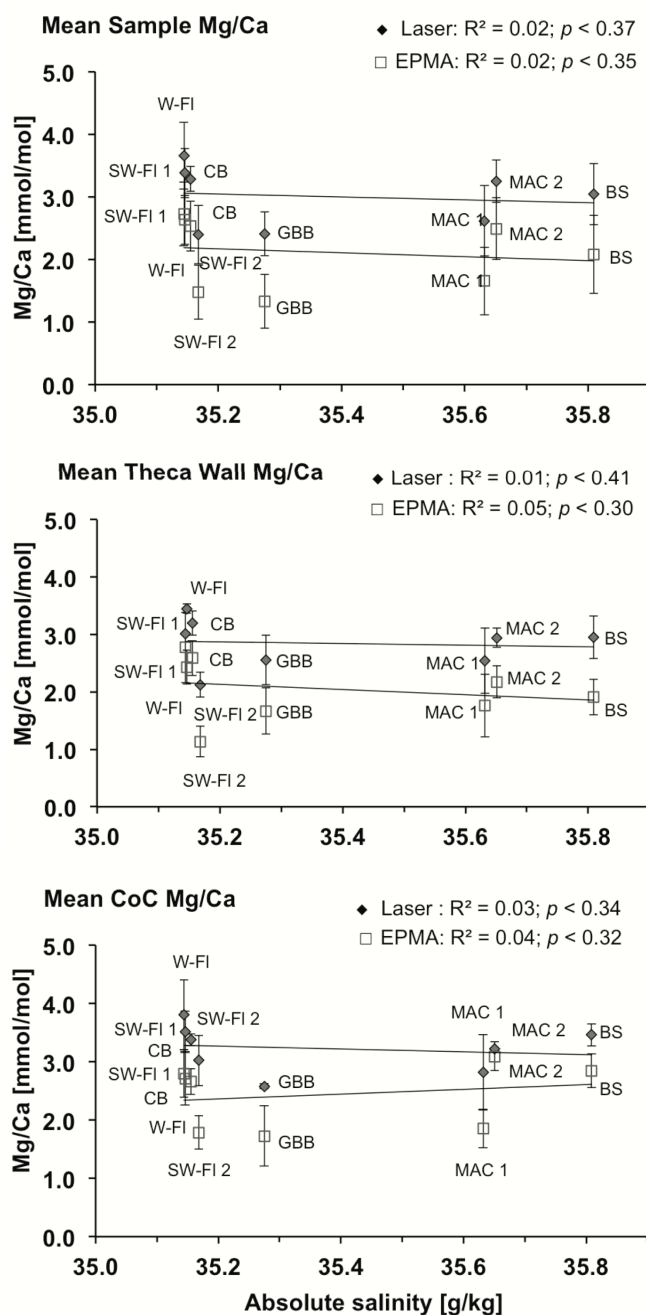


Fig. 3.d Sr/Ca ratios (mmol/mol) versus *in-situ* salinity (g/kg) of EPMA and LA-ICP-MS in *L. pertusa*, differentiated in arithmetic mean sample (overview of the whole sample) *top*, the arithmetic mean TW plotted in the *middle* and the arithmetic mean CoC plotted at the *bottom*. Error bars = ± 1 SD (1σ). The linear regression, the corresponding R^2 and the p -values are given for both EPMA and LA-ICP-MS. Arithmetic mean enrichment factors are presented at Table 3.4

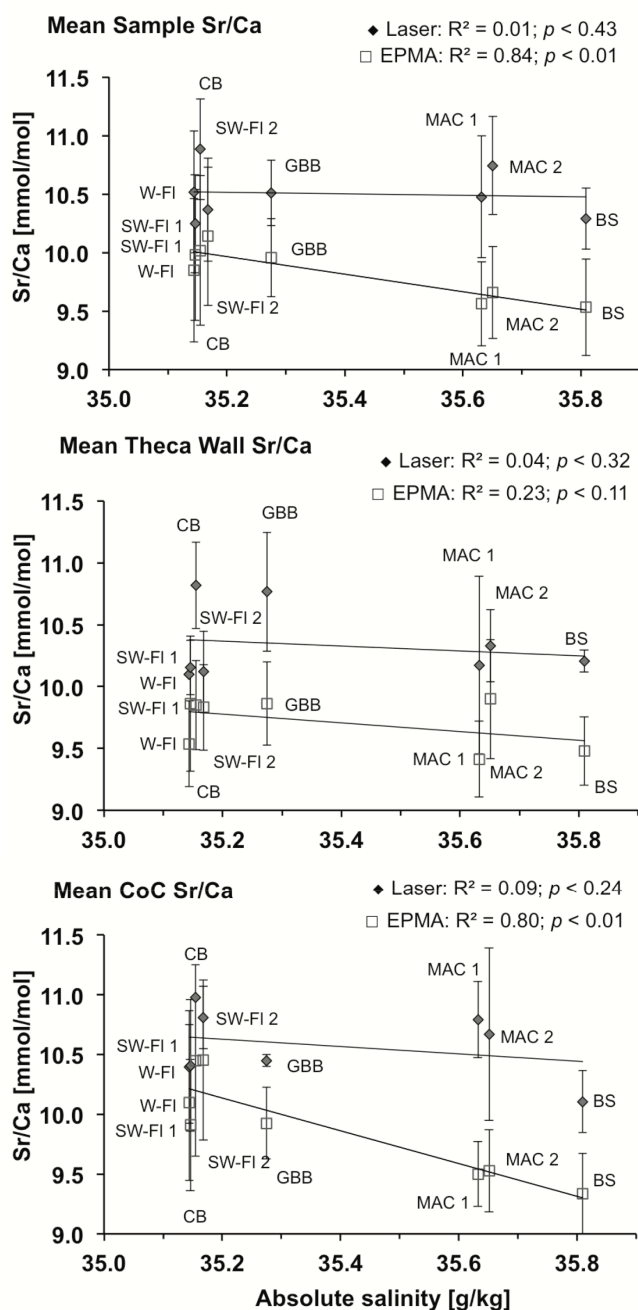


Fig. 3.e top) Calyx length (mm) versus calyx diameters (mm) used for calculating the calyx Factor (CF), differentiated in all arithmetic mean sample at the *top* and the calyx used for geochemical analyses at the *bottom* plot

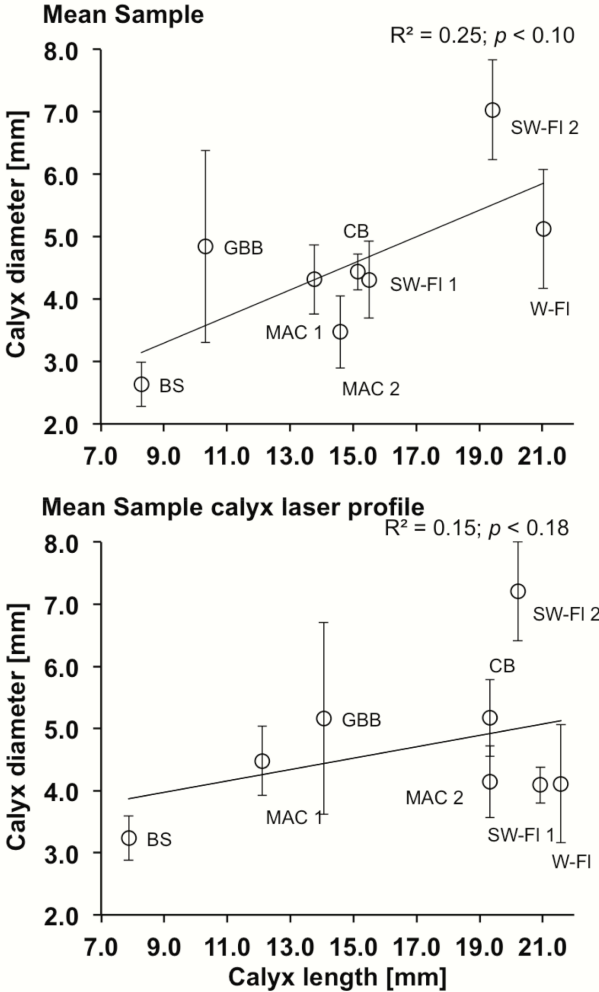


Fig. 3.f Na/Ca ratios versus Calyx factor (CF) derived from all analysed samples, differentiated in arithmetic mean sample (overview of the whole sample) *top*, the arithmetic mean TW plotted in the *middle* and the arithmetic mean CoC plotted at the *bottom*. The linear regression, the corresponding R^2 and the p -values are given for measurements applied by LA-ICP-MS. Error bars = ± 1 SD (1σ)

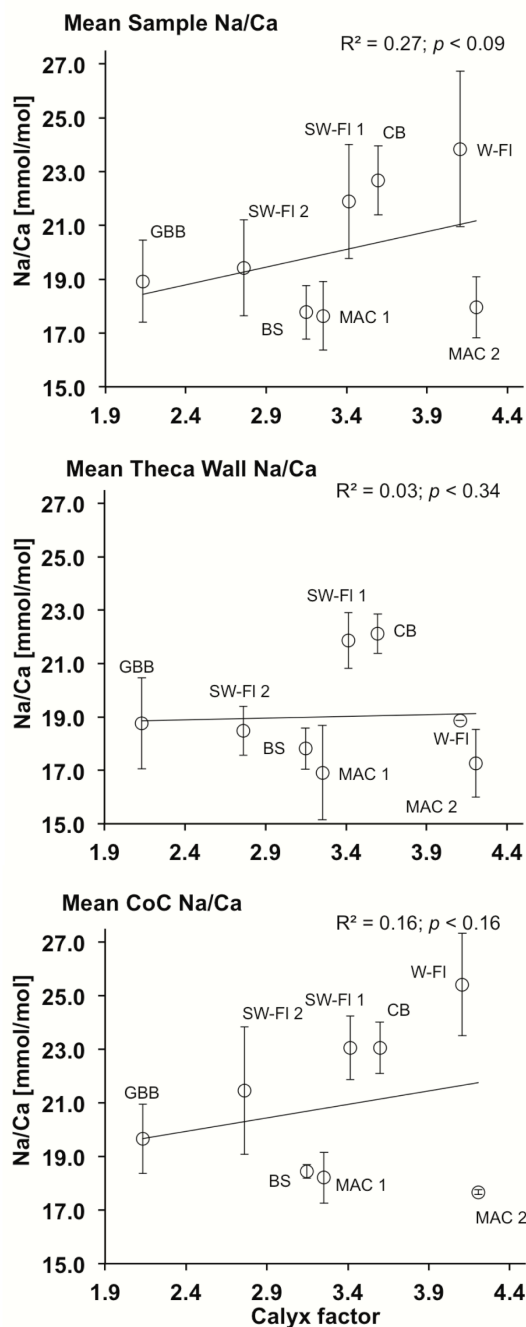


Fig. 3.g Mg/Ca ratios versus Calyx factor (CF) derived from all analysed samples, differentiated in arithmetic mean sample (overview of the whole sample) *top*, the arithmetic mean TW plotted in the *middle* and the arithmetic mean CoC plotted at the *bottom*. The linear regression, the corresponding R^2 and the p -values are given for measurements of both EPMA and LA-ICP-MS. Error bars = ± 1 SD (1σ)

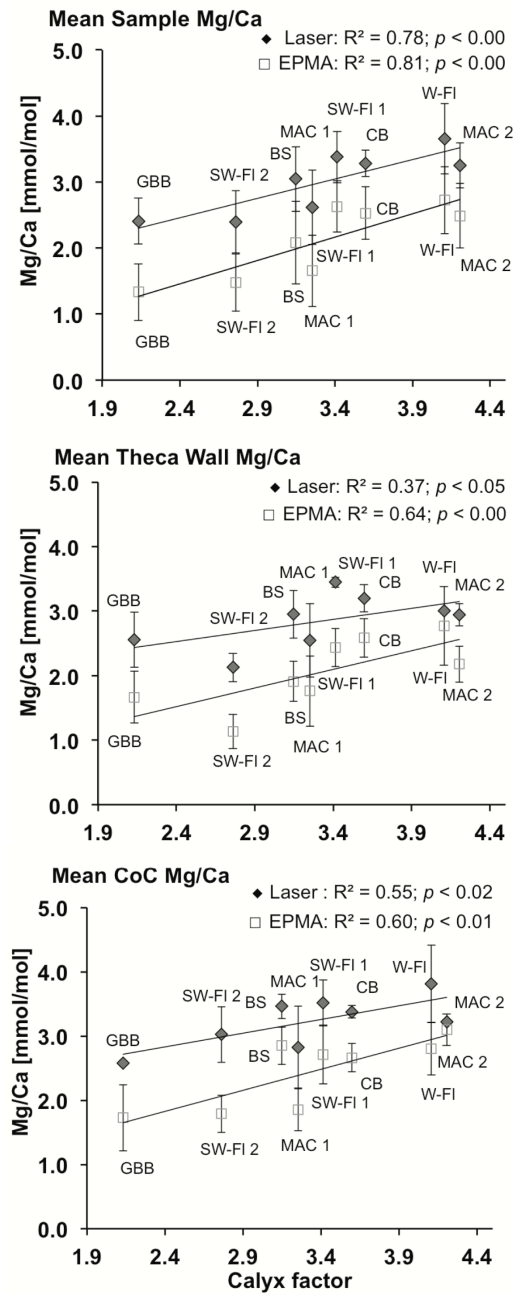
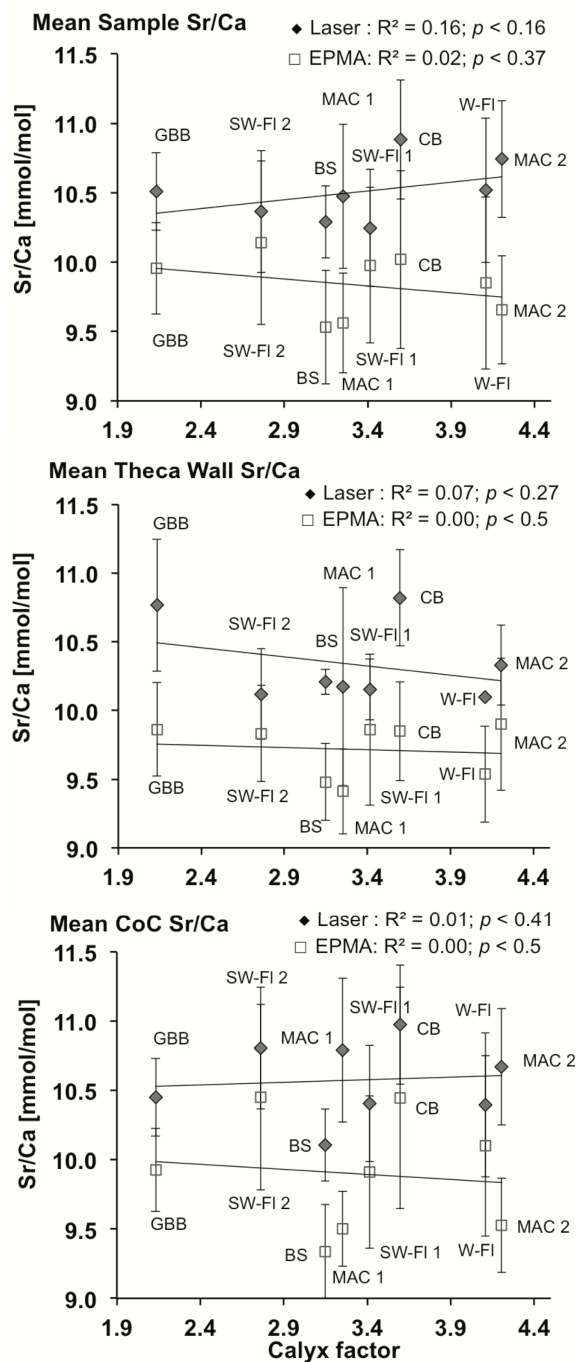


Fig. 3.h Sr/Ca ratios versus Calyx factor (CF) derived from all analysed samples, differentiated in arithmetic mean sample (overview of the whole sample) *top*, the arithmetic mean TW plotted in the *middle* and the arithmetic mean CoC plotted at the *bottom*. The linear regression, the corresponding R^2 and the p -values are given for measurements of both EPMA and LA-ICP-MS. Error bars = ± 1 SD (1σ)



Supplementary Material

Table 3.2 Analytical data for mean sample, TW and CoC for each *L. pertusa* and different methods: EPMA, LA-ICP-MS, binocular camera, Keyence camera. n = the number of individual data points. Analytical results present mean sample values, TW values, and CoC values by different colours (cream=mean sample; grey=TW; green=CoC).

Sample	EPMA Distance outer→inner [μm]						Laser Spot Distance outer→inner number of spots [diameter 60 μm]				Binocular - Camera Spots outer→inner		Keyence - Camera Spots outer→inner	
	Mean Sample [μm]	Mean Sample [n=]	Theca Wall [μm]	Theca Wall [n=]	CoC [μm]	CoC [n=]	Theca Wall [spots=]	Theca Wall [n=]	CoC [spots=]	CoC [n=]	Theca Wall [spots=]	CoC [spots=]	Theca Wall [spots=]	CoC [spots=]
GeoB16312-1	1 - 286	286	26 - 151	125	156 - 245	89	1 - 3	3	6 - 7	2	1 - 4	6 - 7 8=Septum	1 - 4 5=Mix	6 - 7 8=Septum
GeoB16334-1	1 - 281	281	13 - 48	35	49 - 165	116	1	1	2 - 5	4	1	2 - 5 6 - 8=Septum	1	2 - 5 6 - 8=Septum
GeoB16347-1	1 - 436	436	5 - 89	84	99 - 265	166	1 - 2	2	3 - 6	4	1 - 2	3 - 6 7 - 8=Septum	1 - 2	3 - 6 7 - 8=Septum
GeoB16350-1	1 - 729	729	15 - 211	196	230 - 550	320	1 - 5	4	6 - 7	2	1 - 5	6 - 7 8=Septum	1 - 5	6 - 7 8=Septum
GeoB16362-1	1 - 591	591	53 - 266	213	300 - 435	132	1 - 2	2	3 - 5	3	1 - 2	3 - 5 6 - 8=Septum	1 - 2	3 - 5 6 - 8=Septum
GeoB16373-1	1 - 651	651	27 - 145	118	472 - 524	52	1 - 2	2	5 - 6	2	2 - 3 1=Mix 4=Mix	5 - 6 7 - 8=Septum	2 - 3 1=Mix 4=Mix	5 - 6 7 - 8=Septum
MSM32-3-2	1 - 559	559	20 - 154	134	213 - 392	179	2 - 4	3	6 - 7	2	2 - 4 1 and 5=Mix	6 - 7 8=Septum	2 - 4 1 and 5=Mix	6 - 7 8=Septum
MSM32-49-2	1 - 313	313	16 - 99	83	169 - 239	70	1 - 2	2	5 - 6	2	1 - 2 3 - 4=Mix	5 - 6 7 - 8=Septum	1 - 2 3 - 4=Mix	5 - 6 7 - 8=Septum

Table 3.3 Assignment of the LA-ICP-MS analytical spots of Mg/Ca and the analytical points of the EPMA according to each microstructure of the arithmetic mean sample, TW and CoC of each individual section for *L. pertusa* and uncertainties respectively. Enrichment factors of the arithmetic mean and min./max. values are presented (and uncertainties respectively). The total number (n) of measurements as the basis of each individual data point (EMPA and LA-ICP-MA) and different colours for the arithmetic mean sample, the TW and the CoC are listed in detail in Table 3.2

Sample	EPMA Mg/Ca								EPMA Mg/Ca				LA-ICP-MS Mg/Ca								LA-ICP-MS Mg/Ca			
	Mean sample arithmetic mean [mmol/mol]	Mean sample 1 SD [σ]	Theca Wall arithmetic mean [mmol/mol]	Theca Wall 1 SD [σ]	CoC arithmetic mean [mmol/mol]	CoC 1 SD [σ]	Factor arithmetic mean	1 SD [σ]	Theca Wall minimum [mmol/mol]	CoC maximum mmol/mol	Factor min/max	1 SD [σ]	Mean sample arithmetic mean [mmol/mol]	Mean sample 1 SD [σ]	Theca Wall arithmetic mean [mmol/mol]	Theca Wall 1 SD [σ]	CoC arithmetic mean [mmol/mol]	CoC 1 SD [σ]	Factor arithmetic mean	1 SD [σ]	Theca Wall minimum [mmol/mol]	CoC maximum [mmol/mol]	Factor min/max	1 SD [σ]
GeoB16312-1	2.53	0.40	2.59	0.30	2.66	0.22	1.03	0.05	1.66	3.92	2.36	1.60	3.28	0.20	3.20	0.21	3.38	0.10	1.03	0.13	2.96	3.45	1.16	0.34
GeoB16334-1	2.73	0.51	2.77	0.61	2.80	0.41	1.01	0.02	1.69	3.90	2.30	1.56	3.65	0.53	3.01	0.88	3.81	0.60	1.27	0.57	3.01	4.20	1.40	0.84
GeoB16347-1	2.63	0.39	2.43	0.29	2.71	0.45	1.11	0.19	1.75	3.69	2.11	1.37	3.38	0.39	3.45	0.08	3.52	0.35	1.02	0.05	3.39	3.92	1.16	0.37
GeoB16350-1	1.48	0.44	1.13	0.27	1.79	0.29	1.58	0.46	0.65	2.78	4.26	1.51	2.40	0.47	2.13	0.22	3.02	0.43	1.42	0.63	1.87	3.33	1.78	1.03
GeoB16362-1	2.08	0.62	1.91	0.31	2.85	0.29	1.49	0.66	1.01	3.44	3.40	1.72	3.05	0.49	2.95	0.37	3.46	0.19	1.17	0.36	2.69	3.58	1.33	0.63
GeoB16373-1	1.33	0.43	1.67	0.40	1.73	0.52	1.04	0.04	0.77	2.87	3.71	1.48	2.41	0.35	2.56	0.43	2.58	0.04	1.01	0.02	2.25	2.61	1.16	0.26
MSM32-3-2	1.65	0.54	1.76	0.55	1.85	0.33	1.05	0.06	0.76	2.79	3.67	1.44	2.62	0.56	2.55	0.57	2.83	0.64	1.11	0.20	1.98	3.28	1.65	0.91
MSM32-49-2	2.49	0.49	2.18	0.28	3.09	0.24	1.42	0.65	1.47	3.68	2.51	1.57	3.25	0.34	2.94	0.17	3.22	0.02	1.09	0.20	2.82	3.24	1.15	0.29
Factor mean of all samples	n=8						1.22				3.04							1.14				1.35		
Factor ranges of all samples	n=8						1.01 - 1.58				2.11 - 6.89							1.01 - 1.42				1.15 - 1.78		

Table 3.4 Assignment of the LA-ICP-MS analytical spots of Sr/Ca and the analytical points of the EPMA according to each microstructure of the arithmetic mean sample, TW and CoC of each individual section for *L. pertusa* and uncertainties respectively. Enrichment factors of the arithmetic mean and min./max. values are presented (and uncertainties respectively). The total number (n) of measurements as the basis of each individual data point (EMPA and LA-ICP-MA) and different colours for the arithmetic mean sample, the TW and the CoC are listed in detail in Table 3.2

Sample	EPMA Sr/Ca								EPMA Sr/Ca				LA-ICP-MS Sr/Ca								LA-ICP-MS Sr/Ca			
	Mean sample arithmetic mean [mmol/mol]	Mean sample 1 SD [σ]	Theca Wall arithmetic mean [mmol/mol]	Theca Wall 1 SD [σ]	CoC arithmetic mean [mmol/mol]	CoC 1 SD [σ]	Factor arithmetic mean	1 SD [σ]	Theca Wall minimum [mmol/mol]	CoC maximum [mmol/mol]	Factor min/max	1 SD [σ]	Mean sample arithmetic mean [mmol/mol]	Mean sample 1 SD [σ]	Theca Wall arithmetic mean [mmol/mol]	Theca Wall 1 SD [σ]	CoC arithmetic mean [mmol/mol]	CoC 1 SD [σ]	Factor arithmetic mean	1 SD [σ]	Theca Wall minimum [mmol/mol]	CoC maximum [mmol/mol]	Factor min/max	1 SD [σ]
GeoB16312-1	10.02	0.64	9.85	0.36	10.45	0.80	1.06	0.42	9.41	11.96	1.27	1.80	10.88	0.43	10.82	0.35	10.97	0.01	1.01	0.11	10.46	10.97	1.05	0.36
GeoB16334-1	9.85	0.62	9.54	0.35	10.10	0.65	1.06	0.40	8.50	11.55	1.36	2.16	10.52	0.52	10.10	0.40	10.40	0.47	1.03	0.21	10.10	10.89	1.07	0.56
GeoB16347-1	9.98	0.56	9.86	0.55	9.91	0.55	1.00	0.03	9.07	11.44	1.26	1.68	10.25	0.42	10.15	0.22	10.41	0.55	1.03	0.18	9.95	11.12	1.12	0.83
GeoB16350-1	10.14	0.59	9.83	0.35	10.45	0.67	1.06	0.44	9.14	12.16	1.33	2.14	10.37	0.44	10.12	0.33	10.81	0.26	1.07	0.49	9.59	10.99	1.15	0.99
GeoB16362-1	9.53	0.41	9.48	0.28	9.34	0.34	0.98	0.10	8.83	10.22	1.16	0.98	10.29	0.26	10.21	0.09	10.11	0.26	1.00	0.07	9.85	10.36	1.05	0.36
GeoB16373-1	9.95	0.33	9.86	0.34	9.93	0.30	1.01	0.04	9.19	11.24	1.22	1.45	10.51	0.28	10.77	0.48	10.45	0.05	1.00	0.22	10.43	10.49	1.01	0.04
MSM32-3-2	9.56	0.36	9.41	0.31	9.50	0.27	1.01	0.06	8.81	10.31	1.17	1.06	10.48	0.52	10.17	0.72	10.79	0.32	1.06	0.44	9.35	11.02	1.18	1.19
MSM32-49-2	9.66	0.39	9.90	0.48	9.53	0.34	0.96	0.26	9.19	10.23	1.11	0.73	10.74	0.42	10.33	0.29	10.67	0.72	1.03	0.24	10.13	11.18	1.10	0.74
Factor mean of all samples	n=8						1.02				1.24								1.03				1.09	
Factor ranges of all samples	n=8						0.98 - 1.06				1.11 - 1.36								1.00 - 1.07				1.04 - 1.18	

Table 3.5 Assignment of the LA-ICP-MS analytical spots of Na/Ca and the analytical points of the EPMA according to each microstructure of the arithmetic mean sample, TW and CoC of each individual section for *L. pertusa* and uncertainties respectively. Enrichment factors of the arithmetic mean and min./max. values are presented (and uncertainties respectively). The total number (n) of measurements as the basis of each individual data point (EMPA and LA-ICP-MA) and different colours for the arithmetic mean sample, the TW and the CoC are listed in detail in Table 3.2

Sample	LA-ICP-MS Na/Ca								LA-ICP-MS Na/Ca				
	Mean sample arithmetic mean [mmol/mol]	Mean sample 1 SD [σ]	Theca Wall arithmetic mean [mmol/mol]	Theca Wall 1 SD [σ]	CoC arithmetic mean [mmol/mol]	CoC 1 SD [σ]	Factor arithmetic mean	1 SD [σ]	Theca Wall min [mmol/mol]	CoC max [mmol/mol]	Factor min/max	1 SD [σ]	
GeoB16312-1	22.67	1.28	22.12	0.74	23.06	0.96	1.04	0.66	21.41	23.74	1.11	1.65	
GeoB16334-1	23.84	2.89	18.87	2.21	25.42	1.91	1.35	4.63	18.87	28.03	1.49	6.48	
GeoB16347-1	21.88	2.12	21.87	1.05	23.06	1.19	1.05	0.84	21.13	23.96	1.13	2.00	
GeoB16350-1	19.42	1.78	18.49	0.92	21.46	2.38	1.16	2.10	17.46	23.15	1.33	4.02	
GeoB16362-1	17.77	1.00	17.82	0.77	18.45	0.26	1.04	0.45	17.27	18.66	1.08	0.98	
GeoB16373-1	18.92	1.52	18.75	1.70	19.65	1.29	1.05	0.63	17.55	20.57	1.17	2.13	
MSM32-3-2	17.63	1.27	16.91	1.77	18.21	0.95	1.08	0.92	15.16	18.88	1.24	2.63	
MSM32-49-2	17.96	1.14	17.27	1.27	17.67	0.09	1.02	0.28	16.37	17.73	1.08	0.96	
Factor mean of all samples	n=8							1.10				1.20	
Factor ranges of all samples	n=8							1.02 - 1.35				1.08 - 1.33	

Supplementary Material

Table 3.a Electron Probe Microanalyser (EPMA) calibration for quantitative measurements (Calcite after Jarosewich and MacIntyre 1983; KAN-1 after Reay et al. 1993)

Element	Standard		Crystal	Peak/Time/Count [sec]
Mg	1 Calcite	USNM 136321	TAPH	20
Ca	3 KAN 1	Kakanui Anorthoclase, Otago, Neuseeland	PETJ	20
Sr	4 Strontianite	R10065	TAP	40

Table 3.b EPMA semi-quantitative measurement of Mg in counts per pixel (cts/pxl). Highest concentration represent of highest cts/pixel, whereas lowest concentration represent of lowest cts/pixel

Calices diameter used for mean sample [mm]	Station ID	Calyx Diameter 1	Calyx Diameter 2	Calyx Diameter 3	Calyx Diameter 4	Calyx Diameter 5	Calyx Diameter 6	Calyx Diameter 1 - 6 arithmetic mean	Calyx Diameter 1 SD [σ]
		→ with location from the budding to the apical zone →							
GeoB16312-1	CB	4.21	4.16	3.70	5.17			4.31	0.62
GeoB16334-1	W-FI	6.37	4.78	5.22	4.11			5.12	0.95
GeoB16347-1	SW-FI1	4.49 (6)	4.79 (4)	4.37 (2)	4.09 (7)			4.44	0.54
GeoB16350-1	SW-FI2	7.46	7.60	5.86	7.21			7.03	0.80
GeoB16362-1	BS	2.66	2.43	2.33	2.51	3.23		2.63	0.36
GeoB16373-1	GBB	3.70	3.61	6.89	5.16			4.84	1.54
MSM32-3-2	MAC1	4.58	4.48	3.72	4.60	4.97	3.55	4.32	0.56
MSM32-49-2	MAC2	3.70	3.77	3.23	3.51	2.47	4.14	3.47	0.57

Calices Length used for mean sample [mm]	Station ID	Calyx Length 1	Calyx Length 2	Calyx Length 3	Calyx Length 4	Calyx Length 5	Calyx Length 6	Calyx Length 1 - 6 arithmetic mean	Calyx Length 1 SD [σ]	CF length/diameter
		→ with location from the budding to the apical zone →								
GeoB16312-1	CB	18.06	13.99	10.63	19.33			15.50	3.97	3.60
GeoB16334-1	W-FI	18.65	22.53	21.35	21.58			21.03	1.67	4.11
GeoB16347-1	SW-FI1	13.04 (5)	16.06 (3)	10.54 (1)	20.93 (8)			15.14	4.47	3.41
GeoB16350-1	SW-FI2	17.31	22.33	17.82	20.21			19.42	2.32	2.76
GeoB16362-1	BS	9.22	9.68	7.90	6.74	7.87		8.28	1.18	3.15
GeoB16373-1	GBB	10.29	9.69	7.25	14.05			10.32	2.81	2.13
MSM32-3-2	MAC1	14.18	12.11	14.17	14.58	16.94	12.27	14.04	1.77	3.25
MSM32-49-2	MAC2	10.97	14.47	14.52	13.40	14.87	19.32	14.59	2.72	4.21

Table 3.c Each coral branch was measured approximately 4 – 6 times from the budding to the apical zone (calyx length) and at the base of each calyx (cross section). Values are averaged for each calyx length and diameter used for the mean sample. The numbers in parentheses (1 – 8) are corresponding to SM Fig. 3.b. Error bars = ± 1 SD (1σ)

Calyx measured by LA-ICP-MS [mm]	Station ID	Calyx Diameter → with location from	Calyx Diameter 1 SD [σ]	Calyx Length the budding to the	Calyx Length 1 SD [σ]	CF length/ diameter
GeoB16312-1	CB	5.17	0.66	19.33	3.84	3.74
GeoB16334-1	W-FI	4.11	0.70	21.58	1.46	5.25
GeoB16347-1	SW-FI1	4.09 (7)	0.54	20.93 (8)	4.66	5.12
GeoB16350-1	SW-FI2	7.21	0.43	20.21	2.04	2.80
GeoB16362-1	BS	3.23	0.47	7.87	0.70	2.44
GeoB16373-1	GBB	5.16	0.72	14.05	2.28	2.72
MSM32-3-2	MAC1	4.48	0.32	12.11	1.77	2.70
MSM32-49-2	MAC2	4.14	0.71	19.32	3.23	4.67

Table 3.d Each sectioned coral sample was measured 2 times from the budding to the apical zone (calyx length) and at the base of each calyx (cross section) for the calyx used for the LA-ICP-MS measurement. The numbers in parentheses (7 – 8) are corresponding to SM Fig. 3.b. Error bars = ± 1 SD (1σ)

Sample ID	Station ID	Counts/pixel for Mg
GeoB16312-1	CB	82–217
GeoB16334-1	W-FI	69–239
GeoB16347-1	SW-FI1	60–242
GeoB16350-1	SW-FI2	67–220
GeoB16362-1	BS	70–264
GeoB16373-1	GBB	76–220
MSM32-3-2	MAC1	75–278
MSM32-49-2	MAC2	55–313

Table 3.e Mg/Ca, Sr/Ca, Na/Ca values for *Lophelia pertusa* measured by LA-ICP-MS versus distance

Sample ID	Spot	Spot Size [µm]	Distance [µm]	Mg/Ca LA-ICP-MS [mmol/mol]	Na/Ca LA-ICP-MS [mmol/mol]	Sr/Ca LA-ICP-MS [mmol/mol]
GeoB 16312-1	1	60	67	3.35	22.07	10.83
	2	60	93	3.29	22.89	11.17
	3	60	123	2.96	21.41	10.46
	4	60	149	3.57	24.23	10.58
	5	60	173	3.03	20.65	10.36
	6	60	201	3.45	23.74	10.98
	7	60	231	3.31	22.38	10.97
	8	60	261	3.32	24.01	11.71
GeoB 16334-1	1	60	25	3.01	18.87	10.10
	2	60	53	4.25	25.10	9.82
	3	60	94	2.95	23.45	10.89
	4	60	124	3.84	25.08	10.65
	5	60	156	4.20	28.03	10.23
	6	60	182	3.85	23.88	10.60
	7	60	211	3.97	25.62	10.08
	8	60	255	3.17	20.69	11.50
GeoB 16347-1	1	60	41	3.39	22.61	10.31
	2	60	75	3.51	21.13	10.00
	3	60	113	3.36	23.88	10.30
	4	60	156	3.12	21.40	11.12
	5	60	214	3.92	23.96	10.43
	6	60	240	3.69	23.01	9.78
	7	60	278	2.61	17.37	9.87
	8	60	367	3.45	21.69	10.17
GeoB 16350-1	1	32	6	2.36	19.79	10.47
	2	32	26	2.25	18.92	10.13
	3	44	44	1.92	17.46	9.59
	4	44	69	1.87	17.79	10.09
	5	44	176	2.22	18.47	10.32
	6	44	276	3.32	23.14	10.99
	7	44	490	2.72	19.77	10.63
	8	44	641	2.50	20.00	10.71
GeoB 16362-1	1	60	55	2.16	15.88	10.51
	2	60	104	2.69	16.87	10.67
	3	60	135	3.22	18.47	10.41
	4	60	185	3.58	18.66	10.36
	5	60	224	3.25	18.15	10.10
	6	60	257	3.56	18.52	9.85
	7	60	350	3.21	18.36	10.15
	8	60	483	2.69	17.27	10.27
GeoB 16373-1	1	44	19	2.25	17.55	10.43
	2	60	69	2.86	19.96	10.10
	3	90	126	2.49	21.06	10.12
	4	44	364	1.84	16.93	10.57
	5	60	447	2.57	19.03	10.60
	6	90	498	2.55	20.57	10.49
	7	44	553	2.61	18.74	10.44
	8	60	607	2.11	17.55	10.37
MSM32-3-2	1	60	25	2.12	17.71	10.91
	2	60	56	1.98	15.16	10.57
	3	60	91	3.13	18.70	10.61
	4	60	126	2.53	16.87	9.35
	5	60	163	3.37	18.97	10.18
	6	60	222	3.28	18.88	10.56
	7	60	336	2.38	17.54	11.02
	8	60	493	2.16	17.25	10.60
MSM32-49-2	1	60	31	2.82	16.37	10.13
	2	60	65	3.06	18.16	10.53
	3	60	105	3.10	17.19	10.95
	4	60	138	3.13	17.71	11.16
	5	60	173	3.23	17.61	10.16
	6	60	208	3.20	17.73	11.18
	7	60	244	3.55	18.63	10.90
	8	60	275	3.92	20.25	10.94

Chapter 4

Seawater mass density gradient of the Campeche cold-water coral province, southern Gulf of Mexico

Based on: *Environmental forcing of the Campeche cold-water coral province, southern Gulf of Mexico* by Dierk Hebbeln, Claudia Wienberg, Paul Wintersteller, Andre Freiwald, M. Becker, Lydia Beuck, Wolf-Christian Dullo, Gregor P. Eberli, Silke Glogowski, Lelia Matos, Nina Forster, Hector Reyes-Bonilla, Marco Taviani, and the MSM 20-4 shipboard scientific party (2014)
Biogosciences (11):1799-1815

Abstract

With an extension of >40 km² the recently discovered Campeche cold-water coral province located at the northeastern rim of the Campeche Bank in the southern Gulf of Mexico belongs to the largest coherent cold-water coral areas discovered so far. The Campeche province consists of numerous 20–40 m-high elongated coral mounds that are developed in intermediate water depths of 500 to 600 m. The recent environmental setting is characterised by a high surface water production caused by a local upwelling center and a dynamic bottom-water regime comprising vigorous bottom currents, obvious temporal variability, and strong density contrasts, which all together provide optimal conditions for the growth of cold-water corals. This setting – potentially supported by the diel vertical migration of zooplankton in the Campeche area – controls the delivering of food particles to the corals. The Campeche cold-water coral province is, thus, an excellent example highlighting the importance of the oceanographic setting in securing the food supply for the development of large and vivid cold-water coral ecosystems.

4.1 Introduction

The last decade has witnessed a tremendous progress in our knowledge about “framework-building cold-water corals” (CWC) as their role as ecosystem engineers creating highly diverse ecosystems in water depths far beyond the shelf edge is becoming more and more obvious (Roberts et al. 2009). The biodiversity associated with these ecosystems may be comparable to that found in tropical coral reefs (Roberts et al. 2006), and they occur almost worldwide except for the highest latitudes (Davies and Guinotte 2011). The availability of advanced deep-sea technologies (e.g., remotely operated vehicles) greatly supported the discovery and investigation of large, thriving and (so far) unknown CWC ecosystems in remote places. Successful studies such as those performed off Mauritania (Colman et al. 2005), off Angola (Le Guilloux et al. 2009), and in various parts of the Mediterranean demonstrate the potential use of these technologies for future discoveries.

The scleractinian coral *Lophelia pertusa* is among the most common and most widespread CWC species worldwide and is particularly abundant in the eastern North Atlantic (Davies and Guinotte 2011). This species withstands a rather wide range of physicochemical conditions (see summary in Davies et al. 2008), a fact that explains its almost global distribution at depths between a few tens of meters to over 2000 m (Freiwald and Roberts 2005). Another critical factor controlling its distribution is sufficient food supply that is commonly driven by the interplay of surface water productivity and the local nature of the bottom current regime (e.g. currents, stratification, internal waves and tides) delivering food particles to the CWC (Duineveld et al. 2004, 2007; White et al. 2005).

In addition to the CWC hotspot in the eastern North Atlantic, *L. pertusa* also contributes to numerous coral mound structures in the western North Atlantic along the continental margin along the Florida–Hatteras slope (Paull et al. 2010), and the Bahamas to the Florida Straits (e.g. Neumann et al. 1977; Mullins et al. 1981; Grasmueck et al. 2006; Correa et al. 2012a, b). Further west in the Gulf of Mexico, *L. pertusa* appears to be more scattered, forming isolated mound-like structures along the west Florida slope (Newton et al. 1987; Hübscher et al. 2010) and in the northern Gulf of Mexico (Moore and Bullis 1960; Schroeder 2002; Reed et al. 2006; Cordes et al. 2008; Becker et al. 2009; Davies et al. 2010).

In this paper, we document for the first time build-ups at the seafloor formed by framework-building scleractinian corals on the slope of the Mexican Campeche Bank, southern Gulf of Mexico. These build-ups are mainly formed by *Enallopsammia profunda*–*Lophelia pertusa* communities. This finding was unexpected as available data from a few dredge haul stations only described the occurrence of the scleractinian CWC *Madrepora oculata* along the margin of the Campeche Bank, north of the Mexican Yucatan Peninsula (Cairns 1979; Schroeder et al. 2005). Only in 2010 was more detailed information provided, when hydroacoustic surveys revealed “mound-like” structures between 500 and 600 m water depth along the margin of the bank (Hübscher et al. 2010). Without any groundtruthing being available at that time, it only has been speculated that these structures might be CWC mounds (Hübscher et al. 2010). This region was revisited in 2012 and extensive field data (bathymetry, hydrography, and video observations) revealed the existence of a large thriving CWC ecosystem, which is the focus of this paper. This hitherto unknown CWC site is here termed the “Campeche CWC province”. The scope of the present study is to describe this extensive (> 40 km²) CWC province with respect to morphology, the megafaunal community, and the oceanographic setting and to put it into a larger framework analysing the overall forcing factors controlling its development.

4.1.1 Regional Settings

The Campeche Bank is a large shelf area extending approximately 200 km northward from the Mexican Yucatan Peninsula into the Gulf of Mexico. The Gulf of Mexico is a largely oligotrophic basin with enhanced productivity only along the continental shelves (Müller-Karger et al. 1991), where seasonal coastal upwelling provides additional nutrients to the surface waters (Zavala-Hidalgo et al. 2006). A major source of nutrients is the Mississippi plume fertilising the northeastern shelves of the Gulf with enhanced productivity partly extending over the continental slope (Wawrik and Paul 2004). The enhanced productivity triggered by the Mississippi plume most likely plays an important role in sustaining CWC populations along the Louisiana and Florida continental slopes (e.g. Newton et al. 1987; Schroeder 2002). Apart from the typical coastal upwelling, another upwelling regime has been described further offshore along the eastern margin of the Campeche Bank (Merino 1997).

As the curl of the prevailing wind stress is not likely to induce upwelling along the eastern Yucatan slope, the upwelling observed there is probably caused by bottom friction or other topographical effects (Merino 1997). Nevertheless, the advection of nutrients into the photic zone (although rarely to the sea surface; Merino 1997) induces very high productivity reaching a peak in September (Zavala-Hidalgo et al. 2006) when sites near the Campeche CWC province appear prominently in satellite-based productivity maps. According to Merino (1997) three main water masses comprise the water column there. Salinity and temperature increase together from the Antarctic Intermediate Water (AAIW, 7°C, salinity 34.9) in the deep towards the salinity maximum of the Subtropical Intermediate Water (STUW, 23°C, salinity 36.8) at ~150 m depth. Further above, temperature rises and salinity declines until from 50m to the surface both parameters remain relatively constant (26°C–27.5°C, salinity < 36.4), representing the Caribbean Surface Water (CSW). At depths greater than ~650 m, the Yucatan and Cuban countercurrents transport water southward while being confined to the western, Mexican side and to the eastern, Cuban side of the Yucatan Strait, respectively (Sheinbaum et al. 2002).

With respect to the strength of the bottom current regime, the best information is provided by mooring data obtained slightly further south in the Yucatan Strait (~21.5°C; N; e.g. Sheinbaum et al. 2002). Along a W–E transect through the area, the mean northward current velocities at the western margin decrease rapidly from almost 100 cm s⁻¹ at the surface to < 10 cm s⁻¹ at 200m water depth. However, at the depth of the Campeche CWC province (~550 m) the bottom current velocities in the Yucatan Strait increase again to > 10 cm s⁻¹ (Sheinbaum et al. 2002).

4.2 Material and Methods

All data presented here were collected during expedition MSM 20-4 with the German R/V *Maria S. Merian* in spring 2012 (Hebbeln et al. 2012). They include hydroacoustic measurements, water column studies, and seabed ROV video observation (Table 4.1).

Instrument specifications and applied settings for all measurements are described in detail in Hebbeln et al. (2012). Hydrographic measurements through the water column were obtained from two single CTD casts in (GeoB 16305-1; GeoB 16303-1) and one Yoyo-CTD covering a full tide cycle of 13 hours (GeoB 16316-1-13; Table 4.1).

4.2.1 Water column analyses

To determine the physical parameters of the water masses in the area of the Campeche CWC province and to trace their variability, CTD measurements were performed as a Yoyo CTD comprising 13 individual casts taken within 12 h at station GeoB 16316 (Fig 4.1; Table 4.1). The CTD measurements of the water column down to a maximum water depth of 1246 m were conducted using a SEABIRD “SBE 9 plus” underwater unit and a SEABIRD “SBE 11 plus V2” deck unit. The vertical profile over the water column provided standard data for conductivity, temperature, pressure, and dissolved oxygen. Conductivity and temperature data were used to compute salinity (with the latter being presented here unitless). The data presented here all refer to the downcast of the individual CTD deployments.

Table 4.1 Metadata of CTD casts conducted at the Campeche cold-water coral province during R/V *Maria S. Merian* cruise MSM 20-4. Abbreviations: WD: water depth

Station [GeoB-No.]	Gear	Lat. [°N]	Long. [°W]	Date	WD [m]	Remark
MSM20-4 GeoB 16316-1	[Yo-Yo CTD]	23°51.51	87°12.12	24.03.12	576	Hourly casts over ~12h; ADCP data
MSM20-4 GeoB 16303-1	[Single CTD]	22°00.98	86°12.27	21.03.12	1246	Sound velocity profile
MSM20-4 GeoB 16305-1	[Single CTD]	23°49.87	87°12.27	22.03.12	506	Sound velocity profile

4.3 Results

4.3.1 Water column structure/dynamics

The CTD measurements allow the identification of the most important regional water masses, based on temperature (potential temperature) and mainly on absolute salinity data (Fig. 4.1). The uppermost ~80m of the water column are characterised by water with salinities of <36.4, which is indicative of the presence of the CSW. The salinity maximum (~36.8) between 100 and 160 m water depth is characteristic for the STUW. At 540 m water depth salinity drops below 35.0, marking the presence of AAIW. In the depth range where living CWC have been observed (520 to 580 m) temperatures range 7.5°C–9.5°C and salinities 34.9–35.1. Dissolved oxygen contents vary between 2.74 and 2.8mLL⁻¹.

The Yoyo-CTD station (GeoB 16316) consisting of 13 individual, hourly taken casts reveal small but significant variations also in the deepest part of the water column just above the Campeche CWC province (Fig. 4.2): for example, at 519 m water depth the temperature varies by almost 1°C up to three times over the 12 h measuring period (Fig. 4.2c). These temperature changes are also reflected in the depth position of individual isotherms (8°C to 9.5°C, Fig. 4.2b). They fluctuate vertically by up to 20 m, thereby reflecting the same temporal forcing as the temperatures at 519m depth. Along with these temperature changes a distinct density gradient induced by temperature and salinity changes, almost reaching 0.7°C and 0.07, respectively, over a 10 m depth interval (Fig. 4.2d) propagates across the site. With ~0.06 kg m⁻³ per 10 m depth interval this density gradient is strongest for the lower part of the water column at 525 m depth and significantly higher than the density gradients between 380 m and the sea floor that otherwise reach maximum values of ~0.04 kg m⁻³ per 10m depth interval (Fig. 4.2a).

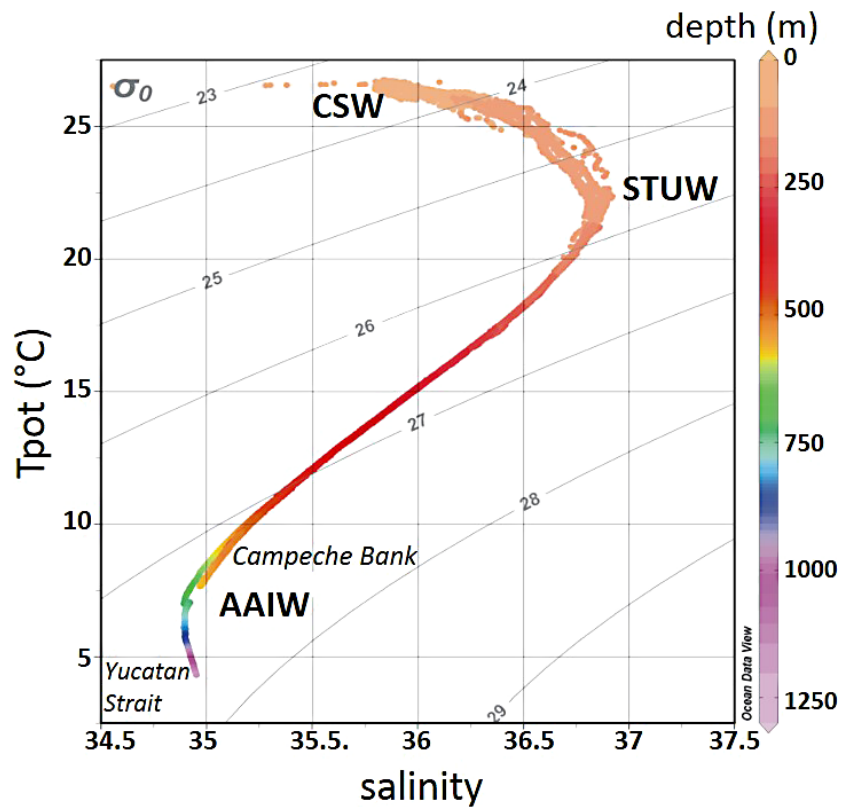


Fig. 4.1 Water mass structure in the Yucatan Strait (GeoB 16303-1) and in the Campeche cold-water coral province (GeoB 16316-1 to - 16, Yoyo CTD station; see Table 4.1). Shown is a temperature–salinity plot; temperature is displayed as potential temperature (T_{pot}), grey lines indicate levels of isodensity (σ_{θ}) in kgm^{-3} (plotted using Ocean Data View v.4.5.1; <http://odv.awi.de>; Schlitzer, 2012). Abbreviations: CSW: Caribbean Surface Water; STUW: Subtropical Intermediate Water; AAIW: Antarctic Intermediate Water

4.4 Discussion

Large CWC-formed seafloor structures have been reported from many regions in the world's oceans (Freiwald and Roberts 2005). In addition to the >300 m high CWC mounds off Ireland (Kenyon et al. 2003; Mienis et al. 2007; Dorschel et al. 2010), the extensive reefs off Norway (e.g. Fosså et al. 2005) are the most impressive features. Extending over tens of kilometers (e.g. the Sula Reef, ~14 x 0.5 km, Freiwald et al. 2002; the Røst Reef, ~40 x 3 km, Fosså et al. 2005) and reaching up to ~40m in height, these reefs generally comprise clusters of individual frameworks rather than a single coalescent structure (Freiwald et al. 2002). The Campeche CWC province shows a similar appearance as it comprises a cluster of individual elongated coral mounds rather than a single clearly confined reef structure.

The term "province" is used for the present study to describe the CWC mounds along the Campeche Bank following the nomenclature developed for the Irish margin where numerous individual CWC mounds occur clustered in provinces (e.g. White and Dorschel 2010). With its mapped area of 10 x 4 km, and most likely further northwest and southeastward extensions, the Campeche CWC province is comparable with the large Norwegian reefs and, thus, belongs to the largest mapped CWC provinces in the world. In addition, the Campeche CWC province represents the most important and extensive flourishing azooxanthellate coral area in the entire Gulf of Mexico discovered so far.

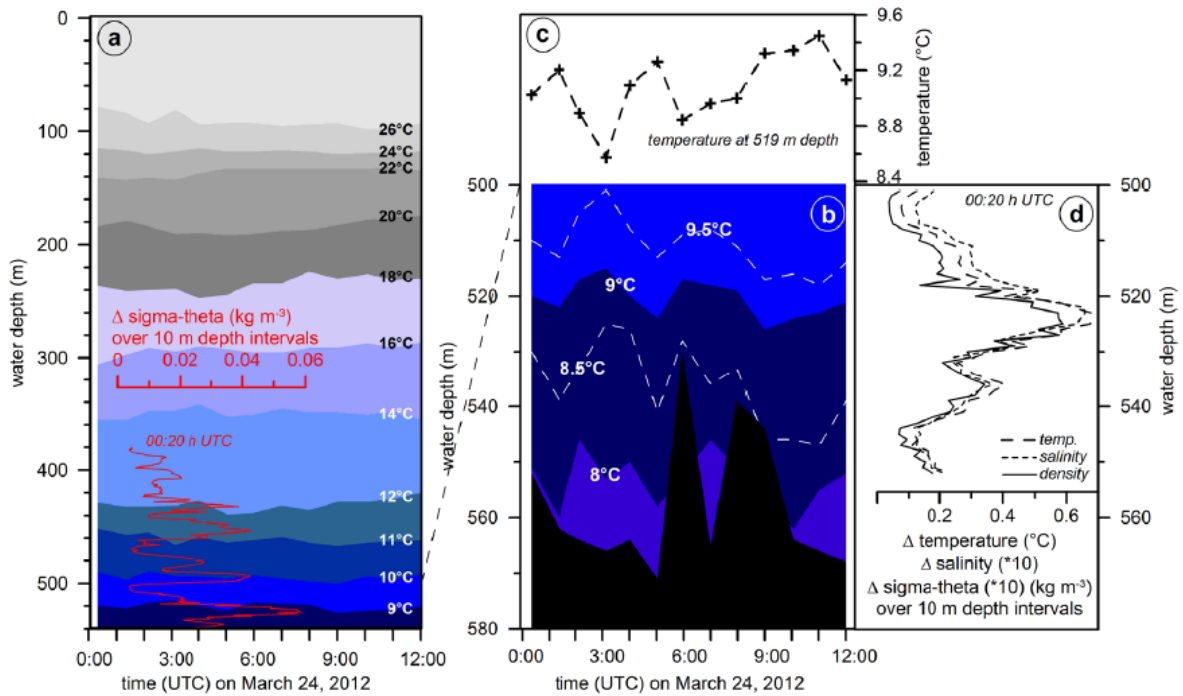


Fig. 4.2 Hydrological variability derived from the Yoyo CTD station GeoB 16316 (see also Table 4.1). **(a)** Variability of the temperature distribution in the entire water column over a time interval of 12 h (comprising 13 individual CTD casts). The red inset shows the density gradient over 10 m depth intervals for the water column below 380 m taken from CTD cast GeoB 16316-1 (00:20 UTC). **(b)** Depth variation of the 8°C to 9.5°C isotherms in the lower part of the water column >500 m water depth over the same time period shows partly vertical movements of >20 m. Variations in water depth (black denotes the sea floor) are caused by slight movements of the vessel (~600m N–S, ~50m E–W) at the Yoyo CTD station (including the crossing of a CWC mound). **(c)** Water temperature at 519 m depth measured over the same time period indicates a variability of up to 1°C. **(d)** Gradients in temperature, salinity, and density over 10 m depth intervals. Data were obtained during the individual CTD cast GeoB 16316-1 (00:20 UTC) and reveal particularly strong gradients around 520 m water depth (see also **a**).

4.4.1 Environmental control on the Campeche cold-water coral ecosystem

The known ranges of temperature (4°C–13.9°C; Roberts et al. 2006; Freiwald et al. 2009), salinity (31.7–38.8; Freiwald et al. 2004; Davies et al. 2008), dissolved oxygen (2.7–7.2mLL⁻¹; Dodds et al. 2007; Davies et al. 2008; Davies et al. 2010) and other physicochemical parameters defining the ecological niche of *L. pertusa* in the eastern North Atlantic (see summary in Davies et al. 2008) are found in many parts of the world's oceans (Davies and Guinotte 2011). Water mass properties obtained for the Campeche margin, such as temperature (9.5°C – 7.5°C) and salinity (35.1 – 34.9), fit well into these defined thresholds). The observed content of dissolved oxygen of ~2.7mLL⁻¹ matches observations from the Viosca Knoll area in the northern Gulf of Mexico, where *Lophelia* colonies currently thrive at the lowest reported oxygen levels of 2.7–2.8mLL⁻¹ (Davies et al. 2010). It is assumed that these extreme oxygen conditions cause decreased growth rates or even inhibit reproductive processes (Brooke and Young 2003).

However, despite a suited physicochemical setting, the presence of suitable hardgrounds for the corals to settle on, and even more importantly the availability of sufficient food, is crucial for the establishment and long-lasting development of a vivid CWC ecosystem. In general CWC feed on fresh phytodetritus (Duineveld et al. 2004; Kiriakoulakis et al. 2005; Duineveld et al. 2007), on zooplankton (Carrier et al. 2009; Dodds et al. 2009) or on a combination of both (Becker et al. 2009; van Oevelen et al. 2009). Recent laboratory studies also revealed the importance of dissolved organic matter which might be actively absorbed by CWC especially during periods when particulate food is scarce (Gori et al. 2014). However, independent of the food source, the sessile CWC rely on sufficient food supply, which is based on primary production in the surface waters and the delivery of food particles to the CWC living at intermediate depths. For the latter, various mechanisms were identified to enhance and transport food particles to the CWC, including strong bottom currents, downwelling and cascading, internal tides and waves, and nepheloid layers which act as a pathway for lateral transport (White et al. 2005; Dorschel et al. 2007; Duineveld et al. 2007; Mienis et al. 2007; Davies et al. 2009; Orejas et al. 2009). On the local to regional scale, topography also influences hydrodynamic processes, as, e.g. internal waves, down- or upwelling. Thus, for any given location it is the interplay of all these factors allowing for or prohibiting the presence of CWC.

Furthermore, the strong density gradient undulating around 520 m (Fig. 4.2d) might act as a decelerator for sinking (food) particles, thereby prolonging their residence time within the reach of the CWC and, thus, enhancing the probability of these particles to be caught by the corals. With salinities varying around 35, this density gradient possibly marks the upper limit of the core of the AAIW. A similar mechanism has been suggested to support the CWC off Ireland, there benefitting from the density gradient developed at the upper limit of the Mediterranean Outflow Water (White and Dorschel 2010). For the northeastern North Atlantic, Dullo et al. (2008) described a narrow potential density envelope of sigma-theta (σ_θ) = 27.35–27.65 kg m⁻³ preferred by the CWC. Along the Campeche Bank the density of the water masses surrounding the CWC is slightly lower, at 27.18–27.29 kg m⁻³, and, thus, close to data reported from the Viosca Knoll area (27.1–27.2 kg m⁻³) (Davies et al. 2010). In contrast, living CWC settings in the Mediterranean Sea are associated with much higher densities of > 29 kg m⁻³. Thus, if applicable, the concept of a narrow density envelope defining the overall habitat range of the CWC as suggested by Dullo et al. (2008) needs to be regionalised (Flögel et al. 2014). However, the obvious steep gradient in density (Fig. 4.2d) seems to be a sensitive indicator for living CWC reef communities.

As indicated by the undulating isotherms the temporal variability of the local hydrographic setting, which might reflect the presence of internal waves, literally might pump the food particles through the CWC ecosystem, especially those particles temporarily accumulating along the strong density gradient, as suggested by Mienis et al. (2012). Over the observed 13 h, the depth range covered by the fluctuating maximum near-bottom density gradient aligns with the upper range of observed living CWC in ~515 – 530 m water depth. Assuming a larger variability associated with monthly (i.e. lunar) to seasonal forcing, one may speculate that the entire depth range of living CWC off the Campeche Bank might intermittently be affected by such a pumping process. Due to the limited length of the 13 h of observation no tidal signal providing additional energy to the bottom current regime could have been clearly detected. However, along the mooring transect across the Yucatan Strait mentioned before (Sheinbaum et al. 2002), a comparably high amplitude of the major axis of the dominant diurnal O_1 tide was observed exactly in the depth range of the Campeche CWC province (Carrillo González et al. 2007).

4.5 Conclusions

The Campeche CWC province is one of the largest coherent CWC areas discovered so far, and the most relevant in the western Atlantic Ocean. A healthy and highly diverse CWC ecosystem is developed on top of a complex system of 20–40 m-high, partly interconnected elongated mounds.

The location of the Campeche CWC province appears to be almost perfect for the establishment of such a large CWC ecosystem. It is (a) located underneath a local upwelling center providing high primary production, (b) influenced by a very dynamic bottom current regime delivering food particles to the corals, and (c) characterised by a physicochemical setting that fits the recognised ecological needs of *L. pertusa*. The observed diel vertical migration of zooplankton possibly reaching the intermediate depth of the CWC ecosystem may even serve as a supplemental food source as already indicated by Mienis et al. (2012).

In many places in the world's oceans the physicochemical setting comply with the niche requirements of *L. pertusa* and other CWC (Davies and Guinotte 2011); however, only in some of these places have CWC ecosystems developed. Thus, the Campeche CWC province appears to be an excellent example showing that food supply – controlled by a variety of mechanisms – plays a major role in the development of CWC ecosystems.

Acknowledgments

The research leading to these results has received support from the Deutsche Forschungsgemeinschaft (DFG) through funding of the WACOM – West Atlantic Cold-water Coral Ecosystems projects, grants HE 3412/17-1 and DU 129/47-1, and through providing ship time. We thank the officers and crew of the *R/V Maria S. Merian*, the MARUM ROV *Cherokee* team, and the scientific crew for on-board assistance during cruise MSM 20-4 (2012). The cruise was further supported through the DFG Research Center/Cluster of Excellence “MARUM – The Ocean in the Earth System”.

We are grateful to the Mexican Government for providing access to conduct scientific work in Mexican waters. A. Freiwald received funds from the Hessian LOEWE BiK-F Project A3.10, and G. P. Eberli acknowledges the donors of the American Chemical Society Petroleum Research Fund (grant no. 49017-ND8) for partial support of this research and the industrial associates of the CSL – Center for Carbonate Research at the University of Miami for additional funding. L. Matos has been supported by the FCT scholarship SFRH/BD/72149/2010. This is ISMAR-CNR Bologna scientific contribution no. 1801. This study contributes to the international research program TRACES –Trans-Atlantic Coral Ecosystem Study.

References

- Becker EL, Cordes EE, Macko SA, Fisher CR (2009) Importance of seep primary production to *Lophelia pertusa* and associated fauna in the Gulf of Mexico. *Deep-Sea Res I* 56:786–800
- Brooke S and Young CM (2003) Reproductive ecology of a deep-water scleractinian coral, *Oculina varicosa*, from the southeast Florida shelf. *Cont Shelf Res* 23: 847–858
- Cairns SD (1979) The Deep-Water Scleractinia of the Caribbean Sea and Adjacent Waters. *Studies on the Fauna of Curaçao and Other Caribbean Islands* 57:341
- Carlier A, Le Guilloux E, Olu-Le Roy K, Sarrazin J, Mastrototaro F, Taviani M, Clavier J (2009) Trophic relationships in a deep Mediterranean cold-water coral bank (Santa Maria di Leuca, Ionian Sea). *Mar Ecol Prog Ser* 397:125–137
- Carrillo González F, Ochoa J, Candela J, Badan A, Sheinbaum J, González Navarro JI (2007) Tidal currents in the Yucatan Channel. *Geof Int* 46:199–209
- Colman JG, Gordaon DM, Lane AP, Forde MJ, Fitzpatrick J (2005) Carbonate mounds off Mauritania, Northwest Africa: status of deep-water corals and implications for management of fishing and oil exploration activities. In: Freiwald A, Roberts JM (eds), *Cold-Water Corals and Ecosystems*. Springer-Verlag, Berlin Heidelberg, ISBN:978-3-540-24136-2:417–441
- Cordes EE, McGinley MP, Podowski EL, Becker EL, Lessard-Pilon S, Viada ST, Fisher CR (2008) Coral communities of the deep Gulf of Mexico. *Deep-Sea Res I* 55:777–787
- Correa TBS, Eberli GP, Grasmueck M, Reed JK, Correa AMS (2012a) Genesis and morphology of cold-water coral ridges in a unidirectional current regime. *Mar Geol* 326–328:14–27
- Correa TBS, Grasmueck M, Eberli GP, Reed JK, Verwer K, Purkis SAM (2012b) Variability of cold-water coral mounds in a high sediment input and tidal current regime, Straits of Florida. *Sedimentology* 59:1278–1304
- Davies A.J, Wisshak M, Orr JC, Roberts JM (2008) Predicting suitable habitat for the cold-water coral *Lophelia pertusa* (Scleractinia). *Deep-Sea Res I* 55:1048–1062
- Davies AJ, Duineveld G, Lavaleye M, Bergman MJ, van Haren H, Roberts JM (2009) Downwelling and deep-water bottom currents as food supply mechanisms to the cold-water coral *Lophelia pertusa* (Scleractinia) at the Mingulay Reef Complex. *Limnol Oceanogr* 54:620–629. doi:10.4319/lo.2009.54.2.0620
- Davies AJ, Duineveld GCA, van Weering TCE, Mienis F, Quattrini AM, Seim HE, Bane JM, Ross SW (2010) Short-term environmental variability in cold-water coral habitat at Viosca Knoll, Gulf of Mexico. *Deep-Sea Res I* 57:199–212
- Davies AJ and Guinotte JM (2011) Global habitat suitability for framework-forming cold-water corals. *Plos One* 6:e18483. doi:10.1371/journal.pone.0018483
- Dodds LA, Roberts JM, Taylor AC, Marubini F (2007) Metabolic tolerance of the cold-water coral *Lophelia pertusa* (Scleractinia) to temperature and dissolved oxygen change. *J Experim Mar Biol Ecol* 349:205–214
- Dodds LA, Black KD, Orr H, Roberts JM (2009) Lipid biomarkers reveal geographical differences in food supply to the cold-water coral *Lophelia pertusa* (Scleractinia). *Mar Ecol Prog Ser* 397:113–124
-

- Dorschel B, Hebbeln D, Foubert A, White M, Wheeler AJ (2007) Hydrodynamics and cold-water coral facies distribution related to recent sedimentary processes at Galway Mound west of Ireland. *Mar Geol* 244:184–195
- Dorschel B, Wheeler A, Monteys X, Verbruggen K (2010) Atlas of the Deep-Water Seabed: Ireland, Springer:164
- Duineveld GCA, Lavleye MSS, Berghuis EM (2004) Particle flux and food supply to a seamount cold-water coral community (Galicia Bank, NW Spain). *Mar Ecol Prog Ser* 277:13–23
- Duineveld GCA, Lavleye MSS, Bergman MJN, De Stigter H, and Mienis F (2007) Trophic structure of a cold-water coral mound community (Rockall Bank, NE Atlantic) in relation to the near-bottom particle supply and current regime. *B Mar Sci* 81:449–467
- Dullo W-C, Flögel S, Rüggeberg A (2008) Cold-water coral growth in relation to the hydrography of the Celtic and Nordic European continental margin. *Mar Ecol Prog Ser* 371:165–176
- Flögel S, Dullo WC, Pfannkuche O, Kiriakoulakis K, Rüggeberg A (2014) Geochemical and physical constraints for the occurrence of living cold-water corals, *Deep-Sea Res II* 99:19–26
- Fosså JH, Lindberg B, Christensen O, Lundälv T, Svellingen I, Mortensen, PB, Alsvag J (2005) Mapping of *Lophelia* reefs in Norway: experiences and survey methods. In: Freiwald A, Roberts JM (eds). *Cold-Water Corals and Ecosystems*. Springer-Verlag, Berlin, pp 359–391. ISBN:978-3-540-24136-2, pp
- Freiwald A, Hühnerbach V, Lindberg B, Wilson JB, Campbell J (2002) The Sula Reef Complex, Norwegian Shelf. *Facies* 47:179–200
- Freiwald A, Fosså JH, Grehan A, Koslow T, Roberts JM (2004) Cold-water Coral Reefs. UNEP-WCMC, Cambridge, UK, *Biodiversity Ser* 22:84
- Freiwald A and Roberts JM (2005) *Cold-water Corals and Ecosystems*. Springer, Berlin-Heidelberg:1243
- Freiwald A, Beuck L, Rüggeberg A, Taviani M, Hebbeln D and R/V Meteor Cruise M70-1 participants (2009) The white coral community in the central Mediterranean Sea revealed by ROV surveys. *Oceanogr* 22:58–74
- Gori A, Grover R, Orejas C, Sikorski S, Ferrier-Pagès C (2014) Uptake of dissolved free amino acids by four cold-water coral species from the Mediterranean Sea. *Deep-Sea Res* 99:42–50
- Grasmueck M, Eberli GP, Viggiano DA, Correa T, Rathwell G, Luo J (2006) Autonomous underwater vehicle (AUV) mapping reveals coral mound distribution, morphology, and oceanography in deep water of the Straits of Florida. *Geophys Res Lett* 33:L23616. doi:10.1029/2006GL027734
- Hebbeln D, Wienberg C and cruise participants: Report and preliminary results of R/V MARIA S. MERIAN cruise MSM20-4, WACOM – West-Atlantic Cold-water Coral Ecosystems (2012) The West Side Story, Bridgetown – Freeport, 14 March–7 April 2012. University of Bremen, 120 pp
- Hübscher C, Dullo WC, Flögel S, Titschack J, Schönfeld J (2010) Contourite drift evolution and related coral growth in the eastern Gulf of Mexico and its gateways. *Int J Earth Sci* 99:S191–S206

- Kenyon NH, Akhmetzhanov AM, Wheeler AJ, vanWeering TCE, de Haas H, Ivanov MK (2003) Giant carbonate mud mounds in the southern Rockall Trough. *Mar Geol* 195:5–30
- Kiriakoulakis K, Harper E, and Wolff GA (2005) Lipids and nitrogen isotopes of two deep-water corals from the North-East Atlantic: initial results and implications for their nutrition. In: Freiwald A, Roberts JM (eds), *Cold-Water Corals and Ecosystems*. Springer-Verlag, Berlin Heidelberg, ISBN:978-3-540-24136-2:715–729
- Le Guilloux E, Olu-Le Roy K, Bourillet JF, Savoye B, Iglésias SP, Sibuet M (2009) First observations of deep-sea coral reefs along the Angola margin. *Deep-Sea Res II* 56:2394–2403
- Merino M (1997) Upwelling on the Yucatan Shelf: hydrographic evidence. *J Mar Syst* 13:101–121
- Mienis F, de Stigter HC, White M, Duineveld G, de Haas H, vanWeering TCE (2007) Hydrodynamic controls on cold-water coral growth and carbonate-mound development at the SW and SE Rockall Trough Margin, NE Atlantic Ocean. *Deep-Sea Res I* 54:1655–1674
- Mienis F, Duineveld GCA, Davies AJ, Ross SW, Seim H, Bane J, Van Weering TCE (2012) The influence of nearbed hydrodynamic conditions on cold-water corals in the Viosca Knoll area, Gulf of Mexico. *Deep-Sea Res I* 60:32–45
- Moore DR and Bullis HR (1960) A deep-water coral reef in the Gulf of Mexico. *Bull Mar Sci Gulf Caribbean* 10:125–128
- Müller-Karger FE, Walsh JJ, Evans RH, Meyers MB (1991) On the seasonal phytoplankton concentration and sea surface temperature cycles of the Gulf of Mexico as determined by satellites. *J Geophys Res* 96:12645–12665
- Mullins HT, Newton CR, Heath K, Vanburen HM (1981) Modern deep-water coral mounds north of Little Bahama Bank: criteria for recognition of deep-water coral bioherms in the rock record. *J Sed Petrol* 51:999–1013
- Neumann AC, Kofoed JW, Keller GH (1977) Lithoherms in the Straits of Florida. *Geology* 5:4–10
- Newton CR, Mullins HT, Gardulski AF (1987) Coral mounds on the West Florida Slope: unanswered questions regarding the development of deepwater banks. *Palaios* 2:359–367
- Orejas C, Gori A, Lo Iacono C, Puig P, Gili JM, Dale MR (2009) Cold-water corals in the Cap de Creus canyon (north-western Mediterranean): spatial distribution, density and anthropogenic impact. *Mar Ecol Prog Ser* 397:37–51
- Paull CK, Neumann AC, am Ende B A, Ussler W, Rodriguez NM (2010) Lithoherms on the Florida–Hatteras slope. *Mar Geol* 166:83–101
- Reed JK, Weaver D, Pomponi SA (2006) Habitat and fauna of deep-water *Lophelia pertusa* coral reefs off the Southeastern USA: Blake Plateau, Straits of Florida, and Gulf of Mexico. *B Mar Sci* 78:343–375
- Roberts JM, Wheeler AJ, Freiwald A (2006) Reefs of the deep: The biology and geology of cold-water coral ecosystems. *Science* 312:543–547
- Roberts JM, Wheeler AJ, Freiwald A, Cairns SD (2009) Coldwater corals. The biology and geology of deep-sea coral habitats. Cambridge University Press:336 pp
- Schlitzer R (2012) Ocean Data View. <http://odv.awi.de>

- Schroeder WW (2002) Observations of *Lophelia pertusa* and the surficial geology at a deep-water site in the northeastern Gulf of Mexico. *Hydrobiol* 471:29–33
- Schroeder WW, Brooke SD, Olson JB, Phaneuf B, McDonough JJ, Etnoyer P (2005) Occurrence of deep-water *Lophelia pertusa* and *Madrepora oculata* in the Gulf of Mexico. In: Freiwald A, Roberts JM (eds), *Cold-Water Corals and Ecosystems*. Springer-Verlag, Berlin Heidelberg, ISBN:978-3-540-24136-2:297–307
- Sheinbaum J, Candela J, Badan A, Ochoa J (2002) Flow structure and transport in the Yucatan Channel. *Geophys Res Lett* 29:1040. doi:10.1029/2001GL013990
- van Oevelen D, Duineveld G, Lavaleye M, Mienis F, Soetaert K, Heip CHR (2009) The cold-water coral community as a hot spot for carbon cycling on continental margins: A food-web analysis from Rockall Bank (northeast Atlantic). *Limnol Oceanogr* 54:1829–1844
- Wawrik B and Paul JH (2004) Phytoplankton community structure and productivity along the axis of the Mississippi River Plume in oligotrophic Gulf of Mexico waters. *Aqua Microb Ecol* 35:185–196
- White M, Mohn C, de Stigter H, Mottram G (2005) Deep-water coral development as a function of hydrodynamics and surface productivity around the submarine banks of the Rockall Trough, NE Atlantic. In: Freiwald A, Roberts JM (eds), *Cold-Water Corals and Ecosystems*. Springer-Verlag, Berlin Heidelberg, ISBN:978-3-540-24136-2:503–514
- White M and Dorschel B (2010) The importance of the permanent thermocline to the cold water coral carbonate mound distribution in the NE Atlantic. *Earth Planet Sci Lett* 296: 395–402
- Zavala-Hidalgo J, Gallegos-García A, Martínez-López B, Morey SL, O'Brien JJ (2006) Seasonal upwelling on the Western and Southern Shelves of the Gulf of Mexico. *Ocean Dynam* 56:333–338

Chapter 5

Hydrographic properties of living cold-water coral reefs in the northern East Atlantic and the Gulf of Mexico

by Silke Glogowski, Wolf-Christian Dullo and Sascha Flögel
(to be submitted)

Abstract

The hydrographic properties of living cold-water coral (CWC) reefs in the North Atlantic are discussed. Cold-water corals (CWCs) are sessile filter feeders and depend on hydrographic properties providing suspended nutrients as well as on the removal of resuspended sediments. Furthermore, living CWC reefs occur in a distinct density ($\sigma\theta$) window as a result of temperature and salinity variabilites. The development of a steep density gradient above living CWC reefs seems to be necessary to advect and accumulate nutrients. The density gradient at the sites on the eastern Atlantic margin north of Gibraltar up to Norway are mainly controlled by changes in salinity, while those south of Gibraltar and in the Gulf of Mexico are more influenced by temperature.

The density gradient is derived by calculating the difference in water mass density between 10 m intervals resulting in the term of $\Delta\sigma\theta_{10m}$. As soon as this gradient is $>0.02 \text{ kg/m}^3$, there is a chance of finding living CWC reefs. Furthermore, if the density gradient of maximum $\Delta\sigma\theta_{10m}$ values forms a thin layer, obviously well developed CWC reefs growth, while a thick layer of maximum $\Delta\sigma\theta_{10m}$ values seem to indicate only thin veneers of living CWC reefs.

5.1 Introduction

Cold-water coral (CWC) reef systems are receiving increasing attention worldwide. The principle cold-water coral species found are the azooxanthellate reef forming scleractinians *Madrepora oculata*, Linneus 1758 and *Lophelia pertusa* (Linneus 1758), living in cold waters of the global ocean (Rogers 1999), with the exception of the polar regions (Le Goff-Vitry et al. 2004; Addamo et al. 2012).

In the northern Atlantic such CWC reefs occur e.g. in the Gulf of Mexico, the Strait of Florida, (Cairns 1984; Bryan and Metaxas 2006; Cairns et al. 2009), Campeche Bank (Hebbeln et al. 2014), NE Atlantic (Zibrowius 1980; Freiwald & Wilson 1998; Rapp & Sneli 1999; Fosså et al. 2002; Freiwald et al. 2004), North Atlantic (Leverette 2004; Braga-Henriques et al. 2013), eastern Atlantic: off Morocco (Glogowski et al. 2015) and Mauretania (Colman et al. 2005; Le Guilloux et al. 2009), and the Mediterranean (Mortensen 2001; Freiwald 2002; Fink et al. 2012; Gori et al. 2013). Temperature and salinity are key factors constraining the distribution of live corals (e.g. Davies et al. 2009; Davies and Guinotte 2011; Vierod et al. 2014), and indirectly ambient seawater density (e.g. Dullo et al. 2008; Flögel et al. 2014). The biogeographical limitation is caused e.g. by changes in sea-surface productivity (Eisele et al. 2011; Wienberg et al. 2011), upwelling regimes (Wienberg et al. 2011), and bottom currents (Huvenne et al. 2005; Rüggeberg et al. 2005), which in turn were affected by changes in intermediate water mass variability (Raddatz et al. 2014).

L. pertusa CWC reefs and coral assemblages occur in different water depths and water masses. This species is found in various depth levels ranging from 39 m (Trondheimsfjord) to 3380 m (western Atlantic Ocean), whereas reefs are most abundant in water depths between 200 and 1000 m (Freiwald and Wilson 1998; Freiwald et al. 2004). Observed temperatures vary between 4°C – 14°C while measured salinities range between 34.8 g/kg and 38.7 g/kg (Davies et al. 2008; Dullo et al. 2008; Mienis et al. 2012; Flögel et al. 2014). This would allow the distribution of living corals over a wide hydrographical range in the water column. However, CWC distribution seems to be limited to suspension-dominated waters (Correa et al. 2011). Furthermore, the investigated sites of living CWC reefs are characterised by a distinct density contrast of the water masses. The habitat of living CWC reefs is characterised by a development of a density gradient (Dullo et al. 2008), which seems to favour lateral nutrient advection and enrichment (Kiriakoulakis et al. 2004; Grasmueck et al. 2007; White et al. 2007; Flögel et al. 2014) and/or larval dispersal. Dullo et al. (2008) indicated that living CWC reefs occur around density surfaces supporting intermediate nepheloid layers (INLs), where food accumulation and availability for bottom biota increases. According to Dullo et al. (2008) most of the pristine and profuse living CWC reefs along the European continental margin occur in water mass densities of $\sigma_{\Theta}=27.35 - 27.65 \text{ kg/m}^3$.

Thus, the concept of a narrow density envelope defining the overall habitat range of the CWC reefs was further related to DIC concentrations resulting in the definition of reef categories by Flögel et al. (2014) with category I: real CWC framework of several 100 m elevation, category II: patchy CWC growth of some horizontal extension but very limited vertical elevation forming a thin veneer, and category III: small, isolated colonies. Hebbeln et al. (2014) further argued that a steep gradient in density seems to be a sensitive indicator for living CWC reef communities.

This study presents the measured and calculated hydrographic gradients at different locations in the northern Atlantic in a comparative way.

5.1.1 Water mass characteristics

The most basic and common tool to describe the distribution of the major water masses is the temperature-salinity (T-S) plot, which has a specific relationship to the observed values of temperature, salinity (Emery and Meincke 1986; Emery 2001) and to the water depth accordingly. This T-S diagram can be used to define water masses by locating their extrema, which are divided into three main sections from the surface to the bottom with the upper surface water, the intermediate water and the deep water.

The current and the water mass regime of the North Atlantic is an essential part of the global thermohaline circulation with large water mass transports (Stramma 2001) driven by temperature and salinity gradients. The surface circulation of the North Atlantic is controlled by the anticyclonic and clockwise subtropical gyre including the East- (EGC), and West- (WGC) Greenland Current the North Atlantic Current (NAC), the Florida Current (FC), the Gulf Stream (GS), the Azores and the Canary Currents (CC), the North Equatorial Current (NEC), and the Loop Current (LC) in the Gulf of Mexico (Stramma 2001; SM Fig. 5.1). The general surface hydrography in the North Atlantic is characterised by the northward transport of warm subtropical water to the higher latitudes, the NAC, which split into two branches (northward into the Norwegian-Greenland Sea and southward into the Bay of Biscay; Pingree 1993). Emery (2001) described this component of the North Atlantic circulation with surface water masses (0 – 500 m water depth) and its separation into Western North Atlantic Central Water (WNACW: 7° – 20°C; 35 – 36.7 g/kg) and Eastern North Atlantic Central Water (ENACW: 8° – 18°C; 35.2 – 36.7 g/kg) (Emery and Meincke 1986; Pollard et al. 1996; White 2007).

In the northern part the North Atlantic interacts with the Arctic Ocean through the Norwegian Sea and the Fram Strait with the Atlantic Subarctic Upper Water (ASUW: 0° – 4°C; 34 – 35 g/kg).

The boundaries between surface and intermediate waters are identified by the shape and the pattern of profiles in T-S plots (Emery and Meincke 1986). The intermediate depth Atlantic Ocean exhibits a northward transport as Western Atlantic Subarctic Intermediate Water (WASIW: 3° – 9°C; 34 – 35.1 g/kg) and an eastward transport as Eastern Atlantic Subarctic Intermediate Water (EASIW: 3° – 9°C; 34.4 – 35.3 g/kg). The WASIW consists of Labrador Sea Water (LSW), which is formed on the offside of the Labrador Current (LAC). Additionally, the Antarctic Intermediate Water (AAIW) is one of the prominent water masses in the North Atlantic. The AAIW is formed at the Antarctic Polar Front and migrates northward between 800 – 1000 m water depth. The AAIW is characterised by low salinities (minimum of 34.9 g/kg), higher oxygen content, nutrient richness and relatively cool temperatures (Emery 2001). Another important component of the intermediate Atlantic Ocean is the Mediterranean Outflow Water (MOW: 2.6° – 11°C; 35 – 36.2 g/kg), which is assigned to an increase of salinity and temperature with respect to surrounding water masses. This salty water flows out of the Mediterranean Sea through the Strait of Gibraltar splitting into two branches. The first one flows northward along the European continental margin beneath the ENAW with mixing processes between both in the eastern North Atlantic and in addition with Subarctic Intermediate Water (SAIW) in the western area of the North Atlantic. The second branch is bathymetrically deeper and mix with Labrador Sea Water (LSW; White et al. 2005; White 2007). The upper level of MOW is associated with a permanent thermocline. The depth of this thermocline matches the mean water depth where living CWC reefs and their associated carbonate mounds are found on the European continental margin. This water depth corresponds to the density envelope of $\sigma_{\theta}=27.35 - 27.65 \text{ kg/m}^3$ (Dullo et al. 2008). There is a link between the top of the MOW and the peak abundance of CWC reefs (Freiwald 2002). De Mol et al. (2005) suggested that this possible relationship between mounds and MOW during different geological periods transported larvae of CWCs from the Mediterranean Sea to initiate the formation of the various mound provinces.

In the North Atlantic the deep and abyssal waters (>1500 m) are the North Atlantic Deep Water (NADW: 1.5° – 4°C; 34.8 – 35 g/kg) and the Arctic Bottom Water (ABW: -1.8° – -10.5°C; 34.88 – 34.94 g/kg); (Emery and Meincke 1986; Emery 2001). The cold and dense NADW is formed in the subpolar gyre in the Greenland Sea (GS) overflows the Denmark Strait and moves southward between 1200 – 4000 m water depth (Stramma 2001). The deep water formed in the Antarctic is the densest water mass, the Antarctic Bottom Water (AABW: -0.9° – -1.7°C; 34.64 – 34.72 g/kg) and can be traced up to north of 40°N (Stramma 2001).

5.1.2 Physical settings of investigated sites

Gulf of Mexico (GoM)

The GoM is a semi-closed basin of approximately 1.5 million km² with continental shelves surrounding a deep abyss (Brooke and Schröder 2007). From the Caribbean Sea and through the Yucatan Strait (YS), Caribbean Surface Water (CSW), Subtropical Intermediate Water (STUW) and Antarctic Intermediate Water (AAIW), inflow and spread throughout the whole GoM-basin, becoming denser while flowing in direction to the Atlantic (Gyory et al. 2005 a). The occurrence of a clockwise flow that extends northward into the GoM and joins the Yucatan Current and the Florida Current is known as the Loop Current (Hofmann and Worley 1986). The Loop Current influences the hydrodynamics even down to 1000 m water depth of the GoM (Hamilton 1990) and is variable in position (Gyory et al. 2005c) with some direct extremes to the Florida Current (Molinari and Mayer 1982; Hofmann and Worley 1986).

Campeche Bank / Yucatan Strait

The Yucatan Strait, at the southeastern slope of the Campeche Bank marks the western boundary of the gateway between the Caribbean and the GoM (Ordonez 1936). The Caribbean Current transports water northward into the GoM via the Yucatan Current through the Yucatan Channel (Sheinbaum et al. 2002; Gyory et al. 2005b; Hübscher et al. 2010; Wei et al. 2012). The Campeche Bank borders the Yucatan Strait on its eastern margin. According to Merino (1997) three main water masses comprise the water column there: the Caribbean Surface Water (CSW), the Subtropical Intermediate Water (STUW) and the Antarctic Intermediate Water (AAIW). The uppermost surface water of ~80 m water depth with salinities of <36.4 g/kg indicating the CSW (26° – 27.5°C).

Between 100 and 160 m water depth the detected salinity maximum (<37 g/kg) characterises the upper STUW (25.3° – 21.2°C, 36.58 – 37.0 g/kg), which comprises the water column down to 540 m. There, salinity drops below 35.0 g/kg, marking the presence of upper AAIW and the homogenous deeper portion portray the AAIW down to the CTD water depth of 1200 m (Fig. 5.2).

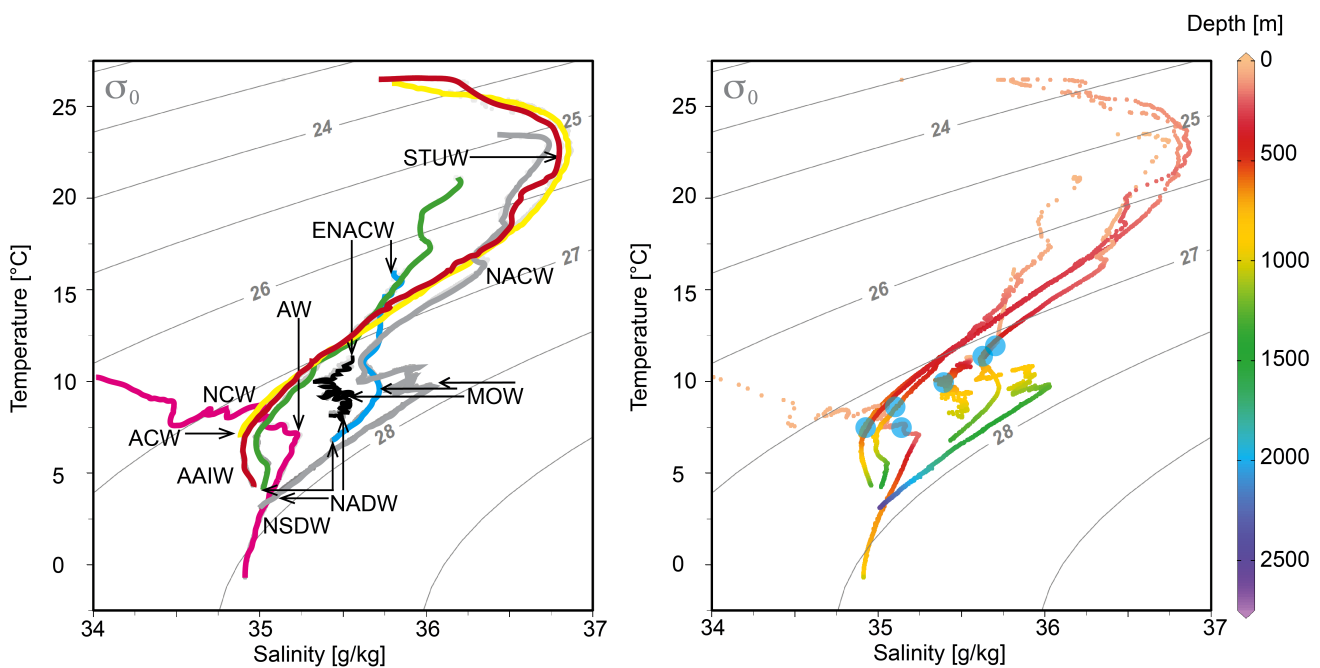


Fig. 5.2 *left*) T-S plot of water masses observed at the studied sites. Each different site is marked by a different color: CB=*red*, GBB=*yellow*, BB=*blue*, PS=*black*, Norwegian margin=*magenta*, MAC=*grey*, MAU=*green*. Abbreviations for water masses are: STUW=Subtropical Intermediate Water; ENACW=Eastern North Atlantic Central Water; AW=Atlantic Water; NCW=Norwegian Coastal Water; ACW=Antilles Current Water; MOW=Mediterranean Outflow Water; AAIW=Antarctic Intermediate Water; NADW=North Atlantic Deep Water; NSDW=Norwegian Sea Deep Water. *right*) The position of living CWC reefs are indicated by blue dots. The color coding represents the depth. The different site to which each T-S profile belongs can be depicted from color coded profiles in the left panel

West-Florida Slope

Off West-Florida the uppermost part of the water column down to 80 m comprises the shallow water mass of the Florida Shelf Surface Water (FSSW) with the lowest salinities around 34.14 g/kg shallower than 50 – 60 m. This water mass is characterised and influenced by the occurrence of relatively fresh water inflow of the Mississippi Water. Below 84 m salinities increase and indicate the onset of the Subtropical Intermediate Water (STUW). The salinity maximum in the water column from 120 – 160 m ranges between 36.72 and 36.87 g/kg, which comprises the water column down to 620 m. There, the upper Antarctic Intermediate Water (AAIW) with a salinity minimum of 34.90 g/kg is found in water depths between 620 – 700 m, and the homogenous deeper portion portray the AAIW down to the CTD water depth of 1280 m.

Great Bahama Bank

The Bahama Archipelago is a complex system of shallow banks and deep basins. It forms a triangle between the Florida Current (FC), the Atlantic Ocean Subtropical gyre and the Antilles Current (AC), and the Carribean Sea (CS) and these water masses reach the Great Bahama Bank (GBB); (Chérubin 2014).

The uppermost part of the water column comprises the shallow water mass of the Tropical Surface Water (TSW) and is influenced by the FC. This water mass is identified by salinities of 36.18 g/kg at ~60 m water depth down ~160 m. There, the onset of the Florida Current Surface Water (FCSW) is indicated by the maximum salinity of 36.9 g/kg, and down to the minimum salinity in ~700 m (35.01 g/kg) indicating the onset of the Antilles Current Water (ACW; Fig. 5.2). At ~1000 m water depth the onset of the Deep Western Boundary Current Water (DWBCW) occurs which is of lower salinity and lower temperature with respect to the intermediate water masses (Chérubin 2014).

St. Nazaire Canyon / Bay of Biscay

The water masses presented in St. Nazaire Canyon on the American Margin are prevalently of North Atlantic and Mediterranean origin (Pollard et. al 1996). The surface water is the Eastern North Atlantic Central Water (ENACW) and extends down to 450 and 550 m respectively. The salinity values are indicated between 35.60 g/kg on the Pagès Escarpment, and 35.71 g/kg in the St. Nazaire Canyon in water depths of 750 – 798 m (Dullo et al. 2017).

The lower part of the ENACW indicated by a salinity minimum of ~ 35.60 g/kg and seemingly influenced by the Subarctic Intermediate Water (SAIW). Below the ENACW, the rapid increase in salinity emblemise the Mediterranean Outflow Water (MOW), which is distributed down to ~ 1500 m water depth. Within this water column the salinity maxima occur between 35.80 and 36.17 g/kg in 900 – 1100 m water depth respectively. The influence of the MOW is highest among the sites on the Galicia margin (36.17 g/kg), while its influence slightly decreases gradually from 35.83 g/kg on Pagès Escarpment to 35.79 g/kg in St. Nazaire Canyon (Dullo et al. 2017). Below the MOW (Fig. 5.2), the North Atlantic Deep Water (NADW) underlies between 1500 m and 3000 m. The detected salinity decreases at 1800 m water depth and is influenced by the Labrador Sea Water (LSW) according to Pingree and Morrison (1973) and Gonzáles-Pola et al. (2006).

Porcupine Seabight

Within the Porcupine Seabight the distribution of water masses show a warm and homogenously distributed surface layer of 40 to 50 m depth. Below, the Eastern North Atlantic Central Water (ENACW) exhibits a linear, uniform distribution down to a salinity minimum in ~ 650 m – 700 m water depth, according to Pollard et al. (1996). Below 700 m water depth the onset of the upper Mediterranean Outflow Water (MOW) appears by increasing salinity with maximum values of 35.6 g/kg and lower temperatures. In this water column ENAW and MOW dominate the intermediate hydrography.

On Rockall Bank margin the surface layer stretches down to 50 m water depth and is further influenced by Subarctic Intermediate Water (SAIW) down to ~ 300 m water depth. This water mass is colder and less saline with respect to the Porcupine Seabight margin. Eastern North Atlantic Central Water (ENACW) follows below down to a salinity minimum in 800 – 1000 m suggesting an insignificant MOW advection to this area. The influence of the MOW might be portayed by a slight increase of salinity (35.6 g/kg). Below 1000 m water depth, with salinity of 35.45 g/kg appears to be the onset of NADW (Fig. 5.2).

Norwegian Sea

The Norwegian margin is characterised by the Norwegian Coastal Water (NCW) with salinities less than 35 g/kg in water depths of >50–250 m with an increase in salinity from 33.5 to 35 g/kg within the first 200 m. Below this surface water and between 250 and 600 m (Skardhamar & Svendsen 2005) the distinct maximum in salinity >35 g/kg and a decrease in temperature <8.5°C indicates the Atlantic Water (AW). Below 600 – 800 m the boundary occurs between AW and Norwegian Sea Deep Water (NSDW) occurs. NSDW is characterised by salinities below 34.95 g/kg and low temperatures less than 0°C (Fig. 5.2). At the Stjernsund sill the variability of temperature and salinity was already reported by Dons (1944), who published the first paper on the occurrence of living CWC reefs from that region. NCW with salinities <35 g/kg occupies the complete water column east of the sill, while Atlantic Water (AW) occurs below ~250 m west of the sill.

At Sveinsgrunen margin salinity values at the surface layer reveal a slight decrease down to 35.01 g/kg at 100 m water depth, indicating the Norwegian Coastal Water (NCW). This surface water mass is influenced by continental river discharge and inflowing fjord water. Below the NCW, salinity increased to 35.24 g/kg at 176 m water depth, and marks the presence of Atlantic Water (AW) with this maximum in salinity. At ~760 m water depth the boundary occurs between AW and the below NSDW, and reveals the salinity minimum with 34.92 g/kg (Fig. 5.2).

Morocco and Mauretania

The uppermost part of the water column down to 52 m comprises the upper surface layer and is identified as shallow water mass of the Subtropical Underwater (SUW), which may be influenced by the Surface Canary Current Water (SCCW) with the lowest salinities around 36.31 g/kg. The salinity maximum values between 99 and 117 m water depth range from 36.35 to 36.36 g/kg and characterise the North Atlantic Central Water (NACW), which reaches up north into the Agadir region. The NACW is a subsurface water mass with moderately temperatures around 16.5°C (Mittelstaedt 1991; Van Camp et al. 1991; Morigi et al. 2001; Vadorpe et al. 2014). According to Mittelstaedt (1991) and Aristegui et al. (2009), the predominantly NACW is upwelling seasonally. Deeper, around a water depth of 650 m, the salinity maximum of 35.69 g/kg is attributed to the Mediterranean Outflow Water (MOW) in combination with relatively high temperatures of 9.87°C. Below ~1250 m water depth, the deepest part of the water column is formed by the North Atlantic Deep Water (NADW) and the topmost portion is characterised by temperatures of 9.7°C and salinities of <35 g/kg (Fig. 5.2).

5.1.3 Density gradient

Different physical properties such as density, potential temperature and salinity have been applied in order to identify the suitable habitats for CWCs. In this study, we focus on the gradients of these properties in relation to depth and their possible influence on living CWC reefs.

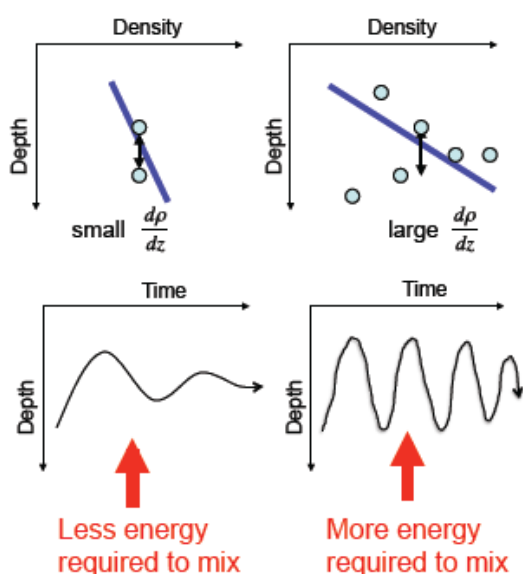


Fig. 5.3 Steepness of density gradients over a very short depth range, e.g. $\Delta\sigma_{\Theta_{10m}}$ maximum, results in very little mixing processes

A steep gradient is characterised by a very rapid change of a property over a very short depth range. This relation portrays the variability in vertical seawater stratification. Steep density gradients therefore result in stable conditions – with only little mixing (Fig. 5.3). Therefore, a steep density gradient at water mass boundaries can have the effect of trapping nutrients, preventing vertical mixing and favour lateral advection and transport of particles (e.g. POC and DOC).

This enhanced stratification as a result of steep gradients may also favour the distribution of larvae (gametes) of *L. pertusa* as a self enhancing process of CWC reef growth Dullo et al. (2008). In this study, we try to relate the measured / calculated gradients to the CWC reef categories (I – III) according to Flögel et al. (2014).

5.2 Material and Methods

5.2.1 Hydrography

Single conductivity-temperature-depth (CTD) data were obtained in order to determine the physical properties of the water masses in the different investigated sites. In addition, repeated CTD measurements were performed as Yoyo-CTDs (Dullo and Flögel 2011) at the same spot, comprising up to 13 individual casts within 12 h to cover a tidal cycle. The CTD measurements of the water column down to each maximum water depth were conducted using a SEABIRD “SBE 9 plus” underwater unit and a SEABIRD “SBE 11 plus V2” deck unit. The vertical profile over the water column provided standard data for conductivity, temperature, pressure and dissolved oxygen (Schlitzer 2013). Conductivity and temperature data were used to compute salinity. All data presented refer to the downcast of the individual CTD deployments.

CTDs were collected at different sites (SM Fig. 5.4) in the Gulf of Mexico (GoM) and on the western margin of the Great Bahama Bank (GBB) during cruise MSM20-4 of *R/V Maria S. Merian* in March/April 2012 (Hebbeln et al. 2014). Additional data derive from the Eugen Seibold coral garden ~40 nautical miles north of the Agadir Canyon off Morocco (Glogowski et al. 2015) sampled during cruise MSM32 with *R/V Maria S. Merian* in October 2013), and on the North-East Atlantic: Ireland / Porcupine Seabight during Meteor cruise M61-1 (April 2004), Norwegian margin during cruises POS325 (July 2005) and POS434 (May 2012), and in the Bay of Biscay during cruise M84-5 (May 2011).

The hydrography of the investigated sites such as Campeche Bank (CB; NE Yucatan Strait Peninsula), West-Florida Slope (W-FI), and Great Bahama Bank Slope (GBB) were reported in Hebbeln et al. (2014), while the respective data off Morocco (MAC; Agadir Canyon) are described in Glogowski et al. (2015). NE-Atlantic: e.g. Porcupine Seabight data and Norwegian Reefs e.g. Sula reef data are described in Dullo et al. (2008) and Flögel et al. (2014).

The derived potential density (σ_{Θ} =sigma-theta) is defined as:

$$\sigma_{\Theta} = 1 / V_{(s,\Theta,p)} - 1000 \text{ kg/m}^3 \quad (\star 5.2)$$

with V =specific volume, S =salinity, Θ =potential temperature and p =pressure at the sea surface.

Since seawater density increases with water depth we calculated the gradient by subtracting the measured seawater density in a distinct depth from the equivalent value 10 m above resulting in $\Delta\sigma_{\Theta_{10m}}$ (kg/m³). This $\Delta\sigma_{\Theta_{10m}}$ varies within the depth range of living *L. pertusa* CWC reef and we selected for each site the $\Delta\sigma_{\Theta_{10m}}$ maximum value to portray this variability. These gradients for other properties like potential temperature and absolute salinity were derived in the same way.

5.3 Results

5.3.1 Hydrography around living CWC reefs

CTD measurements of the ambient seawater were used to identify the distribution of water masses in the North Atlantic. Regional temperature-salinity (T-S) plots (Fig. 5.4) were used to determine the variability of water masses right on top of living *L. pertusa* reefs and are given in SM Table 5.1. The Yoyo-CTDs reveal the variability of the gradients. However, since repeated Yoyo-CTD casts never reach exactly the identical bottom regime due to navigational issues and current regimes only the first cast is being used. Although the plotted measurements of the repeated casts reveal the same information about the different amplitude in gradients within the same water depth.

Campeche Bank

Occurrences of living *L. pertusa* reefs were observed during ROV dives of MSM20-4 (Hebbeln et al. 2012) in water depth from 497 to 560 m. The analysis of the CTD measurement (Fig. 5.5) at 552 m water depth reveal a potential temperature of 7.92 °C, an absolute salinity of 35.16 g/kg and a potential density, sigma-theta σ_{Θ} of 27.27 kg/m³. The calculated maximum values of $\Delta\sigma_{\Theta_{10m}}$ at 0.0621 kg/m³ ($\sigma_{\Theta}=27.28$ kg/m³) were found in water depth of 518 m and are mainly the result of temperature in this area, and $\Delta\sigma_{\Theta_{10m}}$ maximum was found 34 m above the living CWC reefs (SM Table 5.2).

West-Florida

During the cruises MSM20-4 (Hebbeln et al. 2012) and M78/1 (Schönfeld et al. 2009) and ROV dives revealed the occurrences of living *L. pertusa* reefs in the depth range between 513 - 530 m. The potential temperature varies between 7.67° – 7.80°C and the absolute salinity between 35.12 – 35.14 g/kg, and the potential density (sigma-theta; σ_{Θ}) between 27.27 – 27.28 kg/m³ (Fig. 5.5). The density gradients are as well mainly result of temperature in this area and $\Delta\sigma_{\Theta_{10m}}$ maximum was found 10 – 17 m above the living CWC reefs (SM Table 5.2).

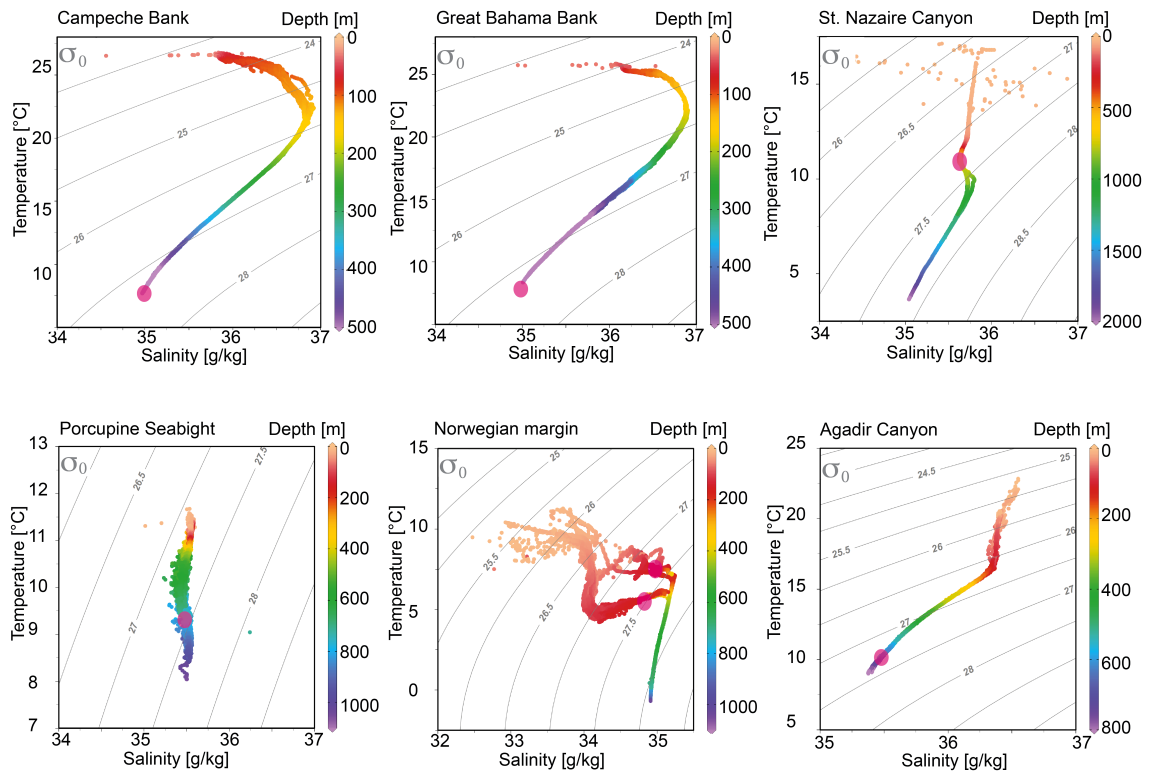


Fig. 5.5 Variability of water masses of the studied sites with respect to potential temperature, salinity and potential density portrayed in T–S diagrams. Living *Lophelia pertusa* reefs are indicated by purple dots. Isopycnals are calculated with the reference pressure at 0 m (σ_θ), i.e. sea level. Abbreviations for localities are: Campeche Bank (CB), Great Bahama Bank (GBB), St. Nazaire Canyon (BB), Porcupine Seabight (PS), Norwegian margin, Agadir Canyon (MAC)

Great Bahama Bank

Occurrences of living *L. pertusa* reefs were observed during ROV dives of cruise MSM20-4 (Hebbeln et al. 2012) in depth between 618 m and deeper. CTD measurement at 618 m revealed a potential temperature of 9.30°C, absolute salinity of 35.28 g/kg and a potential density (sigma-theta; σ_θ of 27.15 kg/m³; Fig. 5.5). The density gradients are more influenced by salinity and less by temperature in this region. The $\Delta\sigma_{\theta 10m}$ maximum was found 60 m above the living CWC reefs (SM Table 5.2).

St. Nazaire Canyon

Living *L. pertusa* reefs were found between 700 – 850 m water depth in the St. Nazaire Canyon during METEOR cruise M84-5 (Flögel et al. 2011). CTD measurements revealed in water depths of 798 and 844 m a potential temperature range between 9.92° and 10.26°C, an absolute salinity between 35.71 and 35.72 g/kg, whereas the potential density ranges between 27.46 and 27.51 kg/m³ (Fig. 5.5). Maximum values of $\Delta\sigma_{10m}$ were found between at 0.0266 kg/m³ ($\sigma_{\Theta}=27.40$ kg/m³) and 0.0449 kg/m³ ($\sigma_{\Theta}=27.47$ kg/m³) at water depth of 765 m and 834 m. The density gradients are mainly driven by temperature in this area and $\Delta\sigma_{10m}$ maximum was found 10 – 55 m above the living CWC reefs (SM Table 5.2).

Porcupine Seabight

Living CWC reefs were found between 600 – 800 m water depth (Rüggeberg et al. 2007; Wienberg et al. 2008), and at 810 – 901 m water depth (Flögel et al. 2014). During METEOR M61-1 (Pfannkuche et al. 2004) occurrences of living *L. pertusa* reefs were observed on the Galway mound in a depth range between 800 – 924 m where the potential temperature ranged from 8.96° - 9.78°C, the absolute salinity varied between 35.46 – 35.53 g/kg, and the potential density σ_{Θ} ranged from 27.38 – 27.54 kg/m³ (Fig. 5.5). Highest calculated gradients range between $\Delta\sigma_{10m}$ maximum values of 0.0769 kg/m³ and 0.0785 kg/m³ at water depth from 783 m to 859 m. The density gradients depend mainly on salinity in this area and $\Delta\sigma_{10m}$ maximum was found 12 - 27 m above the living CWC reefs (SM Table 5.2).

Norwegian margin

On the Norwegian margin living CWC reefs occur in water depth between 150 and 400 m (Dullo et al. 2008). During POSEIDON cruises POS434 (Pannkuche et al. 2012) and POS325 (Freiwald and Dullo 2005) occurrences of living *L. pertusa* reefs were observed in depth range between 140 – 380 m, in detail: at Røst Reef between 300 and 380 m, around 140 and 250 m at Fugløybanken, between 300 and 380 m at Sula Reef, and in Stjærnsund at 208 m, and at Traenadjupet around 297 m. The potential temperature (Θ ; °C) varies between 5.79° at Stjærnsund to 7.24°C at Traenadjupet. Absolute salinity ranges from 34.90 at Stjærnsund to 35.4 g/kg at Røst Reef and Traenadjupet.

The potential density, sigma-theta σ_θ varies between 27.35 at Stjærnsund to 27.61 kg/m³ at Røst Reef (Fig. 5.5). At Røst Reef and Traenadjupet localities the envelope of the maximum density gradient $\Delta\sigma_{\theta_{10m}}$ range between 0.0113 kg/m³ ($\sigma_\theta=27.59$ kg/m³) and 0.0170 kg/m³ ($\sigma_\theta=27.59$ kg/m³) at water depth from 248 m to 286 m. Whereas, the classical locality of Stjærnsund the density gradients ($\Delta\sigma_{\theta_{10m}}$) vary between maximum values of 0.033 kg/m³ ($\sigma_\theta=27.47$ kg/m³) and 0.0704 kg/m³ ($\sigma_\theta=27.36$ kg/m³) at water depth from 163 m to 223 m.

At the classic locality of Stjærnsund the $\Delta\sigma_{\theta_{10m}}$ maximum was found 45 - 60 m above the living CWC reefs like at Røst Reef (54 - 55 m) and Traenadjupet (49 m; SM Table 5.2). The density gradients of all Norwegian sites are mainly driven by changes in salinity.

Morocco

During cruise MSM32 (Krastel et al. 2013) occurrences of living *L. pertusa* reefs reveal a depth range between 674 – 704 m, with detected potential temperature between 9.87° - 10.12°C and absolute salinity between 35.63 – 35.65 g/kg (Fig. 5.5). The potential density (σ_θ) varies between 27.29 – 27.33 kg/m³. The maximum of $\Delta\sigma_{\theta_{10m}}$ was found at 0.0502 kg/m³ ($\sigma_\theta=27.32$ kg/m³) at water depth of 662 m. $\Delta\sigma_{\theta_{10m}}$ maximum was found 9 m above the living CWC reefs (SM Table 5.2).

Mauretania

During POS346 (Westphal et al. 2006; Westphal et al. 2012) living *L. pertusa* reefs were observed around 575 m, having potential temperatures of 9.46°C, absolute salinities of 35.37 g/kg and a potential density, sigma-theta σ_θ of 27.20 kg/m³ (Fig. 5.5). The maximum of $\Delta\sigma_{\theta_{10m}}$ was found at 0.0343 kg/m³ ($\sigma_\theta=27.06$ kg/m³) at water depth of 546 m. $\Delta\sigma_{\theta_{10m}}$ maximum was found 28 m above the living CWC reefs (SM Table 5.2).

For both sites, Morocco and Mauretania the density gradients result more from temperature variabilities than from changes in salinity.

5.4 Discussion

Living CWC reefs occur in water masses of different temperatures and salinities almost everywhere in the global ocean (Rogers et al. 2002; Roberts et al. 2006). A critical factor controlling their distribution is sufficient food supply that is commonly driven by the interplay of surface water productivity and the local hydrographic regime (e.g. stratification, internal waves and tides) delivering food particles to the CWCs (Duineveld et al. 2004 and 2007; White et al. 2005).

However, living CWC reefs seem to be linked to water masses of distinct densities (Dullo et al. 2008; Flögel et al. 2014). This relation was confirmed in several other studies (e.g. van Rooij et al. 2010; De Mol et al. 2011). Hebbeln et al. (2014) argued that one of the main forcing factors favouring the existence of living CWC reefs, is a strong density gradient, which might act as a trap for sinking food particles and may enhance their residence time in the upper intermediate water column leading to an accumulation of nutrients just above the living CWC reefs.

Following the idea of Hebbeln et al. (2014), this study demonstrates that density gradients occur above each investigated locality of living CWC reefs in the North Atlantic, independent from water mass, water depth and region (SM Table 5.2). Looking at the calculated maximum values of $\Delta\sigma_{\Theta_{10m}}$ these range from very low values at e.g. in the Stjærnsund, where CWC reefs cover an existing relief (Rüggeberg et al. 2011) but do not form carbonate mounds such as those in the Porcupine Seabight (Rüggeberg et al. 2007), with highest maximum values of $\Delta\sigma_{\Theta_{10m}}$ (Fig. 5.6).

According to Flögel et al. (2014) both CWC reefs belong to category I, and therefore the maximum values of $\Delta\sigma_{\Theta_{10m}}$ do not tell anything about the reef category. This is also seen at the other investigated sites belonging to other categories like in the St. Nazaire Canyon (Fig. 5.7), or the Campeche Bank CWC reefs (SM Fig. 5.8), and off Morocco region (Fig. 5.9 and SM Table 5.2). The maximum values of $\Delta\sigma_{\Theta_{10m}}$ of the density gradients irrespectively of any reef category vary considerably (Fig. 5.10).

Porcupine Seabight - category I

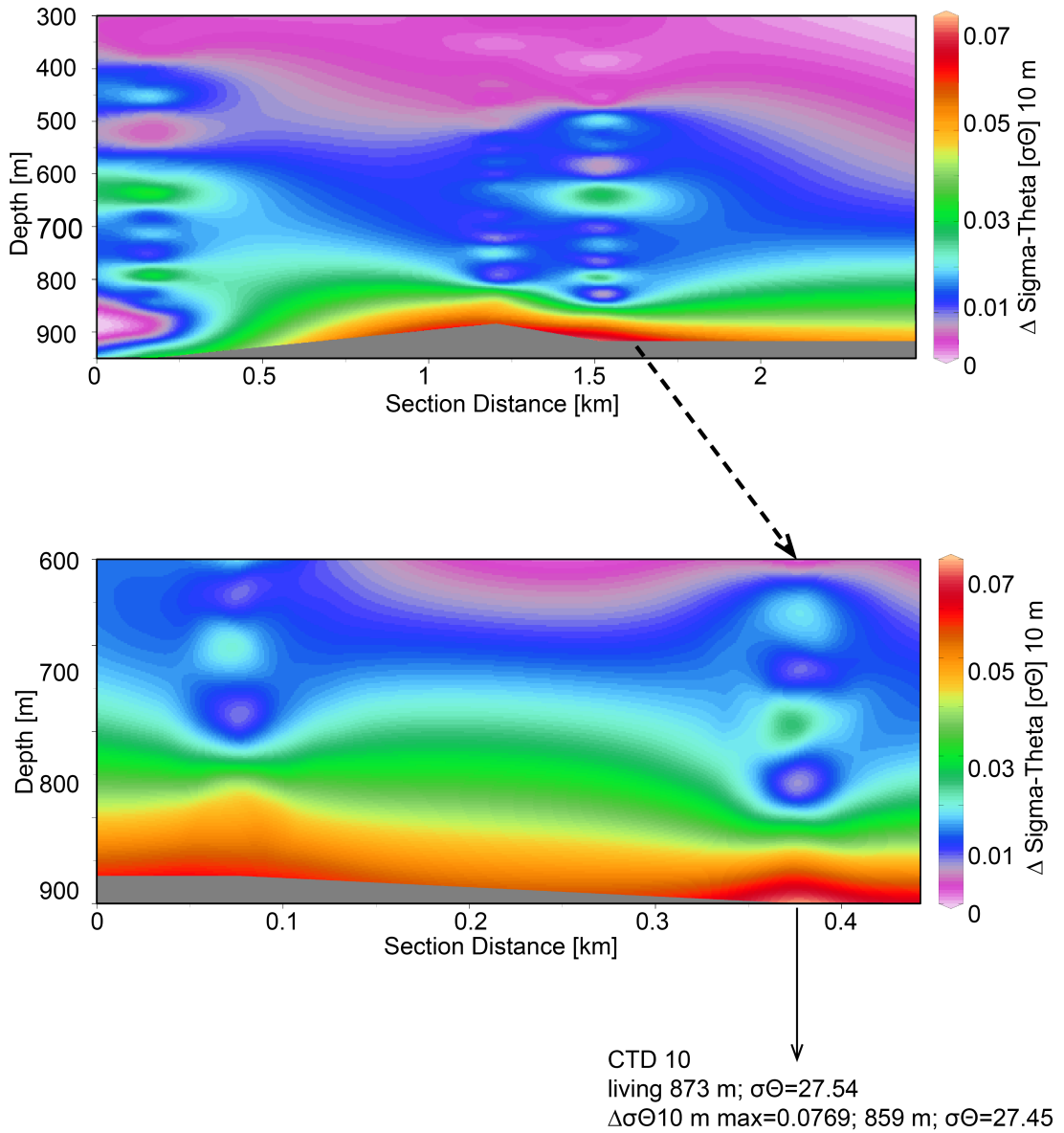


Fig. 5.6 Cross section of density gradients ($\Delta\sigma_{\Theta 10m}$) through water masses in the Porcupine Seabight (PS) – category III. The *upper* section shows the slope over a distance of 2.5 km and the density gradients between 10 m interval. The *bottom* figure zoomed in the section, where living *Lophelia pertusa* reefs were found ($\Delta\sigma_{\Theta 10m}$ maximum >0.07)

St. Nazaire Canyon - category II

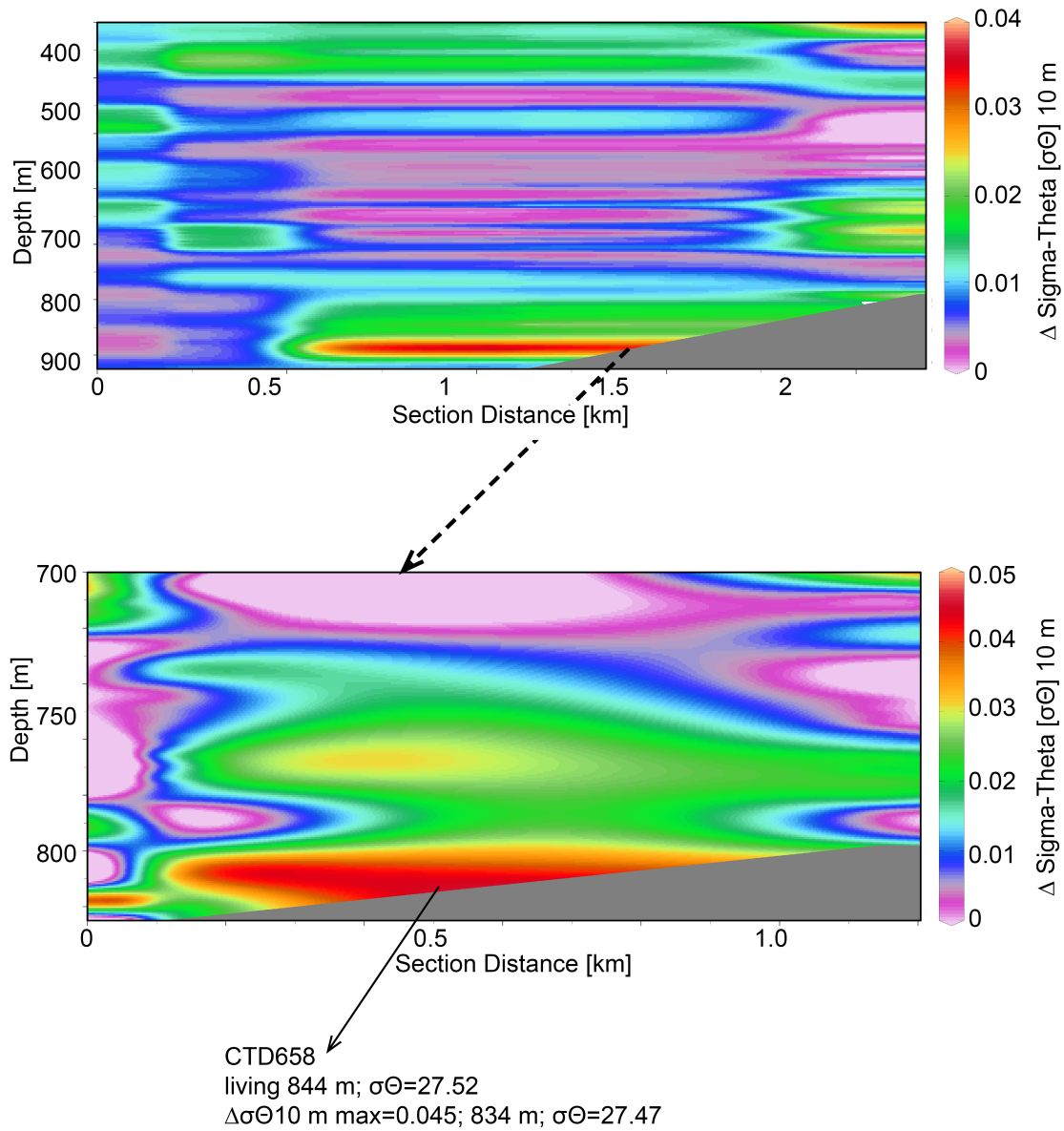


Fig. 5.7 Cross sectioned density gradients ($\Delta\sigma\Theta_{10\text{m}}$) through water masses in the St. Nazaire Canyon (BB) – category II. The *upper* section figure shows the slope over a distance of 310 km. The *bottom* figure zoomed in the section, where living *Lophelia pertusa* reefs were found ($\Delta\sigma\Theta_{10\text{m}}$ maximum >0.04)

Morocco- category III

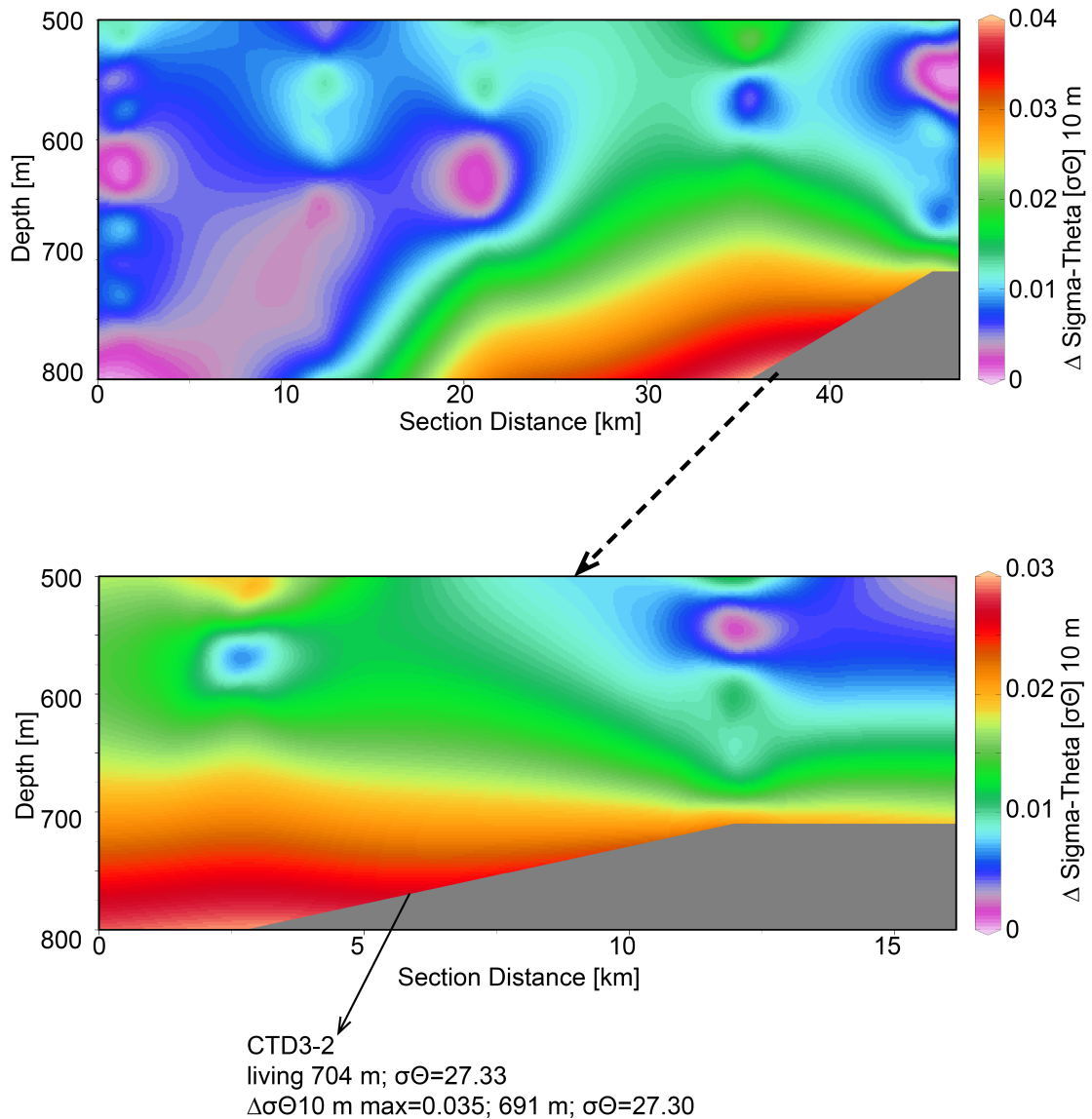


Fig. 5.9 Cross sectioned gradients ($\Delta\sigma_{10m}$) through water masses in the Agadir Canyon (MAC) – category III. The *upper* section figure shows the site over a distance of 65km. The *bottom* figure zoomed in the section, where living *Lophelia pertusa* reefs were found ($\Delta\sigma_{10m}$ maximum >0.03)

Regardless of categories of living CWC reefs *sensu* Flögel et al (2014), there is a link between the regional occurrences of CWC reefs and the yielded density gradient. The calculated density gradient of $\Delta\sigma\Theta_{10m}$ is defined by seawater temperature and salinity (★5.2). This density gradient of $\Delta\sigma\Theta_{10m}$ reaches maximum values up to $>0.07 \text{ kg/m}^3$, which are highest in the studied area of Porcupine Seabight and are driven by changes in salinity. In contrast, the living CWC reefs in the Norwegian Stjernsund occur in much shallower water depth (SM Table 5.2) and are as well salinity controlled density gradients ($\Delta\sigma\Theta_{10m}$). Similarly the density gradient in the Bay of Biscay region is mainly caused by variabilities in salinity (Dullo et al. 2017). This is in contrast to Morocco and Mauretania, and the Campeche Bank province (Fig. 5.10; category III), where the calculated density gradients are mainly driven by temperature on top of the living CWC reefs. Thus, localities mainly driven by salinity, seem to be regions with enhanced productivity like the Porcupine Seabight (White et al. 2005) or off Norway (Freiwald et al. 1997).

Irrespectively of categories, however, the density gradient expressed as $\Delta\sigma\Theta_{10m}$ seems to be indicative for living CWC reefs as soon as its value is $>0.02 \text{ kg/m}^3$. In addition, each studied site shows the density gradient maximum peak $\Delta\sigma\Theta_{10m}$ similar to the maximum peak of the temperature gradient or the salinity gradient respectively, undulating more or less in the same water depth (e.g. GoM SM Fig. 5.11). This is also demonstrated by the repeated Yoyo-CTD measurements of the Campeche Bank, portayed as an example about the amplitude in temperature and salinity variability of uneven casts (SM Fig. 5.12).

Moreover, using the classification of category I the density gradient maximum occurs $\sim 45 - 60 \text{ m}$ above the living CWC reefs on the Norwegian Stjernsund margin, and $\sim 12 - 27 \text{ m}$ in the Porcupine Seabight region. At sites of category II the density gradient maximum is located $\sim 10 - 55 \text{ m}$ above the living CWC reefs, and at sites of category III the density gradient maximum is located $\sim 9 - 60 \text{ m}$ above the living CWC reefs (SM Table 5.2).

The comparison between reef categories *sensu* Flögel et al. (2014) and the presented data of $\Delta\sigma\Theta_{10m}$ density indicates differences around the lower boundaries. While there is a link between the depth range in peak abundance of the maximum of $\Delta\sigma\Theta_{10m}$ above the living CWC reefs, it seems that this particular height of thickness of maximum $\Delta\sigma\Theta_{10m}$ may be indicative for the distribution of living CWC reefs. Living and pristine reef systems of category I (Flögel et al. 2014) exhibit 15 m thickness of $\Delta\sigma\Theta_{10m}$ on the Norwegian Stjernsund margin, same as in the Porcupine Seabight, while the poor occurrences of category III show such a thickness of 50 m over of the living CWC reefs.

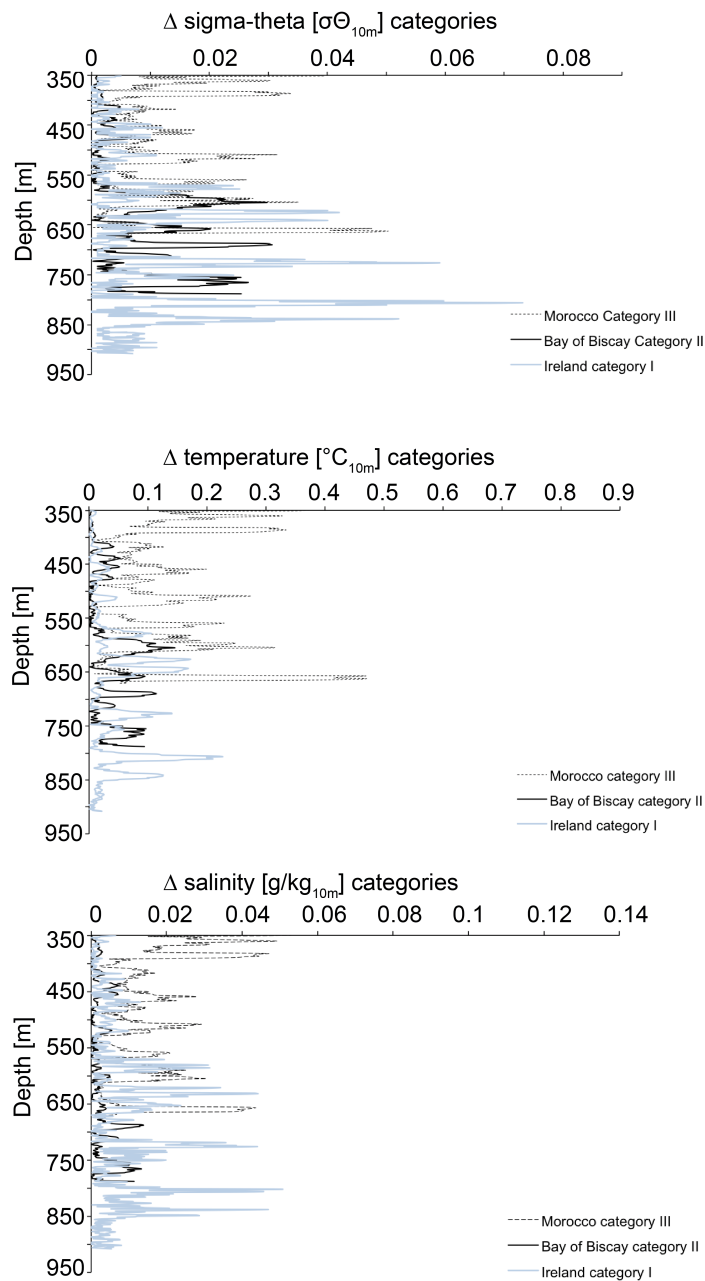


Fig. 5.10 Plots illustrating the relation of hydrological variability derived as $\Delta\sigma\Theta_{10m}$ density, temperature, salinity versus categories I – III for Ireland (Porcupine Seabight) category I, Bay of Biscay (St. Nazaire Canyon) category II and Morocco (Agadir Canyon) category III. Note the strong influence of salinity in the Porcupine Seabight versus the strong influence of temperature in Agadir Canyon, Morocco

These differences may explain a possible vertical deceleration of accumulated food particles (Mienis et al. 2012). A narrow bathymetrical thickness of $\Delta\sigma_{\Theta_{10m}}$ accumulates nutrients but releases them after a shorter time (category I), while a larger bathymetrical thickness of $\Delta\sigma_{\Theta_{10m}}$ accumulates as well, but may capture and retain nutrients over a longer time until they are laterally removed by currents and only a reduced amount may reach the bottom where poor living CWCs are settled (category III).

CWC reefs seem to develop best right below a permanent density gradient, which is either salinity or temperature driven which accumulates nutrients by the interaction of surface and intermediate water masses (Mienis et al. 2007). Localities, which are characterised by salinity driven gradients exhibit a density envelope of $\sigma_{\Theta}=27.34 - 27.61 \text{ kg/m}^3$. In contrast sites, where gradients are mainly driven by temperature the density window is little lower with $\sigma_{\Theta}=27.15 - 27.33 \text{ kg/m}^3$.

5.5 Conclusions

- (1) Irrespectively of the geographical region, water masses, and water depth, all investigated sites exhibit a density gradient expressed as $\Delta\sigma_{\Theta_{10m}}$ above the living CWC reefs. This density gradient seems to be indicative for living CWC reefs as soon as its value is $>0.02 \text{ kg/m}^3$, independently from large CWC reef structures or living CWC cover
- (2) The CWC reefs on the southern part of the North Atlantic margin such as Morocco and Mauretania, as well as those in the semi-closed basin of the Gulf of Mexico belong to CWC reef category III (Flögel et al. 2014). There, the gradients are mainly driven by changes in temperature. In contrast, the living CWC reef on the northern part of the North Atlantic margin off Norway, as well as in the Porcupine Seabight – belong to category I, while those in the Bay of Biscay (St. Nazaire canyon) belong to category II. At these sites, the density gradient is mainly driven by changes in salinity
- (3) The calculated maximum density gradients of $\Delta\sigma_{\Theta_{10m}}$ differ in their bathymetrical thickness right above the living CWC reefs. Healthy and pristine reef systems on the Norwegian margin, of category I exhibit in a range of $\sim 15 \text{ m}$ maximum $\Delta\sigma_{\Theta_{10m}}$ thickness, whereas, the poorly developed structures of category III show $\sim 50 \text{ m}$ thickness
- (4) The development of density gradients favour nutrient accumulations. Thin layers of maximum of $\Delta\sigma_{\Theta_{10m}}$ release nutrients obviously more rapidly, while in thicker layers of maximum of $\Delta\sigma_{\Theta_{10m}}$ nutrients are more retained

Acknowledgments

We acknowledge the superb support by the captains and crew as well as the scientific shipboard parties during cruise 16-3, and cruise 20, and cruise 32 aboard the R/V *MARIA S. MERIAN*, during cruise M61/1, and cruise M78-1, and cruise M84-5, onboard R/V *METEOR* and during cruises of POS325 and POS434 onboard R/V *POSEIDON*. We appreciate very much the scientific discussions with our colleagues Prof. Dr. Hebbeln, Prof. Dr. Freiwald, Dr. Rüggeberg and Dr. Pfannkuche. The Deutsche Forschungsgemeinschaft (DFG) funded ship time and provided further financial support (Du 129/48-1) which is greatly acknowledged.

We greatly thank Jonas von Reumont at GEOMAR, Kiel for his support with the analyses for high performance level to target the density gradients during cruise MSM16-3 and MSM32.

References

- Addamo AM, Reimer JD, Taviani M, Freiwald A, Machordom A (2012) *Desmophyllum dianthus* (Esper, 1794) in the scleractinian phylogeny and its intraspecific diversity. PLoS One 7:e50215
- Arístegui J, Barton ED, Álvarez-Salgado XA, Santos AMP, Figueiras FG, Kifani S, Hernández-León S, Mason E, Machú E, Demarcq H (2009) Sub-regional ecosystem variability in the Canary Current upwelling. Prog Oceanog 83:33–48
- Braga-Henriques A, Porteiro FM, Ribeiro PA, de Matos V, Sampaio Í, Ocaña O, and Santos RS (2013) Diversity, distribution and spatial structure of the cold-water coral fauna of the Azores (NE Atlantic). Biogeosciences 10:4009–4036. doi:10.5194/bg-10-4009-2013
- Brooke S, Schroeder WW (2007) State of deep coral ecosystems in the Gulf of Mexico region. In: Lumsden E, Hourigan TF, Bruckner AW, Dorr G (eds) The state of deep coral ecosystems of the U.S. NOAA Technical Memorandum CRCP-3, Silver Spring, MD:233–270
- Bryan TL and Metaxas A (2006) Distribution of deep-water corals along the North American continental margins: relationships with environmental factors. Deep Sea Res I 53:1865–1879
- Cairns SD (1984) New records of ahermatypic corals (Scleractinia) from the Hawaiian Islands and Line Islands. Ocasional Papers of the Bishop Museum 25:1–30
- Cairns SD, Jaap WC and Lang JC (2009) Scleractinia (Cnidaria) of the Gulf of Mexico, In: Felder DL and Camp DK (eds) Gulf of Mexico – Origins, Waters and Biota. Biodiversity:333–347. Texas A&M, University Press, College Station, Texas
- Carrillo González F, Ochoa J, Candela J, Badan A, Sheinbaum J and González Navarro JI (2007) Tidal currents in the Yucatan Channel. Geof Int 46:199–209
- Chérubin LM (2014) High-resolution simulation of the circulation in the Bahamas and Turks and Caicos Archipelagos. Prog Oceanogr 127:21–46
- Colman JG, Gordaon DM, Lane AP, Forde MJ, Fitzpatrick J (2005) Carbonate mounds off Mauritania, Northwest Africa: status of deep-water corals and implications for management of fishing and oil exploration activities. In: Freiwald A, Roberts JM (eds) Cold-Water Corals and Ecosystems. Springer-Verlag, Berlin-Heidelberg, ISBN:978-3-540-24136-2:417–441
- Correa TBS, Grasmueck M, Eberli GP, Reed JK, Verwer K, Purkis S (2011) Variability of cold-water coral mounds in a high sediment input and tidal current regime, Straits of Florida. Sedimentology. doi:10.1111/j.1365-3091.2011.01306.x
- Davies AJ, Wisshak M, Orr JC and Roberts JM (2008) Predicting suitable habitat for the cold-water coral *Lophelia pertusa* (Scleractinia). doi:10.1016/j.dsr.2008.04.010
- Davies AJ, Duineveld GCA, Lavaleye MSS, Bergmann MJN, Haren HV, Roberts JM (2009) Downwelling and deep-water bottom currents as food supply mechanisms to the cold-water coral *Lophelia pertusa* (Scleractinia) at the Mingulay Reef complex. Limnol Oceanogr 52(2):620
- Davies AJ and Guinotte JM (2011) Global Habitat Suitability for Framework-Forming Cold-Water Corals. PLoS One 6(4): e18483
-

- De Mol B, Henriët J-P, Canals M (2005) Development of coral banks in Porcupine Seabight: do they have Mediterranean ancestors? In: Freiwald A, Roberts M (eds) Cold-water Corals and Ecosystems. Springer-Verlag Berlin Heidelberg: 515–533
- De Mol L, Van Rooij D, Pirlet H, Greinert J, Frank N, Quémeneraid F, Henriët JP (2011) Cold-water habitats in the Penmarch and Guilvinec Canyons (Bay of Biscay): Deep-water versus shallow-water settings. *Mar Geol* 282:40–52
- Dons C (1944) Norges korallrev. Det Kongelige Norske Videnskabers Selskabs Forhandlinger 16:37–82
- Duineveld GCA, Lavleye MSS and Berghuis EM (2004) Particle flux and food supply to a seamount cold-water coral community (Galicia Bank, NW Spain). *Mar Ecol Prog Ser* 277:13–23
- Duineveld GCA, Lavleye MSS, Bergman MJN, De Stigter H and Mienis F (2007) Trophic structure of a cold-water coral mound community (Rockall Bank, NE Atlantic) in relation to the near-bottom particle supply and current regime. *B Mar Sci* 81:449–467
- Dullo W-C, Flügel S, Rüggeberg A (2008) Cold-water coral growth in relation to the hydrography of the Celtic and Nordic European continental margin. *Mar Ecol Prog Ser* 371:165–176. doi:10.3354/meps07623
- Dullo W-C, Flügel S (2011) High-resolution water mass measurements around cold-water corals: a comparative test study between repeated Conductivity-Temperature-Depth (CTD) casts and continuous data acquisition of bottom waters from the West Florida Slope, Gulf of Mexico. *Annalen des Naturhistorischen Museums in Wien. Serie A für Mineralogie und Petrographie, Geologie und Paläontologie, Anthropologie und Prähistorie* 113:209–224
- Dullo W-C, Flügel S, Rüggeberg A (2017) Water mass measurements around benthic communities: a comparative study between Yo-Yo Conductivity-Temperature-Depth (CTD) casts and high-resolution time series data acquisition of bottom waters from the Pagès Escarpment in the southern Bay of Biscay. In: *Diversity in the Coastal Marine Sciences - A Festschrift Volume in Honor of Alexandru Bologa* edited by Charles Finkel, Springer Verlag
- Eisele M, Frank N, Wienberg C, Hebbeln D, Correa ML, Douville E, Freiwald A (2011) Productivity controlled cold-water coral growth periods during the last glacial off Mauretania. *Mar Geol* 280:143–149
- Emery WJ and Meincke J (1986) Global water masses: summary and review. *Oceanol Acta* 9(4):383–391
- Emery WJ (2001) Water Types and Water Masses. In: Academic Press, *Ocean Circulation*:1556–1567. doi:10.1006/rwos.2001.0108
- Fink HG, Wienberg C, Hebbeln D, McGregor HV, Schmiedl G, Taviani M, Freiwald A (2012) Oxygen control on Holocene cold-water coral development in the eastern Mediterranean sea. *Deep-Sea Res I* 62:89–96
- Flügel S and Shipboard Party (2011) RV *METEOR* Cold-water corals in the Bay of Biscay – occurrences and distribution in space and time (TransBiscay) Cruise No. 84, Leg 5, May 32 – June 21, 2011. Vigo (Spain) – Brest (France), *METEOR-Berichte*, Institut für Meereskunde der Universität Hamburg, Leitstelle METEOR, <http://www.ifm.uni-hamburg.de/leitstelle>, 61 pp

- Flögel S, Dullo W-C, Pfannkuche O, Kiriakoulakis K, Rüggeberg A (2014) Geochemical and physical constraints for the occurrence of living cold-water corals. *Deep-Sea Res II* 99:19–26
- Fosså JH, Mortensen PB, Furevik DM (2002) The deep-water coral *Lophelia pertusa* in Norwegian waters; distribution and fishery impacts. *Hydrobiologia* 471:1–12
- Freiwald A, Henrich R, Pätzold J (1997) Anatomy of a deep-water coral reef mound from Stjærnsund, West-Finnmark, northern Norway. In: James NP, Clarke JAD (eds) *Cool-water carbonates*. SEPM, Special Publication 56:141–161
- Freiwald A and Wilson JB (1998) Taphonomy of modern deep, cold-temperate water coral reefs. *Historical Biology* 13:37–52
- Freiwald A (2002) Reef-Forming Cold-Water Corals. In: Wefer G, Billett D, Hebbeln D, Jørgensen BB, Schlüter M and van Weering T (eds) *Ocean Margin Systems*. Springer Verlag: 365–385
- Freiwald A, Fosså JH, Grehan A, Koslow T and Roberts JM (2004) *Cold-water coral reefs*. UNEP-WCMC, Cambridge, UK, pp 84
- Freiwald A, Dullo WC and Shipboard Party (2005) *RV POSEIDON Cruise 325 Bremerhaven – Tromsø, Leg 2: Tromsø – Tromsø, 24 July – 3 August 2005*. POSEIDON Berichte 65 pp
- Glogowski S, Dullo W-C, Feldens P, Liebetrau V, von Reumont J, Hühnerbach V, Krastel S, Wynn RB, Flögel S (2015) The Eugen Seibold coral mounds offshore western Morocco: oceanographic and bathymetric boundary conditions of a newly discovered cold-water coral province. *Geo-Mar Lett* 35(4):257–269. doi:10.1007/s00367-015-0405-7
- González-Pola C, Lavin A, Somavilla R, Vargas-Yáñez M (2006) Central water masses variability in the southern Bay of Biscay from early 90s. The effect of the severe winter 2005. In: ICES Annual Science Conference, Maastricht C:1–12
- Gori A, Grover R, Orejas C, Sikorski S, Ferrier-Pagès C (2013) Uptake of dissolved free amino acids by four cold-water coral species from the Mediterranean Sea. *Deep-Sea Res II* 99:42–50
- Grasmueck M, Eberli GP, Correa TBS, Viggiano DA, Luo J, RSMAS University of Miami; Wyatt GJ, Quester Tangent; Reed JK, Wright AE and Pomponi SA, Harbor Branch Oceanographic Institution (2007) AUV-Based Environmental Characterization of Deep-Water Coral Mounds in the Straits of Florida. Offshore Technology Conference, held in Houston, Texas, U.S.A., 30 April–3 May 2007, OTC 18510
- Gyory J, Rowe E, Mariano AJ, Ryan EH (2005a) “The Florida Current”. *Ocean Surface Currents*. <http://oceancurrents.rsmas.miami.edu/atlantic/florida.html>
- Gyory J, Rowe E, Mariano AJ, Ryan EH (2005b) “The Florida Current”. *Ocean Surface Currents*. <http://oceancurrents.rsmas.miami.edu/atlantic/gulfstream.html>
- Gyory J, Mariano AJ, Ryan EH (2005c) “The Loop Current”. *Ocean Surface Currents*. <http://oceancurrents.rsmas.miami.edu/atlantic/loopcurrent.html>
- Hamilton (1990) Deep currents in the Gulf of Mexico. *J Phys Oceaogr* 20:1087–1104

- Hebbeln D, Wienberg C and cruise participants (2012): Report and preliminary results of R/V *MARIA S. MERIAN* cruise MSM20-4, WACOM – West-Atlantic Cold-water Coral Ecosystems: The West Side Story, Bridgetown – Freeport, 14 March–7 April 2012. University of Bremen, 120 pp
- Hebbeln D, Wienberg C, Wintersteller P, Freiwald A, Becker M, Beuck L, Dullo C, Eberli GP, Glogowski S, Matos L, Forster N, Reyes-Bonilla H, Taviani M (2014) Environmental forcing of the Campeche cold-water coral province, southern Gulf of Mexico. *Biogeosciences* 11:1799–1815
- Hofmann EE and Worley JW (1986) An investigation of the circulation of the Gulf of Mexico. *J Phys Res* 91(12):14221–14236. doi:10.1029/JC091iC12p14221
- Hübscher C, Dullo W-Chr, Flögel S, Titschack J and Schönfeld J (2010) Contourite drift evolution and related coral growth in the eastern Gulf of Mexico and its gateways. *International Journal of Earth Sciences*. doi:10.1007/s00531-010-0558-6
- Huvenne VAI, Beyer A, de Haas H, Dekindt K, Henriët JP, Kozachenko M, Olu-Le Roy K, Wheeler AJ and Participants (2005) The seabed appearance of different coral bank provinces in the Porcupine Seabight, NE Atlantic: results from sidescan sonar and ROV sea-bed mapping. In: Freiwald A, Roberts JM (eds) *Cold-water Corals and Ecosystems*, Springer Verlag, Berlin, Heidelberg: 535–569
- Kiriakoulis K, White M, Bett BJ, Wolff GA (2004) Organic biogeochemistry of the Darwin Mounds, a deep-water coral ecosystem of the NE Atlantic, *Deep-Sea Research I* 51:1937–1954
- Krastel S, Böttner C, Cartigny M, Feldens P, Fu L, Glogowski S, Guggolz T, Hellmann S, Hühnerbach V, Jähmlich H, Kraus K, Kretschmer J, Matthew D, Meier D, Mücke I, von Reumont J, Schönke M, Schürer A, Stevenson C, Unverricht D, Voss D, Webb A, Wynn R (2013) *Maria S. Merian* Berichte. Morphology, processes and geohazards of giant landslides in and around Agadir Canyon, northwest Africa. Cruise No. MSM32. <http://eprints.uni-kiel.de/22613/1/msm32-short-cruise-report.pdf>
- Le Guilloux E, Olu-Le Roy K, Bourillet JF, Savoye B, Iglésias SP, Sibuet M (2009) First observations of deep-sea coral reefs along the Angola margin. *Deep-Sea Res II* 56:2394–2403
- Le Goff-Vitry MC, Rogers AD, Baglow D (2004) A deep-sea slant on the molecular phylogeny of the Scleractinia. *Mol Phylogenet Evol* 30(1):167–177
- Leverette TL (2004) Predicting suitable habitat for deep water corals in the Pacific and Atlantic Continental Margins of North America. Dalhousie University Halifax, Nova Scotia, Department of oceanography, MSc
- Linné C (1758) *Systema naturae*. “The system of Nature“
- Merino M (1997) Upwelling on the Yucatan Shelf: hydrographic evidence. *J Mar Syst* 13:101–121
- Mienis F, De Stigter HC, White M, Duineveld G, De Haas H, Van Weering TC (2007) Hydrodynamic controls on cold-water coral growth and carbonate-mound development at the SW and SE Rockall Trough Margin, NE Atlantic Ocean. *Deep-Sea Res I* 54(9):1655–74
- Mienis F, Duineveld GCA, Davies AJ, Ross SW, Seim H, Bane J and Van Weering TCE (2012) The influence of nearbed hydrodynamic conditions on cold-water corals in the Viosca Knoll area, Gulf of Mexico, *Deep-Sea Res I* 60:32–45

- Mittelstaedt E (1991) The ocean boundary along the northwest African coast: circulation and oceanographic properties at the sea surface. *Prog Oceanog* 26:307–355
- Molinari RL and Mayer JD (1982) Current meter observations on the continental slope at two sites in the eastern Gulf of Mexico. *J Phys Oceanog* 12:1480–1492
- Morigi C, Jorissen FJ, Gervais S, Borsetti AM (2001) Benthic foraminiferal faunas in surface sediments off NW Africa: relationship with organic flux to the ocean floor. *J Foram Res* 31(4):350–368
- Mortensen PB (2001) Aquarium observations on the deep-water coral *Lophelia pertusa* (L., 1758) (Scleractinia) and selected associated invertebrates. *Ophelia* 54:83–104
- Ordóñez E (1936) Principal physiogeographic provinces of Mexico. *Am Assoc Petrol Geol Bull* 20:1277–1307
- Pingree RD and Morrison GK (1973) The relationship between stability and source water for a section in the northeast Atlantic. *Am Meteor Soc* 3:280–285. doi:10.1175/1520-04852
- Pingree RD (1993) Flow of surface waters to the west of the British Isles and in the Bay of Biscay. *Deep-Sea Res II* 40(1-2):369–388. doi:10.1016/0967-0645(93)90022-F
- Pfannkuche O and cruise participants: Report and preliminary results of R/V *METEOR* cruise M61-1 (2004) Geo-Biological Investigations on Azooxanthellate Cold-Water Coral Reefs on the Carbonate Mounds Along the Celtic Continental Slope, 19.4.-04.05.2004, North Atlantic, Leg 1, Lissbon – Cork. *METEOR-Berichte*, Institut für Meereskunde der Universität Hamburg, Leitstelle METEOR, <http://www.ifm.uni-hamburg.de/leitstelle>, 71 pp
- Pfannkuche O (2012) 4D-observation of hydro-dynamical, chemical, and biological properties and its influence on cold-water coral growth in the Stjærnsund, Norway Bergen – Tromsø - Kiel 25. May – 14. June 2012. *POSEIDON Berichte*, 10 pp
- Pollard S, Griffiths CR, Cunningham SA, Read JF, Perez FF, Rios AF (1996) Vivaldi 1991 – a study of the formation, circulation, and ventilation of the eastern North Atlantic Central Water. *Progr Oceanog* 37:167–1925
- Raddatz J, Rüggeberg A, Liebetrau V, Foubert A, Hathorne EC, Fietzke J, Eisenhauer A, Dullo W-Chr (2014) Environmental boundary conditions of cold-water coral mound growth over the last 3 million years in the Porcupine Seabight, Northeast Atlantic. *Deep-Sea Res II* 99:227–236. doi:10.1016/j.dsr2.2013.06.009
- Rapp HT & Snell JA (1999) *Lophelia pertusa* – myths and reality. Second Nordic Mar Sci Meeting, Hirtshals, Denmark
- Roberts JM, Wheeler AJ, Freiwald A (2006) Reefs of the deep: the biology and geology of cold-water coral ecosystems. *Science* 312:543–547. doi:10.1126/science.1119861
- Rogers AD (1999) The biology of *Lophelia pertusa* (Linnaeus 1758) and other deep-water reef forming corals and impact from human activities. *Int Rev Hydrobiologia* 84:315–406
- Rogers AD, Billett D, Berger W, Flach E, Freiwald A, Gage J, Hebbeln D, Heip C, Pfannkuche O, Ramirez-Llodra E, Medlin L, Sibuet M, Soetaert K, Tendal O, Vanreusel A, Włodarska-Kowalczyk M (2002) Life at the edge: achieving prediction from environmental variability and biological variety. In: *Ocean margin systems*. Springer Verlag:387–404

- Rüggeberg A, Dorschel B, Dullo W-Chr, and Hebbeln D (2005) Sedimentary patterns in the vicinity of a carbonate mound in the Hovland Mound province, northern Porcupine Seabight. In: Freiwald A and Roberts JM (eds) *Cold-water Corals and Ecosystems*. Springer-Verlag Berlin, pp 87–112
- Rüggeberg A, Dullo W-Chr, Dorschel B, Hebbeln D (2007) Environmental changes and growth history of Propeller Mound, Porcupine Seabight: Evidence from benthic foraminiferal assemblages. *Int J Earth Sci*. doi: 10.1007/s00531-005-0504-1
- Rüggeberg A, Flögel S, Dullo W-C, Hissmann K, Freiwald A (2011) Water mass characteristics and sill dynamics in a subpolar cold-water coral reef setting at Stjernsund, northern Norway. *Mar Geol* 282:5–12
- Schlitzer R (2013) Ocean Data View. <http://odv.awi.de>
- Schönfeld J and cruise participants: Report and preliminary results of R/V *METEOR* cruise M78-1 (2009) Surface and Intermediate Water hydrography, planktonic and benthic biota in the Caribbean Sea – Climate, Bio and Geosphere linkages (OPOKA). *METEOR-Berichte*, Institut für Meereskunde der Universität Hamburg, Leitstelle METEOR, <http://www.ifm.uni-hamburg.de/leitstelle>, 190 pp
- Sheinbaum J, Candela J, Badan A and Ochoa J (2002) Flow structure and transport in the Yucatan Channel. *Geophys Res Lett* 29:1040. doi:10.1029/2001GL 013990
- Skarøhamar J & Svendsen H (2005) Circulation and shelf–ocean interaction off North Norway. *Cont Shelf Res* 25(12–13):1541–1560
- Stramma L (2001) Overview of current systems in the Atlantic Ocean. doi:10.1006/rwos.2001.0356
- Van Camp L, Nykjier L, Mittelstaedt E, Schlittenhardt B (1991) Upwelling and boundary circulation off Northwest Africa as depicted by infrared and visible satellite observations. *Prog Oceanog* 26:357–402
- Vandorpe T, Van Rooij D, de Haas H (2014) Stratigraphy and paleoceanography of a topography-controlled contourite drift in the Pen Duick area, southern Gulf of Cádiz. *Mar Geol* 349:136–151
- Van Rooij D, Iglesias J, Hernández-Molina FJ (2010b) The Le Danois Contourite Deposirional System: interactions between the Mediterranean Outflow water and the upper Cantabrian slope (North Iberian margin). *Mar Geol* 1–20. doi:10.1016/j.margeo.2010.03.001
- Vierod ADT, Guinotte JM, Davies AJ (2014) Predicting the distribution of vulnerable marine ecosystems in the deep sea using presence-background models. *Deep-Sea Res II* 99:6–18
- Wei CL, Rowe GT, Escobar-Briones E, Nunnally C, Soliman Y and Ellis N (2012) Standing stocks and body size of deep-sea macrofauna: Predicting the baseline of Deepwater Horizon oil spill in the northern Gulf of Mexico. *Deep-Sea Res I* 69:82–99
- Westphal H, Freiwald A, Hanebuth T, Eisele M, Gürs K, Heindel K, Michel J, v Reumont J (2006) Cruise Report *Poseidon* 346 MACUMA Integrating carbonates, siliciclastics and deep-water reefs for understanding a complex environment Las Palmas – Las Palmas 28.12.2006-15.1.2007. *POSEIDON Berichte*, 49 pp
- Westphal H, Beuck L, Braun S, Freiwald A, Hanebuth T, Hetzinger S, Klicpera A, Kudrass H, Lantzsch H, Lundälv T, Mateu-Vicens G, Preto N, v Reumont J, Schilling S, Taviani M, Wienberg C (2012) *Phaeton – Report – Paleoceanographic and paleo-climatic record on the Mauritanian Shelf Cruise No. MSM16-3, Oct 13 – Nov 20, 2010, Bremerhaven (Germany) – Mindelo (Cap Verde)*. Maria S. Merian – *Berichte* 1–53

- White M, Mohn C, de Stigter H and Mottram G (2005) Deep-water coral development as a function of hydrodynamics and surface productivity around the submarine banks of the Rockall Trough, NE Atlantic. In: *Cold-Water Corals and Ecosystems*, Freiwald A and Roberts JM (eds) Springer, Berlin-Heidelberg, pp 503–514
- White M (2007) Benthic dynamics at the carbonate mound regions of the Porcupine Sea Bight continental margin. *Int J Earth Sci* 96 (1):1–9
- Wienberg C, Beuck L, Heidkamp S, Hebbeln D, Freiwald A, Pfannkuche O, Monteys X (2008) In: *Franken Mound - facies and biocoenoses on a newly-discovered 'carbonate mound' on the western Rockall Bank, NE Atlantic*. *Facies* 54:1–24
- Wienberg C, Frank N, Mertens KN, Stuetz J-B, Marchant M, Fietzke J, Mienis F, Hebbeln D (2011) Glacial cold-water coral growth in the Gulf of Cádiz: Implications of increased palaeo-productivity. *Earth Plan Sci Lett* 298(3-4):405–416
- Zibrowius H (1980) *Les Scléactiniaires de la Méditerranée et de l'Atlantique nord-oriental*. In: *Memoires Institute Oceanographic, Monaco* 11:284

Supplementary Material

Fig. 5.1 Simplified map of the thermohaline circulation system in the North Atlantic Ocean (available at: http://pordlabs.ucsd.edu/italley/sio210/Atlantic_deep; Prof. Dr. Lynne Talley, Climate atmospheric science & physical oceanography)

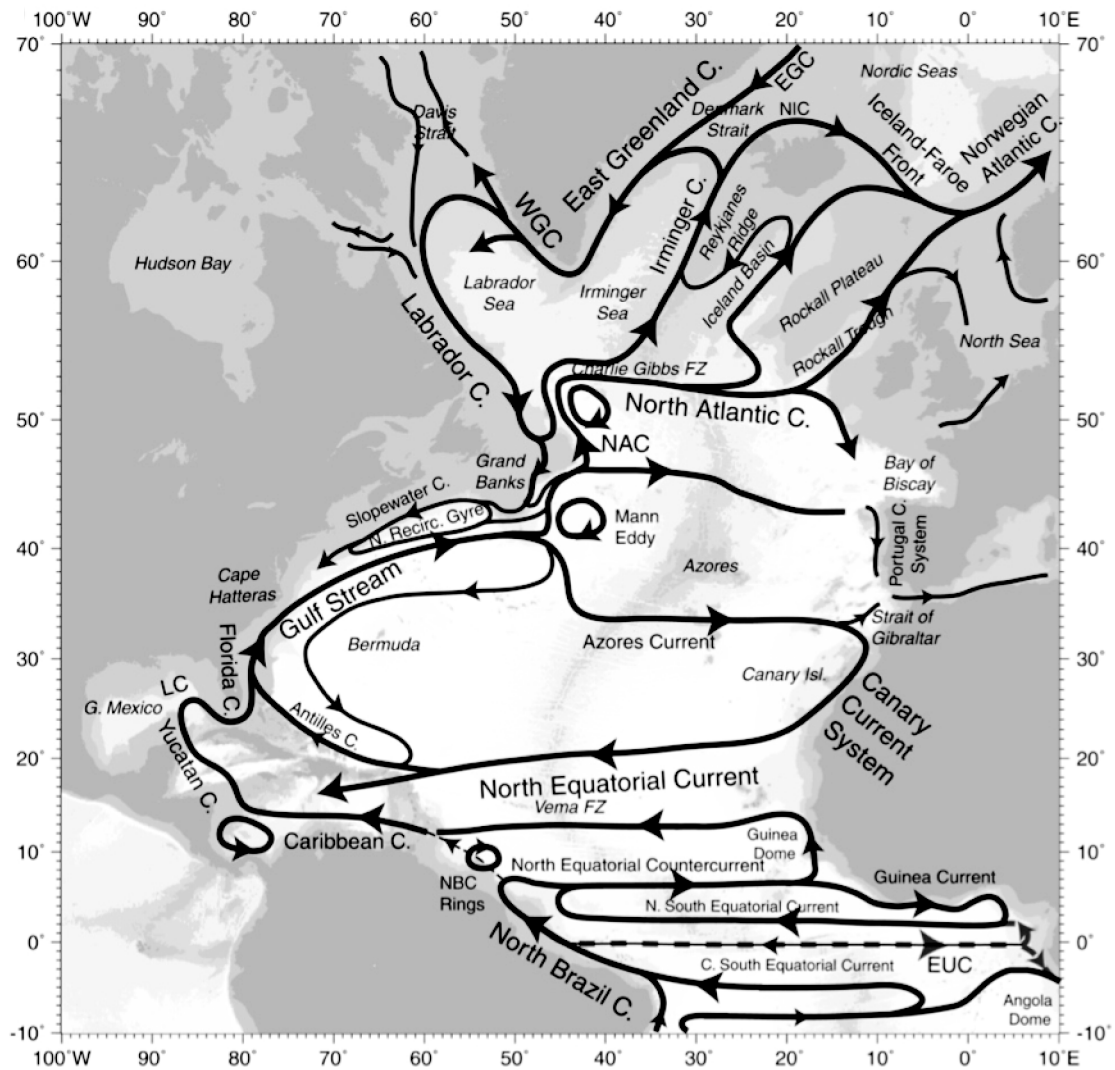


Fig. 5.4 Location map is illustrating sample areas indicated by red dots

Location Map North Atlantic

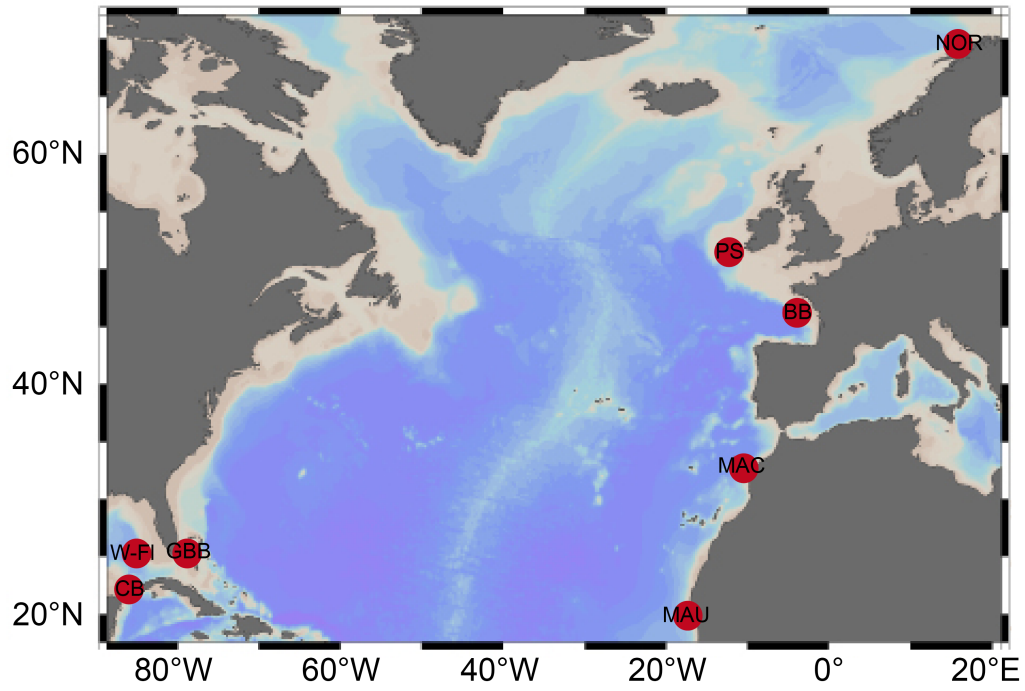


Fig. 5.8 Cross sectioned gradients through ($\Delta\sigma_{\Theta_{10m}}$) water masses Campeche Bank (CB) – category I. The *upper* section displays the site over a distance of 3km. The *bottom* figure zoomed in the section, where living *Lophelia pertusa* reefs were found ($\Delta\sigma_{\Theta_{10m}}$ maximum >0.06)

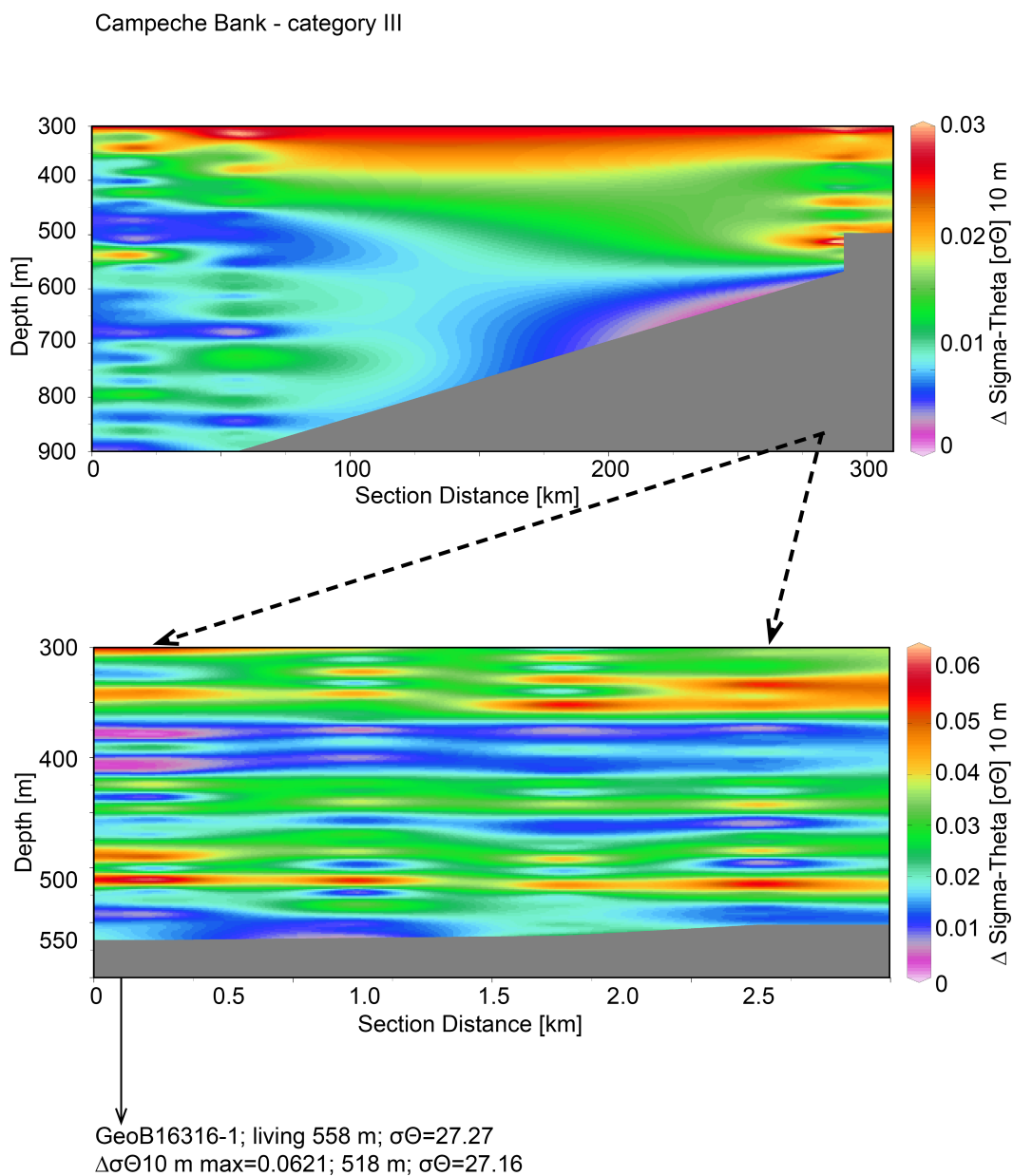


Fig. 5.11 Plots illustrating the relation of hydrological variability derived as $\Delta\sigma_{\Theta_{10m}}$ density, temperature, salinity for Gulf of Mexico (GoM) and the sites of Campeche Bank (CB) and West-Florida Slope (W-FI)

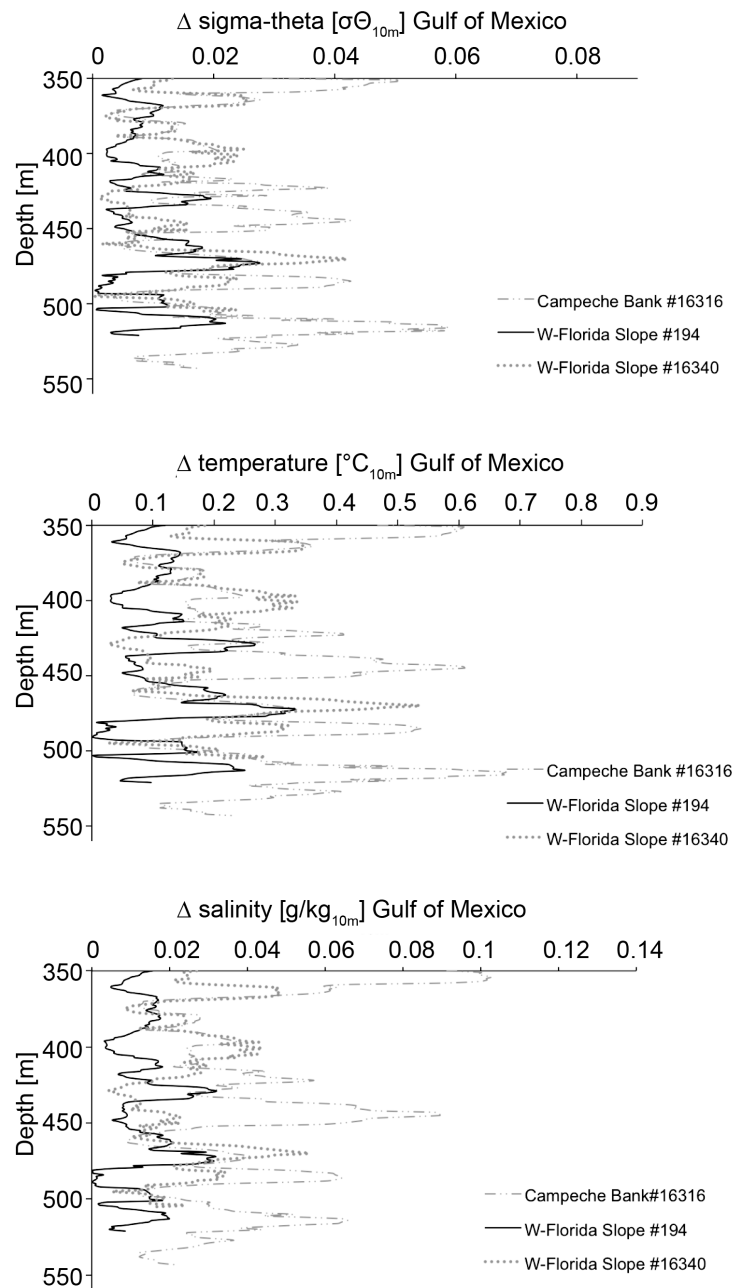
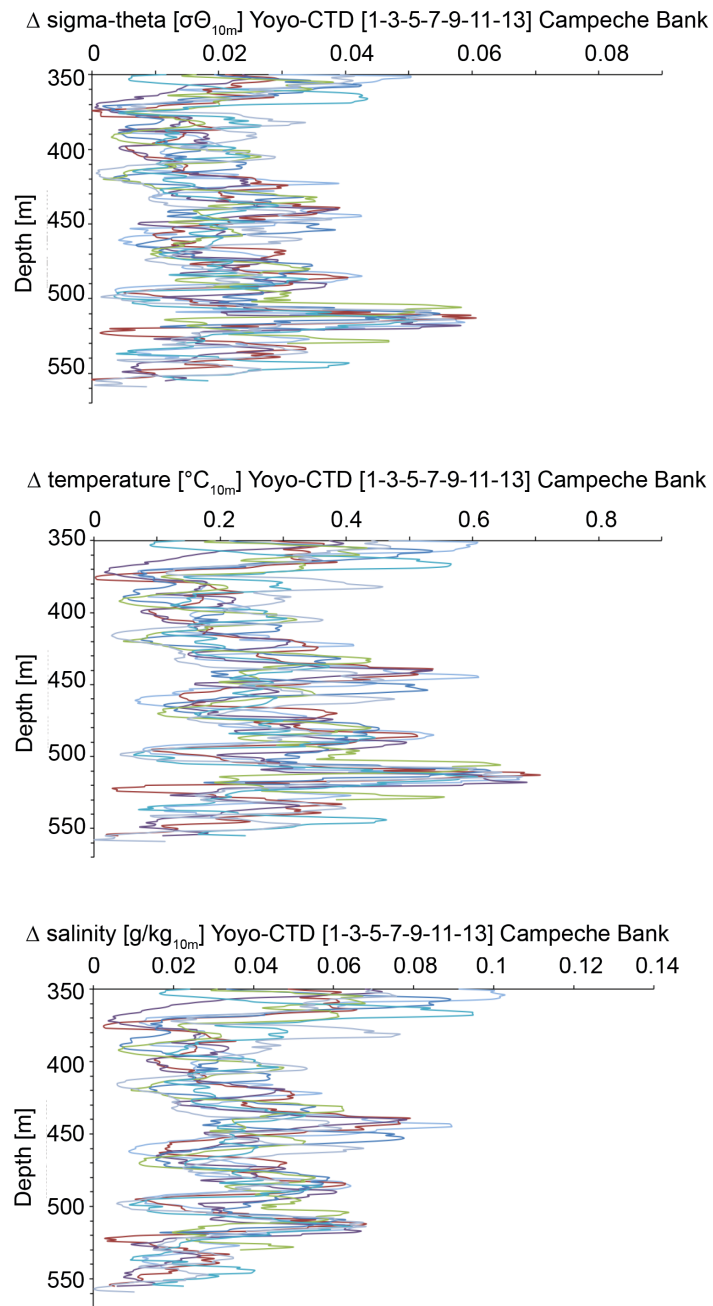


Fig. 5.12 Plots illustrating the relation of hydrological variability derived as $\Delta\sigma_{\Theta_{10m}}$ density, temperature, salinity for the Yoyo-CTD on Campeche Bank (CB)



Supplementary Material

Table 5.1 Sampling location and hydrographical *in-situ* data for the studied regions of Campeche Bank (CB), Great Bahama Bank (GBB), St. Nazaire Canyon (BB), Porcupine Seabight (PS), Norwegian margin, Agadir Canyon (MAC). *Yo-yo-data represent mean values of 13 CTD casts covering a time window of 13 hours

Station	Area	Station ID	Lat. [°N]	Long. [°W]	Sampling Date	Depth living <i>L.pertusa</i> [m]	Conservative Temperature [°C]	Absolute Salinity [psu]	Density [kg/m ³]	Water mass living <i>L.pertusa</i>	Water mass boundary
MSM20-4 GeoB 16316-1 [Yo-Yo CTD]	GoM, Campeche Bank	CB	23°51.511	87°12.124	23.03.12	552	7.92	35.16	27.27	SUW	AAIW
MSM20-4 GeoB 16340-1 [Yo-Yo CTD]	GoM, West Florida Slope	W-FI	26°20.201	84°45.597	27.03.12	513	7.67	35.14	27.28	SUW	AAIW
M78-194 [Yo-Yo CTD]	GoM, West Florida Slope	W-FI	26°12.108	84°43.552	07.03.09	530	7.80	35.12	27.27	SUW	AAIW
MSM20-4 GeoB 16386-1 [Yo-Yo CTD]	Great Bahama Bank Slope	GBB	24°33.635	79°21.211	04.04.12	618	9.30	35.28	27.15	SUW	DWBC
M84-5-666 [Single CTD]	BoB, St. Nazaire Canyon	BB	46°13.588	4°19.300	16.06.11	798	10.26	35.71	27.46	ENACW	MOW
M84-5-656 [Single CTD]	BoB, St. Nazaire Canyon	BB	46°13.480	4°21.1080	15.06.11	1361 no living	6.79	35.43	27.79		
M84-5-658 [Single CTD]	BoB, St. Nazaire Canyon	BB	46°14.204	4°20.960	15.06.11	844	9.92	35.72	27.51	ENACW	MOW
M61-1-1 [Yo-Yo CTD]	Ireland, Porcupine Seabight	PS	51°27.87	11°45.05	23.04.04	810	9.72	35.49	27.38	ENACW	MOW
M61-1-10 [Single CTD]	Ireland, Porcupine Seabight	PS	51°26.39	11°45.51	23.04.04	873	8.96	35.53	27.54	ENACW	MOW
M61-1-4 [Single CTD]	Ireland, Porcupine Seabight	PS	51°27.18	11°45.17	23.04.04	800	9.78	35.46	27.35	ENACW	MOW
M61-1-2 [Single CTD]	Ireland, Porcupine Seabight	PS	51°27.63	11°45.27	23.04.04	901	9.07	35.53	27.52	ENACW	MOW
M61-1-5 [Single CTD]	Ireland, Porcupine Seabight	PS	51°27.10	11°45.14	23.04.04	780	9.90	35.48	27.34	ENACW	MOW
M61-1-17 [Single CTD]	Ireland, Porcupine Seabight	PS	51°26.72	11°48.54	24.04.04	1056 no living	8.16	35.50	27.64		
POS434-143 [Single CTD]	Norway, Stjærnsund	STJ	70°16.303	22°25.928	31.05.05	283	5.90	34.90	27.35	NCW	AW
POS325-421 [Single CTD]	Norway, Stjærnsund	STJ	70°16.01	22°28.46	25.07.05	208	5.79	35.07	27.51	NCW	AW
POS325-375 [Single CTD]	Norway, Røst Reef	RR	67°31.60	09°29.60	19.07.05	301	7.08	35.41	27.61	NCW	AW
POS325-373 [Single CTD]	Norway, Røst Reef	RR	67°31.51	09°29.40	19.07.05	303	7.07	35.41	27.61	NCW	AW
POS325-354 [Single CTD]	Norway, Trænadjupet	TJ	66°58.15	11°07.27	16.07.05	297	7.24	35.41	27.58	NCW	AW
POS325-394 [Single CTD]	Norway, Sveinsgrunen	SV	69°42.82	16°09.81	22.07.05	522 no living	4.64	35.28	27.81		
POS325-383 [Single CTD]	Norway, Sveinsgrunen	SV	69°43.01	16°07.48	21.07.05	1037 no living	sensor defect	35.11	28.07		
MSM32-3-2 [Single CTD]	Morocco, Agadir Canyon	MAC1	31°08.055	10°36.248	02.10.13	704	9.87	35.63	27.33	NACW	MOW
MSM32-49-2 [Yo-Yo CTD]	Morocco, Agadir Canyon	MAC2	31°12.740	10°37.540	25.10.13	674	10.12	35.65	27.29	NACW	MOW
POS346 GeoB14906-1 [Yo-Yo CTD]	Mauretania, Golf d'Arguin	MAU	17°32.489	16°40.122	16.11.10	574	9.46	35.37	27.20	NACW	MOW

Table 5.2 Shown are the various locations and their hydrographic and oceanographic *in-situ* bottom water fingerprints of the presented data set

Cruise	Date	Area	Category	Site	Station ID	Depth m living	Sigma-Theta σ	Reference living	Depth m Δ Gradient max	Depth m Difference	Delta Δ Gradient max (kg/m ³)	Sigma-Theta σ
MSM20-4	Mar 2012	Campeche Bank	III	#16316-1	CB	552	27.28	ROV#4#16312	518	34	0.0621	27.16
MSM20-4	Mar 2012	W-Florida	III	#16340	WFL1	513	27.28	ROV#3#16334	504	10	0.0237	27.25
M78-1	Feb 2009	W-Florida	III	#194-1	WFL2	530	27.27	OFOS#189-1	513	17	0.0219	27.23
MSM20-4	Mar 2012	Great Bahama Bank	III	#16386-1	GBB	618	27.15	ROV#4 #16373	558	60	0.0421	27.03
M84-5	Juni 2011	St. Nazaire Canyon	II	#M666	BB2	798	27.46	TVGrab#M644	765	55	0.0266	27.40
M84-5	Juni 2011	St. Nazaire Canyon	II	#M658	BB3	844	27.52	TVGrab#M644	834	10	0.0449	27.47
M61-1	Apr 2004	Porcupine Seabight	I	CTD 1	PS1	810	27.38	OFOS#203	837	27	0.0527	27.43
M61-1	Apr 2004	Porcupine Seabight	I	CTD 10	PS2	873	27.54	OFOS#203	859	14	0.0769	27.45
M61-1	Apr 2004	Porcupine Seabight	I	CTD 4	PS3	800	27.34	OFOS#203	783	17	0.0785	27.30
M61-1	Apr 2004	Porcupine Seabight	I	CTD 2	PS4	901	27.52	OFOS#203	876	25	0.0484	27.45
M61-1	Apr 2004	Porcupine Seabight	I	CTD 5	PS5	780	27.34	OFOS#203	768	12	0.0341	27.33
POS434	May 2012	Stjernsund	I	#143	STJ1	283	27.35	Jago#412	223	60	0.0330	27.47
POS325	July 2005	Stjernsund	I	#421	STJ2	208	27.51	VVG#416	163	45	0.0704	27.36
POS325	July 2005	Røst Reef	I	#375	RR1	301	27.61	VVG#369	264	37	0.0128	27.59
POS325	July 2005	Røst Reef	I	#373	RR2	303	27.61	VVG#372	286	17	0.0170	27.59
POS325	July 2005	Traenadjupet	I	#354	TRA	297	27.58	ROV#356	248	49	0.0113	27.55
MSM32	Oct 2003	Agadir Canyon	III	#51-2	MOR	671	27.29	Box Corer#3-2	662	9	0.0502	27.32
MSM32	Oct 2003	Agadir Canyon	III	#3-2	MOR	704	27.32	Box Corer#3-2	691	13	0.0350	27.30
MSM16-3	Oct 2010	Golf d'Arguin	III	#14906-1	MAU	574	27.20	ROV#10 #14908	546	28	0.0343	27.06

Summary

The aim of this study was to focus on the environmental control of cold-water coral reefs and to unravel the processes and controlling factors that influence the cold-water coral ecosystems. For this purpose, geochemical proxies from the scleractinian cold-water coral *Lophelia pertusa* - the important and representative reef builder of the cold-water coral reefs - as well as surrounding oceanographic and hydrographic properties have been analysed. In summary, the chapters presented in the context of this thesis have led to some new findings regarding the setting of CWC reefs. These results are summarised and presented in four chapters, which comprise this thesis.

Chapter 2

In this paper, the newly discovered Eugen Seibold coral mounds off western Morocco are presented. Living CWCs dominated by *Lophelia pertusa*, occurred between 678 and 719 m water depth, whereas dead thickets were found at water depths of >710 to 860 m. CTD measurements revealed living CWCs within the NACW, where hydroacoustic data exhibited individual mounds of up to 12 m height. U/Th isotope systematics derived from *L. pertusa* yielded ages of dead coral fragments of the late Holocene at least.

Chapter 3

From different localities geochemical analyses applying EPMA and LA-ICP-MS measurements revealed spatial distributions of Mg/Ca, Sr/Ca and Na/Ca ratios in the CWC *L. pertusa*. One of the key aspects of this research was to resolve the skeletal architecture, i.e. differentiation between theca wall (TW) and the centre of calcification (CoC), and to differentiate both geochemically. The variability of Mg/Ca ratios is the best methodological approach to identify geochemically the different skeletal features in the CWCs. However, most of the CoC records showed stronger correlations to both temperature and salinity with respect to the TW derived data. Moreover, the present thesis demonstrates a negative correlation of Na/Ca ratios to temperature and salinity, with stronger negative correlations within the CoC than within the TW. These observed Na/Ca data (measured by LA-ICP-MS) are crucial to use as a geochemical proxy since their ratio may be entirely controlled by precipitation / biomineralisation processes in *L. pertusa*.

Chapter 4

The Campeche Bank CWC province is a highly diverse CWC ecosystem in the western Atlantic Ocean, dominated by e.g. *Lophelia pertusa*. The rich cold-water coral location is characterised by high surface water production, which appeared to be optimal for the establishment of this CWC ecosystem, supported by the local nutrient rich upwelling regime. Additionally, a dynamic bottom current regime with available supplemental food source for CWC growth, reached the CWC ecosystem by vertical migration. The observed strong density gradient within the intermediate water column controlled the food supply as well and plays a major role in the development of this CWC ecosystem.

Chapter 5

Flourishing cold-water coral reefs seem to depend on the development of a density gradient above the living reef. This density gradient accumulates sinking particulate nutrients and may even advect them laterally. This density gradient expressed as $\Delta\sigma_{\Theta_{10m}}$ right above the living CWC reefs was recognised at each studied locality in the North Atlantic. The eastern North Atlantic margin south of Gibraltar and the Gulf of Mexico exhibit density gradients mainly driven by changes in temperature and these sites have moderately developed CWC reefs. In contrast, the eastern North Atlantic north of Gibraltar shows density gradients mainly driven by changes in salinity. These sites are characterised by well-developed CWC reefs. Further, the bathymetrical thickness of the maximum density gradients of $\Delta\sigma_{\Theta_{10m}}$ may be influential, since CWC reefs below thicker layers are less developed and vice versa. Maybe particulate nutrients are more effectively accumulated on thinner layers.

Index of Figures

Fig. 1.	1
<i>Lophelia pertusa</i> caught during cruise MSM32 off Morocco and redrawn by Gabriel Engelen (Waldorfschule, Kiel)	
Fig. 1.2	3
Living <i>Lophelia pertusa</i> (Photo: R. Wynn; MSM32 off Morocco)	
Fig. 1.3	4
Erich Pontopiddan, Bishop of Norway (1698 – 1764), “Meeresgemüse vegetables – of the ocean” (1755)	
Fig. 1.4	5
Distribution of cold-water reefs after Roberts et al. (2006)	
Fig. 2.1	25
<i>Top</i> Map showing the locations of the study area off western Morocco (<i>black box</i> ; <i>green dot</i> mound field), and the CTD stations (<i>stars</i>) of earlier cruises off Mauritania (MSM16/3) and in the Gulf of Cadiz (MSM1/3; cf. Table 1), with depth contours and water masses. North Atlantic Central Water: <i>solid blue arrows</i> after Vandorpe et al. (2014); <i>dotted blue arrow</i> its continuation, present study. Mediterranean Outflow Water: <i>red area and arrows</i> after Hernández-Molina et al. (2011), including preferred meddy pathways; <i>orange arrows</i> its continuation, CTD data of present study. North Atlantic Deep Water: <i>solid dark grey arrows</i> after Hernández-Molina et al. (2011); <i>dark grey dotted arrow</i> its continuation, present study. <i>Bottom</i> Green Multibeam bathymetry coverage. Note the location of CTD station MSM32-1-1 (cf. Fig. 3, Table 1)	
Fig. 2.2	27
<i>Top</i> 3D perspective view of multibeam bathymetry (lateral pixel resolution 30 m) across the Eugen Seibold coral mounds, and locations of the seven box corer stations (cf. Table 2) with live or dead corals, as well as three areas selected for estimation of coral mound density (cf. Fig. 4). With the exception of CTD station MSM32-1-1, situated further north beyond the currently known boundaries of the coral mound site (cf. Fig. 1), the locations of the other ten CTD stations were essentially identical or very close to those of the box corer stations (cf. Table 1). <i>Bottom</i> Bathymetric profile 1 crosses the site from its shallowest to its deepest part, profile 2 incorporates a coral mound with living CWCs, and profile 3 a coral mound with dead corals (box corer stations MSM32-49-2 and 46-1 respectively). <i>V.E.</i> Vertical exaggeration	

Fig. 2.3

31

T–S plot (Θ cons. temperature, S_A absolute salinity) for CTD stations MSM32-1-1 (see Fig. 1 for location) and MSM32-3-2 (location as for box corer station MSM32-3-1 in Fig. 2). Water masses comprise (from shallowest to deepest) an upper surface layer, Subtropical Under Water (SUW), South Atlantic Central Water (SACW), North Atlantic Central Water (NACW), Mediterranean Outflow Water (MOW), and North Atlantic Deep Water (NADW). Living CWCs, especially *Lophelia pertusa*, occur in the deeper part of the NACW roughly 150 m above the MOW characterised by still relatively elevated salinities and limited variation in temperature. Isopycnals are calculated with the reference pressure at 0 m (σ_Θ), i.e. sea level

Fig. 2.4

31

Shaded relief (*top row*) and slope map (*bottom row*) across selected coral mound areas at three different water depths based on multibeam bathymetry data. Abundance, elevation and slope of coral mounds decrease as water depths increase from area 1 to area 3 (700, 780 and 890 m respectively). See Fig. 2 for locations of selected areas

Fig. 2.5

46

Number of mounds with respect to height for the three selected areas (each 4 km²) shown in Fig. 4. Mound height decreases from shallower depths of area 1, where living corals have been sampled, to deeper depths of area 3. Mean elevation and standard deviation for area 1 = 6.9±2.2 m, area 2 = 6.0±1.4 m, and area 3 = 3.6±1.0 m. Refer to Fig. 2 for area locations

Fig. 2.6

47

Left TOBI side scan sonar (30 kHz) imagery across the carbonate mound province (swath width 6 km). Individual coral mounds are recognized by high acoustic backscatter on flanks inclined towards the side scan sonar track, and low backscatter shadows on the lee sides. *Right* Higher-resolution imagery in the vicinity of two box corer stations (*red stars*): *top right* MSM32-49-2, with living corals; *bottom right* MSM32-50-2, with dead corals. For corresponding locations in study area, see Fig. 2

Fig. 2.7

33

Photograph showing the contents of the box core recovered from station MSM32-3-1. The large colony of *Lophelia pertusa* (1) exhibits up to 15 consecutive living polyps in one branch. *Madrepora oculata* (2) settled on dead branches of *L. pertusa*, which evidently collapsed prior to settlement as indicated by the different orientation of the polyps of both corals. This is the only living *M. oculata* recovered during the cruise. *Desmophyllum* sp. (3) settled also on dead *L. pertusa* branches. In this box core, the numerous dead corals partly buried in the muddy, bioclast-rich sediment comprise only *L. pertusa*. Among the coral debris, a few bivalves occur. See Fig. 2 for location of box core station

Fig. 2.8

35

Detailed T–S plot (cf. Fig. 3) of water masses bathing living and dead CWCs of the Eugen Seibold coral mounds north of Agadir Canyon (cruise MSM32 of the present study, *colour*), compared with dead CWC sites in the Gulf of Cadiz (cruise MSM1/3, *light grey*) and living CWC sites off Mauritania (cruise MSM16/3, *dark grey*). *Dashed ellipses* Temperature–salinity occurrence range of dead CWCs; *yellow, white circles* living CWCs, all category III of Flögel et al. (2014). Isopycnals are calculated with the reference pressure at 0 m (σ_Θ), i.e. sea level

Fig. 3.1 SM

84

Coral sample locations. Gulf of Mexico (GoM; MSM20-4), CB = Campeche Bank, W-FI = West-Florida Slope, SW-FI (1,2) = South-West-Florida Slope. Left: West-Atlantic (MSM20-4), BS = Bimini Slope, GBB = Great Bahama Bank. Right: East-Atlantic (MSM32), MAC (1,2) = Morocco

Fig. 3.2 SM

84

a) ROV image showing the coral habitat at the Campeche Bank (image copyright MARUM, Bremen, ROV Cherokee team, MSM20-4). Note the squat lobster within. b) – c) Sample GeoB16312-1, b) the analysed calyx shown within the red rectangle and c) the resin embedded, polished *L. pertusa*. The red point within the red rectangle indicates the location used for geochemical analyses exactly (in order to avoid the organic interior lining in brownish colour)

Fig. 3.3 SM

85

Mg/Ca ratios (mmol/mol) versus *in-situ* temperature ($^{\circ}\text{C}$) derived by EPMA and LA-ICP-MS in *L. pertusa*, differentiated in arithmetic mean sample (overview of the whole sample) *top*, the arithmetic mean TW plotted in the *middle* and the arithmetic mean CoC plotted at the *bottom*. Error bars = ± 1 SD (1σ). The linear regression, the corresponding R^2 and the p -values are given for both EPMA and LA-ICP-MS. Arithmetic mean enrichment factors are presented at Table 3

Fig. 3.4

64

Sr/Ca ratios (mmol/mol) versus *in-situ* temperature ($^{\circ}\text{C}$) of EPMA and LA-ICP-MS in *L. pertusa*, differentiated in arithmetic mean sample (overview of the whole sample) *top*, the arithmetic mean TW plotted in the *middle* and the arithmetic mean CoC plotted at the *bottom*. Error bars = ± 1 SD (1σ). The linear regression, the corresponding R^2 and the p -values are given for both EPMA and LA-ICP-MS. Arithmetic mean enrichment factors are presented at Table 4

Fig. 3.5

66

Na/Ca ratios (mmol/mol) versus *in-situ* temperature (°C) of LA-ICP-MS in *L. pertusa*, differentiated in arithmetic mean sample (overview of the whole sample) *top*, the arithmetic mean TW plotted in the *middle* and the arithmetic mean CoC plotted at the *bottom*. Error bars = ± 1 SD (1σ). The linear regression, the corresponding R^2 and the p -values are given for LA-ICP-MS. Arithmetic mean enrichment factors are presented at Table 5

Fig. 3.6

66

Na/Ca ratios (mmol/mol) versus *in-situ* salinity (g/kg) of LA-ICP-MS in *L. pertusa*, differentiated in arithmetic mean sample (overview of the whole sample) *top*, the arithmetic mean TW plotted in the *middle* and the arithmetic mean CoC plotted at the *bottom*. Error bars = ± 1 SD (1σ). The linear regression, the corresponding R^2 and the p -values are given for LA-ICP-MS. Arithmetic mean enrichment factors are presented at Table 5

Fig. 3.7

72

Na/Ca ratios versus Calyx factor (CF) derived from the analysed calices, differentiated in arithmetic mean sample (overview of the whole sample) *top*, the arithmetic mean TW plotted in the *middle* and the arithmetic mean CoC plotted at the *bottom*. Error bars = ± 1 SD (1σ). The linear regression, the corresponding R^2 and the p -values are given for LA-ICP-MS

Fig. 3.8

72

Mg/Ca ratios versus Calyx factor (CF) derived from the analysed calices, differentiated in arithmetic mean sample (overview of the whole sample) *top*, the arithmetic mean TW plotted in the *middle* and the arithmetic mean CoC plotted at the *bottom*. Error bars = ± 1 SD (1σ). The linear regression, the corresponding R^2 and the p -values are given for both EPMA and LA-ICP-MS

Fig. 3.9 SM

86

Sr/Ca ratios versus Calyx factor (CF) derived from the analysed calices, differentiated in arithmetic mean sample (overview of the whole sample) *top*, the arithmetic mean TW plotted in the *middle* and the arithmetic mean CoC plotted at the *bottom*. Error bars = ± 1 SD (1σ). The linear regression, the corresponding R^2 and the p -values are given for both EPMA and LA-ICP-MS

Mg concentrations and Me/Ca ratios derived by different methods from *L. pertusa* (GeoB16312-1; Campeche Bank) are shown to illustrate their distribution in relation to the different microstructures and are representative for all samples.

a) Semi-quantitative mapping of Mg distribution (EPMA) exhibiting low concentrations in blue (82 counts per pixel=cts/pixel) and high concentrations in red (>217 cts/pixel). The boundary between the theca wall (TW) and the center of calcification (CoC) would be assigned at ~150 μm distance from the outer rim (=DFOR). The elongated red rectangle indicates the measured profile in *b*

b) Mg/Ca ratio EPMA profile (spot size 3 μm) plotted as overlay on a black and white binocular image (*c*). The boundary between TW and CoC is almost identical to the mapping in *a*) and is located at 156 μm DFOR (Mg/Ca $1\sigma = \pm 0.4$; see Table 3). The spots refer to the LA-ICP-MS measurements in *d*)

c) The corresponding boundary between TW and CoC on the basis of the binocular image is indicated by the black line

d) The resolution of the LA-ICP-MS spot (light, large circles) is more than one order of magnitude larger than the EPMA spot. Note that the diameter of the shooted spot is not similar to the diameter of the mapped shot. The boundary between TW and CoC based on minima for the TW and maxima for the CoC would assign it between spot 4 and 5. The large spot size of the laser may capture Mg/Ca ratios (mmol/mol) from the CoC crystals below the ablated surface and vice versa.

The lowest Mg/Ca ratios at spot 5 (Mg/Ca $1\sigma = \pm 0.2$; see Table 3), although visually located within the CoC, also according to the Keyence image (*e*) may result from such a "mixing" signal.

Na/Ca ratio (mmol/mol) measured by LA-ICP-MS (Na/Ca $1\sigma = \pm 1.28$; see Table 5) overlain on the Keyence image demonstrate the maximum within the TW at spot 4 and the minimum at the "mixing" signal of spot 5 within the CoC. The large spot size does not allow a clear differentiation between TW, CoC and the septum. The individual spot 8 might result from density differences within the material, or from a pore under the epoxy resin, or from an exploded crystal under the 150 shots of the laser ablation

e) Based on the Keyence© image the corresponding boundary between TW and CoC is indicated by the black line (bottom panel). Differentiation between TW and CoC on the basis of the different method a) – e) of TW (yellow) and CoC (red)

Fig. 4.1

107

Water mass structure in the Yucatan Strait (GeoB 16303-1) and in the Campeche cold-water coral province (GeoB 16316-1 to - 16, Yoyo CTD station; see Table 4.1). Shown is a temperature–salinity plot; temperature is displayed as potential temperature (T_{pot}), grey lines indicate levels of isodensity (σ_{θ}) in kgm^{-3} (plotted using Ocean Data View v.4.5.1; <http://odv.awi.de>; Schlitzer, 2012). Abbreviations: CSW: Caribbean Surface Water; STUW: Subtropical Intermediate Water; AAIW: Antarctic Intermediate Water

Fig. 4.2

109

Hydrological variability derived from the Yoyo CTD station GeoB 16316 (see also Table 4.1). (a) Variability of the temperature distribution in the entire water column over a time interval of 12 h (comprising 13 individual CTD casts). The red inset shows the density gradient over 10 m depth intervals for the water column below 380 m taken from CTD cast GeoB 16316-1 (00:20 UTC). (b) Depth variation of the 8°C to 9.5°C isotherms in the lower part of the water column >500 m water depth over the same time period shows partly vertical movements of >20 m. Variations in water depth (black denotes the sea floor) are caused by slight movements of the vessel (~600m N–S, ~50m E–W) at the Yoyo CTD station (including the crossing of a CWC mound). (c) Water temperature at 519 m depth measured over the same time period indicates a variability of up to 1°C. (d) Gradients in temperature, salinity, and density over 10 m depth intervals. Data were obtained during the individual CTD cast GeoB 16316-1 (00:20 UTC) and reveal particularly strong gradients around 520 m water depth (see also a)

Fig. 5.1 SM

148

Simplified map of the thermohaline circulation system in the North Atlantic Ocean (available at: http://pordlabs.ucsd.edu/ltalley/sio210/Atlantic_deep; Prof. Dr. Lynne Talley, Climate atmospheric science & physical oceanography)

Fig. 5.2

123

left) T-S plot of water masses observed at the studied sites. Each different site is marked by a different color: CB=*red*, GBB=*yellow*, BB=*blue*, PS=*black*, Norwegian margin=*magenta*, MAC=*grey*, MAU=*green*. Abbreviations for water masses are: STUW=Subtropical Intermediate Water; ENACW=Eastern North Atlantic Central Water; AW=Atlantic Water; NCW=Norwegian Coastal Water; ACW=Antilles Current Water; MOW=Mediterranean Outflow Water; AAIW=Antarctic Intermediate Water; NADW=North Atlantic Deep Water; NSDW=Norwegian Sea Deep Water. *right*) The position of living CWC reefs are indicated by blue dots. The color coding represents the depth. The different site to which each T-S profile belongs can be depicted from color coded profiles in the left panel

Fig. 5.3	127
Steepness of density gradients over a very short depth range, e.g. $\Delta\sigma_{\Theta_{10m}}$ maximum, results in very little mixing processes (Ocean dynamics stability in the water column; available at: www.maths.unsw.edu.au/~katrinmeissner/.../wk4_handouts_large)	
Fig. 5.4 SM	149
Location map is illustrating sample areas indicated by red dots	
Fig. 5.5	130
Variability of water masses of the studied sites with respect to potential temperature, salinity and potential density portrayed in T–S diagrams. Living <i>Lophelia pertusa</i> reefs are indicated by purple dots. Isopycnals are calculated with the reference pressure at 0 m (σ_{Θ}), i.e. sea level. Abbreviations for localities are: Campeche Bank (CB), Great Bahama Bank (GBB), St. Nazaire Canyon (BB), Porcupine Seabight (PS), Norwegian margin, Agadir Canyon (MAC)	
Fig. 5.6	134
Cross section of density gradients ($\Delta\sigma_{\Theta_{10m}}$) through water masses in the Porcupine Seabight (PS) – category III. The <i>upper</i> section shows the slope over a distance of 2.5 km and the density gradients between 10 m interval. The <i>bottom</i> figure zoomed in the section, where living <i>Lophelia pertusa</i> reefs were found ($\Delta\sigma_{\Theta_{10m}}$ maximum >0.07)	
Fig. 5.7	135
Cross sectioned density gradients ($\Delta\sigma_{\Theta_{10m}}$) through water masses in the St. Nazaire Canyon (BB) – category II. The <i>upper</i> section figure shows the slope over a distance of 310 km. The <i>bottom</i> figure zoomed in the section, where living <i>Lophelia pertusa</i> reefs were found ($\Delta\sigma_{\Theta_{10m}}$ maximum >0.04)	
Fig. 5.8 SM	150
Cross sectioned gradients through ($\Delta\sigma_{\Theta_{10m}}$) water masses Campeche Bank (CB) – category I. The <i>upper</i> section displays the site over a distance of 3km. The <i>bottom</i> figure zoomed in the section, where living <i>Lophelia pertusa</i> reefs were found ($\Delta\sigma_{\Theta_{10m}}$ maximum >0.06)	
Fig. 5.9	136
Cross sectioned gradients ($\Delta\sigma_{\Theta_{10m}}$) through water masses in the Agadir Canyon (MAC) – category III. The <i>upper</i> section figure shows the site over a distance of 65km. The <i>bottom</i> figure zoomed in the section, where living <i>Lophelia pertusa</i> reefs were found ($\Delta\sigma_{\Theta_{10m}}$ maximum >0.03)	

Fig. 5.10

138

Plots illustrating the relation of hydrological variability derived as $\Delta\sigma_{\Theta_{10m}}$ density, temperature, salinity versus categories I – III for Ireland (Porcupine Seabight) category I, Bay of Biscay (St. Nazaire Canyon) category II and Morocco (Agadir Canyon) category III. Note the strong influence of salinity in the Porcupine Seabight versus the strong influence of temperature in Agadir Canyon, Morocco

Fig. 5.11 SM

151

Plots illustrating the relation of hydrological variability derived as $\Delta\sigma_{\Theta_{10m}}$ density, temperature, salinity for Gulf of Mexico (GoM) and the sites of Campeche Bank (CB) and West-Florida Slope (W-FI)

Fig. 5.12 SM

152

Plots illustrating the relation of hydrological variability derived as $\Delta\sigma_{\Theta_{10m}}$ density, temperature, salinity for the Yoyo-CTD on Campeche Bank (CB)

Index of Tables

Table 1.1		3
Taxonomy <i>Lophelia pertusa</i>		
Table 2.1	SM	48
CTD stations off Morocco during cruise MSM32 (present study), and off Mauritania (cruise MSM16/3) and in the Gulf of Cadiz (cruise MSM1/3 (for data sources, see main text). T, S, density and oxygen values are given for the deepest sampling locations		
Table 2.2	SM	50
Box corer stations off Morocco during cruise MSM32		
Table 2.3	SM	51
U-Th isotope systematics and age determination of <i>Lophelia pertusa</i> from box core MSM32-3-1-1 (719 m water depth), cruise MSM32 off Morocco (uncertainties at 2 SE level)		
Table 3.1		55
Sampling location and hydrographical <i>in-situ</i> data (according to Hebbeln et al. 2014; Glogowski et al. 2015). *Yo-yo-data represent mean values of 13 CTD casts covering a time window of 13 hours		
Table 3.2	SM	84
Analytical data for mean sample, TW and CoC for each <i>L. pertusa</i> and different methods: EPMA, LA-ICP-MS, binocular camera, Keyence camera. n = the number of individual data points. Analytical results present mean sample values, TW values, and CoC values by different colours (cream=mean sample; grey=TW; green=CoC).		
Table 3.3	SM	95
Assignment of the LA-ICP-MS analytical spots of Mg/Ca and the analytical points of the EPMA according to each microstructure of the arithmetic mean sample, TW and CoC of each individual section for <i>L. pertusa</i> and uncertainties respectively. Enrichment factors of the arithmetic mean and min./max. values are presented (and uncertainties respectively). The total number (n) of measurements as the basis of each individual data point (EMPA and LA-ICP-MA) and different colours for the arithmetic mean sample, the TW and the CoC are listed in detail in Table 2		

Table 3.4 SM 96

Assignment of the LA-ICP-MS analytical spots of Sr/Ca and the analytical points of the EPMA according to each microstructure of the arithmetic mean sample, TW and CoC of each individual section for *L. pertusa* and uncertainties respectively. Enrichment factors of the arithmetic mean and min./max. values are presented (and uncertainties respectively). The total number (n) of measurements as the basis of each individual data point (EMPA and LA-ICP-MA) and different colours for the arithmetic mean sample, the TW and the CoC are listed in detail in Table 2

Table 3.5 SM 97

Assignment of the LA-ICP-MS analytical spots of Na/Ca and the analytical points of the EPMA according to each microstructure of the arithmetic mean sample, TW and CoC of each individual section for *L. pertusa* and uncertainties respectively. Enrichment factors of the arithmetic mean and min./max. values are presented (and uncertainties respectively). The total number (n) of measurements as the basis of each individual data point (EMPA and LA-ICP-MA) and different colours for the arithmetic mean sample, the TW and the CoC are listed in detail in Table 2

Table 4.1 105

Metadata of CTD casts conducted at the Campeche cold-water coral province during R/V *Maria S. Merian* cruise MSM 20-4. Abbreviations: WD: water depth

Table 5.1 SM 153

Sampling location and hydrographical *in-situ* data for the studied regions of Campeche Bank (CB), Great Bahama Bank (GBB), St. Nazaire Canyon (BB), Porcupine Seabight (PS), Norwegian margin, Agadir Canyon (MAC). *Yo-yo-data represent mean values of 13 CTD casts covering a time window of 13 hours

Table 5.2 SM 154

Shown are the various locations and their hydrographic and oceanographic *in-situ* bottom water fingerprints of the presented data set

Acknowledgments

I would like to sincerely thank my supervisor, Prof. Dr. **Wolf-Christian Dullo** (GEOMAR, Kiel) for the given opportunity to carry out my PhD-Thesis. Regardless of the circumstance your door was always open, you were always a patient and helpful supervisor! Thank you very much!

Dr. **Sascha Flögel** (GEOMAR, Kiel) and Dr. **Jacek Raddatz** (Goethe Institute, Frankfurt), Prof. Dr. **Priska Schäfer** (University Kiel), who are to be thanked for continually believing in this project, even at times when it seemed to be unachievable. Your guidance, support and encouragement were instrumental throughout this entire process.

I would also like to thank all members of my committee, Prof. Dr. **Martin Frank**, Prof. Dr. **Ute Hentschel Humeida**, Prof. Dr. **Dirk Nürnberg** for providing valuable input through the various stages of this project and for comments on this manuscript.

Furthermore, I am very grateful to Dr. **Volker Liebetrau**, Dr. **Dorothea Bauch**, Dr. **Steffen Hetzinger**, Dr. **Daniela Henkel**, Dr. **Hanno Kinkel**, Dr. **Kristin Döring**, Dr. **Georgi Laukert** and **Martina Hars** (GEOMAR, Kiel) for co-correcting the manuscripts and for helpful discussions.

My colleague Dipl.-Geol. **Jonas von Reumont** (GEOMAR, Kiel) who is deeply to be thanked for his encouragement, support, ship cruise MSM32, and for uncountable discussions.

The laboratory team, namely Dr. **Jan Fietzke**, Dr. **Matthias Frische**, **Mario Thöner**, **Jutta Heinze**, **Anke Beyer**, **Bettina Domeyer**, **Nadine Gehre**, **Ana Kolevica** are highly acknowledged for their technical assistance and help on all questions concerning the laboratory management.

Dr. **Robert van Geldern** (University of Erlangen-Nuremberg) who is to be thanked for his DIC analyses and Dr. **Sonja Enders** (GEOMAR, Kiel) for transporting the samples from Kiel to Erlangen.

I also would like to express my gratitude to the “Kaffeerunde“ from the **Arctic-Group** (Geb. 4) named personally: Robert, Henning, Dorothea, Georgi, Kirstin, Nadezda, Carolyn, Karen and Heidi.

Special thanks to **Gabriel Engelen** for beautiful pictures of the *L. pertusa*.

Greatly acknowledgements to the *R/V MARIA S. MERIAN* crew during MSM20-4 for their friendly and professional cooperation as well as their efficient technical assistance. Special thanks to the Masters, Crew, Shipboard and Science staff onboard *R/V Maria S. Merian* for their continuous support during cruise MSM32. The cruises were funded by the Deutsche Forschungsgemeinschaft (DFG).

My colleagues and friends at the GEOMAR: Hanno, Doris, Veit, Clauschi, Steffie, Anna, Stefan, David, Jacky, Peer.

Special thanks to my close friends: Henri und Ralf, Re-Nate, Susanne, Tina, Verena, Claudia, Jochen, Alexandra, Franzi, Inka und Jörg, Bea und Andi, Sanni, Hermann, Tobi, Nicole, Andrea, Hubschi, Frauke, Uli, Domenica and Erika.

The greatest thank will be given to my sons Keke and Mika. I love you!

Apendix

Chapter 4

Environmental forcing of the Campeche cold-water coral province, southern Gulf of Mexico by Dierk Hebbeln, Claudia Wienberg, Paul Wintersteller, Andre Freiwald, M. Becker, Lydia Beuck, Wolf-Christian Dullo, Gregor P. Eberli, [Silke Glogowski](#), Lelia Matos, Nina Forster, Hector Reyes-Bonilla, Marco Taviani, and the MSM 20-4 shipboard scientific party (2014). *Biogosciences* (11):1799-1815



Environmental forcing of the Campeche cold-water coral province, southern Gulf of Mexico

D. Hebbeln¹, C. Wienberg¹, P. Wintersteller¹, A. Freiwald², M. Becker¹, L. Beuck², C. Dullo³, G. P. Eberli⁴, S. Glogowski³, L. Matos^{1,5,6}, N. Forster², H. Reyes-Bonilla⁷, M. Taviani^{8,9}, and the MSM 20-4 shipboard scientific party

¹Center for Marine Environmental Sciences (MARUM), University of Bremen, Bremen, Germany

²Senckenberg am Meer, Marine Research Department, Wilhelmshaven, Germany

³Helmholtz Centre for Ocean Research Kiel (GEOMAR), Kiel, Germany

⁴Rosenstiel School for Marine and Atmospheric Science (RSMAS), University of Miami, Miami, USA

⁵Instituto Portugues do Mar e da Atmosfera (IPMA), Lisbon, Portugal

⁶Centro de Estudos do Ambiente e do Mar (CESAM), Aveiro, Portugal

⁷Universidad Autónoma de Baja California Sur, La Paz, Mexico

⁸Institute of Marine Sciences, National Research Council, Bologna, Italy

⁹Biology Department, Woods Hole Oceanographic Institution, Woods Hole, USA

Correspondence to: D. Hebbeln (dhebbeln@marum.de)

Received: 30 October 2013 – Published in Biogeosciences Discuss.: 28 November 2013

Revised: 11 February 2014 – Accepted: 13 February 2014 – Published: 7 April 2014

Abstract. With an extension of $> 40 \text{ km}^2$ the recently discovered Campeche cold-water coral province located at the northeastern rim of the Campeche Bank in the southern Gulf of Mexico belongs to the largest coherent cold-water coral areas discovered so far. The Campeche province consists of numerous 20–40 m-high elongated coral mounds that are developed in intermediate water depths of 500 to 600 m. The mounds are colonized by a vivid cold-water coral ecosystem that covers the upper flanks and summits. The rich coral community is dominated by the framework-building Scleractinia *Enallopsammia profunda* and *Lophelia pertusa*, while the associated benthic megafauna shows a rather scarce occurrence. The recent environmental setting is characterized by a high surface water production caused by a local upwelling center and a dynamic bottom-water regime comprising vigorous bottom currents, obvious temporal variability, and strong density contrasts, which all together provide optimal conditions for the growth of cold-water corals. This setting – potentially supported by the diel vertical migration of zooplankton in the Campeche area – controls the delivering of food particles to the corals. The Campeche cold-water coral province is, thus, an excellent example highlighting the

importance of the oceanographic setting in securing the food supply for the development of large and vivid cold-water coral ecosystems.

1 Introduction

The last decade has witnessed a tremendous progress in our knowledge about “framework-building cold-water corals” (CWC) as their role as ecosystem engineers creating highly diverse ecosystems in water depths far beyond the shelf edge is becoming more and more obvious (Roberts et al., 2009). The biodiversity associated with these ecosystems may be comparable to that found in tropical coral reefs (Roberts et al., 2006), and they occur almost worldwide except for the highest latitudes (Davies and Guinotte, 2011). The availability of advanced deep-sea technologies (e.g., remotely operated vehicles) greatly supported the discovery and investigation of large, thriving and (so far) unknown CWC ecosystems in remote places. Successful studies such as those performed off Mauritania (Colman et al., 2005), off Angola (Le Guilloux et al., 2009), and in various parts of the Mediterranean

Sea (Freiwald et al., 2009; Orejas et al., 2009; Fink et al., 2013; Gori et al., 2013) demonstrate the potential use of these technologies for future discoveries.

With their rigid carbonate skeletons that can persist over geological timescales CWC shape the sea floor by creating large three-dimensional structures, e.g., > 300 m-high coral carbonate mounds along the Irish margin (e.g., Kenyon et al., 2003; Mienis et al., 2007) reaching back to Pliocene times (~ 2.6 Ma; Kano et al., 2007) and > 100 km²-large reef structures off Norway (Fosså et al., 2005) formed during the Holocene (e.g., López Correa et al., 2012). These structures consist of a mixture of coral skeletons, the skeletal remains of the coral-associated megafaunal community, and pelagic or hemipelagic sediments that can serve as paleoenvironmental archives allowing to reconstruct the long-term development of the CWC ecosystems (e.g., Dorschel et al., 2005; Frank et al., 2009; Titschack et al., 2009; Wienberg et al., 2009; Eisele et al., 2011; Fink et al., 2012; López Correa et al., 2012; Douarin et al., 2013; Thierens et al., 2013).

The scleractinian coral *Lophelia pertusa* is among the most common and most widespread CWC species worldwide and is particularly abundant in the eastern North Atlantic (Davies and Guinotte, 2011). This species withstands a rather wide range of physicochemical conditions (see summary in Davies et al., 2008), a fact that explains its almost global distribution at depths between a few tens of meters to over 2000 m (Freiwald and Roberts, 2005). Another critical factor controlling its distribution is sufficient food supply that is commonly driven by the interplay of surface water productivity and the local nature of the bottom current regime (e.g., currents, stratification, internal waves and tides) delivering food particles to the CWC (Duineveld et al., 2004, 2007; White et al., 2005). Paleoenvironmental studies revealed that food supply often is the decisive factor triggering on- or off-sets of coral growth in a given setting (e.g., Dorschel et al., 2005; Wienberg et al., 2010; Eisele et al., 2011; Fink et al., 2013).

In addition to the CWC hotspot in the eastern North Atlantic, *L. pertusa* also contributes to numerous coral mound structures in the western North Atlantic along the continental margin from North Carolina (Ross and Nizinski, 2007), along the Florida–Hatteras slope (Paull et al., 2010), and The Bahamas to the Florida Straits (e.g., Neumann et al., 1977; Mullins et al., 1981; Grasmueck et al., 2006; Correa et al., 2012a, b). Further west in the Gulf of Mexico, *L. pertusa* appears to be more scattered, forming isolated mound-like structures along the west Florida slope (Newton et al., 1987; Hübscher et al., 2010) and in the northern Gulf of Mexico (Moore and Bullis, 1960; Schroeder, 2002; Reed et al., 2006; Cordes et al., 2008; Becker et al., 2009; Davies et al., 2010). Summarizing the current knowledge, Mienis et al. (2012) conclude that within the Gulf of Mexico CWC mound structures have been rarely found, except on the west Florida slope and in the Viosca Knoll area (Fig. 1). The latter area has been considered the most extensive *Lophelia* habitat found

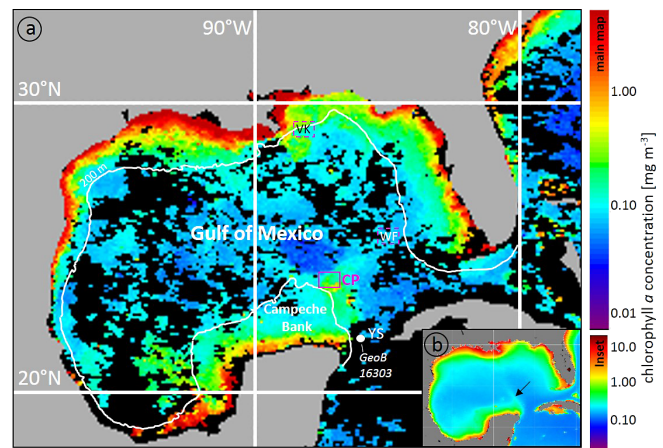


Fig. 1. SEAWIFS satellite ocean color data transferred into chlorophyll *a* concentrations for the Gulf of Mexico (source: <http://oceancolor.gsfc.nasa.gov>). **(a)** The map refers to an 8-day composite representing the period 22–29 September 2010. Black indicates data gaps. The Campeche cold-water coral province (CP) is influenced by increased productivity probably forced by local upwelling at the northeastern rim of the Campeche Bank (Molinari and Morrison, 1988). The white dot in the Yucatan Strait (YS) indicates CTD station GeoB 16303-1. The white line marks the 200 m isobath within the Gulf of Mexico. VK: Viosca Knoll cold-water coral setting (e.g., Brooke and Schroeder, 2007); WF: west Florida cold-water coral mounds (Newton et al., 1987). **(b)** The inset shows the same data as a composite for the entire SEAWIFS mission (4 September 1997 to 30 November 2010). The black arrow indicates the area of the Campeche cold-water coral province that is located in a region marked by a long-term enhanced productivity.

so far in this region (Brooke and Schroeder, 2007; Davies et al., 2010) probably as a consequence of enhanced productivity driven by nutrient-enriched Mississippi River outflow (Wawrik and Paul, 2004). Apart from the Campeche Bank, the southern Gulf of Mexico is generally characterized by meager planktonic biomass along the Mexican slope mirroring the low-productivity Caribbean water that enters the Gulf of Mexico through the Yucatan Strait (Wei et al., 2012).

In this paper, we document for the first time build-ups at the sea floor formed by framework-building scleractinian corals on the slope of the Mexican Campeche Bank, southern Gulf of Mexico. These build-ups are mainly formed by *Enallopsammia profunda*–*Lophelia pertusa* communities. This finding was unexpected as available data from a few dredge haul stations only described the occurrence of the scleractinian CWC *Madrepora oculata* along the margin of the Campeche Bank, north of the Mexican Yucatan Peninsula (Cairns, 1979; Schroeder et al., 2005). Only in 2010 was more detailed information provided, when hydroacoustic surveys revealed “mound-like” structures between 500 and 600 m water depth along the margin of the bank (Hübscher et al., 2010). Without any groundtruthing being available at

that time, it only has been speculated that these structures might be CWC mounds (Hübscher et al., 2010).

This region was revisited in 2012 and extensive field data (bathymetry, hydrography, and video observations) revealed the existence of a large thriving CWC ecosystem, which is the focus of this paper. This hitherto unknown CWC site is here termed the “Campeche CWC province”. The scope of the present study is to describe this extensive ($> 40 \text{ km}^2$) CWC province with respect to morphology, the megafaunal community, and the oceanographic setting and to put it into a larger framework analyzing the overall forcing factors controlling its development.

2 Regional setting

The Campeche Bank is a large shelf area extending approximately 200 km northward from the Mexican Yucatan Peninsula into the Gulf of Mexico (Fig. 1). The Gulf of Mexico is a largely oligotrophic basin with enhanced productivity only along the continental shelves (Müller-Karger et al., 1991), where seasonal coastal upwelling provides additional nutrients to the surface waters (Zavala-Hidalgo et al., 2006). A major source of nutrients is the Mississippi plume fertilizing the northeastern shelves of the Gulf with enhanced productivity partly extending over the continental slope (Wawrik and Paul, 2004). The enhanced productivity triggered by the Mississippi plume most likely plays an important role in sustaining CWC populations along the Louisiana and Florida continental slopes (e.g., Newton et al., 1987; Schroeder, 2002; Fig. 1).

Apart from the typical coastal upwelling, another upwelling regime has been described further offshore along the eastern margin of the Campeche Bank (Merino, 1997). As the curl of the prevailing wind stress is not likely to induce upwelling along the eastern Yucatan slope, the upwelling observed there is probably caused by bottom friction or other topographical effects (Merino, 1997). Nevertheless, the advection of nutrients into the photic zone (although rarely to the sea surface; Merino, 1997) induces very high productivity reaching a peak in September (Zavala-Hidalgo et al., 2006) when sites near the Campeche CWC province appear prominently in satellite-based productivity maps (Fig. 1).

Along its eastern edge the Campeche Bank borders the Yucatan Strait that forms the main passage connecting the Caribbean Sea and the Gulf of Mexico through which the Yucatan Current transports $\sim 24 \text{ Sv}$ from south to north (Sheinbaum et al., 2002). According to Merino (1997) three main water masses comprise the water column there. Salinity and temperature increase together from the Antarctic Intermediate Water (AAIW, 7°C , salinity 34.9) in the deep towards the salinity maximum of the Subtropical Intermediate Water (STUW, 23°C , salinity 36.8) at $\sim 150 \text{ m}$ depth. Further above, temperature rises and salinity declines until from 50 m to the surface both parameters remain relatively constant

($26\text{--}27.5^\circ\text{C}$, salinity < 36.4), representing the Caribbean Surface Water (CSW). At depths greater than $\sim 650 \text{ m}$, the Yucatan and Cuban countercurrents transport water southward while being confined to the western, Mexican side and to the eastern, Cuban side of the Yucatan Strait, respectively (Sheinbaum et al., 2002).

With respect to the strength of the bottom current regime, the best information is provided by mooring data obtained slightly further south in the Yucatan Strait ($\sim 21.5^\circ \text{N}$; e.g., Sheinbaum et al., 2002). Along a W–E transect through the area, the mean northward current velocities at the western margin decrease rapidly from almost 100 cm s^{-1} at the surface to $< 10 \text{ cm s}^{-1}$ at 200 m water depth. However, at the depth of the Campeche CWC province ($\sim 550 \text{ m}$) the bottom current velocities in the Yucatan Strait increase again to $> 10 \text{ cm s}^{-1}$ (Sheinbaum et al., 2002).

3 Methods

All data presented here were collected during expedition MSM 20-4 with the German R/V *Maria S. Merian* in spring 2012 (Hebbeln et al., 2012). They include hydroacoustic measurements, water column studies, and seabed ROV video observation (see Table 1 and Fig. 2 for relevant site information). Instrument specifications and applied settings for the hydroacoustic measurements are described in detail in Hebbeln et al. (2012). For all hydroacoustic measurements introduced below, the essential sound velocity profile through the water column was obtained from two CTD casts in (GeoB 16305-1) and close to (GeoB 16303-1) the working area (Figs. 1 and 2, Table 1).

3.1 Hydroacoustic measurements

3.1.1 Multibeam echosounder (MBES)

Seabed mapping was performed using a KONGSBERG EM1002 multibeam echosounder system (MBES) operating at a frequency of 95 kHz. The EM1002 emitted 111 beams per ping, covered a depth range of 2 to 1000 m and achieved a high depth resolution of 2–8 cm, depending on the pulse length (0.2–2 ms). Achievable swath width on a flat bottom was up to 5 times the water depth dependent on the character of the seafloor. Spatial integrity of the mapping data were achieved by combining the ship’s SEAPATH 200 inertial navigation system (INS) including differential global positioning system (DGPS) information with motion data (roll, pitch, heave) provided by the motion reference unit (MRU) 5. The open-source software package MB-System v.5.3.1 (Caress and Chayes, 1996) and the Generic Mapping Tool (GMT) v.4.3.1 (Wessel and Smith, 1998) were used for bathymetric data processing, editing and evaluation. ESRI ArcGIS v.10 was used to create maps (grid cell size: 10 m) and a sustainable spatial data management.

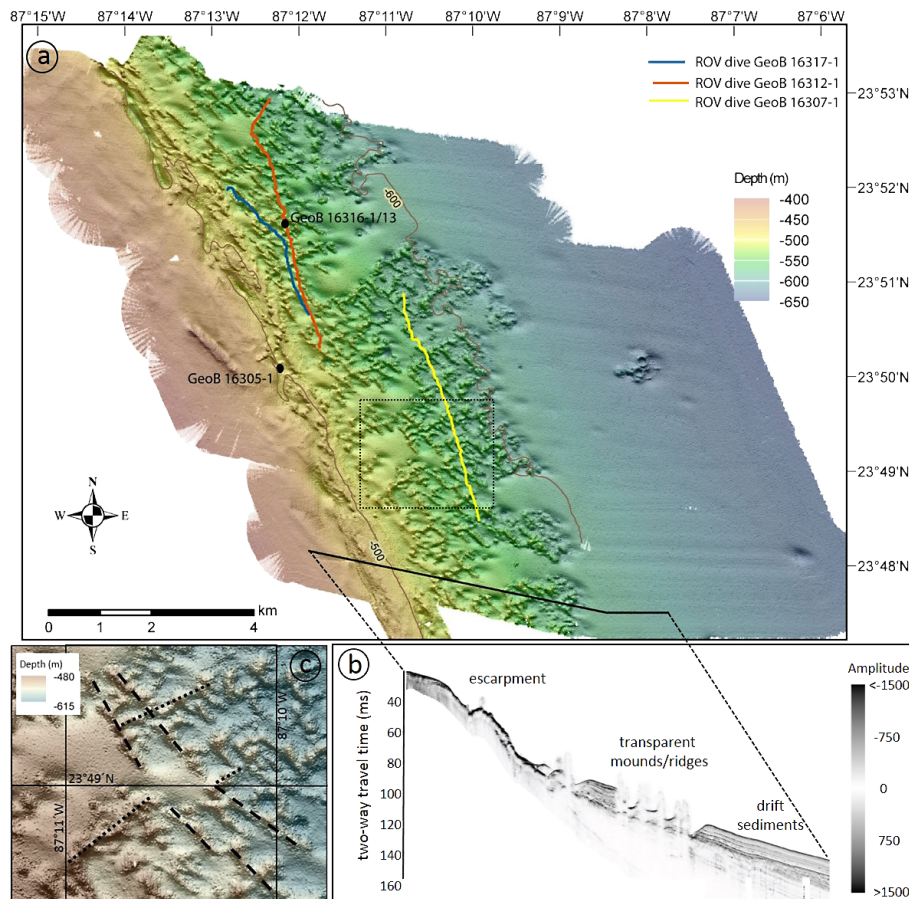


Fig. 2. Overview on the Campeche cold-water coral province (for location see Fig. 1). **(a)** Detailed bathymetric map showing the eastern margin of the Campeche Bank comprising the Campeche cold-water coral province revealing numerous individual elongated coral mounds located mainly between 500 and 600 m water depth. Indicated are CTD sites (black dots) and ROV dive tracks (colored lines; GeoB station numbers are indicated) conducted during R/V *Maria S. Merian* cruise MSM 20-4 (for detailed site information see Table 1). **(b)** PARASOUND profile crossing the slope and highlighting the main morphological units. **(c)** High-resolution view on some of the elongated coral mounds (for position see dotted rectangle in **a**), with the dominant northwesterly directions marked by dashed lines and with the sub-dominant northeasterly directions marked by the dotted lines.

3.1.2 Acoustic Doppler current profiler (ADCP)

Current velocity and direction, and backscatter data through the water column were measured with an RDI Ocean Surveyor acoustic Doppler current profiler (ADCP) operating at a frequency of 75 kHz. Data were acquired using the RDI software VMDAS (Vessel-Mount Data Acquisition) using 128 depth bins of 5 m bin size. Backscatter data were corrected for beam spreading and water absorption (Deines, 1999). For the backscatter data set presented in this study, a constant water absorption coefficient of 0.0272 dB m^{-1} was used (Schulkin and Marsh, 1962). Due to the simultaneous deployment of several hydroacoustic devices, backscatter and current velocity data were affected by acoustic interference, which was removed using appropriate filters. Backscatter data close to the seafloor were biased by side-lobe interferences and not used for interpretation. ADCP data are

presented as a stationary 12 h record collected at site GeoB 16316 (Fig. 2, Table 1).

3.2 ROV video observation and sampling

Three video surveys (GeoB 16307-1, GeoB 16312-1, GeoB 16317-1; Table 1, Fig. 2) were conducted with the ROV *Cherokee* (Sub-Atlantic, Aberdeen, Scotland; operated by MARUM, Bremen, Germany) crossing several CWC mounds along the Campeche margin. The ship-based IXSEA global acoustic positioning system (GAPS) coupled with the ship's DGPS provided an absolute positioning accuracy within 1–2 % of the slant range. The ROV was equipped with a hydraulic manipulator system for sampling purposes, four video cameras including a color video zoom camera for detailed seafloor observation and a digital still camera. The cameras were equipped with two lasers for object size measurements on the seabed; laser scaling was adjusted to

Table 1. Metadata of CTD casts and ROV *Cherokee* video surveys conducted at the Campeche cold-water coral province during R/V *Maria S. Merian* cruise MSM 20-4. Abbreviations: WD: water depth.

Station [GeoB-No.]	Gear	Date [2012]	UTC [hh:mm]	Latitude [N]	Longitude [W]	WD [m]	Remark
16303-1	CTD	21 March	14:59	22° 00.98'	86° 02.95'	1246	Sound velocity profile
16305-1	CTD	22 March	05:21	23° 49.87'	87° 12.27'	506	Sound velocity profile
16316-1 to 16316-13	Yoyo CTD	Start:	24 March 00:20	23° 51.51'	87° 12.12'	576	Hourly casts over ~ 12 h; ADCP data were recorded simultaneously over ~ 13 h
		End:	24 March 12:01	23° 51.52'	87° 12.13'	558	
16307-1	ROV	Start:	22 March 13:51	23° 40.83'	87° 10.03'	547	Video observation
		End:	22 March 16:20	23° 50.49'	87° 10.71'	577	
16312-1	ROV	Start:	23 March 14:31	23° 50.35'	87° 11.76'	523	Video observation
		End:	23 March 18:31	23° 52.52'	87° 12.49'	531	
16317-1	ROV	Start:	24 March 13:37	23° 51.12'	87° 12.53'	555	Video observation
		End:	24 March 15:02	23° 51.77'	87° 12.16'	556	

11.5 cm in a horizontal direction. All video and still-image data were digitally stored. Navigational data (ship, ROV), video recordings, and still images are all time-referenced. With the manipulator of the ROV several coral samples were collected to assess the phenotypes of the different CWC species.

3.3 Water column analyses

To determine the physical parameters of the water masses in the area of the Campeche CWC province and to trace their variability, CTD measurements were performed as a Yoyo CTD comprising 13 individual casts taken within 12 h at station GeoB 16316 (Fig. 2, Table 1). The CTD measurements of the water column down to a maximum water depth of 1246 m were conducted using a SEABIRD “SBE 9 plus” underwater unit and a SEABIRD “SBE 11 plus V2” deck unit. The vertical profile over the water column provided standard data for conductivity, temperature, pressure, and dissolved oxygen. Conductivity and temperature data were used to compute salinity (with the latter being presented here unitless). The data presented here all refer to the downcast of the individual CTD deployments.

4 Results

4.1 Morphology and dimensions of the Campeche cold-water coral province

The hydroacoustic mapping encompasses an area of 180 km² along the northeastern slope of the Campeche Bank and displays three distinct topographical features (Fig. 2). The western part of the map shows an extensive more or less plain area at ~ 440 m water depth. A NNW–SSE orientated and ~ 40 m-high escarpment separates this rather shallow and

plain area from a gently dipping slope to the east, which covers the water depths between 480 and 600 m. Further downslope below ~ 600 m water depth, the slope is followed by a more gently dipping area which comprises smooth sediment of a major drift sediment body (Hübscher et al., 2010). The first 3–5 km of the dipping slope east of the edge are covered by linear and steep-sided elongated mounds between 500 and 600 m water depth. This belt of parallel elongated mounds is situated between the escarpment and the continuous drift deposit, with a few stratified sediment bodies also occurring between the mounds. Both the mounds and the sediment drift overlay a regional truncation surface (Fig. 2b; Hübscher et al., 2010).

The mounds have average heights between 20 and 40 m but can even reach heights of up to 50 m. They vary in length from a few tens of meters to > 1000 m, and trend in two directions. The dominant direction is NW–SE and the second one NE–SW (Fig. 2c). In many cases both directions merge, thereby forming V-shaped elongated mounds pointing with the tip to the WNW. ROV-based video observations reveal that the morphology of these mounds is mostly rather steep with estimated angles of up to 30° (e.g., Fig. 3e). These elongated mounds are often aligned by a moat towards the next mound (Fig. 2). In addition, on some of the mound flanks exhumed carbonate crusts with irregular upper and lower surfaces have been observed (Fig. 3h). As the video observations clearly indicate that these mounds are covered by a vivid CWC ecosystem (Figs. 3a, b and 4a, b), the entire structure is termed here the Campeche CWC province. The minimum extension of the Campeche CWC province is 40 km²; however, most likely this CWC province is even larger, as it still has a significant width at the northern and southern boundaries of the mapped area (Fig. 2). Thus, the ultimate northern and southern boundaries of the Campeche CWC province still need to be verified.

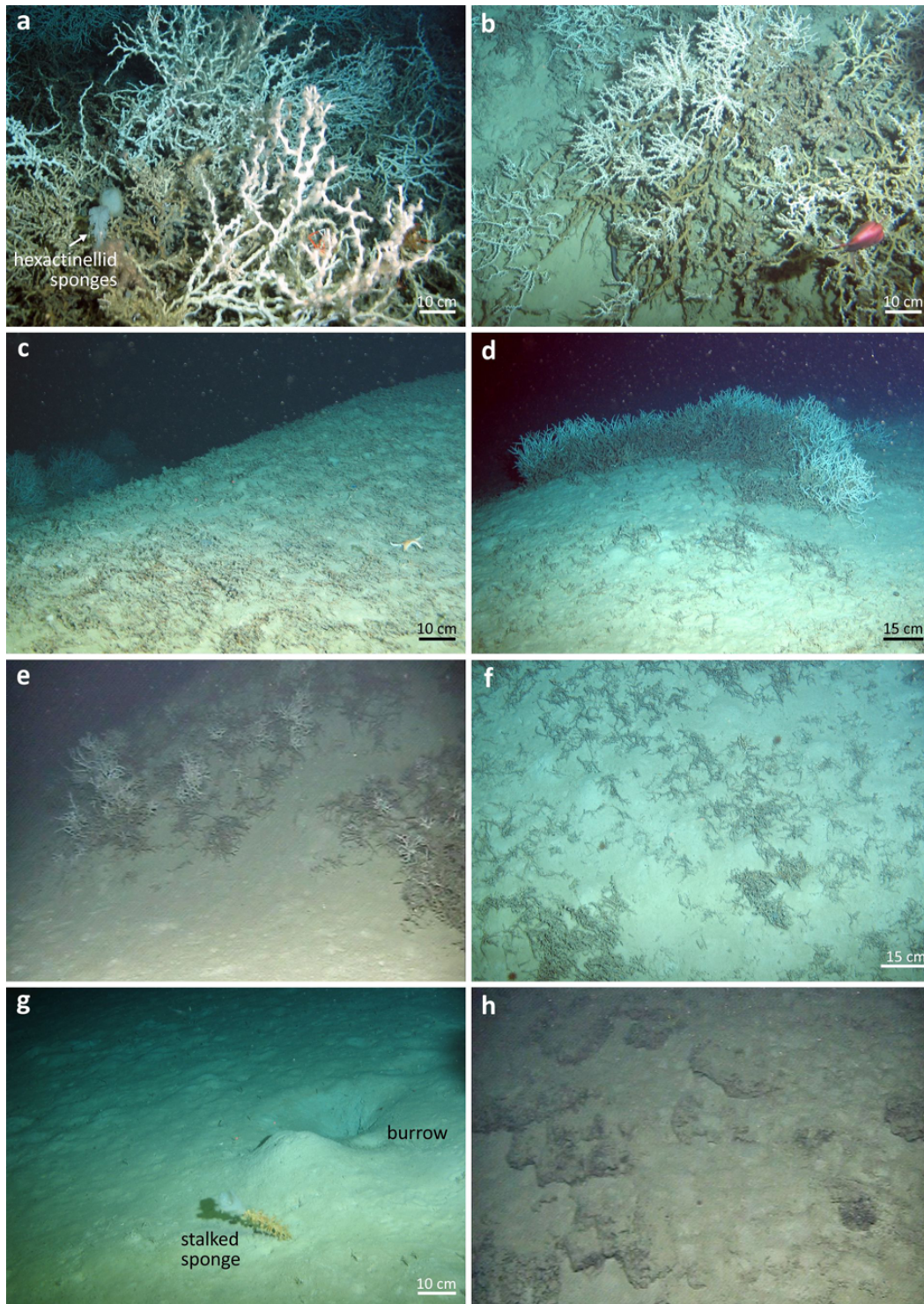


Fig. 3. ROV images showing the variety of facies types observed for the Campeche cold-water coral province (images copyright MARUM, Bremen, ROV *Cherokee* team). **(a)** Coral mound summit: dense colonies of *Lophelia pertusa* – note Hexactinellid sponges (*Aphrocallistes* sp.) and squat lobster; **(b)** current-exposed coral mound flank: ensemble of the fragile *Enallopsammia profunda* and the *brachycephala* morphotype of *L. pertusa*; **(c)** mound flank packed with dead coral framework; **(d)** arcuate *E. profunda* thicket on a low-relief mound; **(e)** sudden facies change from flat soft sediment plain to steeply inclined coral mound flank; **(f)** lower coral mound flank: dispersed fragments of *E. profunda*; **(g)** intermound area: strongly bioturbated soft sediment – note stalked sponge (*Hyalonema* sp.) colonized by actinarians; and **(h)** occasionally observed outcropping carbonate crusts.

4.2 The Campeche cold-water coral ecosystem

Observations during three ROV dives that cross several mounds of the Campeche CWC province reveal the composition of the structure-forming CWC and their associated megafaunal community. The dive tracks of the video surveys had an NNW–SSE orientation in water depths ranging 510–580 m (Fig. 2). All mounds studied are colonized by colonial scleractinians representing *Enallopsammia profunda*–*Lophelia pertusa* communities (Figs. 3 and 4), whereas the flat seabed between the mounds consists of pelagic unconsolidated mud enriched by globigerinid foraminifers and thecosomatous gastropods, locally admixed with patches of coral rubble and mollusk shell hash (see detailed description of collected sediment samples in Hebbeln et al. (2012)). These intermound areas are strongly bioturbated as indicated by widespread lebensspuren and burrows (Fig. 3g).

Coral colonization, coral density and coral species distribution show a clear zonation related to current exposure and position on the mound flank. In general, living corals occur at the highest parts of the mounds, followed downslope by a zone of coral rubble and by plain soft sediments in the lower parts of the mounds and in the areas between the mounds (Fig. 3). However, on some steeply inclined mounds (up to 30°), coral colonization starts already at the base of their current-exposed side (SSE), thereby generating a sharp change of sedimentary facies from pelagic muds to a living CWC ecosystem. On less steep mounds live coral colonies start to appear halfway upslope the current-exposed flank, or the mound flanks are entirely covered by a dead and collapsed coral framework or coral rubble with only few live coral colonies in between. For both types of mounds, corals fade off halfway along the leeward flanks of the mounds. Overall, the density of coral framework and the proportion of live coral colonies become progressively higher towards the summit, where they can form very dense coral thickets up to 60 cm thick. The mound flanks are dominated by *E. profunda*, whereas *L. pertusa* becomes increasingly abundant, if not dominant on the summits.

The dendroid *E. profunda* colonies display an open-spaced growth habit with individual colony branches pointing in all directions (Fig. 4a and b). This growth habit results in a loose mesh of coral framework, thus facilitating framework disintegration of individual branches into stick-like fragments. Colony heights vary from 20 to 60 cm; thus only the upper 10–15 cm of a colony yields live coral polyps and translucent tissue. *Lophelia pertusa* also constructs an open-spaced coral framework. However, secondary fusion between adjacent coral branches is a very common feature, thus increasing the structural integrity of the entire framework considerably in comparison to *E. profunda*. The branches of *L. pertusa* are strongly calcified and slender with individual corallite lengths of 2.5–3.5 cm and calicular diameters of 0.5–0.8 cm. This phenotype has been described as forma *gracilis* by Duncan (1873) and is in contrast to the stout

branches with extremely wide calicular diameters of the *brachycephala* form (Fig. 4a) described by Moseley (1881) and Cairns (1979). The latter phenotype occurs in low numbers in the Campeche CWC province, but the co-occurrence of the two *L. pertusa* growth forms is a well-known phenomenon in the northern Gulf of Mexico (Newton et al., 1987; Brooke et al., 2009). The *Lophelia* framework can attain heights of 50 cm, and the zone of live polyps and translucent tissue coverage stretch over a range of 20–30 cm.

The live coral zone is utilized by the associated community in various ways and differs largely in terms of species composition and richness from the associated community found in the tissue-barren, exposed coral framework beneath. Common organisms observed (although not exclusively) in the live zone are the predatory decapods *Bathynectes longispina*, *Eumunida picta*, *Chaceon fenneri*, *Munidopsis* sp. and *Rochinia crassa* and the grazing echinoids *Cidaris* sp. and *Gracilechinus* sp. (Fig. 4e). The latter echinoid has been recognized as a corallivore in CWC habitats of the eastern North Atlantic (Stevenson and Rocha, 2013). Other organisms with corallivore affinities in the live coral zone are star fishes of the genus *Hippasteria* (Mah et al., 2010) and the muricid gastropod *Coralliophila richardi* (Taviani et al., 2009), which were commonly collected from the live coral zone. Stalkless crinoids have been occasionally observed to take advantage of the elevated and current-exposed position of live coral branches for filtering particles from the water. Indication of probably necrotic epibiosis of live scleractinians by zoanthids and actinarians in some scleractinian colonies is a common feature and seems to cause local mortality. Polychaetes of the genus *Eunice*, from which several species are known as symbionts of *L. pertusa* and other colonial CWC (e.g., Buhl-Mortensen and Mortensen, 2004; Mueller et al., 2013), are surprisingly rare in the Campeche CWC province.

Characteristic organisms of the tissue-barren, exposed coral framework are flytrap anemones (probably *Actinoscyphia* sp.; Fig. 4b), isidid corals (*Keratoisis* sp.), and solitary scleractinians (*Desmophyllum dianthus*, *Javania cailetti*, *Stenocyathus vermiformis*, *Trochopsammia infundibulum*). The glass sponge *Aphrocallistes* sp. was found attached to the coral framework. Apparently the glass sponges are living together with masses of yellow actinarians (Fig. 4f), thus resembling the recently described symbiotic relationship between the glass sponge *Hyalonema sieboldi* with the actinarian *Spongiactis japonica* (Sanamyan et al., 2012). Common fishes encountered frequently in the coral framework were *Helicolenus dactylopterus* and *Nettenchelys exoria*. Gorgonians and antipatharians that are elsewhere common in CWC ecosystems are extremely rare here.

The coral rubble is strongly admixed with unconsolidated pelagic mud, thereby providing small hard-substrate islands within soft sediment. Common megafaunal organisms are large astrorhizid foraminifers, cerianthids, pennatulaceans, stalked glass sponges (*Hyalonema* sp.), and the

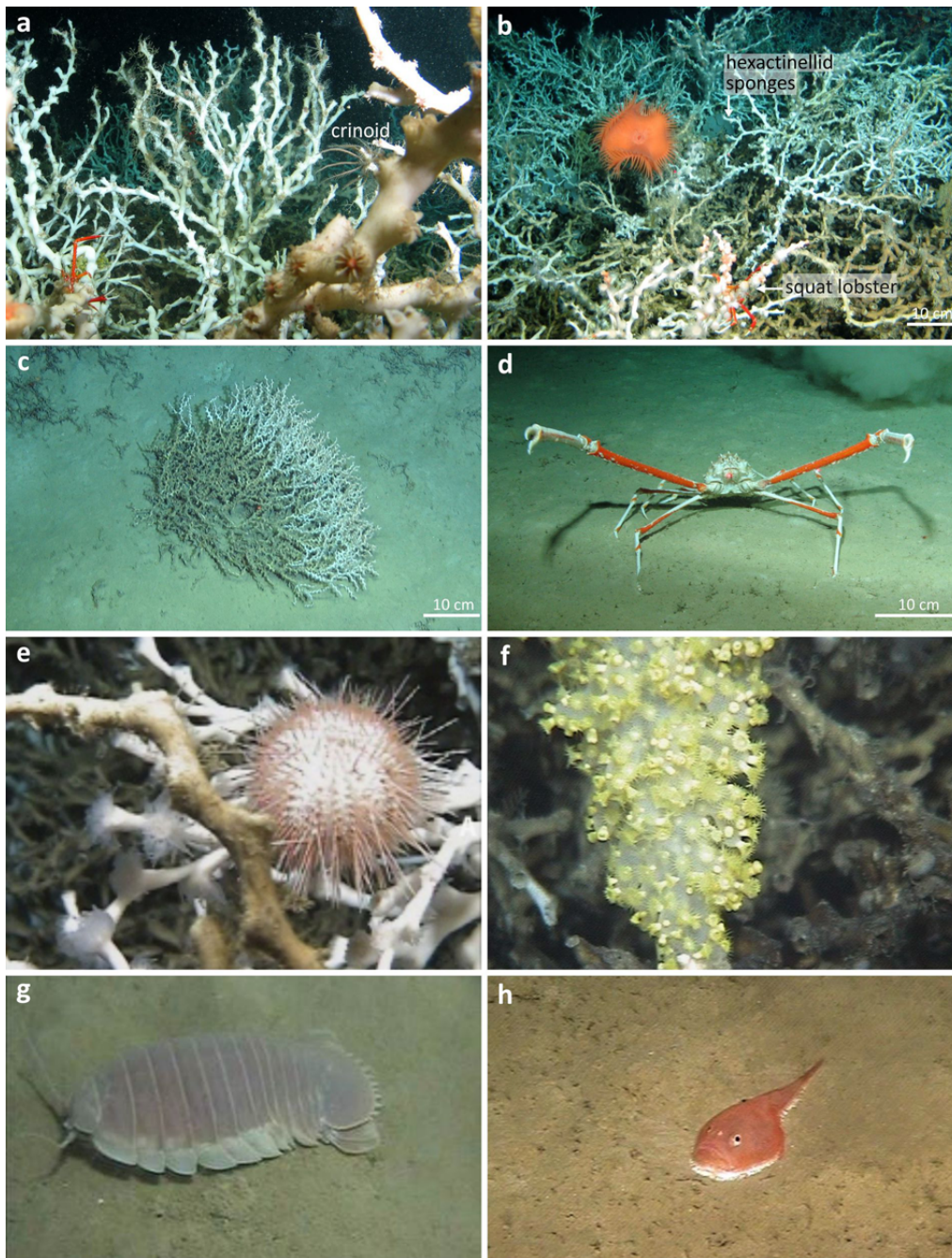


Fig. 4. ROV images showing examples for the megafaunal community present in the Campeche cold-water coral province (images copyright MARUM, Bremen, ROV *Cherokee* team). (a) Dense colonization of *Lophelia pertusa* at the coral mound top; (b) flytrap anemone (probably *Actinoscyphia* sp.) colonizing tissue-barren, exposed coral framework; (c) displaced but still alive colony of *Enallopsammia profunda*; (d) brachyuran crab *Rochinia crassa*; (e) grazing of living corals by the echinoid *Gracilechinus* sp.; (f) glass sponge *Aphrocallistes* sp. living together with masses of yellow actinarians; (g) the giant cirrolanid isopod *Bathynomus giganteus*; and (h) the anglerfish *Chaunax suttkusi* commonly spotted near the coral mounds resting on the seabed.

common decapods (same as in the live zone) and shrimps. Amongst the mobile organisms, the giant isopod crustacean *Bathynomus giganteus* was detected (Fig. 4g). Like in other coral rubble habitats elsewhere in the Gulf of Mexico and

in the northern North Atlantic, the anglerfish *Chaunax suttkusi* (Fig. 4h), was commonly spotted near the coral mounds resting on the seabed (Caruso et al., 2007). Other common fishes observed in the coral rubble and pelagic mud areas

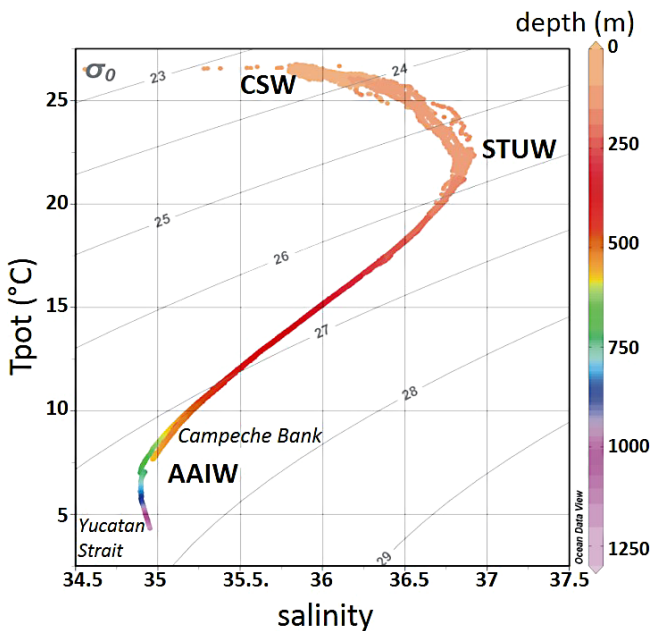


Fig. 5. Water mass structure in the Yucatan Strait (GeoB 16303-1) and in the Campeche cold-water coral province (GeoB 16316-1 to -16, Yoyo CTD station; see Table 1). Shown is a temperature–salinity plot; temperature is displayed as potential temperature (T_{pot}), grey lines indicate levels of isodensity (σ_{θ}) in kg m^{-3} (plotted using Ocean Data View v.4.5.1; <http://odv.awi.de>; Schlitzer, 2012). Abbreviations: CSW: Caribbean Surface Water; STUW: Subtropical Intermediate Water; AAIW: Antarctic Intermediate Water.

are *Chlorophthalmus agassizi*, *Laemonema* sp., *Nezumia* sp., Phycidae and Rajidae.

4.3 Water column structure/dynamics

The CTD measurements allow the identification of the most important regional water masses, based on temperature (potential temperature) and mainly on salinity data (Fig. 5). The uppermost ~ 80 m of the water column are characterized by water with salinities of < 36.4 , which is indicative of the presence of the CSW. The salinity maximum (~ 36.8) between 100 and 160 m water depth is characteristic for the STUW. At 540 m water depth salinity drops below 35.0, marking the presence of AAIW. In the depth range where living CWC have been observed (520 to 580 m) temperatures range $7.5\text{--}9.5\text{ }^{\circ}\text{C}$ and salinities $34.9\text{--}35.1$. Dissolved oxygen contents vary between 2.74 and 2.8 mL L^{-1} .

The Yoyo CTD station (GeoB 16316) consisting of 13 individual, hourly taken casts reveal small but significant variations also in the deepest part of the water column just above the Campeche CWC province (Fig. 6): for example, at 519 m water depth the temperature varies by almost $1\text{ }^{\circ}\text{C}$ up to three times over the 12 h measuring period (Fig. 6c). These temperature changes are also reflected in the depth position of individual isotherms (8 to $9.5\text{ }^{\circ}\text{C}$, Fig. 6b). They fluctuate

vertically by up to 20 m, thereby reflecting the same temporal forcing as the temperatures at 519 m depth. Along with these temperature changes a distinct density gradient induced by temperature and salinity changes, almost reaching $0.7\text{ }^{\circ}\text{C}$ and 0.07 , respectively, over a 10 m depth interval (Fig. 6d) propagates across the site. With $\sim 0.06\text{ kg m}^{-3}$ per 10 m depth interval this density gradient is strongest for the lower part of the water column at 525 m depth and significantly higher than the density gradients between 380 m and the sea floor that otherwise reach maximum values of $\sim 0.04\text{ kg m}^{-3}$ per 10 m depth interval (Fig. 6a).

The ADCP data collected over a 13 h time interval (simultaneously to the Yoyo CTD data; see Table 1) allow distinguishing between three major layers that show some internal (although less pronounced) horizontal structuring (Figs. 7 and 8). Within the upper 130 m of the water column, the highest current velocities ($74\text{--}83\text{ cm s}^{-1}$) occur together with a high backscatter ($94\text{--}98\text{ dB}$). Current directions vary between 322° and 335° . The second layer between 130 and 460 m is characterized by continuously decreasing current velocities from 63 to 42 cm s^{-1} , again by rather stable current directions similar to the uppermost layer (325° to 336°), and by low backscatter values ($84\text{--}94\text{ dB}$). The bottom layer (> 460 m) is marked by a significant change in current direction (343° to 360°) and by the lowest but still strong currents flowing at a rate of 24 to 42 cm s^{-1} .

At the beginning of the stationary ADCP record (ca. 00:00 UTC, 24 March 2012) enhanced backscatter signals move upward through the water column towards the sea surface. By the end (ca. 11:30 UTC), similar signals move downward towards the seabed (Fig. 7). Similar observations were made during additional ADCP surveys in the working area during cruise MSM 20-4 (Hebbeln et al., unpublished data). In total, four upward (always at around 0:00 UTC, corresponding to 18:15 local “solar” time at 86° W, i.e., sunset) and two downward movements (always at around 11:30 UTC, corresponding 05:45 local solar time at 86° W, i.e., sunrise) were observed.

5 Discussion

Large CWC-formed seafloor structures have been reported from many regions in the world’s oceans (see compilation in Freiwald and Roberts (2005)). In addition to the > 300 m-high CWC mounds off Ireland (Kenyon et al., 2003; Mienis et al., 2007; Dorschel et al., 2010), the extensive reefs off Norway (e.g., Fosså et al., 2005) are the most impressive features. Extending over tens of kilometers (e.g., the Sula Reef, $\sim 14 \times 0.5$ km, Freiwald et al., 2002; the Røst Reef, $\sim 40 \times 3$ km, Fosså et al., 2005) and reaching up to ~ 40 m in height, these reefs generally comprise clusters of individual frameworks rather than a single coalescent structure (Freiwald et al., 2002). The Campeche CWC province shows a similar appearance as it comprises a cluster of individual

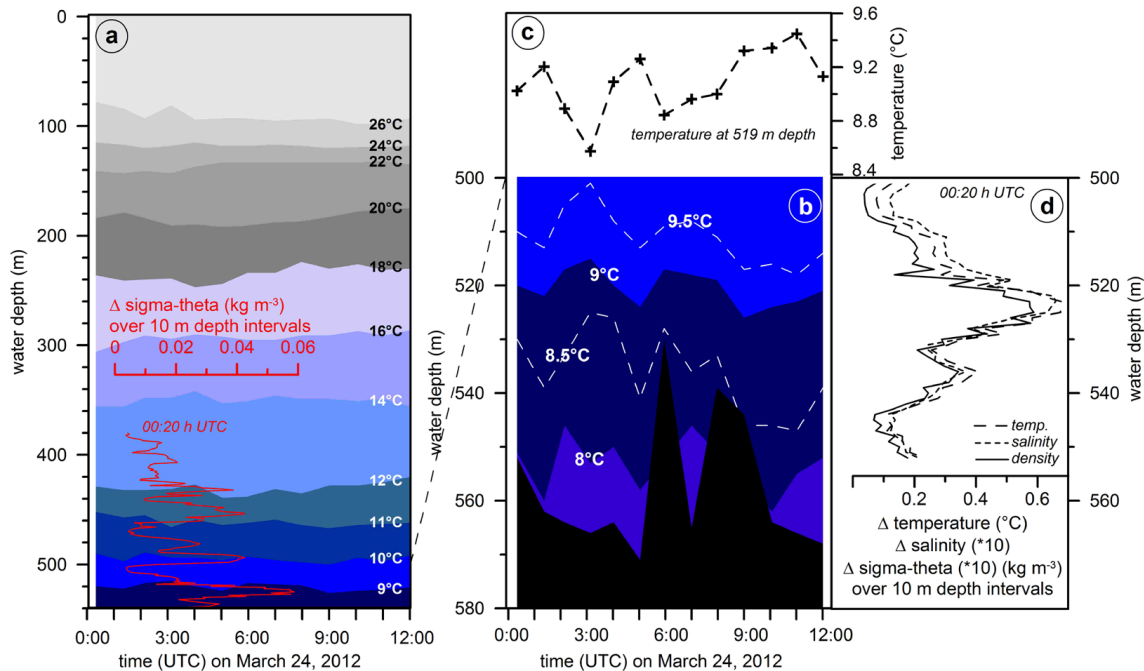


Fig. 6. Hydrological variability derived from the Yoyo CTD station GeoB 16316 (see also Table 1 and Fig. 1). **(a)** Variability of the temperature distribution in the entire water column over a time interval of 12 h (comprising 13 individual CTD casts). The red inset shows the density gradient over 10 m depth intervals for the water column below 380 m taken from CTD cast GeoB 16316-1 (00:20 UTC). **(b)** Depth variation of the 8 °C to 9.5 °C isotherms in the lower part of the water column > 500 m water depth over the same time period shows partly vertical movements of > 20 m. Variations in water depth (black denotes the sea floor) are caused by slight movements of the vessel (~ 600 m N–S, ~ 50 m E–W) at the Yoyo CTD station (including the crossing of a CWC mound). **(c)** Water temperature at 519 m depth measured over the same time period indicates a variability of up to 1 °C. **(d)** Gradients in temperature, salinity, and density over 10 m depth intervals. Data were obtained during the individual CTD cast GeoB 16316-1 (00:20 UTC) and reveal particularly strong gradients around 520 m water depth (see also a).

elongated coral mounds rather than a single clearly confined reef structure. The term “province” is used for the present study to describe the CWC mounds along the Campeche Bank following the nomenclature developed for the Irish margin where numerous individual CWC mounds occur clustered in provinces (e.g., White and Dorschel, 2010). With its mapped area of 10×4 km, and most likely further northwest- and southeastward extensions, the Campeche CWC province is comparable with the large Norwegian reefs and, thus, belongs to the largest mapped CWC provinces in the world. In addition, the Campeche CWC province represents the most important and extensive flourishing azooxanthellate coral area in the entire Gulf of Mexico discovered so far. The geographically closest CWC province is situated along the Miami Terrace in the Straits of Florida, where 27 km² of elongated coral mounds are mapped in detail by an autonomous underwater vehicle (Correa et al., 2012a) in an area where earlier studies have reported occurrences of “muddy mounds” and “sand ridges” (Neumann and Ball, 1970).

Whereas the large Irish coral mounds have been accumulated over > 2 million years (Kano et al., 2007), the Norwegian reefs have been formed only during the last

~ 10 000 years of the Holocene (e.g., López Correa et al., 2012), when during the last deglaciation the Fennoscandian Ice Sheet retreated beyond the present-day coastline. Large seafloor structures formed by CWC cannot easily be transferred into age, as, for example, the Irish mounds at some point in time changed from a distinct accumulation stage into an almost stagnation stage marked by CWC growth and sediment deposition alternating with extensive periods dominated by erosion (Dorschel et al., 2005; Kano et al., 2007; Eisele et al., 2008). Thus, the average height of the Campeche coral mounds of 20 to 40 m does not allow for estimating the onset of coral growth in the region. Nevertheless, their size and the collection of a > 10 m-long sediment core containing abundant coral fragments embedded in a matrix of hemipelagic sediments (Hebbeln et al., 2012) reveal that also the Campeche CWC ecosystem has a relevant, although yet not constrained, history.

This sedimentary record adds to the PARASOUND evidence for a “CWC origin” of these mounds. The coral mounds show little to no internal layering and are often transparent (Fig. 2b), which is a common feature for coral carbonate mounds (e.g., Van Rooij et al., 2003; Savini et al.,

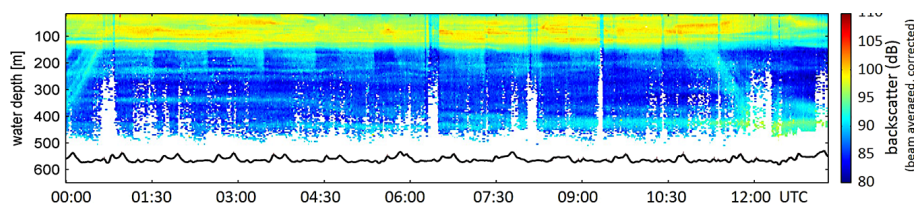


Fig. 7. ADCP-derived backscatter data obtained during a 13 h stationary measurement from 00:00 to 13:00 UTC on 24 March 2012. ADCP data were recorded simultaneously to the Yoyo CTD station GeoB 16316 (see Table 1). This backscatter record shows the upward (0:00–0:30 UTC, local sunset) and downward (11:30–12:00 UTC, local sunrise) migration of the zooplankton. Probably biased data close to the seafloor have been omitted.

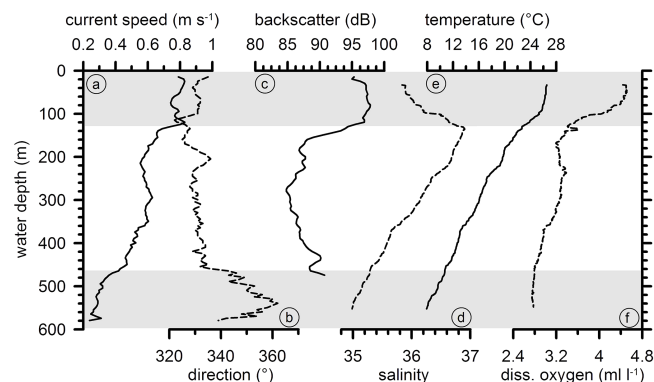


Fig. 8. Water column data for the Yoyo CTD site GeoB 16316. Mean values for (a) current speed, (b) current direction, and (c) backscatter averaged from the 13 h stationary ADCP measurement. CTD data from cast GeoB 16316-1 for (d) salinity, (e) temperature, and (f) dissolved oxygen. The dashed lines refer to the lower x axes. The grey shadings delineate the different layers of the water column as derived from the ADCP data.

2014). The PARASOUND profile crossing the Campeche CWC province from west to east displays a strong reflection underneath the drift sediment bodies and the CWC mounds developed along the Campeche Bank slope (Hübscher et al., 2010). It is assumed that this continuous strong reflector forms the base of the coral mounds (Hübscher et al., 2010) that might have provided the hardground allowing for the initial coral settlement similar to the erosional unconformity forming the base of the Irish CWC mounds (Van Rooij et al., 2003; Kano et al., 2007).

CWC often form coral mounds that can have a variety of shapes, from circular to elongate (Roberts et al., 2009). Elongated mounds often have been related to the presence of an unidirectional bottom current regime, however, with elongated coral mounds sometimes occurring perpendicular (Correa et al., 2012a) and sometimes parallel (Messing et al., 1990) to the main current direction. The elongated coral mounds within the Campeche CWC province appear to be generally aligned parallel to the main current direction possibly following an upstream growth pattern as outlined by Messing et al. (1990). They mostly stretch towards 330° with

some heading towards 300° (with a second-order direction NE–SW; see above). These directions are close to the two main current directions of 330° (above ~ 470 m) and 360° (below ~ 470 m) derived from the ADCP data (Fig. 8) which, however, only represent a snapshot in time. Temporal variations (e.g., lunar, seasonal) below 470 m might result in the different directions of the coral mounds observed. Then, the 30° offset between both current directions and both mound directions observed could speculatively be related to an inherent 30° relationship between coral mound extension and prevailing current direction.

5.1 The Campeche cold-water corals and associated community

The Campeche CWC province is constructed by *Enallopsammia profunda* and to a lesser degree by *Lophelia pertusa*. Neither of the scleractinians have been reported in previous publications from the Campeche slope (e.g., Cairns, 1979; Cairns et al., 1993) but are known from several locations in the Caribbean Sea and northern Gulf of Mexico (see compilations of published and unpublished information by Brooke and Schroeder, 2007; Lutz and Ginsburg, 2007; Messing et al., 2008). While *L. pertusa* has a nearly cosmopolitan distribution, *E. profunda* is endemic to the western Atlantic from the Antilles in the south to off Massachusetts in the north at water depths of 146–1748 m (Cairns, 1979). Structure-forming *Enallopsammia*–*Lophelia* frameworks are known from the base of the Florida–Hatteras slope in 500–800 m water depth and from Miami to South Carolina (Reed, 2002). Correa et al. (2012a) describe an approximately 20 km² field of *Enallopsammia*–*Lophelia* coral mounds at the base of the Miami Terrace, Straits of Florida, at 630–870 m depth, with a denser coral framework on current-facing flanks and summits. The same coral association is present in the CWC mound province at the toe of the Great Bahama Bank (Correa et al., 2012b). Interestingly, on the ROV tracks studied only a low abundance of associated megafauna in the Campeche CWC province was documented. This is in contrast to other scleractinian coral framework habitats in the northern Gulf of Mexico (Lessard-Pilon et al., 2010) or in the eastern North Atlantic (e.g., Henry and Roberts, 2007; Roberts et al., 2006). For instance, with the exception of

Aphrocallistes sp. and a few *Keratoisis* sp., no other large suspension-feeding megabenthos were observed during the three ROV dives. It should be kept in mind that the visually inspected portion of the Campeche coral province is far too small for a solid conclusion at present and further inspections may change this first impression considerably.

Regarding the structure-forming CWC from the Campeche Bank on a wider perspective, this newly found CWC province is located at a key position, namely at the beginning of the Loop Current that passes over the well-known CWC occurrences of Louisiana and west Florida before it becomes the Florida Current flowing through the Straits of Florida. North of the Straits of Florida the Florida Current forms 90 % of the Gulf Stream, passing north along the margins of South Carolina and Georgia, from where also large CWC provinces have been reported (Ross, 2007; Ross and Quattrini, 2007; Messing et al., 2008). South of the Campeche CWC province, *Lophelia* is known from off Brazil, Venezuela and Colombia and was recently mapped off Roatan, Honduras (Reyes et al., 2005; Lutz and Ginsburg, 2007; Arantes et al., 2009; Mangini et al., 2010; Etnoyer et al., 2011), thus following the path of the northward-flowing AAIW that bypasses the Campeche Bank (Merino, 1997). Such an oceanic intermediate water gateway (sensu Henry, 2011) may exert strong control on coral larval dispersal routes as has been documented for *Desmophyllum dianthus* populations in the South Pacific (Miller et al., 2011).

5.2 Environmental control on the Campeche cold-water coral ecosystem

The known ranges of temperature (4–13.9 °C; Roberts et al., 2006; Freiwald et al., 2009), salinity (31.7–38.8; Freiwald et al., 2004; Davies et al., 2008), dissolved oxygen (2.7–7.2 mL L⁻¹; Dodds et al., 2007; Davies et al., 2008; Davies et al., 2010) and other physicochemical parameters defining the ecological niche of *L. pertusa* in the eastern North Atlantic (see summary in Davies et al., 2008) are found in many parts of the world's oceans (Davies and Guinotte, 2011). Water mass properties obtained for the Campeche margin, such as temperature (9.5–7.5 °C) and salinity (35.1–34.9), fit well into these defined thresholds (Fig. 7). The observed content of dissolved oxygen of ~2.7 mL L⁻¹ matches observations from the Viosca Knoll area in the northern Gulf of Mexico, where *Lophelia* colonies currently thrive at the lowest reported oxygen levels of 2.7–2.8 mL L⁻¹ (Davies et al., 2010). It is assumed that these extreme oxygen conditions cause decreased growth rates or even inhibit reproductive processes (Brooke and Young, 2003).

However, despite a suited physicochemical setting, the presence of suitable hardgrounds for the corals to settle on, and even more importantly the availability of sufficient food, is crucial for the establishment and long-lasting development of a vivid CWC ecosystem. In general CWC feed on fresh phytodetritus (Duineveld et al., 2004; Kiriakoulakis et al.,

2005; Duineveld et al., 2007), on zooplankton (Carlier et al., 2009; Dodds et al., 2009) or on a combination of both (Becker et al., 2009; van Oevelen et al., 2009). Recent laboratory studies also revealed the importance of dissolved organic matter which might be actively absorbed by CWC especially during periods when particulate food is scarce (Gori et al., in press). However, independent of the food source, the sessile CWC rely on sufficient food supply, which is based on primary production in the surface waters and the delivery of food particles to the CWC living at intermediate depths. For the latter, various mechanisms were identified to enhance and transport food particles to the CWC, including strong bottom currents, downwelling and cascading, internal tides and waves, and nepheloid layers which act as a pathway for lateral transport (White et al., 2005; Dorschel et al., 2007; Duineveld et al., 2007; Mienis et al., 2007; Davies et al., 2009; Orejas et al., 2009). On the local to regional scale, topography also influences hydrodynamic processes, as, e.g., internal waves, down- or upwelling. Thus, for any given location it is the interplay of all these factors allowing for or prohibiting the presence of CWC.

For the Campeche CWC province, the provision of food to the CWC appears to be almost optimal, and therefore the observed paucity of the coral-associated megafauna remains to be explained. Primary productivity in the surface waters is high (up to ~1 mg Chl *a* m⁻³; Fig. 1) due to the local upwelling center that is located just above the Campeche CWC province (Merino, 1997). Current meter data from the Yucatan Strait (Sheinbaum et al., 2002) as well as the ADCP data collected during cruise MSM 20-4 reveal reasonably strong bottom currents with average velocities of ~30 cm s⁻¹ between 500 and 600 m water depth (Fig. 8). These numbers are in line with in situ current measurements at other CWC sites indicating maximum velocities of > 50 cm s⁻¹ (Dorschel et al., 2007; Mienis et al., 2007), whereas average current velocities can be as low as 8 cm s⁻¹ (Mienis et al., 2007).

Furthermore, the strong density gradient undulating around 520 m (Fig. 6d) might act as a decelerator for sinking (food) particles, thereby prolonging their residence time within the reach of the CWC and, thus, enhancing the probability of these particles to be caught by the corals. With salinities varying around 35, this density gradient possibly marks the upper limit of the core of the AAIW. A similar mechanism has been suggested to support the CWC off Ireland, there benefitting from the density gradient developed at the upper limit of the Mediterranean Outflow Water (White and Dorschel, 2010). For the northeastern North Atlantic, Dullo et al. (2008) described a narrow potential density envelope of sigma-theta (σ_θ) = 27.35–27.65 kg m⁻³ preferred by the CWC. Along the Campeche Bank the density of the water masses surrounding the CWC is slightly lower, at 27.18–27.29 kg m⁻³, and, thus, close to data reported from the Viosca Knoll area (27.1–27.2 kg m⁻³) (Davies et al., 2010). In contrast, living CWC settings in the Mediterranean Sea are

associated with much higher densities of $> 29 \text{ kg m}^{-3}$. Thus, if applicable, the concept of a narrow density envelope defining the overall habitat range of the CWC as suggested by Dullo et al. (2008) needs to be regionalized (see also Flögel et al., in press). However, the obvious steep gradient in density (Fig. 6d) seems to be a sensitive indicator for living CWC reef communities.

As indicated by the undulating isotherms (Fig. 6), the temporal variability of the local hydrographic setting, which might reflect the presence of internal waves, literally might pump the food particles through the CWC ecosystem, especially those particles temporarily accumulating along the strong density gradient, as suggested by Mienis et al. (2012). Over the observed 13 h, the depth range covered by the fluctuating maximum near-bottom density gradient aligns with the upper range of observed living CWC in $\sim 515\text{--}530 \text{ m}$ water depth. Assuming a larger variability associated with monthly (i.e., lunar) to seasonal forcing, one may speculate that the entire depth range of living CWC off the Campeche Bank might intermittently be affected by such a pumping process. Due to the limited length of the 13 h of observation no tidal signal providing additional energy to the bottom current regime could have been clearly detected. However, along the mooring transect across the Yucatan Strait mentioned before (Sheinbaum et al., 2002), a comparably high amplitude of the major axis of the dominant diurnal O_1 tide was observed exactly in the depth range of the Campeche CWC province (Carrillo González et al., 2007).

The ADCP data also point to another possible food source for the corals. The strong upward-rising backscatter signal at dusk and the down-going signal at dawn (Fig. 7) are indicative of the diel vertical migration of zooplankton (Heywood, 1996). According to the backscatter data shown in Fig. 7 the migrating zooplankton spend the day at depths of $> 300 \text{ m}$, with any deeper-reaching migration being obscured by bottom interferences of the backscatter signal. In case the zooplankton actively descend to the depths of the CWC, it might serve as an additional process enhancing the delivery of food to the CWC. The depth range of the Campeche CWC is often reached by migrating zooplankton. For instance, off the California coast, a depth of $\sim 560 \text{ m}$ has been shown to be a preferred depth of the zooplankton at which to spend the daytime (Plüddemann and Pinkel, 1989). The potential of daily migrating zooplankton as an additional food source for the CWC has also been put forward by Mienis et al. (2012) based on ADCP observations in the Viosca Knoll area in the northern Gulf of Mexico.

6 Conclusions

The Campeche CWC province is one of the largest coherent CWC areas discovered so far, and the most relevant in the western Atlantic Ocean. A healthy and highly diverse CWC ecosystem is developed on top of a complex system

of 20–40 m-high, partly interconnected elongated mounds, which probably can serve as a paleoenvironmental archive enabling the reconstruction of the long-term development of the Campeche CWC province over the Late Quaternary climatic cycles.

The location of the Campeche CWC province appears to be almost perfect for the establishment of such a large CWC ecosystem. It is (a) located underneath a local upwelling center providing high primary production, (b) influenced by a very dynamic bottom current regime delivering food particles to the corals, and (c) characterized by a physicochemical setting that fits the recognized ecological needs of *L. pertusa*. The observed diel vertical migration of zooplankton possibly reaching the intermediate depth of the CWC ecosystem may even serve as a supplemental food source as already indicated by Mienis et al. (2012). These observations fits several paleoenvironmental studies, highlighting the controlling role of the food supply on the long-term development of such ecosystems (Dorschel et al., 2005; Wienberg et al., 2010; Eisele et al., 2011; Fink et al., 2013).

In many places in the world's oceans the physicochemical setting comply with the niche requirements of *L. pertusa* and other CWC (Davies and Guinotte, 2011); however, only in some of these places have CWC ecosystems developed. Thus, the Campeche CWC province appears to be an excellent example showing that food supply – controlled by a variety of mechanisms – plays a major role in the development of CWC ecosystems.

Acknowledgements. The research leading to these results has received support from the Deutsche Forschungsgemeinschaft (DFG) through funding of the WACOM – West Atlantic Cold-water Coral Ecosystems projects, grants HE 3412/17-1 and DU 129/47-1, and through providing ship time. We thank the officers and crew of the R/V *Maria S. Merian*, the MARUM ROV *Cherokee* team, and the scientific crew for on-board assistance during cruise MSM 20-4 (2012). The cruise was further supported through the DFG Research Center/Cluster of Excellence “MARUM – The Ocean in the Earth System”. We are grateful to the Mexican Government for providing access to conduct scientific work in Mexican waters. A. Freiwald received funds from the Hessian LOEWE BiK-F Project A3.10, and G. P. Eberli acknowledges the donors of the American Chemical Society Petroleum Research Fund (grant no. 49017-ND8) for partial support of this research and the industrial associates of the CSL – Center for Carbonate Research at the University of Miami for additional funding. L. Matos has been supported by the FCT scholarship SFRH/BD/72149/2010. This is ISMAR-CNR Bologna scientific contribution no. 1801. This study contributes to the international research program TRACES – Trans-Atlantic Coral Ecosystem Study.

Edited by: J. Bijma

References

- Arantes, R. C. M., Castro, C. B., Pires, D. O., and Seoane, J. C. S.: Depth and water mass zonation and species associations of cold-water octocoral and stony coral communities in the southwestern Atlantic, *Mar. Ecol.-Prog. Ser.*, 397, 71–79, 2009.
- Becker, E. L., Cordes, E. E., Macko, S. A., and Fisher, C. R.: Importance of seep primary production to *Lophelia pertusa* and associated fauna in the Gulf of Mexico, *Deep-Sea Res. Pt. I*, 56, 786–800, 2009.
- Brooke, S. and Schroeder, W. W.: State of the U.S. deep coral ecosystems in the northern Gulf of Mexico region: Florida Straits to Texas, in: *The State of Deep Coral Ecosystems of the United States*, edited by: Lumsden, S. E., Hourigan, T. F., and Bruckner, A. W., NOAA Technical Memorandum CRCP-3, Silver Spring MD, 271–306, 2007.
- Brooke, S. and Young, C. M.: Reproductive ecology of a deep-water scleractinian coral, *Oculina varicosa*, from the southeast Florida shelf, *Cont. Shelf Res.*, 23, 847–858, 2003.
- Brooke, S. D., Holmes, M. W., and Young, C. M.: Sediment tolerance of two different morphotypes of the deep-sea coral *Lophelia pertusa* from the Gulf of Mexico, *Mar. Ecol.-Prog. Ser.*, 390, 137–144, 2009.
- Buhl-Mortensen, L. and Mortensen, P. B.: Symbiosis in deep-water corals, *Symbiosis*, 37, 33–61, 2004.
- Cairns, S. D.: The Deep-Water Scleractinia of the Caribbean Sea and Adjacent Waters, *Studies on the Fauna of Curaçao and Other Caribbean Islands*, 57, 341 pp., 1979.
- Cairns, S. D., Opresko, D. M., Hopkins, T. S., and Schroeder, W. W.: New records of deep-water Cnidaria (Scleractinia and Antipatharia) from the Gulf of Mexico, *Northeast Gulf Science*, 13, 1–11, 1993.
- Caress, D. W. and Chayes, D. N.: Improved processing of Hydrosweep DS Multibeam Data on the R/V MAURICE EWING, *Geophys. Res.*, 18, 631–650, 1996.
- Carlier, A., Le Guilloux, E., Olu-Le Roy, K., Sarrazin, J., Mas-trototaro, F., Taviani, M., and Clavier, J.: Trophic relationships in a deep Mediterranean cold-water coral bank (Santa Maria di Leuca, Ionian Sea), *Mar. Ecol.-Prog. Ser.*, 397, 125–137, 2009.
- Carrillo González, F., Ochoa, J., Candela, J., Badan, A., Sheinbaum, J., and González Navarro, J. I.: Tidal currents in the Yucatan Channel, *Geof. Int.*, 46, 199–209, 2007.
- Caruso, J. H., Ross, S. W., Sulak, K. J., and Sedberry, G. R.: Deep-water chaunacid and lophiid anglerfishes (Pisces: Lophiiformes) off the south-eastern United States, *J. Fish Biol.*, 70, 1015–1026, 2007.
- Colman, J. G., Gordaon, D. M., Lane, A. P., Forde, M. J., and Fitzpatrick, J.: Carbonate mounds off Mauritania, Northwest Africa: status of deep-water corals and implications for management of fishing and oil exploration activities, in: *Cold-water Corals and Ecosystems*, edited by: Freiwald, A., and Roberts, J. M., Springer, Berlin-Heidelberg, 417–441, 2005.
- Cordes, E. E., McGinley, M. P., Podowski, E. L., Becker, E. L., Lessard-Pilon, S., Viada, S. T., and Fisher, C. R.: Coral communities of the deep Gulf of Mexico, *Deep-Sea Res. Pt. I*, 55, 777–787, 2008.
- Correa, T. B. S., Eberli, G. P., Grasmueck, M., Reed, J. K., and Correa, A. M. S.: Genesis and morphology of cold-water coral ridges in a unidirectional current regime, *Mar. Geol.*, 326–328, 14–27, 2012a.
- Correa, T. B. S., Grasmueck, M., Eberli, G. P., Reed, J. K., Verwer, K., and Purkis, S. A. M.: Variability of cold-water coral mounds in a high sediment input and tidal current regime, *Straits of Florida, Sedimentology*, 59, 1278–1304, 2012b.
- Davies, A. J. and Guinotte, J. M.: Global habitat suitability for framework-forming cold-water corals, *Plos One*, 6, e18483, doi:10.1371/journal.pone.0018483, 2011.
- Davies, A. J., Wisshak, M., Orr, J. C., and Roberts, J. M.: Predicting suitable habitat for the cold-water coral *Lophelia pertusa* (Scleractinia), *Deep-Sea Res. Pt. I*, 55, 1048–1062, 2008.
- Davies, A. J., Duineveld, G., Lavaleye, M., Bergman, M. J., van Haren, H., and Roberts, J. M.: Downwelling and deep-water bottom currents as food supply mechanisms to the cold-water coral *Lophelia pertusa* (Scleractinia) at the Mingulay Reef Complex, *Limnol. Oceanogr.*, 54, 620–629, doi:10.4319/lo.2009.54.2.0620, 2009.
- Davies, A. J., Duineveld, G. C. A., van Weering, T. C. E., Mienis, F., Quattrini, A. M., Seim, H. E., Bane, J. M., and Ross, S. W.: Short-term environmental variability in cold-water coral habitat at Viosca Knoll, Gulf of Mexico, *Deep-Sea Res. Pt. I*, 57, 199–212, 2010.
- Deines, K. L.: Backscatter estimation using broadband acoustic Doppler current profilers, *Proceedings of the Sixth Working Conference on Current Measurement*, San Diego, CA, IEEE, 249–253, 1999.
- Dodds, L. A., Roberts, J. M., Taylor, A. C., and Marubini, F.: Metabolic tolerance of the cold-water coral *Lophelia pertusa* (Scleractinia) to temperature and dissolved oxygen change, *J. Experim. Mar. Biol. Ecol.*, 349, 205–214, 2007.
- Dodds, L. A., Black, K. D., Orr, H., and Roberts, J. M.: Lipid biomarkers reveal geographical differences in food supply to the cold-water coral *Lophelia pertusa* (Scleractinia), *Mar. Ecol.-Prog. Ser.*, 397, 113–124, 2009.
- Dorschel, B., Hebbeln, D., Rüggeberg, A., and Dullo, W.-C.: Growth and erosion of a cold-water coral covered carbonate mound in the Northeast Atlantic during the Late Pleistocene and Holocene, *Earth Planet. Sci. Lett.*, 233, 33–44, 2005.
- Dorschel, B., Hebbeln, D., Foubert, A., White, M., and Wheeler, A. J.: Hydrodynamics and cold-water coral facies distribution related to recent sedimentary processes at Galway Mound west of Ireland, *Mar. Geol.*, 244, 184–195, 2007.
- Dorschel, B., Wheeler, A., Monteys, X., and Verbruggen, K.: Atlas of the Deep-Water Seabed: Ireland, Springer, 164 pp., 2010.
- Douarin, M., Elliot, M., Noble, S. R., Sinclair, D., Henry, L.-A., Long, D., Moreton, S. G., and Murray Roberts, J.: Growth of north-east Atlantic cold-water coral reefs and mounds during the Holocene: A high resolution U-series and 14C chronology, *Earth Planet. Sci. Lett.*, 375, 176–187, 2013.
- Duineveld, G. C. A., Lavaleye, M. S. S., and Berghuis, E. M.: Particle flux and food supply to a seamount cold-water coral community (Galicia Bank, NW Spain), *Mar. Ecol.-Prog. Ser.*, 277, 13–23, 2004.
- Duineveld, G. C. A., Lavaleye, M. S. S., Bergman, M. J. N., De Stigter, H., and Mienis, F.: Trophic structure of a cold-water coral mound community (Rockall Bank, NE Atlantic) in relation to the near-bottom particle supply and current regime, *B. Mar. Sci.*, 81, 449–467, 2007.
- Dullo, W.-C., Flögel, S., and Rüggeberg, A.: Cold-water coral growth in relation to the hydrography of the Celtic and Nordic

- European continental margin, *Mar. Ecol.-Prog. Ser.*, 371, 165–176, 2008.
- Duncan, P. M.: A description of the Madreporaria dredged up during the expeditions of HMS Porcupine in 1869 and 1870. Part I, *Trans. Zool. Soc. London*, 8, 303–344, 1873.
- Eisele, M., Hebbeln, D., and Wienberg, C.: Growth history of a cold-water coral covered carbonate mound – Galway Mound, Porcupine Seabight, NE-Atlantic, *Mar. Geol.*, 253, 160–169, 2008.
- Eisele, M., Frank, N., Wienberg, C., Hebbeln, D., López Correa, M., Douville, E., and Freiwald, A.: Productivity controlled cold-water coral growth periods during the last glacial off Mauritania, *Mar. Geol.*, 280, 143–149, 2011.
- Etnoyer, P., Shirley, T., and Lavelle, K. A.: Deep coral and associated species taxonomy and ecology (DeepCAST) II expedition report, NOAA Technical Memorandum. NOAA/NOS Center for Coastal Environmental Health and Biomolecular Research, Charleston, 1–42, 2011.
- Fink, H. G., Wienberg, C., Hebbeln, D., McGregor, H. V., Schmiedel, G., Taviani, M., and Freiwald, A.: Oxygen control on Holocene cold-water coral development in the eastern Mediterranean Sea, *Deep-Sea Res. Pt. I*, 62, 89–96, 2012.
- Fink, H. G., Wienberg, C., De Pol-Holz, R., Wintersteller, P., and Hebbeln, D.: Cold-water coral growth in the Alboran Sea related to high productivity during the Late Pleistocene and Holocene, *Mar. Geol.*, 339, 71–82, 2013.
- Flögel, S., Dullo, W. C., Pfannkuche, O., Kiriakoulakis, K., and Rüggeberg, A.: Geochemical and physical constraints for the occurrence of living cold-water corals, *Deep-Sea Res. Pt. II*, 99, 19–26, 2014.
- Fosså, J. H., Lindberg, B., Christensen, O., Lundälv, T., Svellingen, I., Mortensen, P. B., and Alsvag, J.: Mapping of *Lophelia* reefs in Norway: experiences and survey methods, in: *Cold-water Corals and Ecosystems*, edited by: Freiwald, A., and Roberts, J. M., Springer, Berlin-Heidelberg, 359–391, 2005.
- Frank, N., Ricard, E., Lutringer-Paquet, A., van der Land, C., Colin, C., Blamart, D., Foubert, A., Van Rooij, D., Henriot, J.-P., de Haas, H., and van Weering, T.: The Holocene occurrence of cold water corals in the NE Atlantic: Implications for coral carbonate mound evolution, *Mar. Geol.*, 266, 129–142, 2009.
- Freiwald, A. and Roberts, J. M.: *Cold-water Corals and Ecosystems*, Springer, Berlin-Heidelberg, 1243 pp., 2005.
- Freiwald, A., Hühnerbach, V., Lindberg, B., Wilson, J. B., and Campbell, J.: The Sula Reef Complex, Norwegian Shelf, *Facies*, 47, 179–200, 2002.
- Freiwald, A., Fosså, J. H., Grehan, A., Koslow, T., and Roberts, J. M.: *Cold-water Coral Reefs*, UNEP-WCMC, Cambridge, UK, Biodiversity Series 22, 84 pp., 2004.
- Freiwald, A., Beuck, L., Rüggeberg, A., Taviani, M., Hebbeln, D., and R/V Meteor Cruise M70-1 participants: The white coral community in the central Mediterranean Sea revealed by ROV surveys, *Oceanography*, 22, 58–74, 2009.
- Gori, A., Orejas, C., Madurell, T., Bramanti, L., Martins, M., Quintanilla, E., Marti-Puig, P., Lo Iacono, C., Puig, P., Requena, S., Greenacre, M., and Gili, J. M.: Bathymetrical distribution and size structure of cold-water coral populations in the Cap de Creus and Lacaze-Duthiers canyons (northwestern Mediterranean), *Biogeosciences*, 10, 2049–2060, doi:10.5194/bg-10-2049-2013, 2013.
- Gori, A., Grover, R., Orejas, C., Sikorski, S., and Ferrier-Pagès, C.: Uptake of dissolved free amino acids by four cold-water coral species from the Mediterranean Sea, *Deep-Sea Res. Pt. II*, 99, 42–50, 2014.
- Grasmueck, M., Eberli, G. P., Viggiano, D. A., Correa, T., Rathwell, G., and Luo, J.: Autonomous underwater vehicle (AUV) mapping reveals coral mound distribution, morphology, and oceanography in deep water of the Straits of Florida, *Geophys. Res. Lett.*, 33, L23616, doi:10.1029/2006GL027734, 2006.
- Hebbeln, D., Wienberg, C., and cruise participants: Report and preliminary results of R/V MARIA S. MERIAN cruise MSM20-4, WACOM – West-Atlantic Cold-water Coral Ecosystems: The West Side Story, Bridgetown – Freeport, 14 March–7 April 2012, University of Bremen, 120 pp., 2012.
- Henry, L. A.: A deep-sea coral “gateway” in the Northwestern Caribbean, in: *Too precious to drill: The marine biodiversity of Belize*, edited by: Palomares, M. L. D. and Pauly, D., Fisheries Centre Research Reports, 120–124, 2011.
- Henry, L. A. and Roberts, J. M.: Biodiversity and ecological composition of macrobenthos on cold-water coral mounds and adjacent off-mound habitat in the bathyal Porcupine Seabight, NE Atlantic, *Deep Sea Res. Part I*, 54, 654–672, 2007.
- Heywood, V. H.: The Global Biodiversity Assessment, *The Globe*, 30, 2–4, 1996.
- Hübscher, C., Dullo, W. C., Flögel, S., Titschack, J., and Schönfeld, J.: Contourite drift evolution and related coral growth in the eastern Gulf of Mexico and its gateways, *Int. J. Earth Sci.*, 99, S191–S206, 2010.
- Kano, A., Ferdelman, T. G., Williams, T., Henriot, J.-P., Ishikawa, T., Kawagoe, N., Takashima, C., Kakizaki, Y., Abe, K., Sakai, S., Browning, E. L., Li, X., and Integrated Ocean Drilling Program Expedition 307 Scientists: Age constraints on the origin and growth history of a deep-water coral mound in the northeast Atlantic drilled during Integrated Ocean Drilling Program Expedition 307, *Geology*, 35, 1051–1054, 2007.
- Kenyon, N. H., Akhmetzhanov, A. M., Wheeler, A. J., van Weering, T. C. E., de Haas, H., and Ivanov, M. K.: Giant carbonate mud mounds in the southern Rockall Trough, *Mar. Geol.*, 195, 5–30, 2003.
- Kiriakoulakis, K., Harper, E., and Wolff, G. A.: Lipids and nitrogen isotopes of two deep-water corals from the North-East Atlantic: initial results and implications for their nutrition, in: *Cold-water Corals and Ecosystems*, edited by: Freiwald, A., and Roberts, J. M., Springer, Berlin-Heidelberg, 715–729, 2005.
- Le Guilloux, E., Olu-Le Roy, K., Bourillet, J. F., Savoye, B., Iglésias, S. P., and Sibuet, M.: First observations of deep-sea coral reefs along the Angola margin, *Deep-Sea Res. Pt. II*, 56, 2394–2403, 2009.
- Lessard-Pilon, S., Podowski, E. L., Cordes, E. E., and Fisher, C. R.: Megafauna community composition associated with *Lophelia pertusa* colonies in the Gulf of Mexico, *Deep-Sea Res. Part II*, 57, 1882–1890, 2010.
- López Correa, M., Montagna, P., Joseph, N., Rüggeberg, A., Fietzke, J., Flögel, S., Dorschel, B., Goldstein, S. L., Wheeler, A., and Freiwald, A.: Preboreal onset of cold-water coral growth beyond the Arctic Circle revealed by coupled radiocarbon and U-series dating and neodymium isotopes, *Quat. Sci. Rev.*, 34, 24–43, 2012.

- Lutz, S. J. and Ginsburg, R. N.: State of the U.S. deep coral ecosystems in the United States Caribbean region: Puerto Rico and U.S. Virgin Islands, in: The State of Deep Coral Ecosystems of the United States, edited by: Lumsden, S. E., Hourigan, T. F., and Bruckner, A. W., NOAA Technical Memorandum CRCP-3, Silver Spring MD, 307–365, 2007.
- Mah, C., Nizinski, M., and Lundsten, L.: Phylogenetic revision of the Hippasterinae (Goniasteridae; Asteroidea): systematics of deep sea corallivores, including one new genus and three new species, *Zool. J. Linnean Soc.*, 160, 266–301, 2010.
- Mangini, A., Godoy, J. M., Godoy, M. L., Kowmann, R., Santos, G. M., Ruckelshausen, M., Schroeder-Ritzrau, A., and Wacker, L.: Deep sea corals off Brazil verify a poorly ventilated Southern Pacific Ocean during H2, H1 and the Younger Dryas, *Earth Planet. Sci. Lett.*, 293, 269–276, 2010.
- Merino, M.: Upwelling on the Yucatan Shelf: hydrographic evidence, *J. Marine Syst.*, 13, 101–121, 1997.
- Messing, C. G., Neumann, A. C., and Lang, J. C.: Biozonation of deep-water lithoherms and associated hardgrounds in the north-eastern Straits of Florida, *Palaeo*, 5, 15–33, 1990.
- Messing, C. G., Reed, J. K., Brooke, S. D., and Ross, S. W.: Deep-Water Coral Reefs of the United States, in: Coral Reefs of the USA, edited by: Riegl, B. and Dodge, R. E., Springer, 763–787, 2008.
- Mienis, F., de Stigter, H. C., White, M., Duineveld, G., de Haas, H., and van Weering, T. C. E.: Hydrodynamic controls on cold-water coral growth and carbonate-mound development at the SW and SE Rockall Trough Margin, NE Atlantic Ocean, *Deep-Sea Res. Pt. I*, 54, 1655–1674, 2007.
- Mienis, F., Duineveld, G. C. A., Davies, A. J., Ross, S. W., Seim, H., Bane, J., and Van Weering, T. C. E.: The influence of near-bed hydrodynamic conditions on cold-water corals in the Viosca Knoll area, Gulf of Mexico, *Deep-Sea Res. Pt. I*, 60, 32–45, 2012.
- Miller, K. J., Rowden, A. A., Williams, A., and Häussermann, V.: Out of their depth? Isolated deep populations of the cosmopolitan coral *Desmophyllum dianthus* may be highly vulnerable to environmental change, *Plos One*, 6, e19004, doi:10.1371/journal.pone.0019004, 2011.
- Molinari, R. L. and Morrison, J.: The separation of the Yucatan Current from the Campeche Bank and the intrusion of the Loop Current into the Gulf of Mexico, *J. Geophysic. Res.*, 93, 10645–10654, 1988.
- Moore, D. R. and Bullis, H. R.: A deep-water coral reef in the Gulf of Mexico, *Bull. Mar. Sci. Gulf Caribbean*, 10, 125–128, 1960.
- Moseley, H. N.: Report on certain hydroid, alcyonarian, and madreporarian corals procured during the voyage of H.M.S. Challenger, in the years 1873–1876. Report of Scientific Research of H.M.S. Challenger, *Zoology*, 2, 1–248, 1881.
- Mueller, C. E., Lundälv, T., Middelburg, J. J., and Van Oevelen, D.: The symbiosis between *Lophelia pertusa* and *Eunice norvegica* stimulates coral calcification and worm assimilation, *Plos One*, 8, e58660, doi:10.1371/journal.pone.0058660, 2013.
- Müller-Karger, F. E., Walsh, J. J., Evans, R. H., and Meyers, M. B.: On the seasonal phytoplankton concentration and sea surface temperature cycles of the Gulf of Mexico as determined by satellites, *J. Geophysic. Res.*, 96, 12645–12665, 1991.
- Mullins, H. T., Newton, C. R., Heath, K., and Vanburen, H. M.: Modern deep-water coral mounds north of Little Bahama Bank: criteria for recognition of deep-water coral bioherms in the rock record, *J. Sed. Petrol.*, 51, 999–1013, 1981.
- Neumann, A. C. and Ball, M. M.: Submersible observations in Straits of Florida – geology and bottom currents, *Geol. Soc. Americ. Bull.*, 81, 2861–2873, 1970.
- Neumann, A. C., Kofoed, J. W., and Keller, G. H.: Lithoherms in the Straits of Florida, *Geology*, 5, 4–10, 1977.
- Newton, C. R., Mullins, H. T., and Gardulski, A. F.: Coral mounds on the West Florida Slope: unanswered questions regarding the development of deepwater banks, *Palaeo*, 2, 359–367, 1987.
- Orejas, C., Gori, A., Lo Iacono, C., Puig, P., Gili, J. M., and Dale, M. R.: Cold-water corals in the Cap de Creus canyon (north-western Mediterranean): spatial distribution, density and anthropogenic impact, *Mar. Ecol.-Prog. Ser.*, 397, 37–51, 2009.
- Paull, C. K., Neumann, A. C., am Ende, B. A., Ussler III, W., and Rodriguez, N. M.: Lithoherms on the Florida–Hatteras slope, *Mar. Geol.*, 166, 83–101, 2010.
- Plüddemann, A. J., and Pinkel, R.: Characterization of the patterns of diel migration using a doppler sonar, *Deep-Sea Res.*, 36, 509–530, 1989.
- Reed, J. K.: Comparison of deep-water coral reefs and lithoherms off southeastern USA, *Hydrobiol.*, 471, 57–60, 2002.
- Reed, J. K., Weaver, D., and Pomponi, S. A.: Habitat and fauna of deep-water *Lophelia pertusa* coral reefs off the Southeastern USA: Blake Plateau, Straits of Florida, and Gulf of Mexico, *B. Mar. Sci.*, 78, 343–375, 2006.
- Reyes, J., Santodomingo, N., Gracia, A., Borrero-Pérez, G., Navas, G., Mejía-Ladino, L. M., Bermudéz, A., and Benavidos, M.: Southern Caribbean azooxanthellate coral communities off Colombia, in: Cold-water Corals and Ecosystems, edited by: Freiwald, A., and Roberts, J. M., Springer, Berlin-Heidelberg, 309–330, 2005.
- Roberts, J. M., Wheeler, A. J., and Freiwald, A.: Reefs of the deep: The biology and geology of cold-water coral ecosystems, *Science*, 312, 543–547, 2006.
- Roberts, J. M., Wheeler, A. J., Freiwald, A., and Cairns, S. D.: Cold-water corals. The biology and geology of deep-sea coral habitats, Cambridge University Press, 336 pp., 2009.
- Ross, S. W.: Unique deep-water ecosystems off the southeastern United States, *Oceanography*, 20, 130–139, 2007.
- Ross, S. W. and Nizinski, M. S.: State of the U.S. deep coral ecosystems in the southeastern United States region: Cape Hatteras to the Florida Straits, in: The State of Deep Coral Ecosystems of the United States, edited by: Lumsden, S. E., Hourigan, T. F., and Bruckner, A. W., NOAA Technical Memorandum CRCP-3, Silver Spring MD, 233–270, 2007.
- Ross, S. W. and Quattrini, A. M.: The fish fauna associated with deep coral banks off the southeastern United States, *Deep-Sea Res. Pt. I*, 54, 975–1007, 2007.
- Sanamyan, N. P., Sanamyan, K. E., and Tabachnick, K. R.: The first species of Actiniaria, *Spongiactis japonica* gen.n., sp.n. (Cnidaria: Anthozoa), an obligate symbiont of a glass sponge, *Invert. Zool.*, 9, 127–141, 2012.
- Savini, A., Vertino, A., Marchese, F., Beuck, L., and Freiwald, A.: Mapping Cold-Water Coral Habitats at Different Scales within the Northern Ionian Sea (Central Mediterranean): An Assessment of Coral Coverage and Associated Vulnerability, *PLoS ONE*, 9, e87108, doi:10.1371/journal.pone.0087108, 2014.

- Schroeder, W. W.: Observations of *Lophelia pertusa* and the surficial geology at a deep-water site in the northeastern Gulf of Mexico, *Hydrobiol.*, 471, 29–33, 2002.
- Schroeder, W. W., Brooke, S. D., Olson, J. B., Phaneuf, B., McDonough, J. J., and Etnoyer, P.: Occurrence of deep-water *Lophelia pertusa* and *Madrepora oculata* in the Gulf of Mexico, in: *Cold-water Corals and Ecosystems*, edited by: Freiwald, A. and Roberts, J. M., Springer, Berlin-Heidelberg, 297–307, 2005.
- Schulkin, M. and Marsh, H. W.: Sound absorption in seawater, *J. Acoust. Soc. Am.*, 34, 864–865, 1962.
- Sheinbaum, J., Candela, J., Badan, A., and Ochoa, J.: Flow structure and transport in the Yucatan Channel, *Geophys. Res. Lett.*, 29, 1040, doi:10.1029/2001GL013990, 2002.
- Stevenson, A. and Rocha, C.: Evidence for the bioerosion of deep-water corals by echinoids in the Northeast Atlantic, *Deep-Sea Res. Pt. I*, 71, 73–78, 2013.
- Taviani, M., Angeletti, L., Dimech, M., Mifsud, C., Freiwald, A., Harasewych, M. G., and Oliverio, M.: Coralliophilinae (Gastropoda: Muricidae) associated with deep-water coral banks in the Mediterranean, *The Nautilus*, 123, 106–112, 2009.
- Thierens, M., Browning, E., Pirlet, H., Loutre, M. F., Dorschel, B., Huvenne, V. A. I., Titschack, J., Colin, C., Foubert, A., and Wheeler, A. J.: Cold-water coral carbonate mounds as unique palaeo-archives: the Plio-Pleistocene Challenger Mound record (NE Atlantic), *Quaternary Sci. Rev.*, 73, 14–30, 2013.
- Titschack, J., Thierens, M., Dorschel, B., Schulbert, C., Freiwald, A., Kano, A., Takashima, C., Kawagoe, N., and Li, X.: Carbonate budget of a cold-water coral mound (Challenger Mound, IODP Exp. 307), *Mar. Geol.*, 259, 36–46, 2009.
- van Oevelen, D., Duineveld, G., Lavaleye, M., Mienis, F., Soetaert, K., and Heip, C. H. R.: The cold-water coral community as a hot spot for carbon cycling on continental margins: A food-web analysis from Rockall Bank (northeast Atlantic), *Limnol. Oceanogr.*, 54, 1829–1844, 2009.
- Van Rooij, D., De Mol, B., Huvenne, V., Ivanov, M., and Henriët, J. P.: Seismic evidence of current-controlled sedimentation in the Belgica mound province, upper Porcupine slope, southwest of Ireland, *Mar. Geol.*, 195, 31–53, 2003.
- Wawrik, B. and Paul, J. H.: Phytoplankton community structure and productivity along the axis of the Mississippi River Plume in oligotrophic Gulf of Mexico waters, *Aqua. Microb. Ecol.*, 35, 185–196, 2004.
- Wei, C. L., Rowe, G. T., Escobar-Briones, E., Nunnally, C., Solomon, Y., and Ellis, N.: Standing stocks and body size of deep-sea macrofauna: Predicting the baseline of 2010 Deepwater Horizon oil spill in the northern Gulf of Mexico, *Deep-Sea Res. Pt. I*, 69, 82–99, 2012.
- Wessel, P. and Smith, W. H. F.: New, improved version of Generic Mapping Tools released, *EOS*, 79, p. 579, doi:10.1029/98EO00426, 1998.
- White, M. and Dorschel, B.: The importance of the permanent thermocline to the cold water coral carbonate mound distribution in the NE Atlantic, *Earth Planet. Sci. Lett.*, 296, 395–402, 2010.
- White, M., Mohn, C., de Stigter, H., and Mottram, G.: Deep-water coral development as a function of hydrodynamics and surface productivity around the submarine banks of the Rockall Trough, NE Atlantic, in: *Cold-Water Corals and Ecosystems*, edited by: Freiwald, A. and Roberts, J. M., Springer, Berlin-Heidelberg, 503–514, 2005.
- Wienberg, C., Hebbeln, D., Fink, H. G., Mienis, F., Dorschel, B., Vertino, A., López Correa, M., and Freiwald, A.: Scleractinian cold-water corals in the Gulf of Cádiz – first clues about their spatial and temporal distribution, *Deep-Sea Res. Pt. I*, 56, 1873–1893, 2009.
- Wienberg, C., Frank, N., Mertens, K. N., Stuut, J.-B., Marchant, M., Fietzke, J., Mienis, F., and Hebbeln, D.: Glacial cold-water coral growth in the Gulf of Cádiz: Implications of increased palaeo-productivity, *Earth Planet. Sci. Lett.*, 298, 405–416, 2010.
- Zavala-Hidalgo, J., Gallegos-García, A., Martínez-López, B., Morey, S. L., and O'Brien, J. J.: Seasonal upwelling on the Western and Southern Shelves of the Gulf of Mexico, *Ocean Dynam.*, 56, 333–338, 2006.

Profile: A committed Diploma-Geologist with best achievements in main ocean studies: paleoceanography, coastal geology and sedimentology. Also a proven assistant manager, an excellent communicator and teacher (education). As well as being highly motivated, creative with strong administrative, analytical and structural skills.

Name: Silke Glogowski, geb. Reimer
Nationality: german
Marital status: singled (2 sons; born in 1996 and 1998)
e-Mail: silke-glogowski@t-online.de

Last Education and Training

Date: 01/2013 – today
Applied Sciences: GEOMAR Helmholtz Centre for Ocean Research Kiel
Qualification: PhD student, Paleoceanography
Ocean Circulation and Climate Dynamics

Date: 10/2003 – 11/2010
Applied Sciences: University Kiel (CAU)
Qualification: Diploma in Geology
Focus: paleoceanography, coastal geology,
sedimentology

Date: 3/2007 – 8/2007
Applied Sciences: University Kiel (CAU);
Scientific Diving Centre (CAU)
Qualification: Scientific Diver

Date: 12/2010 – 9/2011
Applied Sciences: University Kiel (CAU)
Qualification: Period of practical training and as auditor at University
Kiel

Date: 2/1987 – 1/1989
Position: New Yorker OHG, Russeer Weg 101-103, 24109 Kiel
Qualification: Trainee wholesale and foreign trader

Date: 08/1983 – 07/1984
Technic Secondary
School: Berufliche Schulen am Schützenpark”, Kiel
Qualification: Certificate of higher education (polytechnic degree)

Date: 8/1980 – 6/1983
Position: Otlepp Sportlepp KG
Qualification: Trainee window displayer

Last Work Experience

Date: 1/1991 – 9/2003
Position: Assistant to director of sales (management)
Employer: New Yorker OHG, Russeer Weg 101-103, 24109 Kiel
Sector: Retailing
Achievements: Coordinated, organized and arranged the assistant job independently
Within this job: since 11/1994
Qualification: Instructor for trainees (with examination)

Personal Skills

Languages: German (mother tongue)
English (C1*, Independent User)
*Common European Framework (CEF) level

Social Skills: Good oral and written communication skills.
Considerable experience of working in multicultural teams

Organizational skills: Extensive experience in leading project teams

Computer Skills: Excellent knowledge of Word, Excel, Power-Point.
Working knowledge in GIS and Matlab

Activities, Hobbies: Diving, skiing, motorcycling, rescue work with my dog,
Jogging (10 km distance)

Additional information: Clean driving licence (car and motorcycle)

References: Available upon request

Silke Glogowski

Publications

Non published „Diploma“:

2011

Diploma

Glogowski S

Rekonstruktion der spätquartären Paläo-Boden-Strömungen im zentralen Arktischen Ozean anhand von Sedimentkernen vom Lomonosov-Rücken / Arktis. GEOMAR Library

Article in a Scientific Journal - peer reviewed

2012

Hebbeln D, Wienberg C, Beuck L, Dehning K, Dullo C, Eberli G, Freiwald A, **Glogowski S**, Garlich T, Jansen F, Joseph N, Klann M, Matos L, Nowald N, Reyes Bonilla H, Ruhland G, Taviani M, Wilke T, Wisenack M, Wintersteller P (2012) Report and preliminary results of R/V MARIA S. MERIAN cruise MSM20-4. WACOM-West-Atlantic Cold-water Coral Ecosystem: The West Side Story. Bridgetown-Freeport, 14. March – 7. April 2012, University of Bremen:120 pp

2014

Hebbeln D, Wienberg C, Wintersteller P, Freiwald, A, Becker M, Beuck L, Dullo C, Eberli G, **Glogowski S**, Freiwald A, Matos L, Joseph N, Reyes-Bonilla H, Taviani M, and the MSM20-4 shipboard scientific party (2014) Environmental forcing of the Campeche cold-water coral province, southern Gulf of Mexico. Biogeosciences 11: 1799-1815, doi: 10.5194/bg-11-1799-2014.

Keywords: cold-water corals, Campeche Bank, Gulf of Mexico, coral mounds, living *Lophelia pertusa*

2015

Glogowski S, Dullo W-C, Feldens P, von Reumont J, Hühnerbach V, Krastel S, Wynn RB and Flögel S (2015) „Eugen Seibold Coral Mounds“ offshore northwest Morocco: Oceanographic and bathymetric controls on a newly discovered cold-water coral province. Geo-Marine Letters. doi: 10.1007/s00367-015-0405-7

Keywords: cold-water coral, living *Lophelia pertusa*, coral mounds, Agadir Canyon, Morocco

2017 (submitted)

Glogowski, S, Dullo W-C, Flögel S and Raddatz J

Geochemical, optical, microstructure and growth systematics of the scleractinian cold-water coral *Lophelia pertusa*.

Keywords: cold-water coral, living *Lophelia pertusa*, Mg/Ca, Na/Ca, theca wall, center of calcification

2017 (to be submitted)

Glogowski S, Dullo W-C and Flögel S

Control mechanism of the density gradients in the water column above scleractinian cold-water coral *Lophelia pertusa* in the East- and West Atlantic and the Gulf of Mexico

2017

Glogowski S

Water mass dynamics around Cold-Water Coral reefs in the North Atlantic
Dissertation zur Erlangung des Doktorgrades Dr. rer. nat. an der Mathematisch-Naturwissenschaftlichen Fakultät der Christian-Albrechts-Universität zu Kiel, vorgelegt am: GEOMAR Helmholtz-Zentrum für Ozeanforschung Kiel FB 1 Paläo-Ozeanographie

Conference Presentation

2011

Spielhagen RF, **Glogowski S**, Nørgaard-Pedersen N und Schmidt A (2011) *Arctic Ocean Paleoenvironmental Change in the last 50 kyr Reconstructed from an Alpha Ridge to Gakkel Ridge Transect*. In: AGU Fall Meeting 2011, 05.-09.12.2011, San Francisco, USA

Conference Poster

2014

1.

Glogowski S, Feldens P, Hühnerbach V, von Reumont J, Krastel S, Flögel S, Dullo W-C, Wynn RB (2014)

Living cold water corals off Morocco: Water Masses and Bathymetry, GeoHab (Marine **Geological** and Biological **Habitat** Mapping), Lorne (Victoria, Australia), 05.-09.05.2014

2.

Krastel S, Wynn RB, Feldens P, Hühnerbach V, Unverricht D, Schürer A, **Glogowski S**, Stevenson C (2014)

High-resolution acoustic imaging in the Agadir-Canyon region, NW-Africa: Morphology, processes and geohazards. AGU Fall Meeting, San Franzisko, 15.-19.12.2014

2015

Glogowski S, Dullo W-C, Feldens P, von Reumont J, Hühnerbach V, Krastel S, Wynn RB, and Flögel S (2015) „The Eugen Seibold coral mounds“ offshore north-west Morocco: Oceanographic and bathymetric steering of a newly discovered cold-water coral province. EGU Vienna, April 2015